In vivo Charakterisierung Amyloid-β-Oligomer eliminierender D-enantiomerer Peptide zur Therapie der Alzheimer'schen Demenz

Inaugural-Dissertation

zur Erlangung des Doktorgrades
der Mathematisch-Naturwissenschaftlichen Fakultät
der Heinrich-Heine-Universität Düsseldorf

vorgelegt von

Sarah Schemmert
aus Herzogenrath

Düsseldorf, Januar 2018

Aus dem Institut für Physikalische Biologie
der Heinrich-Heine-Universität Düsseldorf

Gedruckt mit der Genehmigung der
Mathematisch-Naturwissenschaftlichen Fakultät der
Heinrich-Heine-Universität Düsseldorf

1. Berichterstatter:	Prof. Dr. Dieter Willbold
2. Berichterstatter:	Prof. Dr. Karl-Josef Langen
3. Berichterstatter:	Prof. Dr. Heinrich Sticht
Tag der mündlichen Prüfung:	28.03.2018

Eidesstaatliche Erklärung

Hiermit erkläre ich an Eides statt, dass ich die vorliegende Dissertation selbständig verfasst und keine anderen als die von mir angegebenen Quellen und Hilfsmittel verwendet und Zitate kenntlich gemacht habe.

Ferner erkläre ich, dass ich in keinem anderen Dissertationsverfahren mit oder ohne Erfolg versucht habe, diese Dissertation einzureichen.

Düsseldorf, den

_____

(Sarah Schemmert)

Jedes Leben ist wertvoll.

Den Mäusen dieser Arbeit gewidmet.

Danksagung

Viele Menschen haben zu dem Gelingen dieser Arbeit beigetragen, bei denen ich mich von Herzen bedanken möchte!

Ich danke Herrn Prof. Dr. Dieter Willbold für die Möglichkeit, meine Dissertation in seinem Institut des Forschungszentrums Jülich und der Heinrich-Heine-Universität erarbeiten zu können. Darüber hinaus danke ich Ihm für die vielen Möglichkeiten, die er mir während meiner Doktorarbeit ermöglicht hat. Die fachlichen Diskussionen und die zahlreichen Anlässe, meine spannenden Projekte auf nationalen und internationalen Konferenzen mit Wissenschaftlern weltweit austauschen zu dürfen, haben mir viele Möglichkeiten eröffnet, meine Arbeit zu verbessern.

Des Weiteren Danke ich Herrn Prof. Dr. Karl-Josef Langen, für die Übernahme meines Zweitgutachtens. Die herausragende Kooperation zwischen dem ICS-6 und Ihrer Arbeitsgruppe des INM-4 hat mir viele Möglichkeiten eröffnet.

Ein Großer Dank gilt Dr. Antje Willuweit und Dr. Janine Kutzsche für die intensive, unermüdliche Betreuung, das stets offene Ohr und die fachliche Hilfe. Eure Ratschläge haben immer dazu beigetragen, dass sich meine wissenschaftliche Arbeit verbessert!

Darüber hinaus möchte ich meinen lieben Kolleginnen und Kollegen – Dr. Anne Elfgen, Dr. Tamar Ziehm, Markus Tusche, Dominik Honold, Julia Post-Schulz, Dr. Franziska Weirich, Michelle Hupert, Dr. Bea Santiago-Schübel, Alexandra Drechsel, Bettina Kass, Dr. Nan Jiang, Dr. Oleksandr Brener, Dr. Lothar Gremer, Dr. Christian Zafiu, Dr. Andreas Kulawik, Dr. Dagmar Jürgens, Anne Cousin, Volker Söhnitz, Caroline Folz, Michael Schöneck, Nicole Niemietz, Verena Graf, Dennis Oliveira, Carina Stegmayer und Arbia Khezami - für die vielen wunderbaren Momente, die zahlreichen fachlichen Diskussionen und privaten Freuden danken. Ihr alle habt zum Gelingen dieser Arbeit beigetragen! Mein größter Dank gilt der anderen Hälfte des Team „ElSa“! Elena, die gemeinsame Arbeit mit dir, die vielen Stunden, die wir stets motiviert und mit größter Freude und „ein kleines bisschen verrückt“ im Labor, im Tierhaus und im Büro verbracht haben, bleiben unvergesslich!

Ein weiterer Dank gilt dem Tierhausteam des Forschungszentrums Jülich, für seine fürsorgliche Betreuung unserer Mäuschen und der tatkräftigen Unterstützung unserer Studien.

Zu guter Letzt danke ich meinen Freunden und meiner Familie, die mich stetes unterstützt und ermutigt haben. Dominik, dir danke ich für dein Vertrauen und dein Verständnis. Wie immer: Danke, dass ihr meines Wahnsinns nicht leid seid ☺

Liste der Publikationen und Kongressbeiträge

Publikationen

2017

- Kutzsche J.*, **Schemmert S.***, Tusche M., Neddens J., Rabl R., Jürgens D., Brener O., Willuweit A., Hutter-Paier B., Willbold D. (2017) Large-Scale Oral Treatment Study with the Four Most Promising D3 Derivatives for the Treatment of Alzheimer's Disease. *Molecules 22 (10).*

- van Groen T., **Schemmert S.**, Brener O., Gremer L., Ziehm T., Tusche M., Nagel-Steger L., Kadish I., Schartmann E., Elfgen A., Jurgens D., Willuweit A., Kutzsche J., Willbold D. (2017) The Aβ oligomer eliminating D-enantiomeric peptide RD2 improves cognition without changing plaque pathology. *Sci Rep* 7, 16275.

- Hupert M, Elfgen A., Schartmann E., **Schemmert S.**, Buscher B., Kutzsche J., Willbold D., Santiago-Schubel B. (2017) Development and validation of an UHPLC-ESI-QTOF-MS method for quantification of the highly hydrophilic amyloid-beta oligomer eliminating all-D-enantiomeric peptide RD2 in mouse plasma. *J Chromatogr B Analyt Technol Biomed Life Sci* **1073**, 123-129.

- Dunkelmann T., Teichmann K., Ziehm T., **Schemmert S.**, Frenzel D., Tusche M. Dammers C., Jürgens D., Demuth H-U., Langen K-J., Kutzsche J., Willuweit A., Willbold D. (2017) Aβ oligomer eliminating compounds interfere successfully with pEAβ(3–42) induced motor neurodegenerative phenotype in transgenic mice. *Neuropeptides.*

- Schartmann E., **Schemmert S.,** Ziehm T., Leithold L.H.E., Jiang N., Tusche M., Shah N. J., Langen K.-J., Kutzsche J., Willbold D., Willuweit A. (2017) Comparison of blood-brain barrier penetration efficiencies between linear and cyclic all-D-enantiomeric peptides developed for the treatment of Alzheimer's disease. *Eur J Pharm Sci* **114**, 93-102.

2018

- Dunkelmann T.*, **Schemmert S.***, Honold D., Teichmann K., Butzküven E., Demuth H-U., Shah N. J., Langen K-J., Kutzsche J., Willbold D., Willuweit A. (2018) Comprehensive characterization of the pyroglutamate Aβ induced motor neurodegenerative phenotype of TBA2.1 mice. *J. Alzheimer's Dis.*

- **Schemmert S**., Schartmann E., Zafiu C., Kass B., Hartwig S., Lehr S., Bannach O., Langen K-J., Shah N.J., Kutzsche J., Willbold D., Willuweit A. (2018) Aβ oligomer elimination restores cognition in transgenic Alzheimer's mice with full-blown pathology. *EMBO Rep.*

- **Schemmert S**., Schartmann E., Honold D., Zafiu C., Ziehm T., Langen K-J., Shah N.J., Kutzsche J., Willuweit A., Willbold D (2018) Oral treatment with an Aβ oligomer eliminating compound decelerates the neurodegenerative phenotype in pyroglutamate-Aβ accumulating transgenic mice. *Neuron.*

- Schartmann E., **Schemmert S**., Niemietz N., Honold D., Ziehm T., Tusche M., Elfgen A., Gering I., Brener O., Shah N.J., Langen K-J., Kutzsche J., Willbold D., Willuweit A. (2018) *In vitro* potency and preclinical pharmacokinetic comparison of all-D-enantiomeric peptides developed for the treatment of Alzheimer's disease. *J. Alzheimer's Dis*.

Kongressbeiträge national/international

2016

- **Schemmert S.**, Schartmann E., Willuweit A., Kutzsche J., Willbold D.
  Therapeutic Treatment with a D-enantiomeric peptide improves cognitive impairment in aged APPswe/PS1 transgenic mice
  Alzheimer's Association International Conference (AAIC), Toronto 2016

- Schartmann E., **Schemmert S.**, Ziehm T., Leithold L.H.E., Jiang N., Kutzsche J., Willuweit A., Willbold D.
  Raising available brain concentrations of a potential Alzheimer's disease drug candidate by peptide cyclization
  Alzheimer's Association International Conference (AAIC), Toronto 2016

2017

- **Schemmert S.**, Schartmann E., Willuweit A., Kutzsche J., Willbold D.
  Therapeutic Treatment with a D-enantiomeric peptide improves cognitive impairment in aged APPswe/PS1 transgenic mice
  The 13th International Conference on Alzheimer's & Parkinson's Diseases and Related Neurological Disorders (ADPD), Vienna 2017

- Schartmann E., **Schemmert S.**, Ziehm T., Leithold L.H.E., Jiang N., Kutzsche J., Willuweit A., Willbold D.
  The cyclized version of an all-D-enantiomeric peptide AD drug candidate reaches the brain more efficiently than its linear version
  The 13th International Conference on Alzheimer's & Parkinson's Diseases and Related Neurological Disorders (ADPD), Vienna 2017

- **Schemmert S.**, Schartmann E., Willuweit A., Kutzsche J., Willbold D.
  Treatment with an all-D-enantiomeric peptide improves cognitive and motoric impairment in two different Alzheimer mouse models
  Alzheimer's Association International Conference (AAIC), London 2017

- Schartmann E., **Schemmert S.**, Ziehm T., Leithold L.H.E., Jiang N., Kutzsche J., Willuweit A., Willbold D.
  Cyclic D-enantiomeric peptide targeting Amyloid-beta in Alzheimer's disease
  Alzheimer's Association International Conference (AAIC), London 2017

- **Schemmert S**., Schartmann E., Ziehm T., Kutzsche J., Kass B., Zafiu C., Willuweit A., Willbold D.
  Treatment with the all-D-enantiomeric peptide RD2 improves cognitive and motor impairment in two different Alzheimer's disease mouse models
  Düsseldorf-Jülich Symposium on Neurodegenerative Diseases: Formation, aggregation and propagation of amyloids, Düsseldorf 2017

- Schartmann E., **Schemmert S.**, Ziehm T., Leithold L.H.E., Jiang N., Langen K.-J., Kutzsche J., Willbold D., Willuweit A.
  Comparison of blood-brain barrier penetration efficiencies between linear and cyclic all-D-enantiomeric peptides developed for the treatment of Alzheimer's disease
  Düsseldorf-Jülich Symposium on Neurodegenerative Diseases: Formation, aggregation and propagation of amyloids, Düsseldorf 2017

Inhaltsverzeichnis

Tabellenverzeichnis

Abbildungsverzeichnis

Kurzfassung

Die Alzheimer'sche Demenz (AD) ist eine unheilbare, neurodegenerative Erkrankung, pathologisch charakterisiert durch zerebrale Amyloid-β (Aβ)-Ablagerungen und neurofibrilläre Bündel, einhergehend mit einem progressivem Verlust der Gedächtnisleistung. Die Suche nach einer kausalen Therapie gegen die AD stellt Forscher, aufgrund der Komplexität der multifaktoriellen Erkrankung, weltweit vor eine enorme Herausforderung. Derzeit zugelassene Medikationen bewirken ausschließlich eine Verzögerung der klinischen Symptome, oft einhergehend mit unerwünschten Nebenwirkungen, ohne die kausale Ursache der Erkrankung zu behandeln. Seit mehreren Jahren forscht die Arbeitsgruppe um Prof. Dr. Willbold am Forschungszentrum Jülich und der Heinrich-Heine-Universität Düsseldorf an einer kausalen Therapie gegen die AD, die selektiv toxische Amyloid-β-Oligomere eliminiert, um deren Neurotoxizität zu reduzieren. Diese Therapie beruht auf Peptiden, einzig bestehend aus D-enantiomeren Aminosäureresten, die mittels Spiegelbild-Phagendisplay gegen monomeres Aβ selektiert worden sind. Ausgehend von der Leitsubstanz D3, die sowohl *in vitro* gezielt toxische Aβ-Oligomere eliminiert und *in vivo* in verschiedenen AD-Mausmodellen den Wirksamkeitsnachweis erbracht hat, wurden verschiedene D3-Derivate entwickelt. Das vielversprechendste dieser Derivate, RD2, wurde in dieser Arbeit ausgiebig charakterisiert. Dazu erfolgte eine detaillierte *in vitro* Charakterisierung die zeigte, dass RD2 toxische Aβ-Oligomere effizienter eliminiert als die Leitsubstanz D3 sowie anschließend Behandlungsstudien in verschiedenen AD-Mausmodellen. In einer initialen Studie konnte belegt werden, dass RD2 nach einer vierwöchigen intraperitonealen Behandlung die kognitiven Fähigkeiten steigert ohne die AD-assoziierte Pathologie zu beeinflussen. Aufgrund der erfolgreichen initialen Behandlungsstudie und der zu diesem Zeitpunkt bekannten Daten über die orale Verfügbarkeit wurden verschiedene orale Behandlungsstudien mit RD2 in verschiedenen AD-Mausmodellen durchgeführt. In einer groß angelegten *in vivo* Studie, in der mehrere D3-Derivate zeitgleich im APP_{SL} AD-Mausmodell oral getestet worden sind, konnte belegt werden, dass RD2 und das D3-Tandemderivat D3D3 die kognitiven Fähigkeiten der Mäuse steigerte. Jedoch konnte auch hier keine Änderung der AD-assoziierten Pathologie verzeichnet werden. In einer weiteren Behandlungsstudie, in der alte APPswe/PS1ΔE9 Mäuse mit starken kognitiven Beeinträchtigungen und einer ausgeprägten AD-assoziierten Pathologie oral behandelt wurden, konnte gezeigt werden, dass RD2 die kognitiven Fähigkeiten in diesem AD-Modell signifikant steigert. Neben der Steigerung der kognitiven Fähigkeiten konnte ein signifikanter Rückgang der Aβ-Ablagerungen im Kortex gezeigt werden. Weiterhin wurde erstmalig der Beweis erbracht, dass RD2 signifikant toxische Aβ-Oligomere in den Gehirnen der behandelten Mäuse reduziert (sog. „Target Engagement"). Trotz der hoch eingesetzten Dosierung wurden keine unerwünschten Arzneimittelwirkungen

nachgewiesen, welches durch eine Analyse diverser Plasmaenzymparameter sowie verschiedener Zytokine und Chemokine im Plasma belegt wurde. In einer weiteren oralen Behandlungsstudie an einem AD-Mausmodell, den sog. TBA2.1 Mäusen, welches durch motorische Defizite und eine enorme Neurodegeneration charakterisiert ist, konnte demonstriert werden, dass RD2 den sich progressiv ausbildenden Phänotyp signifikant verringert. Zusammenfassend zeigte RD2 in drei AD-Mausmodellen, in drei verschiedenen Laboratorien, selbst nach oraler Applikation eine signifikante Verbesserung, ohne unerwünschte Arzneimittelwirkungen aufzuweisen. Die erfolgsversprechenden pharmakokinetischen Eigenschaften, wie eine lange terminale Halbwertszeit, eine hohe orale Bioverfügbarkeit (über 70%) und ein Überwinden der Blut-Hirn-Schranke, sodass der Wirkstoff seinen Zielort erreichen kann sowie die herausragenden pharmakodynamischen Eigenschaften (selbst nach oraler Applikationen) qualifizieren RD2 als einen möglichen Kandidaten für eine erste Anwendung im Menschen und bietet eine neuartige Substanzklasse zur kausalen und erkrankungsmodifizierenden Therapie der AD.

Abstract

Alzheimer's disease (AD) is an incurable neurodegenerative disorder, mainly characterized by amyloid-β (Aβ)-deposits and neurofibrillary tangles, resulting in cognitive decline of the affected patients. Despite considerable efforts by scientists all over the world, no disease modifying or curative treatment against this multifactorial disease is available so far. Currently, approved medications only slow down the disease symptoms accompanied by undesirable adverse drug reactions. Since several years, Prof. Dr. Dieter Willbold's group at the Forschungszentrum Jülich and the Heinrich-Heine-Universität Düsseldorf is looking for a disease modifying therapy against AD. Their approach is based on the specific and direct elimination of toxic Aβ-oligomers. The elimination of toxic Aβ-oligomers is achieved by peptides solely consisting of D-enantiomeric amino acid residues, which were identified by mirror image phage display. Originating from the lead compound D3, which eliminates toxic Aβ-oligomers *in vitro* and enhances cognition *in vivo* in several AD mouse models, different lead optimization approaches were conducted. In this thesis, RD2, the most promising D3-derivative, was intensively characterized. For this purpose, several *in vitro* experiments were conducted, revealing that RD2 eliminates toxic Aβ oligomers more efficiently than D3. Moreover, treatment studies were performed to verify RD2's *in vivo* efficacy. In an initial intraperitoneal treatment study, it was proven that RD2 enhances cognition impairment without changing the AD-associated pathology in the brain. Based on the positive outcome of this study and the determined oral bioavailability, different oral RD2-treatment studies were conducted. In a large-scale oral treatment study in APP_{SL} AD mice several D3-derivatives were directly compared. This study revealed that RD2, as well as the D3-tandem derivative D3D3, improved cognition. Again, there were no differences in the AD-associated pathology. Within a further treatment study, old-aged APPswe/PS1ΔE9 with severe cognitive impairments and a full-blown pathology were orally treated, resulting in a significant improvement of cognition. Besides the amelioration of cognitive impairments, a significant reduction of Aβ-deposits was demonstrated in this study. For the first time, it was proven that RD2 eliminates toxic Aβ-oligomers out of RD2-treated brains (target engagement). Despite the high administered dose, no adverse drug reactions were observed by analysis of different plasma enzymes, as well as different cytokines and chemokines. Additionally, an oral treatment study was performed in an AD mouse model, the TBA2.1 mouse model, which is characterized by a motor phenotype and enormous neurodegeneration. It was shown that RD2 significantly decelerates the neurodegenerative phenotype.

In this thesis, the proof of concept of RD2 was demonstrated in various AD mouse models in different laboratories, even after oral administration. Amelioration of cognition and the deceleration of a neurodegenerative phenotype were demonstrated without exhibiting

adverse drug reactions. The promising pharmacokinetic properties, e.g. the high oral bioavailability, the long terminal half-life, and the favorable blood-brain-barrier penetration, even after oral administration, qualify RD2 as a potential first-in-man, first-in-class drug candidate for a disease modifying and curative treatment of AD.

1. Einleitung

Als Alois Alzheimer im Jahr 1907 erstmalig eine bis dahin unbekannte Krankheit beschrieb [1] ahnte er nicht, dass die Alzheimer'sche Demenz (AD) über 100 Jahre später ein großes medizinisches und volkwirtschaftliches Problem darstellen würde Der Fall seiner Patientin Auguste Deter ließ sich mit keinem bisher bekannten Krankheitsbild in Einklang bringen, ihr „Gebaren (trug) den Stempel volliger Ratlosigkeit", sie litt unter fortschreitender „Gedächtnisschwäche" und „Merkfähigkeit" [1]. Bis zu ihrem Tod konnte sich Alzheimer die Ursache ihres absonderlichen Verhaltens nicht erklären. Untersuchungen ihres Gehirns zeigten schon damals die bis heute als charakteristisch geltenden pathologischen Veränderungen der AD: 1) extrazelluläre Ablagerungen des Amyloid-β(Aβ)-Proteins, die sogenannten Aβ-Plaques, 2) neurofibrilläre Bündel (NFT), bestehend aus dem hyperphosphorylierten Tau-Protein, 3) eine Atrophie der grauen Substanz des Gehirns, einhergehend mit einer Vergrößerung der Ventrikel und 4) eine pathologische Anhäufung von Entzündungszellen (Abbildung 1) [1].

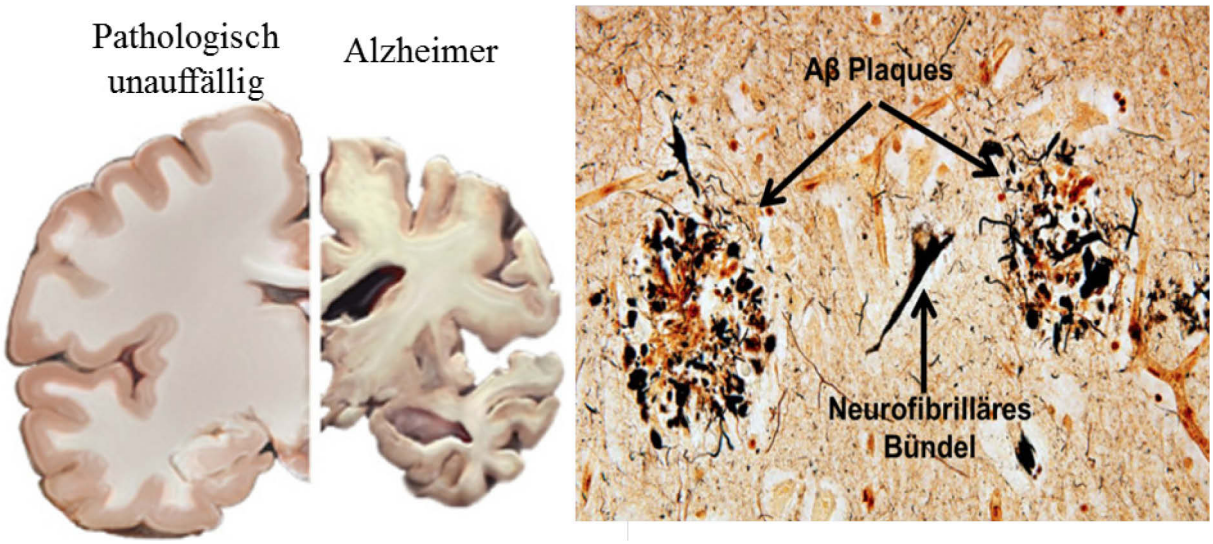

Abbildung 1: Die Alzheimer'sche Demenz.
Links: Abbildung eines pathologisch unauffälligen Gehirns im Vergleich zu einem Gehirn eines Alzheimer Patienten, mit deutlich sichtbarer Atrophie und vergrößerten Ventrikeln. Rechts: Mikroskopische Hauptkennzeichen der AD; Aβ-Plaques und neurofibrilläre Bündel.
Quellen: https://www.nia.nih.gov/sites/default/files/inline-images/brain_slices_alzheimers_0.jpg und Perl, 2010.

Heutzutage gilt die AD, eine neurodegenerative, irreversible Erkrankung, generell einhergehend mit Gedächtnisverlust und Abbau der kognitiven Fähigkeiten der betroffenen Patienten, als die am häufigsten verbreitete Form der Demenz. Klassisch wird die AD in zwei Formen gegliedert: Die familiäre, vererbte Form (fAD, oder auch „early onset AD", (EOAD)) und die sporadische Form (sAD, oder auch „late onset AD", (LOAD)). Während die Ursachen der sAD bis heute wissenschaftlich unzulänglich aufgeklärt sind, gelten Mutationen in den

Genen, die für die Proteine Präsenilin-1 und -2 (PS1 und PS2) sowie dem Amyloid-Vorläufer-Protein (APP) kodieren, ursächlich als Auslöser der fAD [2].

Trotz intensiver Forschungsbemühungen (Publikationen (pubmed) im Feld der AD Forschung ca. 130.000, Stand Januar 2018) und erheblicher Förderungen gilt die AD nach wie vor als unheilbar. Zugelassene Medikationen wie Acetylcholinesteraseinhibitoren (AChEI) und N-methyl-D-Aspartat(NMDA)-Rezeptor-Antagonisten bewirken nur eine kurzzeitige Linderung der Symptome ohne die kausale Ursache zu behandeln.

1.1 Ätiologie der multifaktoriellen Erkrankung AD: Genetik, Epidemiologie und Risikofaktoren

Der Begriff „Demenz“ ist eine generalisierte Bezeichnung für eine verminderte geistige Fähigkeit, insbesondere des Gedächtnisses. Die Prävalenz an Demenz zu erkranken liegt bei Personen, die jünger als 60-65 Jahre alt sind unter einem Prozent. Diese steigt jedoch exponentiell mit dem Alter, sodass Menschen in der westlichen Welt mit einem Alter über 85 Jahren ein Risiko von 24 bis 33 % haben, an einer Form der Demenz zu erkranken [3]. Des Weiteren wird mit einer exponentiellen Verdopplung der Fälle alle 20 Jahre von 46,8 Millionen Patienten im Jahr 2015 bis hin zu 131,5 Millionen Betroffenen im Jahr 2050 gerechnet [3], auch bedingt durch den demographischen Wandel der Bevölkerung.

Die AD ist die am häufigsten verbreitete Form der Demenz, mit 60 bis 80 % der an Demenz erkrankten Patienten [4]. Bezugnehmend auf den „World Alzheimer’s Report“ aus dem Jahr 2015, betragen die weltweiten Kosten für die Therapie und Versorgung aller Demenzerkrankten 818 Milliarden US$, wobei für 2030 bereits mit Kosten in Höhe von 2 Billionen US$ gerechnet wird [4].

Die kausale Ursache für die Entwicklung der AD ist höchstwahrscheinlich durch eine Vielzahl diverser Umstände geprägt, zu denen unter anderem genetische, epigenetische und Umwelteinflüsse zählen. Der größte und offensichtlichste Risikofaktor, an AD zu erkranken, ist das Alter. Neben diesem gelten weitere Aspekte als mögliche Risikofaktoren. Zu diesen zählen persönliche und teilweise vermeidbare Faktoren wie Fettleibigkeit, Rauchen, zu geringe physische Aktivität, ein geringer Bildungsstatus sowie eine reduzierte Aktivität im weiteren Lebensverlauf [5]. Des Weiteren können Erkrankungen wie Diabetes mellitus, Hypertonie, Depressionen, koronare Herzerkrankung, vaskuläre Erkrankungen, Hypercholesterinämie und Atherosklerose zu einem erhöhten Risiko beitragen an AD zu erkranken [2, 6-9].

Die AD gilt als eine heterogene genetische Erkrankung, die in eine familiäre, vererbte und eine sporadische Form gegliedert werden kann. Die fAD ist eine autosomal dominant

vererbte Erkrankung, besonders geprägt durch einen frühzeitigen Ausbruch der Demenz unter 65 Jahren. Das klinische Erscheinungsbild der fAD und sAD lässt sich hinsichtlich der kognitiven Beeinträchtigungen und der Pathologie nicht unterscheiden [10]. Es wurden drei Gene identifiziert die, wenn sie mutiert sind, zur Ausprägung der fAD führen: APP, PS1 und PS2 [11]. Die erste bekannte Mutation, die ursächlich für die familiäre Form der AD beschrieben wurde, ist eine Mutation des APP-Gens. Das APP-Gen liegt auf Chromosom 21q21 und ist ein ubiquitär exprimiertes Transmembranprotein. Es gibt drei verschiedene Isoformen des APP-Gens: APP695, APP751 und APP770. APP695 wird hauptsächlich in Neuronen und APP751 in Astrozyten exprimiert [12]. In der Literatur werden über 30 Mutationen beschrieben, die vermehrt in der Aβ-Domäne auftreten (Exon 16 und 17), vor allem im C-terminalen Bereich [13]. Die daraus resultierende Verschiebung der APP-Prozessierung, die unter Kapitel 1.3 näher erläutert wird, führt zu einer vermehrten Bildung des stark amyloidogenen $A\beta_{42}$, einer reduzierten $A\beta_{40}$-Bildung und somit zu einer Änderung des $A\beta_{42/40}$ Verhältnisses, ohne die Aβ-Gesamtmenge zu verändern [14]. Trotz der vielen verschiedenen Mutationen sind jene im APP-Gen vorkommenden nicht die dominantesten. Mutationen in den Genen PS1 und PS2 hingegen kommen in nahezu allen Fällen der fAD vor [15, 16]. Die beiden Gene PS1 (Chromosom 14q23.4) und PS2 (Chromosom 1q31-q42) weisen eine strukturelle Ähnlichkeit auf und sind wesentliche Bestandteile des γ-Sekretase-Komplexes, welcher APP zu Aβ spaltet [17]. Zusammengefasst sind diese Mutationen für 30 bis 50 % der autosomal vererbten AD-Fälle verantwortlich und nur für 0,5% der sAD-Fälle [13]. Obwohl diese Mutationen nur für eine verschwindend geringe Zahl der gesamten AD-Fälle verantwortlich sind, kann man sich diese in der Gentechnik zu Nutze machen, z.B. um Mausmodelle zu generieren. Mit Hilfe dieser ist es möglich, die Entstehung der AD sowie neue therapeutische Ansätze auf deren Wirksamkeit zu untersuchen. Diese werden unter Kapitel 1.5 näher erläutert. Neben Mutationen in den genannten Genen (APP, PS1 und PS2), die hautsächlich für die Entstehung der fAD verantwortlich sind gelten Mutationen im Apolipoprotein E (ApoE) ε4 Allel als stärkster Risikofaktor für die sAD. Ein heterozygotes Vorliegen des ApoEε4 trägt zu einem dreifach erhöhten Risiko bei, ein homozygotes Vorliegen des ApoEε4 zu einem fünfzehnfachen Risiko [18].

1.2 Diagnose und Pathologie/Pathophysiologie der AD

Der pathophysiologische Verlauf der AD beginnt viele Jahre, wenn nicht sogar Jahrzehnte bevor die klinische Diagnose der AD gestellt werden kann. D.h. bevor eine Manifestation kognitiver Beeinträchtigung sichtbar wird, können über diverse Nachweisverfahren, wie bildgebende Verfahren (Positronen-Emissions-Tomographie (PET)) und Magnetresonanztomographie (MRT)) und der Nachweis von Biomarkern aus z.B. der Cerebrospinalflüssigkeit (CSF)), erste pathologische Veränderungen detektiert werden

(Abbildung 2) [19]. Kriterien für die Diagnose der AD wurden bereits vor über 30 Jahren festgelegt, wobei bis heute eine definitive Diagnose zumeist erst *post mortem* gestellt werden kann [20].

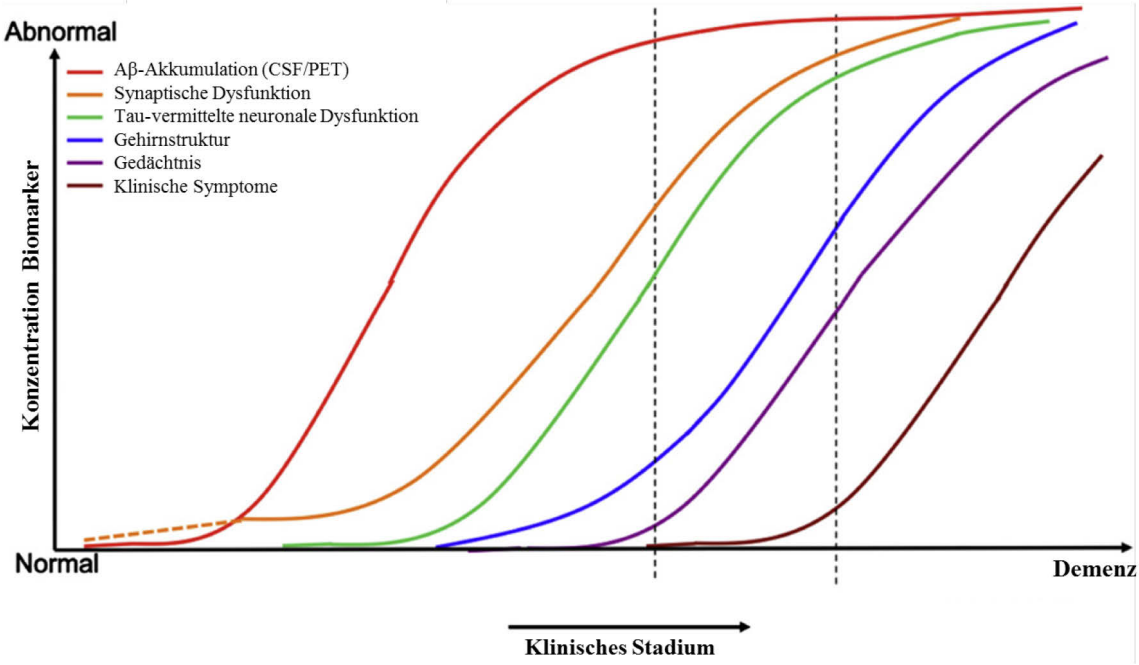

Abbildung 2: Theoretisches Modell des Auftreten von typischen Biomarkern der Alzheimer'schen Demenz und Auftreten der klinischen Symptome.
Weit vor dem Auftreten erster kognitiver Beeinträchtigungen (klinischer Symptome) können sowohl über Biomarker aus der Cerebrospinalflüssigkeit (CSF), als auch über bildgebende Verfahren, wie der Positronen-Emissions-Tomographie (PET) pathologische Veränderungen nachgewiesen werden. Abbildung modifiziert nach [19].

Der Beginn einer Demenzerkrankung beginnt in der Regel damit, dass sich der Erkrankte an alltägliches nicht mehr erinnern kann, jedoch sehr wohl an vergangene Ereignisse. Durch die Beeinträchtigung des episodischen Gedächtnisses können neue Informationen nicht aufgenommen und verarbeitet werden, da das Lernen, und somit die Verarbeitung neuer Informationen, durch fehlende neuronale Verbindungen, vor allem in kortikalen und hippocampalen Strukturen, beeinträchtigt ist. All unsere Sinneswahrnehmungen werden über neokortikale Regionen aufgenommen und von dort aus in entorhinale Regionen projiziert. Von dort aus werden die Informationen in den Hippocampus weitergeleitet, verarbeitet und zurück in tiefe entorhinale Regionen und, schlussendlich, wieder zurück in den Neokortex projiziert. Ein Verlust dieser für das Lernen und somit für die Gewinnung neuer Erinnerungen essentiellen Verbindungen bewirkt die typischen klinischen Symptome einer Demenz [21]. Wie bereits zu Beginn dieses Abschnittes beschrieben, können pathologische Veränderungen im Gehirn eines AD Patienten bereits Jahrzehnte bevor klinische Symptome erkennbar sind detektiert werden. Mittels verschiedener bildgebender Verfahren konnte, vor allem im Frontallappen, eine Atrophie des Gehirns bei AD Patienten dokumentiert werden

[22]. Die Atrophie des entorhinalen Kortex korreliert mit der Einschränkung des episodischen Gedächtnisses und geht mit einer Reduktion der grauen Substanz (Neuronen) einher. Die beschriebene Atrophie eines Gehirns eines an AD erkrankten Patienten ist auf den Verlust von Dendriten, Synapsen und Axonen sowie einer reduzierten Myelinisierung, resultierend in einer Neurodegeneration, zurückzuführen.

Der pathologische Verlauf und somit die Schwere der AD lässt sich unter anderem in sechs sog. „Braak-Stadien“ (engl. Braak stages) gliedern [23]. Ausgehend vom medialen Temporallappen (Stadien 1 und 2, prodromale AD) breitet sich die Pathologie in limbische Regionen aus (Stadien 3 und 4, frühe moderate AD) und manifestiert sich schlussendlich im Neokortex (Stadien 5 und 6, späte moderate AD, klinische Manifestation der Erkrankung) [24]. Braak-Stadien wurden ursprünglich in Bezug auf die Ausbreitung neurofibrillärer Bündel entwickelt, lassen sich jedoch auch auf die Aβ Verteilung übertragen [21]. Aβ-Ablagerungen entwickeln sich immer zunächst im Neokortex, gefolgt von Aβ-Ablagerungen im entorhinalen Kortex und medialen Schläfenlappen. Anschließend sind Aβ-Ablagerungen im Hippocampus und diesen assoziierten Regionen zu finden (z.B. Striatum) sowie im basalen Vorhirn (z.B. Nucleus basalis Meynert), bis Aβ Ablagerungen final im Hirnstamm sowie im Kleinhirn zu finden sind [25].

Auf der mikroskopischen Ebene gibt es eine Vielzahl von Merkmalen, die als charakteristisch für die AD gelten. Die Hauptmerkmale der AD sind senile Plaques und NFT‘s in verschiedenen Bereichen des Gehirnes. Mitochondriale Dysfunktionen, oxidativer Stress, Veränderungen des Zellzyklus, neurovaskuläre Veränderungen, inflammatorische Prozesse sowie die Hyperphosphorylierung des tau Proteins mit Bildung von neurofibrillären Bündeln und die Aβ-Aggregation sind einige der zugrundeliegenden pathogener Mechanismen der charakteristischen Neuropathologie der AD [2].

1.3 Das Amyloid β Protein

1.3.1 Prozessierung

Während der letzten Jahre wurde der Fokus der Wissenschaft zur kausalen Therapie der AD unter anderem auf Aβ und dessen (toxische) Prozessierung gelegt, da Aβ eine zentrale Rolle in der Pathogenese der AD einnimmt. Nichtsdestotrotz darf nicht außer Acht gelassen werden, dass monomeres Aβ auch normale physiologische Funktionen, wie z.B. Genregulation, Entwicklung des Gehirns und Zell-Zell-Interaktionen, zugesprochen werden [26]. Es konnte gezeigt werden, dass eine Überexpression des APP-Gens einen positiven Effekt auf Zellen hat, z.B. führt es zu vergrößerten Neuronen [27] und gesteigerte kognitive Fähigkeiten sowie einer erhöhten synaptischen Dichte [28, 29]. Des Weiteren wurde erst

kürzlich über eine Mutation im APP-Gen berichtet, die dazu führt, dass die Betroffenen nicht an AD erkranken (Island-Mutation) [30].

Hauptbestandteil der extrazellulären Plaques ist das Aβ, das kontinuierlich durch enzymatische Proteolyse des humanen APP gepalten wird [31]. Das humane APP ist ein 110 bis 130 kDa großes Protein, zugehörig zu einer konservierten Familie Typ 1 transmembraner Glykoproteine, zu denen ebenfalls die APP ähnlichen Proteine APLP1 und APLP2 gehören [32], die funktionelle Ähnlichkeiten aufweisen, jedoch nicht die Aβ-Sequenz enthalten [33]. APP kann über zwei Wege, abhängig von der Sekretase, proteolytisch gespalten und prozessiert werden: den amyloidogenen und den nicht-amyloidogenen Weg. Unter physiologischen Bedingungen wird APP kontinuierlich im normalen Zellmetabolismus über den nicht-amyloidogenen Weg prozessiert (Abbildung 3) [2]. Dabei wird APP initial von der α-Sekretase innerhalb der Aβ-Domäne geschnitten, sodass die Bildung und Freisetzung des Aβ-Peptides verhindert wird [31]. Neben dem löslichem sAPPα-Fragment, welches in den extrazellulären Raum sekretiert wird [34], entsteht das C83-Fragment (83-amino-acid C-terminal fragment), welches über die γ-Sekretase weiter zu dem P3 und AICD Protein (amino-terminal APP intracellular domain) gespalten wird (Abbildung 3) [32].

Aβ wird über den amyloiden Weg generiert [35]. Dabei wird APP oberhalb der Aβ-Domäne mittels der β-Sekretase (auch β-site APP cleaving enzyme (BACE-1) genannt) geschnitten, sodass der N-terminale Teil, als sAPPβ, in den extrazellulären Raum freigesetzt wird. Über eine γ-Sekretase wird die Aβ-Domäne vom C-terminalen Rest (C99-Fragment) gespalten und ebenfalls in den extrazellulären Raum sezerniert [32]. Wie auch beim nicht-amyloiden Weg entsteht das AICD Protein, welches im Zytosol verbleibt (Abbildung 3). Abhängig von der spaltenden γ-Sekretase können verschieden große Aβ-Fragmente entstehen (38 bis 42 Aminosäuren lang), wobei $Aβ_{(1-40)}$ die dominanteste Form ist [36]. Einigen Formen, z.B. $Aβ_{(1-42)}$ und $Aβ_{(3-40)}$ wird ein erhöhtes amyloidogenes Potential zugesprochen [37], als anderen, z.B. $Aβ_{(1-40)}$ und $Aβ_{(1-38)}$ [35]. Ein erhöhtes amyloidogenes Potential bedeutet, dass diese Isoformen eine erhöhte Neigung zur Aggregation und ein toxischeres Potential haben sowie vermehrt in den Aβ-Plaques in Gehirnen von transgenen AD Mäusen sowie an AD erkrankten Patienten zu finden sind [31, 38]. Neben extrazellulärem Aβ wurde dieses ebenfalls intrazellulär nachgewiesen, sowohl in verschiedenen transgenen AD Mausmodellen, als auch im Menschen [35].

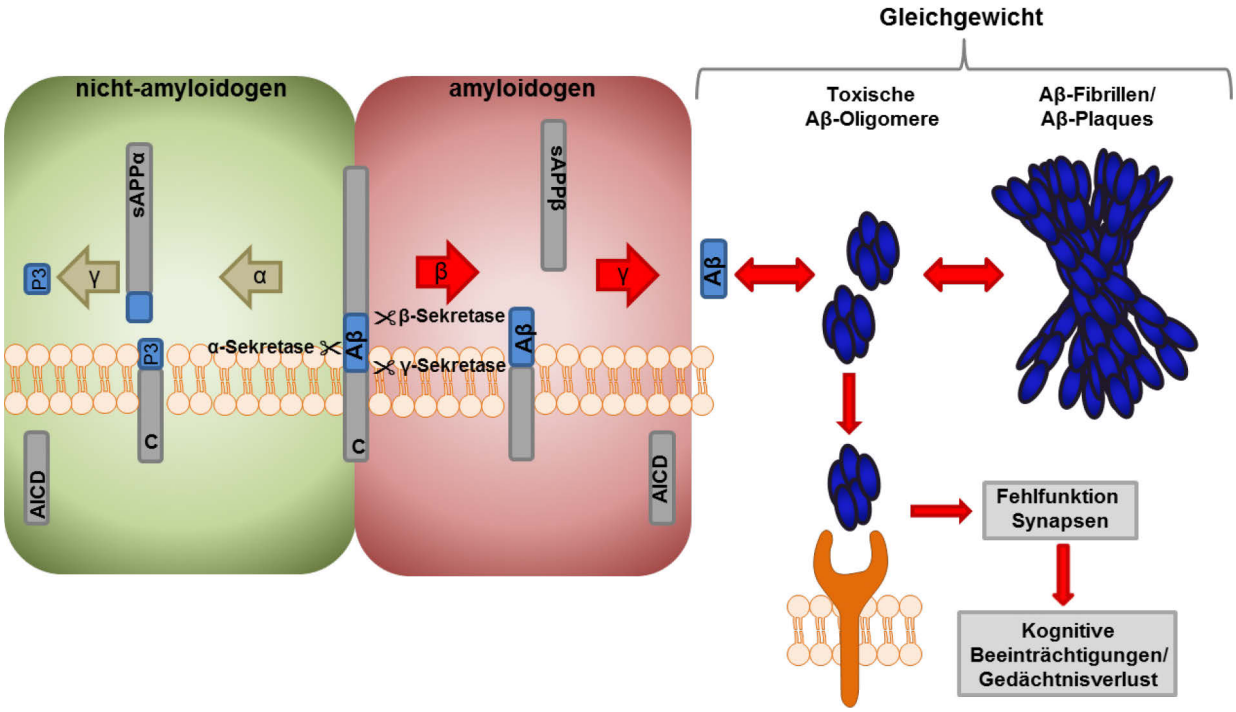

Abbildung 3:Bildung und Prozessierung des Amyloid-β-Proteins (Aβ).
Aβ kann über den nicht-amyloidogenen Weg, oder über den amyloidogenen Weg gebildet werden. Während über den nicht-amyloidogenen Weg das Amyloid-Vorläuferprotein (APP) mittels der α- und γ –Sekretase geschnitten und in nicht toxische Produkte prozessiert wird, entsteht über den amyloidogenen Weg das Aβ-Protein durch Prozessierung des APP mittels der β- und γ –Sekretase (links). Monomeres Aβ kann im weiteren Verlauf zu toxischen Aβ-Oligomeren, Aβ-Protofibrillen, Aβ-Fibrillen bis hin zu Aβ-Plaques aggregieren. Die Bildung der Aβ-Oligomere kann unter anderem zu einer Fehlfunktion der Synapsen führen, und die synaptische Dichte reduzieren was im weiteren Verlauf zu den der klinischen Symptomatik der Alzheimer'schen Demenz führt (rechts).

1.3.2 Aβ-Isoformen und -Modifikationen

Neben den bereits beschrieben Aβ-Spezies gibt es weitere Modifikationen/Isoformen, z.B. posttranslationale Modifikationen (PTM), denen eine besondere Rolle, wie eine erhöhte Toxizität und ein erhöhtes Aggregationspotential, zugesprochen werden. Da Aβ-Ablagerungen/Plaques generell sehr heterogen sind, bestehen sie aus einer Vielzahl Aβ-Isoformen, die sowohl C- als auch N-terminal verändert sein können [39, 40]. Neben $Aβ_{(1-40)}$ und $Aβ_{(1-42)}$ gelten N-terminal modifizierte Aβ-Spezies als die dominantesten Formen [41].

Die häufigste vorkommende N-terminale Modifikation des Aβ-Peptids ist das Pyroglutamat-modifizierte Aβ-Peptid (pEAβ) [42, 43]. Die Bildung des pEAβ ist ein mehrstufiger Prozess, der mit einer N-terminal verkürzten Form des Aβ als Substrat, an den Stellen 3 oder 11 (Glutamat) startet. Daraufhin erfolgt die Zyklisierung des Glutamat, durch die Glutaminylzyklase, an den entsprechenden Stellen zu Pyroglutamat. Die Verkürzung des Aβ kann entweder durch Endoproteolyse des APPs durch eine bestimmte β-Sekretase erfolgen, oder durch PTM des Gesamtlängen Aβ durch Aminopeptidasen (Abbildung 4) [42].

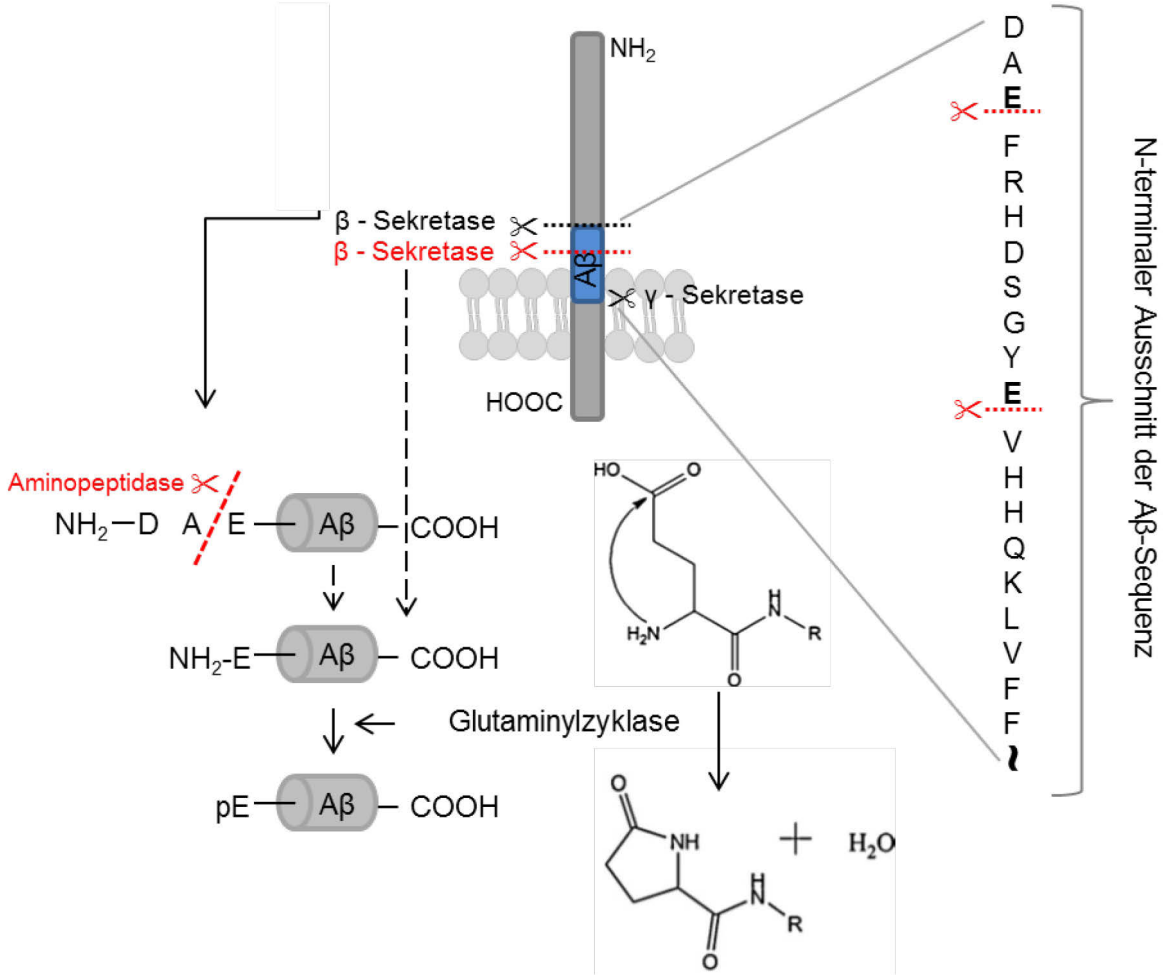

Abbildung 4: Schematische Darstellung der pEAβ-Bildung
Der exakte Mechanismus zur Entstehung der N-terminal verkürzten Aβ-Isoform zur Bildung des pEAβ ist wissenschaftlich unzulänglich geklärt. Er wird vermutet, dass Aβ entweder durch eine alternativ schneidende β-Sekretase endoproteolytisch vom APP gespalten wird, oder durch eine posttranslationale Modifikation über Aminopeptidasen verkürzt wird. Liegt Glutamat an den Stellen 3 oder 11 frei erfolgt die Zyklisierung durch die Glutaminylzyklase zur Bildung des pEAβ. Abbildung modifiziert nach [42].

Es wird dokumentiert, dass $pEA\beta_{(3\text{-}42)}$ im Vergleich zu $A\beta_{(1\text{-}42)}$ eine erhöhte Tendenz zur Aggregation zeigt und dadurch eine verstärke Neurotoxizität aufweist und zu einer Beeinträchtigung der Langzeitpotenzierung führt [42, 44-49]. Daneben konnte ebenfalls beschrieben werden, dass $pEA\beta_{(3\text{-}42)}$ die Aggregationskinetik von $A\beta_{(1\text{-}42)}$ beeinflussen kann [50]. Des Weiteren ist es resistent gegenüber einem proteolytischem Abbau [42, 44-47]. Die Bedeutung dieser PTM des Aβ-Peptides wird von der Tatsache gestützt, dass es die einzige PTM ist, gegen die nicht nur gezielt therapeutisch aktive Substanzen entwickelt und sowohl *in vitro* als auch *in vivo* getestet werden, sondern bereits klinische Studien am Menschen durchgeführt wurden [51].

1.3.3 Aβ-Oligomere

Bereits 1984 wurde postuliert, dass die amyloidogene Proteinakkumulation des Aβ-Peptids die kausale Ursache für die Entstehung der AD sei [52]. Für lange Zeit wurde angenommen, dass senile Aβ-Plaques in den Gehirnen der AD erkrankten Personen die hauptsächliche Ursache für die Fehlfunktion der Synapsen, Neurodegeneration und letztendlich die kognitiven Defizite sind. Nachdem Aβ aus APP generiert wurde, aggregiert dieses zunächst über Aβ-Oligomere (AβO), zu Aβ-Protofibrillen, Aβ-Fibrillen bis hin zu den senilen Aβ-Plaques (Abbildung 3). Da Aβ-Plaques auch in kognitiv unauffälligen/gesunden Individuen nachgewiesen wurde, entstand immer größerer Zweifel, dass die Aβ-Plaques das toxische Agens sind [53]. Neueren Studien zufolge wurde determiniert, dass lösliche AβO verantwortlich für die Entstehung und Progression der AD sind und diese unter anderem die NMDA- und AMPA (α-amino-3-hydorxy-5-methyl-4-isoxazole) vermittelte synaptische Übertragung inhibieren und schlussendlich für den Verlust von Synapsen, Neurodegeneration, Inflammation und Gedächtnisverlust verantwortlich sind [53, 54]. Durch die Entwicklung spezifischer Nachweismethoden, wie spezialisierte biochemische Analysen (ELISA, Westen Blot) und Massenspektroskopie konnte gezeigt werden, dass der Gehalt löslicher AβO, im Gegensatz zum Vorkommen von Aβ-Plaques, eine erhöhte Korrelation mit Anwesenheit und Progression kognitiver Defizite darstellt [55-60]. Der exakte AβO-vermittelte Mechanismus, der dazu führt, dass eine kognitive Beeinträchtigung entwickelt wird, ist noch nicht final geklärt [53]. Es konnte gezeigt werden, dass isolierte AβO die Langzeitpotenzierung, ein essentieller Mechanismus für das Lernen, einschränken, speziell in hippocampalen Strukturen [61, 62].

1.3.4 Die Amyloid-Kaskaden-Hypothese

Die zentrale Hypothese der ursächlichen Entstehung der AD ist die sogenannte „Amyloid-Kaskaden-Hypothese“, die im Jahre 1992 von John Hardy und Gerald Higgins erstmalig beschrieben wurde [63]. Das zentrale Dogma der Hypothese besagt, dass eine Disparität zwischen Aβ-Bildung und –Abbau zu der AD führen. Eine erhöhte Bildung des Aβ-Peptids in der fAD ist durch Mutationen bedingt, welche zu einer Lebenslangen Überproduktion des Aβ führen. Ein verringerter Aβ-Abbau in der sAD ist unter anderem durch Prädispositionen bedingt [63-65]. Die aktualisierte Form der Amyloid-Kaskaden-Hypothese führt auf, dass in beiden Formen der AD eine erhöhte Präsenz des Aβ-Peptids im Gehirn und dessen Akkumulation und Oligomerisierung vorliegt, wodurch die AβO ihr toxisches Potential auf Synapsen ausüben können [64]. Neben der Bildung der senilen Aβ-Plaques, der Aktivierung von Entzündungszellen wie Mikroglia und Astrozyten und einer gestörten Homöostase, führen die AβO zur direkten Bildung der NTF’s. Alle fehlerhaften Prozesse, ausgelöst durch

AβO, führen final zu einer ausgedehnten synaptischen Dysfunktion, Neurodegeneration und final zur Demenz.

1.4 Behandlung der Alzheimer'schen Demenz

Die AD gilt trotz intensivster Forschungsbemühungen immer noch als irreversible, unheilbare neurodegenerative Erkrankung. Die derzeitigen zugelassenen Behandlungen sind einzig darauf ausgelegt, die Progression der mit der AD einhergehenden Symptomatik zu verlangsamen und beruhen darauf, den gestörten Neurotransmitterhaushalt zu normalisieren, um die verbleibende Aktivität der Transmission zu erhöhen [66].

1.4.1 Erste Generation: symptomatische Behandlung

Bevor Aβ als AD auslösendes Agens identifiziert wurde, wurde lange Zeit vermutet, dass ein Mangel an dem Neurotransmitter Acetylcholin (ACh), einem der wichtigsten Neurotransmitter des zentralen Nervensystems, die ursächliche Veränderung der Erkrankung darstellt [67, 68]. Um das Verbleiben des Neurotransmitters im synaptischen Spalt zu erhöhen und somit die physiologischen Funktionen aufrechtzuerhalten, wurden sogenannte Acetylcholinesteraseinhibitoren (AChEI) entwickelt, die den Abbau von ACh im synaptischen Spalt durch die Acetylcholinesterase inhibieren. Für diese pharmakologische Intervention sprechen diverse Aspekte. Zum einen konnte in präklinischen und klinischen Studien belegt werden, dass cholinerge Agonisten die Lernfähigkeit erhöhen, sodass anzunehmen ist, dass ACh eine wichtige Rolle im Lernprozess einnimmt [69]. Des Weiteren wurde in Gehirnbiopsien und Autopsien von AD Patienten nachgewiesen, dass das ACh synthetisierende Enzym in kortikalen Strukturen eine verminderte Aktivität zeigt sowie ein Verlust cholinerger Neurone in jenen kortikalen Strukturen, die zum Hippocampus projizieren und somit Einfluss auf das Lernverhalten haben [70, 71]. Unter den vielen verschiedenen pharmakologischen Interventionen zur Modifikation der cholinergen Neurotransmission hat sich nur die Klasse der AChEI zu Behandlung der AD manifestiert. Zu diesen zählen Donezepil, Rivastigmine und Galantamine, welche bei milder bis moderater AD eingesetzt werden [72].

Neben einem Mangel an ACh besteht bei AD eine pathologisch erhöhte Erregung des NMDA-Rezeptors durch den Neurotransmitter Glutamat, dem exzitatorischen Neurotransmitters des Gehirns/Nervensystems [66]. Die so entstehende Dauererregung des glutamatergen Systems und der entsprechenden Neurone resultiert in Schädigung der Neurone, bis hin zur Neurodegeneration, einem der charakteristischen Merkmale der AD. Die glutamaterge und über den NMDA-Rezeptor vermittelte Reizübertragung spielt eine enorme Rolle in Gedächtnisprozessen, welche bei AD Patienten beeinträchtigt sind [73].

Aufgrund dessen wurde an Substanzen geforscht, die spezifisch den NMDA-Rezeptor blockieren (sog. Antagonisten), um so die pathologisch erhöhte Reizweiterleitung zu inhibieren. Memantine, welches nun seit mehr als 10 Jahren zugelassen ist, ist der einzige NMDA-Rezeptor-Antagonist, der zu Behandlung von mittlerer bis schwerer AD eingesetzt wird.

1.4.2 Zweite Generation: kausale Behandlung

Neue Bestrebungen zur Entwicklung einer kurativen und krankheitsmodifizierenden Medikation zur Behandlung der AD basieren, aufgrund der pathologischen Komplexität, auf verschiedenen Targets und Wirkansätzen (Abbildung 4). In den letzten Jahren wurden verschiedene therapeutische Strategien entwickelt. Wie vielfältig die Ansätze einer möglichen Therapie sind spiegelt auch die Anzahl jener Substanzen wider, die sich in einer der Phasen der klinischen Forschung befinden [74]. Wie in Abbildung 5 gezeigt, setzten die möglichen kausalen Behandlungen auf die hauptsächlichen pathologischen Kennzeichen der AD an: Geringere/erhöhte Konzentrationen diverser Neurotransmitter (ACh, Glutamat) (Neurotransmittermodulation), Aβ-Aggregate (Anti-Amyloid-Strategien), NFT's (Anti-Tau-Strategien), Modulation verschiedener Signalkaskaden, Reduktion des oxidativen Stresses und Neuroinflammation, wobei das Hauptaugenmerk der Wissenschaft auf Anti-Amyloide- und Anti-Tau-Strategien gelegt ist.

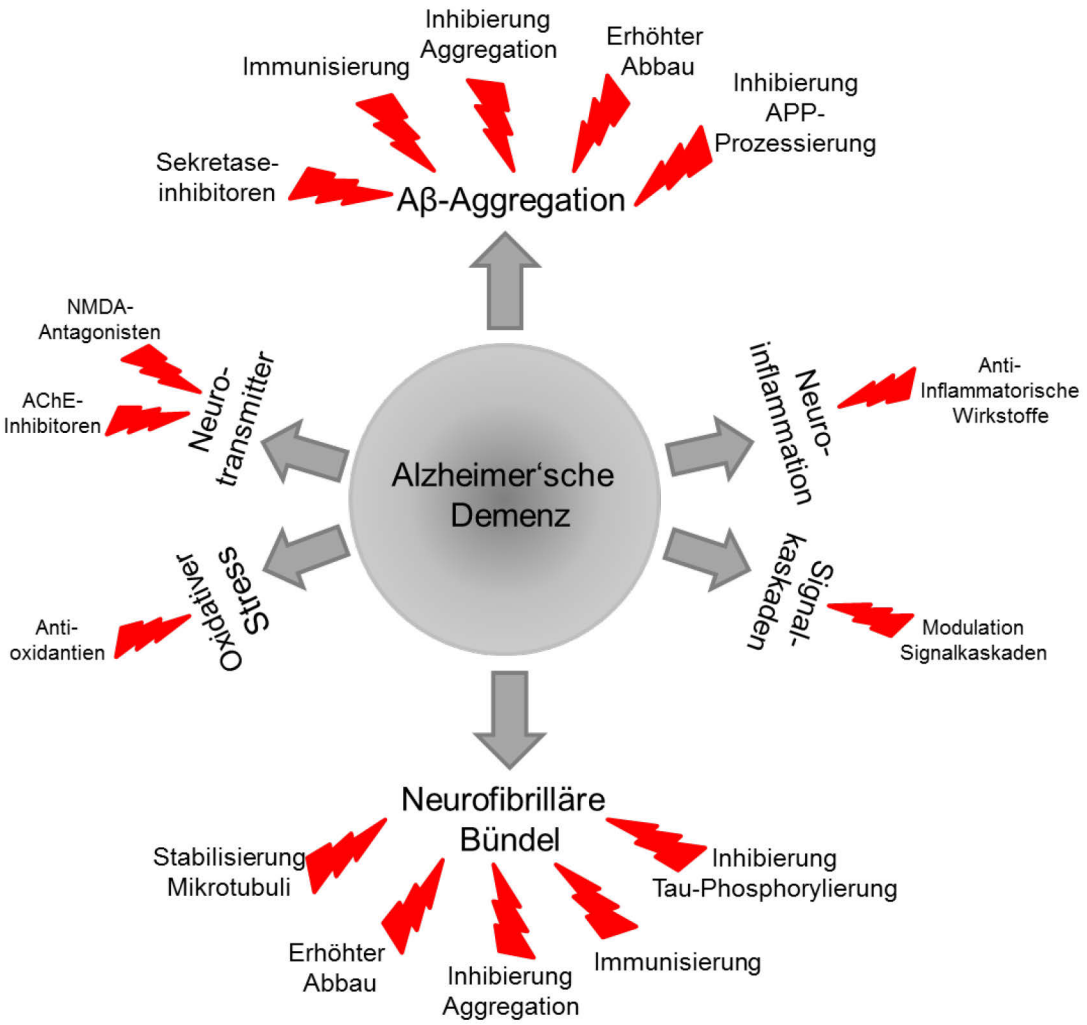

Abbildung 5: Mögliche Ansätze einer kausalen Therapie der Alzheimer'schen Demenz (AD).
Die AD ist eine multifaktorielle Erkrankung, deren klinisches Erscheinungsbild durch diverse pathologische Veränderungen geprägt ist. Die pathologischen Hauptmerkmale sind zum einen die zerebralen Amyloid β-Ablagerungen sowie neurofibrilläre Bündel, bestehend aus dem Protein Tau. Beide pathologischen Merkmale bieten einen möglichen Ansatz neuer potentiell kurativer Therapien, in dem unter anderem die Aggregation der Proteine gehemmt wird oder der Abbau der fehlgefalteten Proteine gefördert wird.

Neurotransmittermodulation

Trotz der intensiven Forschung an kausalen Behandlungen werden Behandlungsstrategien der ersten Generation weiter verfolgt. Neben möglichen Optimierungen der AChE-Inhibition wird an Medikationen geforscht, die zusätzlich einen Effekt auf den APP-Metabolismus haben (Huperzin A). Neben den AChEIs besteht unter anderem die Möglichkeit der Modulation GABAerger Neuronen, eine Weiterentwicklung der NMDA-Rezeptor-Antagonisten, eine Modulation des Serotoninrezeptors, oder eine Reduktion des oxidativen Stresses zur Behandlung der AD [75].

Anti-Tau-Strategien

In seiner physiologischen Form nimmt das Tau-Protein eine wichtige Rolle zur Stabilisierung der Mikrotubuli ein, um für eine zuverlässige Funktion der Neurone zu sorgen. Zur Inhibierung der Hyperphosphorylierung gelten verschiede Enzyme als Target. Eines der erfolgversprechendsten Enzyme ist die Glykogensynthase-Kinase 3 (GSK3), für die Inhibitoren bereits in klinischen Phasen getestet werden. Neben diesen wird, ebenso wie bei den Anti-Amyloiden-Strategien, durch pharmakologische Interventionen versucht, die Aggregation des Tau-Proteins zu verhindern. Auch hier wird daran geforscht, ob Immuntherapien eine mögliche therapeutische Wirkung zeigen [76].

Anti-Amyloide-Strategie

Anti-Amyloide-Strategien können auf vielfältige Weisen in den APP-Metabolismus eingreifen. Zu diesen zählen unter anderem die Modulation der für die APP-Prozessierung verantwortlichen Sekretasen, ein aktives Eingreifen in die Aβ-Aggregation, um diese zu inhibieren, ein erhöhter Aβ-Abbau, oder auf Impfungen beruhende Therapien.

Sekretase-Inhibitoren

Ein Ansatz für eine mögliche Therapie der AD ist die Inhibierung der für die APP-Prozessierung verantwortlichen β- oder γ-Sekretasen [77], sodass die Aβ-Bildung inhibiert wird (Abbildung 6). Vielfältige Substanzen wurden bereits erfolgreich präklinisch *in vivo* getestet, jedoch stellte sich bei der klinischen Testung einiger γ-Sekretase-Inhibitoren heraus, dass unerwünschte On-Target Effekte entstehen, unter anderem da die γ-Sekretase für die Prozessierung einiger wesentlicher Proteine verantwortlich ist [78]. Eines jener Proteine ist das sog. Notch-Protein, das zahlreiche Funktionen, wie z.B. Regulation der Zellproliferation, -entwicklung und –kommunikation einnimmt [79]. Da der Einsatz von γ-Sekretase-Inhibitoren dieses Enzym völlig inhibiert, werden diese nicht weiter eingesetzt. Stattdessen wird, auf γ-Sekretase-Modulatoren umgestellt, oder auf jene gesetzt, die eine Spezifität für die APP-spaltende γ-Sekretase aufweisen [78]. Ein ähnliches Bild zeigte sich bisher für β-Sekretase-Inhibitoren (BACE1-Inhibitoren). In einigen klinischen Studien konnte gezeigt werden, dass einige β-Sekretase-Inhibitoren die Aβ-Produktion senken (Nachweis über Aβ-Konzentrationsbestimmung im CSF) [80, 81]. Jedoch konnten auch hier Nebenwirkungen nachgewiesen werden, die ebenfalls darauf beruhen, dass neben APP noch weitere, physiologisch relevante Substrate dieser Sekretase existieren (z.B. ADAM10) [82].

Eine weitere Möglichkeit bietet die Erhöhung der Aktivität der α-Sekretase über z.B. die Proteinkinase C (PKC), um eine Prozessierung des APPs über den nicht-amyloidogenen Weg zu fördern [83]. Bryostatin, ein natürlicher PKC-Aktivator, wurde bereits erfolgreich *in vivo* getestet [84] und befindet sich zurzeit in der klinischen Testung [83]. Des Weiteren kann die PKC über M1-und M3 muskarine Rezeptor-Agonisten aktiviert werden [85]. Jedoch wird beschrieben, dass eine chronische Aktivierung dieser beiden Rezeptoren zu unerwünschten Nebeneffekten führen kann [85].

Anti-Amyloide-Immuntherapie

Die Anti-Amyloide-Immuntherapie schließt die aktive, wie auch die passive Immunisierung gegen Aβ ein, wobei in beiden Ansätzen versucht wird, den Aβ-Abbau zu fördern und somit den Aβ-Gehalt zu reduzieren (Abbildung 6).

Bei der aktiven Immunisierung werden entweder Gesamtlängen $Aβ_{(1-42)}$ oder synthetische Fragmente dessen genutzt, um eine durch stimulierte B- und T-Zellen ausgelöste Immunreaktion zu bewirken. D.h. Aβ wird durch Bindung der gebildeten Antikörper in seiner Funktion so verändert, dass es nicht mehr seine „toxische“ Funktion auf den Körper ausüben kann. Die ablaufende Immunreaktion ist ähnlich wie bei einer Impfung z.B. gegen den Masernerreger. Die erste Generation dieser Wirkstoffgruppe (z.B. AN1792) zeigte vielversprechende Effekte in präklinischen Studien. Jedoch stellte sich in einer klinischen Studie II heraus, dass es zu schwerwiegenden Nebenwirkungen kommt. Aufgrund einer Autoimmunantwort erlitten 6% der Patienten eine Meningoencephalitis [86]. Bei der zweiten Generation wurde darauf verzichtet, Gesamtlängen $Aβ_{(1-42)}$ zu verwenden, sondern ausschließlich Fragmente dessen (z.B. $Aβ_{(1-6)}$), die ebenfalls eine therapeutische Aktivität aufweisen [87].

Bei der passiven Immunisierung wird darauf verzichtet, die körpereigene Antikörperbildung anzuregen. Somit wird das Risiko einer T-Zellen-vermittelten Entzündung als Quelle möglicher Nebenwirkungen minimiert. Zwei für lange Zeit als therapeutisch vielversprechend geltende Antikörper waren der erste humanisierte monoklonale Antikörper Bapineuzumab und Solanezumab, ein ebenfalls humanisierter monoklonaler Antikörper. Der Antikörper Bapineuzumab bindet bevorzugt an Aβ-Plaques gegenüber löslicher Aβ-Spezies, zu denen auch die toxischen AβO zählen. Da heutzutage angenommen wird, dass lösliche AβO das toxische Agens sind und nicht Aβ-Plaques, ist der Umstand, dass Bapineuzumab bevorzugt an Aβ-Plaques bindet ein denkbarer Grund, warum es in klinischen Studien nicht erfolgreich war. Trotz ausschließlich minimaler Erfolge in klinischen Phasen II wurde eine klinische Phase III mit einer großen Patientenkohorte durchgeführt. In dieser stellte sich heraus, dass die Immunisierung mit diesem Antikörper keine therapeutische Wirksamkeit erzielte, jedoch

schwerwiegende Nebenwirkungen auftraten, wie z.B. arterielle Ödeme oder zerebrale Mikroblutungen [88]. Solanezumab, der anstelle unlöslicher Aβ-Plaques lösliche Aβ-Spezies bindet, zeigte während der klinischen Phasen II vielversprechendere Ergebnisse ohne erkennbare Nebenwirkungen. Jedoch scheiterte auch dieser Antikörper in einer groß angelegten Phase III Studie mangels Wirksamkeit [89]. Ein derzeit vielversprechender monoklonaler Antikörper zur kurativen Behandlung der AD ist Aducanumab. Im Gegensatz zu den zuvor beschriebenen Antikörpern ist dieser nicht humanisiert sondern wurde aus humanen Gedächtnis-B-Zellen gewonnen, die eine Reaktivität gegen aggregiertes Aβ aufwiesen. Wie in präklinischen Studien gezeigt wurde, reagiert dieser mit verschiedenen Aβ-Aggregaten, vor allem auch mit toxischen AβO und unlöslichen Aβ-Fibrillen und zeigt eine geeignete Blut-Hirn-Schranken-Gängigkeit [90]. In einer klinischen Phase Ib Studie konnte gezeigt werden, dass nach einjähriger Behandlung mit Aducanumab Aβ-Plaques deutlich zurückgingen. Von größerer Wichtigkeit: es konnte gezeigt werden, dass durch die Behandlung die Progression der kognitiven Beeinträchtigung signifikant verringert wurde [91]. Neben der erfolgsversprechenden therapeutischen Wirksamkeit zeigt diese Studie ebenfalls, dass AβO, bzw. die Eliminierung dieser, eine vielversprechende Zielstruktur für eine erfolgreiche AD Therapie sind.

Inhibierung der Aβ-Aggregation

Die Aggregation von monomeren Aβ zu toxischen AβO gilt als ursächlich für die Neurotoxizität. Aufgrund dessen ist die Inhibierung der Aβ-Aggregation (Abbildung 6) ein weiterer höchst interessanter Ansatz für eine kausale Behandlung der AD, mit der bereits vielversprechende Ergebnisse in Behandlungsstudien an transgenen AD Mausmodellen gezeigt werden konnte. Einige dieser Substanzen zeigten ein so großes Potential, dass sie den Schritt in klinische Studien schafften. Homotaurin, oder auch Tramiprosat, ein Glykosaminoglykan (GAG) Mimetikum, verhindert die Aggregation von Aβ-Monomeren, indem es um die GAG-Bindungsstelle des Aβ konkurriert. Nach dem Abschluss erfolgreicher präklinischer Studien ist Tramiprosat die erste Aggregationsinhibitor, die in verschiedenen klinischen Studien getestet worden ist. Jedoch stellte sich in einer großangelegten klinischen Phase II heraus, dass Tramiprosat keine therapeutische Wirksamkeit aufweisen konnte. Ein weiterer Kandidat dieser Gruppe, Scyllo Inositol (ELND005), zeigte ebenfalls Wirksamkeit in präklinischen Studien sowie positive Ergebnisse in einigen klinischen Studien. Jedoch bleibt noch offen, ob diese Substanz einen Effekt auf die Gedächtnisleistung erzielt. Colostrinin, ein Prolin-reiches Peptid, gewonnen aus dem ovinen Kolostrum, zeigte ebenfalls Potential zur Steigerung der Gedächtnisleistung in transgenen AD Mäusen [92] sowie in einer ersten klinischen Pilotstudie [93].

Peptide zur Therapie der AD

Peptide, (i.d.R. lineare) Moleküle bestehend aus zwei oder mehr Aminosäureresten, zeigen diverse Vorteile gegenüber anderen Pharmazeutika, die zur kausalen Behandlung der AD eingesetzt werden, wie ihre hohe Spezifität. Diese kann durch einfachen Austausch einer oder mehrerer Aminosäureresten weiter optimiert werden, d.h. es besteht ein großer Spielraum für eine rationale Umstrukturierung der Aminosäurerestesequenz zur Steigerung der Effektivität oder Wirksamkeit, in dem z.B. die Affinität für die entsprechende Zielstruktur (Aβ) erhöht wird. Des Weiteren können Peptide die Blut-Hirn-Schranken (BHS), im Vergleich zu anderen Therapien, effizienter passieren und zeigen eine geringe Akkumulation in Organen und Geweben [94]. Die meisten Peptide, die zur kausalen Therapie der AD entwickelt wurden, sind von der $A\beta_{(1-42)}$-Sequenz abgeleitet und weisen aufgrund dessen charakteristische Eigenschaften, wie z.B. die Inkorporation mit dem β-Faltblatt, auf oder zeigen eine starke Bindungsaffinität [95]. Ursprünglich wurden Peptide hinsichtlich dessen entwickelt, dass sie eine starke Bindung mit bestimmten Sequenzen innerhalb des Aβ-Peptids aufzeigen, z.B. dem aus fünf Aminosäuren (KLVFF) bestehenden hydrophoben Kern (dieser gilt als besonders aggregationsfreudig) [96, 97], oder dem C-Terminus. Seither wurde eine große Anzahl Peptide für eine kausale Therapie der AD entwickelt (eine ausführliche Zusammenfassung dieser kann unter [94] gefunden werden).

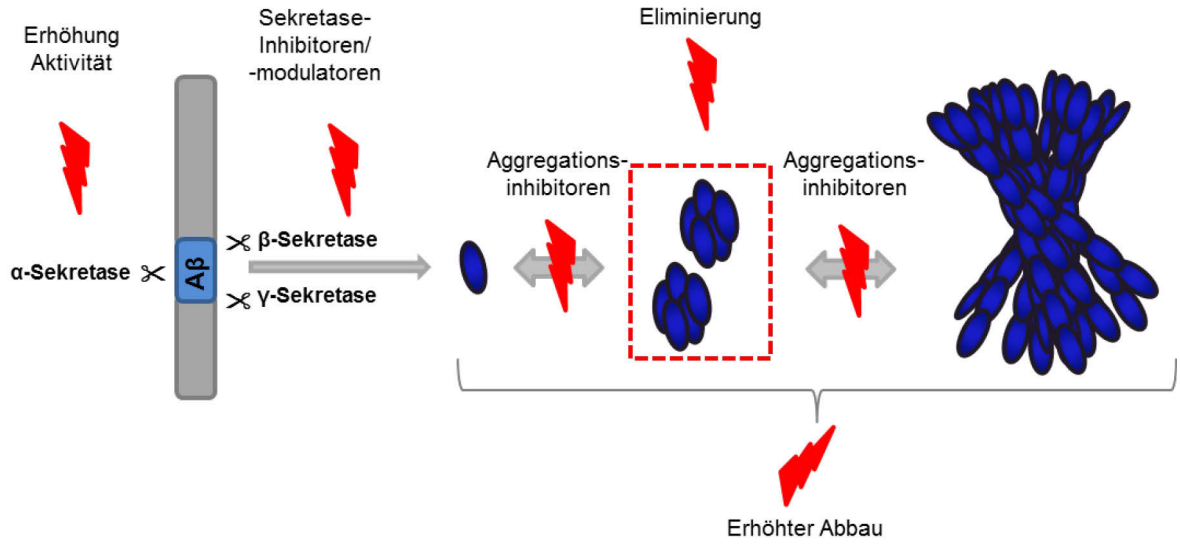

Abbildung 6: Anti Amyloid β (Aβ) Therapieansätze gegen die Alzheimer'sche Demenz (AD).
Die Prozessierung des Amyloidvorläuferproteins (APP) zu Aβ und dessen Aggregation gewährt eine Vielzahl möglicher Angriffspunkte für eine kausale Therapie der AD. Durch eine Erhöhung der α-Sekretaseaktivität soll eine Verschiebung der APP-Prozessierung in Richtung des nicht-amyloiden Weges bewirkt werden, sodass APP nicht zu Aβ prozessiert werden kann. Der gezielte Einsatz von β- und γ-Sekretaseinhibitoren/modulatoren soll bewirken, dass diese APP nicht mehr schneiden können und keine Aβ-Monomere entstehen und somit eine mögliche Aggregation zu toxischen Aβ-Oligomeren verhindert wird. Neben diesen stellen Antikörper-basierte Immuntherapien einen vielversprechenden Ansatz für eine kausale Therapie der AD dar. Antikörper sollen dabei verschiedene Aβ-Spezies (Monomere, Oligomere, Fibrillen) binden und so deren Abbau durch das Immunsystem fördern. Aggregationsinhibitoren werden eingesetzt, um eine Aggregation von Aβ-Monomeren zu Aβ-Oligomeren zu verhindern. Eine weitere Möglichkeit besteht darin, Aβ-Monomere zu stabilisieren (z.B. durch D-enantiomere Peptide). Dies führt dazu, dass das herrschende Gleichgewicht hin zu Aβ-Monomeren verschoben wird.

D-enantiomere Peptide zur selektiven Eliminierung toxischer Aβ-Oligomere

Der in dieser Arbeit beschriebene Ansatz für eine kausale Behandlung der AD beruht ebenfalls auf Peptiden, genauer auf D-enantiomeren Peptiden, die nur aus D-enantiomeren Aminosäureresten bestehen. Diese D-Peptide wurden zur spezifischen Eliminierung toxischer AβO entwickelt. Dabei binden einige der beschrieben D-Peptide an monomeres $Aβ_{(1-42)}$ und verschieben so das Gleichgewicht zwischen AβO und Aβ-Monomeren in Richtung Aβ-Monomere (Abbildung 6). So entstehen *in vitro* nicht-toxische, aggregationsinkompetente Kopräzipitate [98]. Die Leitsubstanz D3 (Tabelle 1), ein aus 12 D-enantiomeren Aminosäureresten bestehendes Peptid, wurde im Jahr 2003 mittels Spiegelbild-Phagendisplay gegen monomeres $Aβ_{(1-42)}$ selektiert [99]. In zahlreichen *in vitro* Untersuchungen konnte belegt werden, dass D3 eine Bindungsaffinität im mikromolaren Bereich an monomeres $Aβ_{(1-42)}$ zeigt, die $Aβ_{(1-42)}$-Fibrillenbildung inhibiert, die $Aβ_{(1-42)}$ induzierte Zelltoxizität hinabsetzt sowie effizient toxische $Aβ_{(1-42)}$-Oligomere eliminiert [98, 100-104]. Neben der *in vitro* Charakterisierung wurden ausgiebige pharmakokinetische- und Stabilitätsuntersuchungen mit D3 durchgeführt. Dabei stellte sich heraus, dass D-Peptide gegenüber ihrem L-enantiomeren Äquivalent diverse Vorteile aufweisen, da sie eine erhöhte Stabilität gegenüber einer Proteolyse sowie eine erhöhte orale Bioverfügbarkeit aufweisen [105]. Es konnte gezeigt werden, dass D3 eine hohe proteolytische Stabilität in verschiedenen Medien (simulierter Magen- und Darmsaft sowie humane Lebermikrosomen und humanes Plasma) aufweist [105] sowie aussichtsreiche pharmakokinetische Parameter (hohe orale Bioverfügbarkeit, lange terminale Halbwertszeit) und ein Überwinden der BHS, sowohl *in vitro*, als auch *in vivo* [106, 107]. In zahlreichen *in vivo* Studien in verschiedenen transgenen AD Mauslinien konnte die Wirksamkeit von D3 belegt werden. Intraperitoneale, wie auch orale Behandlungsstudien ergaben eine signifikante Steigerung kognitiver wie auch motorischer Defizite sowie eine Reduktion von Aβ-Plaques und inflammatorischen Zellen (Mikroglia und Astrozyten) [100-103, 108-110].

Zur Optimierung der Leitstruktur D3 wurden verschiedene Ansätze durchgeführt. Basierend auf Peptid-Mikroarrays wurde systematisch nach möglichen, optimierten D3-Derivaten selektiert, die eine erhöhte Affinität sowie Spezifität gegenüber monomerem $Aβ_{(1-42)}$ aufweisen. Resultierend aus diesen Ansätzen entstanden die sogenannten DB3 und ANK D-Peptide [111, 112]. Durch ein rationales Wirkstoffdesign wurden weitere D3-Derivate entwickelt. Eines der vielversprechendsten D-Peptide dieser Entwicklung ist RD2 (Tabelle 1). Erste pharmakokinetische Analysen und Stabilitätstest wiesen darauf hin, dass auch RD2 eine vielversprechende orale Verfügbarkeit zeigt sowie effizient an seinen Zielort (das Gehirn) gelangt und eine lange terminale Halbwertszeit (über 50 Stunden) aufweist [113].

Die lange terminale Halbwertszeit und die orale Verfügbarkeit bieten eine hohe Therapietreue.

D-Peptid	Sequenz Aminosäurereste
D3	rprtrlhthrnr
D3D3	rprtrlhthrnrrprtrlhthrnr
cD3r	rprtrlhthrnrr (N- zu C-terminale Verbindung)
RD2	ptlhthnrrrrr
RD2D3	ptlhthnrrrrrrprtrlhthrnr
cRD2D3	ptlhthnrrrrrrprtrlhthrnr (N- zu C-terminale Verbindung)
ANK6	rkrirlvtkkkr
tANK6	rkrirlvtkkkrrkrirlvtkkkr
cANK6	rkrirlvtkkkrr (N- zu C-terminale Verbindung)

Tabelle 1: Auflistung der Sequenzen der Aminosäurereste der verschiedenen D-Peptide

1.5 Pharmakologie - Pharmakokinetische und pharmakodynamische Analysen

Die Pharmakologie, die Lehre der Wechselwirkung zwischen Wirkstoffen (Pharmaka) und biologischen Systemen (Organismen/Lebewesen), ist ein Überbegriff für diverse Teilbereiche und wurde erstmalig 1953 von F.H. Dost eingeführt [114]. Allgemein lässt sich die Pharmakologie in zwei große Teilbereiche gliedern, die **Pharmakokinetik** - *Was macht der Körper mit dem Wirkstoff?* und die **Pharmakodynamik** – *Was macht der Wirkstoff mit dem Körper?* (Abbildung 7).

In der **Pharmakokinetik** werden verschiedene Aspekte der Metabolisierung und des Transportes eines Pharmakons basierend auf dem (L)ADME-Schema (Liberation, Absorption, Distribution, Metabolisierung und Exkretion) beschrieben. Nach Applikation des Pharmakon/Wirkstoffs erfolgt zunächst die Freisetzung/Liberation [115]. Unter der Freisetzung versteht man das Herauslösen des Arzneistoffes aus seiner Darreichungsform (z.B. Tablette). Die Applikation eines Wirkstoffes kann über verschiedene Wege erfolgen, unter anderem davon abhängig, ob der Wirkstoff schnell in den Körper gelangen soll (intravenöse Applikation), oder ob er oral verfügbar ist. Die einfachste Applikationsform bei Menschen ist die orale Darreichung eines Wirkstoffes, da diese nicht invasiv ist und eine hohe Therapietreue (Compliance) gewährleistet, jedoch muss bei dieser der sogenannte First-Pass-Effekt (erste Metabolisierung in der Leber vor systemischer Verteilung) berücksichtigt werden [116]. Mit der Absorption wird die Aufnahme des Wirkstoffes von der Applikation, über die Freisetzung des Wirkstoffes, bis ins Plasma beschrieben. Die Absorption eines Wirkstoffes ist vor allem bei einer oralen Verabreichung von Bedeutung, da hier der Wirkstoff den Gastrointestinaltrakt passieren muss. Um eine systemische Verteilung

(Distribution) eines Wirkstoffes zu gewährleisten, muss dieser verschiedene Zellmembranen des Köpers passieren, wobei die BHS eine besondere Stellung einnimmt und Wirkstoffe, die als Zielorgan das Gehirn haben diese zwingend (aktiv oder passiv) überschreiten müssen. Die systemische Verteilung eines Wirkstoffes wird über den Blutkreislauf gewährleistet. Die Elimination eines Wirkstoffes erfolgt über die Metabolisierung (Biotransformation) und/oder die Exkretion (Ausscheidung) [114-117]. Die Metabolisierung eines Wirkstoffes durch den Organismus dient dem Zweck sie chemisch so zu modifizieren, dass sie leichter ausgeschieden werden können. Die chemische Modifikation erfolgt i.d.R. in zwei Phasen (Phase I: hinzufügen einer funktionellen Gruppe, z.B. –OH Gruppe, Phase II: Konjugation einer z.B. Glucuronsäure oder Schwefelsäure) und dient der renalen Exkretion. Enzyme des Cytochrom-P450-Systems (CYP), die hauptsächlich in der Leber vorkommen, nehmen eine besondere Rolle in der Metabolisierung von Wirkstoffen ein. CYP-Enzyme können durch Wirkstoffe (z.B. Omeprazol, Rifampicin), aber auch durch Genussmittel (Grapefruitsaft, Tabakrauch) inhibiert oder induziert werden. Wechselwirkungen eines Arzneistoffes mit diesen sollten aufgrund dessen zwingend berücksichtigt werden. Einige Wirkstoffe, sog. „Prodrugs“, erlangen erst durch eine Metabolisierung im Organismus (i.d.R. hepatisch) ihre Wirksamkeit [114-117].

Die Pharmakokinetik eines Wirkstoffes lässt sich hauptsächlich über sog. Plasmakonzentrations-Zeit-Kurven darstellen. Neben diesen können diverse Parameter berechnet werden, mit denen eine Aussage über die Bioverfügbarkeit, die Halbwertszeit u.v.m. eines Wirkstoffes getroffen werden kann [115] (Abbildung 7).

Ergänzend zur Pharmakokinetik, untersucht die **Pharmakodynamik** die erwünschte, aber auch mögliche unerwünschte (toxische) Wirkung eines Pharmakons auf den Organismus (zeigt ein Medikament seine gewünschte Wirkung?). Weitergehend befassen sich pharmakodynamische Analysen mit komplexen Dosis-Wirkungsbeziehungen und zugrundeliegenden Wirkmechanismen [118]. Dosis-Wirkungsbeziehungen lassen sich anhand diverser experimenteller Verfahren (Zellkultur, isolierte Organe, Tierversuche, Probanden) untersuchen. Ziel dieser ist es oft, eine therapeutische Breite zu determinieren, d.h. ab welcher eingesetzten Dosierung kann ein (gewünschter) Effekt erzielt werden und ab welcher Konzentration sind erste unerwünschte (toxische) Wirkungen zu verzeichnen. Für Wirkstoffe, die z.B. einen Rezeptor oder ein Enzym aktivieren oder inhibieren sollen, sind solche Studien mit geringem Aufwand und etablierten Testsystemen durchführbar, da das Target (die Zielstruktur, z.B. Rezeptor oder Enzym) und das Wirkprinzip klar definiert und angreifbar sind.

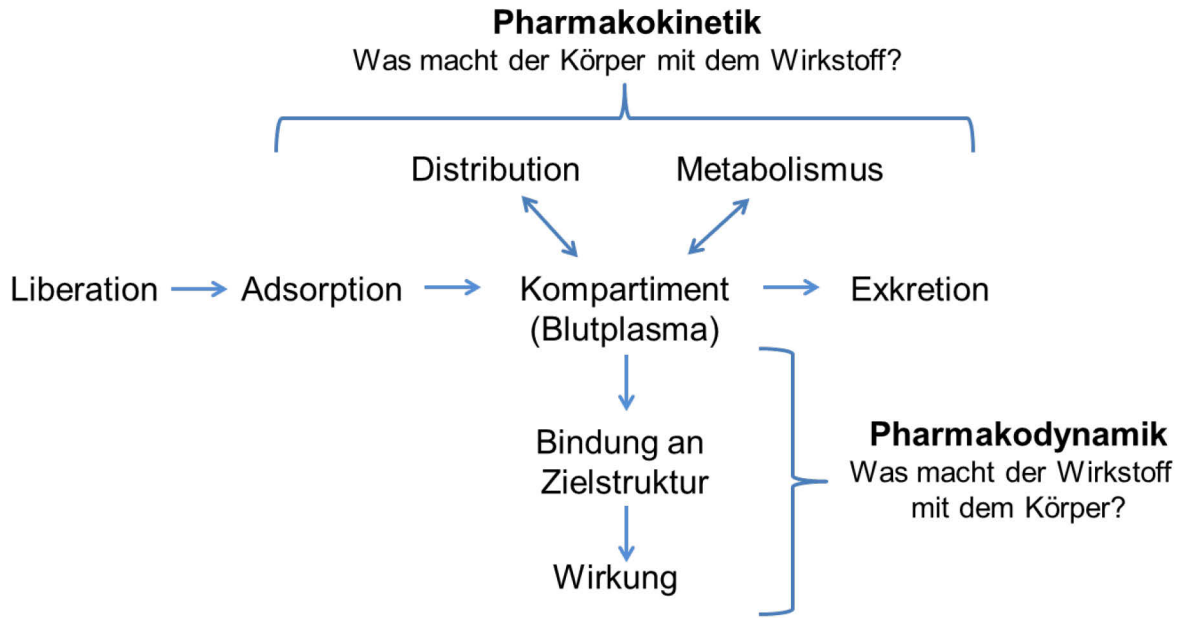

Abbildung 7: Beziehung von Pharmakokinetik und Pharmakodynamik. Abbildung modifiziert nach [115].

1.6 Mausmodelle der AD

Mausmodelle stellen ein wichtiges Werkzeug in der Erforschung von Erkrankungen sowie zur Entwicklung neuer Medikationen dar. Die Entwicklung transgener Mausmodelle war eine herausragende wissenschaftliche Errungenschaft, für jene drei Wissenschaftler (Mario Capecchi, Sir Martin Evans und Oliver Smithies) 2007 den Nobelpreis für Physiologie oder Medizin erhielten.

Transgene Mausmodelle der AD basieren unter anderem darauf, dass man sich die bekannten Mutationen der fAD (z.B. APP, PS1 und PS2) zu Nutze macht, um gezielt verschiedene Aspekte der Neuropathologie und Verhaltensbeeinträchtigungen der Erkrankung zu modellieren. Jedoch ist zu bedenken, dass keines der verfügbaren Mausmodelle alle Aspekte der humanen AD widerspeigelt (Translation auf den Menschen). In der Regel tragen Mausmodelle zur Erforschung der AD entweder APP- oder Tau-Mutationen, die entweder eine Amyloidose, oder eine Tauopathie zeigen. Dies bedeutet, dass jeweils nur ein wichtiger Aspekt der AD-Pathologie widergespiegelt wird, ohne den jeweils anderen zu berücksichtigen. Es gibt jedoch auch einige Mausmodelle, die sowohl eine APP- als auch eine Tau-Mutationen tragen (z.B. das biAT AD-Mausmodell [119] oder das dreifach-transgene AD-Mausmodell 3xTg-AD [120]). Ein großer Nachteil jener Modelle ist, dass sie in der Regel keine Neurodegeneration aufweisen. Derzeit gibt es kein Mausmodell der AD, welches alle Aspekte in Gänze widerspiegelt.

Das erste transgene AD Mausmodell (PDAPP, V717F Indiana-Mutation), welches eine manifestierte Aβ-Pathologie aufweist, wurde im Jahr 1995 von Games und Kollegen

generiert [121]. Seitdem wurden weit über 100 Mausmodelle entwickelt (aufgelistete AD Mausmodelle (ALZFORUM) im Feld der AD Forschung ca. 127, Stand Januar 2018), die entweder eine oder mehrere Mutationen humaner AD-relevanter Gene tragen. Aufgrund der Vielzahl der Modelle werden nur jene beschrieben, die eine Relevanz für diese Arbeit haben (Abbildung 8).

APPswe/PS1dΔE9

Das ausgiebig charakterisierte APPswe/PS1dΔ9 (kurz APP/PS1) AD-Mausmodell ist unter Wissenschaftlern, die sich mit der AD befassen, weit verbreitet. Entwickelt 2004 von Jankowsky und Kollegen, trägt dieses Mausmodell zwei Transgene unter Kontrolle eines murinen Thy2.1 Promoters bzw. einer Expressionskassette auf Chromosom 9 der Maus: die schwedische APP-Doppelmutation (APPswe, Austausch der Aminosäuren K670N/M671L, die eine Änderung der Schnittstelle der β-Sekretase bewirk) und die ΔE9-Mutation des humanen PS1-Gens (Deletion des Exon 9, bewirkt eine Form der EOAD)[122]. Das Mausmodell ist durch ein relativ frühes Auftreten der Aβ-Plaques (ab einem Alter von 6 Monaten), vor allem im Hippocampus charakterisiert. Ab diesem Zeitpunkt steigt die Anzahl der zerebralen Aβ-Ablagerungen progressiv, einhergehend mit einer Gliose, gekennzeichnet durch Astrozyten und Mikroglia, vor allem in unmittelbarer Nähe von Aβ-Plaques [122-124]. Kognitive Defizite können in diesem Mausmodell ab einem Alter von 12 Monaten gefunden werden, vor allem innerhalb der Trainingsphase des sogenannten Morris Water Maze [125]. Neben den kognitiven Defiziten konnten auch weitere Verhaltensbeeinträchtigungen, wie z.B. ein vermindertes Nestbauverhalten in dieser Linie nachgewiesen werden [126] (Abbildung 8).

APP_{SL}

Das APPswedish-london (kurz APP_{SL}) AD Mausmodell wurde im Jahr 2001 erstmalig von Rockenstein und Kollegen beschrieben [127]. Es trägt, wie auch die APP/PS1 Linie, die schwedische APP-Mutation, zusätzlich jedoch noch eine weitere APP-Mutation, die APP-London Mutation (V717I) unter Kontrolle einer murinen Thy2.1 Promoters bzw. Expressionskassette. Dieses Modell ist durch einen progressiven Anstieg der kognitiven Defizite, die vor allem im Morris water maze (MWM) nachgewiesen wurden, charakterisiert, ohne Defizite in der Motorik oder im allgemeinen Verhalten (z.B. Hyper- oder Hypoaktivität) zu zeigen [128]. Die AD-typische Pathologie dieser Linie beginnt mit der Ausprägung zerebraler Aβ-Ablagerungen im frontalen Kortex ab einem Alter von 3 Monaten, die sich progressiv mit dem Alter über verschiedene Regionen des Gehirns ausbreitet. Ab einem Alter von 11 Monaten sind Aβ-Plaques nahezu über den gesamten Neokortex verteilt zu finden sowie im Hippocampus, insbesondere im Subiculum und im Thalamus [127-129]. Neben diesen steigt auch die Anzahl der die Aβ-Plaques umgebenden Entzündungszellen (Gliose), wie Astrozyten und Mirkoglia [129] (Abbildung 8).

TBA2.1

Das TBA2.1 AD Mausmodell wurde im Jahr 2011 von Alexandru und Kollegen entwickelt [130]. Im Gegensatz zu den bereits erwähnten Mausmodellen produziert dieses Mausmodell, durch PTM, Pyroglutamat-modifiziertes $Aβ_{(3-42)}$. Unter der Kontrolle einer murinen Thy1.2 regulatorischen Sequenz wurde $Aβ_{(Q3-42)}$ in das Chromosom transgener Tiere integriert. Durch eine Fusion des Thyreotropin-freisetzenden Hormons (TRH) an den N-Terminus des $Aβ_{(Q3-42)}$ kann dieses Schrittweise durch endogene Glutaminylzyklasen posttranslational zu $pEAβ_{(3-42)}$ modifiziert werden [130]. Die Freisetzung des $pEAβ_{(3-42)}$ bewirkt, dass transgene Tiere Aβ-Ablagerungen entwickeln, die sich stark von Aβ-Plaques unterscheiden. Im Gegensatz zu Aβ-Plaques anderer Mausmodelle (z.B. APP/PS1) sind diese um ein Vielfaches kleiner und zeigen klare Abgrenzungen zu dem umliegenden Gewebe. Wie auch in den anderen Mausmodellen steigt die Anzahl der Aβ-Ablagerungen, die insbesondere in der CA1 Region des Hippocampus, im sensomotorischen Kortex und im Striatum zu finden sind, progressiv mit dem Alter (Abbildung 8). Eines der herausragendsten charakteristischen Merkmale dieses transgenen Mausmodells ist der Verlust von Neuronen innerhalb der CA1 Region in homozygoten Tieren (Abbildung 7). Ein Verlust von Neuronen, unabhängig von der Region, tritt in den klassischen Modellen der Amyloidose (z.B. Tg2576 oder APP/PS1) nicht oder nur unzureichend auf. Neben den pathologischen Veränderungen zeigen homozygote Tiere einen stark ausgeprägten motorisch eingeschränkten Phänotyp, der sich vor allem in einem hohem SHIRPA-Score (siehe Kapitel 1.5.1, Allgemeine und motorische

Verhaltenstests) sowie einer verschlechterten Leistung im Rotarod (siehe Kapitel 1.5.1, Allgemeine und motorische Verhaltenstests) widerspiegelt und progressiv mit dem Alter ansteigt [109, 130]. Durch den Schweregrad der phänotypischen Belastung müssen homozygote Tiere dieser Linie (aus tierschutzrechtlichen und ethischen Gründen) mit einem Alter von 22 Wochen euthanasiert werden, da sie sonst, aufgrund des Phänotyps, sterben würden. Bisher ist nicht bekannt, ob dieses Mausmodell kognitive Defizite ausprägt.

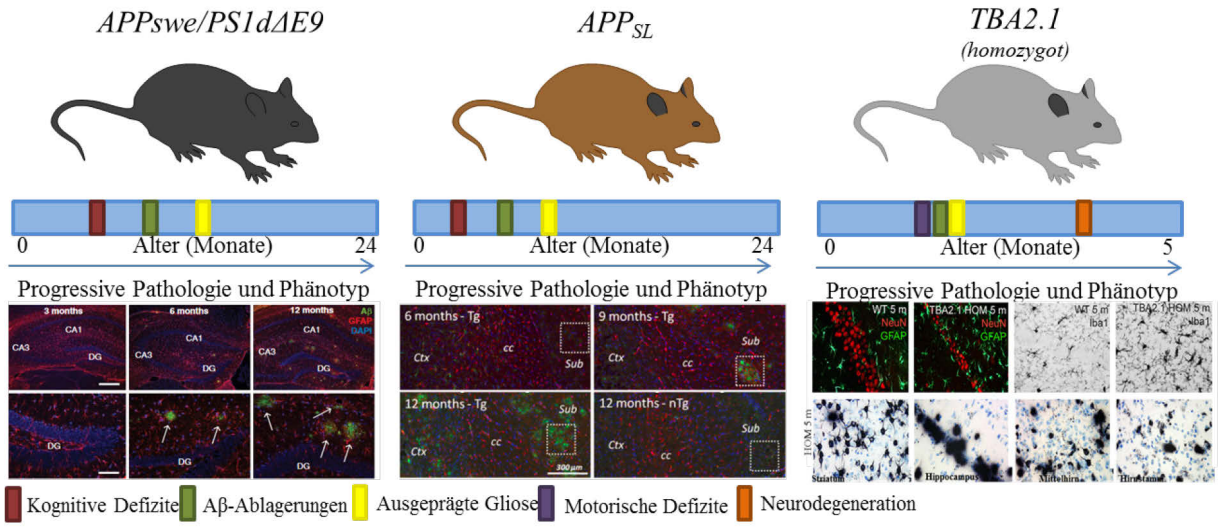

Abbildung 8: Übersicht der pathologischen und phänotypischen Charakteristika der Mausmodelle APPswe/PS1ΔE9 (APP/PS1), APPSL und TBA2.1..
Die Mausmodelle APP/PS1 (links) und APP_{SL} (Mitte) sind durch ein Auftreten zerebraler Aβ-Plaques und kognitiver Defizite charakterisiert, die beide progressiv mit fortschreitendem Alter zunehmen. Das TBA2.1 Mausmodell (rechts), insbesondere homozygote Tiere, sind durch einen sensomotorischen Phänotyp beschrieben. Als besonders charakteristisches Merkmal gilt der Verlust von Neuronen innerhalb der CA1-Region des Hippocampus. Histologische Abbildungen modifiziert nach [129-131].

1.5.1 Testung der Kognition und des Verhaltens in Mäusen

In der präklinischen Entwicklung neuer Medikamente für eine Therapie der AD spielen Verhaltenstests, insbesondere jene zur Darstellung der kognitiven Leistung, eine kritische Rolle. Der Hippocampus ist u.a. für die Gedächtniskonsolidierung verantwortlich. Er ist einer jener Regionen, die aufgrund einer AD beeinträchtigt sind. Neben der Langzeitpotenzierung (dem Lernen und dem Gedächtnis) ist der Hippocampus am räumlichen Lernen beteiligt. Diese Gegebenheit lässt sich anhand des Hippocampus von Londoner-Taxifahrern veranschaulichen. Während ihrer Berufsjahre nimmt das Volumen des Hippocampus, aufgrund ihres räumlichen Lernverhaltens, zu [132, 133]. Folglich können definierte Tests zur Untersuchung des räumlichen Gedächtnisses genutzt werden, um mögliche Defizite zu analysieren.

Kognitive Verhaltenstests

Unter der Vielzahl der beschriebenen Verhaltenstests gilt der sog. Morris Water Maze (MWM), der erstmalig von Richard Morris im Jahr 1984 beschrieben wurde [134], als Goldstandard zur Testung kognitiver Fähigkeiten (räumliches Lernen) der Ratte und, im späteren Verlauf der Entwicklung des Testes, auch der Maus. Während der Durchführung eines MWM ist es das Ziel, dass Mäuse oder Ratten eine sich unter der Wasseroberfläche befindliche Plattform finden, die aufgrund einer Trübung des Wassers nicht erkennbar ist. Dabei können sich die Tiere anhand von Markierungen, die entweder außerhalb oder innerhalb des Beckens angebracht sind, orientieren. Während der Trainingsphase lernen die Tiere, sich an die Lage der Plattform zu erinnern. Innerhalb der Testphase von mehreren Tagen können sich Mäuse bzw. Ratten ohne kognitive Beeinträchtigung an die Lage der Plattform erinnern und diese nach kurzer Schwimmdauer wiederfinden [135]. Kognitiv beeinträchtigte transgene AD Mäuse können dies aufgrund ihrer pathologischen Veränderungen nicht. Darüber hinaus kann mit Hilfe des MWM das Langzeitgedächtnis untersucht werden. Zusätzlich zum MWM gibt es noch weitere Labyrinthe zur Analyse der Kognition (z.B. „Y-Maze“, „T-Maze“, „Radial-Arm-Maze“) [136].

Neben diesen gibt es auch Tests, die nicht ausschließlich auf dem Prinzip des räumlichen Erinnerungsvermögens beruhen. Der sogenannte Object recognition test (ORT) [137, 138] beruht auf der natürlichen Neigung der Tiere ein gestärktes Interesse an neuen, unbekannten Objekten zu zeigen [139]. Es konnte gezeigt werden, dass hippocampale und kortikale Regionen für das visuelle Gedächtnis der Objekterkennung verantwortlich sind [140]. Da diese Regionen aufgrund pathologischer Veränderungen der AD besonders beeinträchtigt sind, findet der ORT hier Anwendung. Ein Vorteil dieses Testes ist, dass er ohne negative oder positive Verstärkung durchgeführt werden kann. Der MWM nutzt hingegen bei der Maus das Wasser als negative Verstärkung, da Mäuse zwar schwimmen können, jedoch eine Aversion gegen Wasser zeigen und somit einen inneren Antrieb zeigen, dem Wasser zu entkommen.

Allgemeine und motorische Verhaltenstests

Bei der Entwicklung neuer transgener AD Mausmodelle mit kognitiven Defiziten sollte vor Verwendung dieser in kognitiven Tests sichergestellt werden, dass etwaige motorische Defizite diese nicht in der Durchführung beeinflussen [141]. Des Weiteren stellen Tests für das generelle Verhalten sowie motorische Verhaltenstests ein wichtiges Werkzeug zur Analyse des Phänotyps von transgenen Mäusen dar. Motorische Verhaltenstests nehmen eine wichtige Rolle in der Evaluation eines motorisch defizitären Phänotyps ein. Es gibt eine

Vielzahl solcher Verhaltenstest. Zu den am häufigsten verwendeten Tests zählen z.B. der Offenfeldtest, die SHIRPA-Testbatterie oder der Rotarod-Test.

Der Offenfeldtest ist ein experimentelles Prozedere zur Determination der Motorik (Lokomotion) und des Angstverhaltens von Mäusen [142]. Zu diesem Zweck werden Mäuse in eine Arena gesetzt, die imaginär in zwei Bereiche gegliedert wird: einen Rand- und einen Zentrumsbereich. Da Mäuse eine Aversion gegen offene und helle Flächen zeigen, sollten diese mehr Zeit im Randbereich der Arena verbringen [143]. In der Regel dauert der Test 30 Minuten. Eine Einteilung der Explorationszeit in einzelne Zeiteinheiten, z.B. 5 Minuten, kann dazu genutzt werden, um einen möglichen Habituationseffekt oder das generelle Explorationsverhalten zu untersuchen.

Die SHIRPA-Testbatterie (SmithKline Beecham, Harwell, Imperial College, Royal London Hospital, phenotype assessment) wurde zur semiquantitativen Analyse eines Phänotyps von Mäusen entwickelt [144]. Dieser Test beinhaltet eine Reihe von Subtests, wie z.B. das Verhalten einer Maus im Käfig, die Beurteilung des Erscheinungsbildes und Evaluation der Reflexe (z.B. Pinna-Pedal-Reflex). Dabei werden die Tiere anhand eines definierten Auswerteschemas (Punkteskala null bis drei) beurteilt. Null Punkte bedeuten, dass sich die Maus in den jeweiligen Eigenschaften ganz normal verhält. Drei Punkte bedeuten, dass das Tier stak von normalen Verhalten abweicht. Beispiel: Ohrmuschelreflex. Hierbei werden die Haut und Haare am bzw. im Ohr stimuliert. Null Punkte (keine Auffälligkeiten) - vehementes Kopfumdrehen und Abwehrhaltung; Ein Punkt: Reaktion vorhanden; Zwei Punkte: kaum Reaktion; Drei Punkte: keine Reaktion.

Der Rotarod-Test dient zur Analyse der Motorik und der Koordination [141]. Originär wurde der Test im Jahr 1957 entwickelt unter Anwendung einer gleichbleibenden Geschwindigkeit [145]. Während der Durchführung des Rotarod-Tests laufen die Tiere über einen definierten Zeitraum auf einem sich rotieren Zylinder, dessen Geschwindigkeit im Laufe der Testzeit ansteigt. Motorisch unauffällige Tiere sollten es schaffen, sich während der Testzeit auf dem rotierenden Zylinder zu halten. Fallen Tiere von diesem, so bedeutet es, dass sie einen motorischen defizitären Phänotyp haben. Heutzutage können Apparaturen erworben werden, die Vielfältige Funktionen aufweisen (aufsteigende Geschwindigkeiten usw.).

2. Zielsetzung

Trotz intensivster Forschungsbemühungen gibt es bisher kein Medikament, welches die AD heilen kann. Zugelassene Medikationen dienen ausschließlich dem Zweck, die Symptome kurzzeitig zu unterdrücken oder auch nur kurzzeitig zu verlangsamen, ohne die Progression nachhaltig zu verlangsamen. Aufgrund dessen wurden für eine kausale Therapie der AD, unter Leitung von Prof. Willbold im Institut für komplexe System des Forschungszentrums Jülich und dem Institut für Physikalische Biologie der Heinrich-Heine-Universität Düsseldorf, D-enantiomere Peptide entwickelt, die spezifisch toxische Aβ-Oligomere eliminieren, welche neuesten Kenntnissen zufolge als krankheitsauslösend gelten. Für die Leitstruktur D3 konnte in einer Vielzahl erfolgreicher Studien der Wirksamkeitsnachweis demonstriert werden. Zur Optimierung des Wirkstoffprofils wurden verschiedene systematische, aber auch rationale Ansätze durchgeführt. Das erfolgversprechendste D-Peptid des rationalen Wirkstoffdesigns ist RD2 (Abkürzung für „rationales Design“). Nach Erstellung des *in vitro* Profils war das Hauptziel dieser Arbeit die ausführliche ***in vivo*** **Charakterisierung der pharmakodynamischen Eigenschaften** des D-enantiomeren Peptides RD2. Des Weiteren sollten D3-Derivate, für die bereits herausragende *in vitro* Eigenschaften beschrieben worden sind, aufgrund ihrer pharmakokinetischen Eigenschaften untersucht werden.

Zur Charakterisierung des D-enantiomeren Peptides RD2 sollten verschiedene Fragestellungen beantwortet werden.

Zeigt RD2 in vivo Wirksamkeit?

Zeigt RD2 Wirksamkeit nach oraler Applikation?

Zeigt RD2 nicht nur präventive, sondern auch kurative Wirksamkeit, d.h. nach Krankheitsausbruch?

Zeigt RD2 Wirkung in einem weiteren AD-Mausmodell mit einem pEAβ induzierten neurodegenerativen Phänotyp?

Die Aufklärung der Fragestellungen sollte mit Hilfe von verschiedenen Behandlungsstudien an verschiedenen AD-Mausmodellen verschiedener Altersstufen durchgeführt werden. In einer initialen Studie sollte überprüft werden, ob RD2 eine Wirksamkeit, nach intraperitonealer Behandlung, in einem jungen AD-Mausmodell zeigt, welches zwei AD-relevante Mutationen trägt (APP und PS1) (Zeigt RD2 ***in vivo*** **Wirksamkeit**?). Die intraperitoneale Applikation sollte dabei gewährleisten, dass der Wirkstoff schnell und unverändert an seinen Wirkort (das Gehirn) gelangt. Darüber hinaus sollte, auch in einem

jungen AD-Mausmodell, überprüft werden, ob RD2 nach oraler Darreichung eine Wirksamkeit aufweist, da eine orale Applikation die bevorzugte Darreichungsform beim Menschen darstellt (Zeigt RD2 Wirksamkeit nach **oraler Applikation**?). Im Vergleich zu dem zuvor verwendeten AD-Mausmodell trägt dieses keine PS1-Mutation, sodass ebenfalls evaluiert werden sollte, ob eine Wirkung auf verschiedene Aβ-Spezies erzielt werden kann. Zur Ermittlung einer kurativen Wirkung sollte eine orale Behandlungsstudie an gealterten, 18 Monate alten AD-Mäusen durchgeführt werden, die sowohl schwere kognitive Defizite, als auch eine ausgeprägte Pathologie aufweisen (Zeigt RD2 **kurative Wirksamkeit nach oraler Applikation**?). Viele potentiell kausale AD-Medikationen scheitern in späteren klinischen Studien. Dieser Umstand könnte darauf zurückzuführen sein, dass diese ausschließlich in AD-Mausmodellen mit APP-Mutationen getestet worden sind. Ein Nachteil vieler AD-Mausmodelle ist, dass diese oft nur die Amyloidose widerspiegeln, ohne andere wichtige Aspekte der AD-assoziierten Pathologie, z.B. die Neurodegeneration, zu berücksichtigen. Aufgrund dessen sollte in einer weiteren Studie überprüft werden, ob eine orale RD2-Behandlung die Progression des neuromotorischen Phänotyps des TBA2.1 AD-Mausmodells aufhält (Zeigt RD2 Wirkung in einem weiteren **AD-Mausmodell mit einem pEAβ induzierten neurodegenerativen Phänotyp**?). Im Vorfeld dieser Studie wurde darüber hinaus zunächst das TBA2.1 Modell ausgiebig charakterisiert, um die für die Behandlungsstudie passenden motorischen Tests zu etablieren.

Nach Abschluss der erfolgreichen Therapiestudien, in denen der Wirksamkeitsnachweis demonstriert wurde, erfolgte ein Vergleich aller Behandlungsstudien.

3. Manuskripte

3.1 Large-Scale Oral Treatment Study with the Four Most Promising D3 Derivatives for the Treatment of Alzheimer's Disease

Autoren:	Kutzsche J.*, **Schemmert S.***, Tusche M., Neddens J., Rabl R., Jürgens D., Brener O., Willuweit A., Hutter-Paier B., Willbold D.
	*Autoren sind gleichberechtigt
Journal:	Molecules (2017), veröffentlicht am 10. Oktober 2017
DOI:	10.3390/molecules22101693
Impact Factor:	2,861 (2016)
Beitrag:	Auswertung und Darstellung der Daten
	Anfertigung der meisten Abbildungen
	statistische Auswertung
	Hauptverfasserin des Manuskriptes gemeinsam mit J. Kutzsche

molecules

MDPI

Article

Large-Scale Oral Treatment Study with the Four Most Promising D3-Derivatives for the Treatment of Alzheimer's Disease

Janine Kutzsche [1,†], Sarah Schemmert [1,†], Markus Tusche [1], Jörg Neddens [2], Roland Rabl [2], Dagmar Jürgens [1], Oleksandr Brener [3], Antje Willuweit [4], Birgit Hutter-Paier [2] and Dieter Willbold [1,3,*]

1 Institute of Complex Systems, Structural Biochemistry (ICS-6), Forschungszentrum Jülich, Jülich 52425, Germany; j.kutzsche@fz-juelich.de (J.K.); s.schemmert@fz-juelich.de (S.S.); m.tusche@fz-juelich.de (M.T.); d.juergens@fz-juelich.de (D.J.)

2 QPS Austria GmbH, Grambach A-8074, Austria; joerg.neddens@qps.com (J.N.); roland.rabl@qps.com (R.R.); birgit.hutter-paier@qps.com (B.H.-P.)

3 Institut für Physikalische Biologie, Heinrich-Heine-Universität Düsseldorf, Düsseldorf 40225, Germany; brener@biophys.uni-duesseldorf.de

4 Institute of Neuroscience and Medicine, Medical Imaging Physics (INM-4), Forschungszentrum Jülich, Jülich 52425, Germany; a.willuweit@fz-juelich.de

* Correspondence: d.willbold@fz-juelich.de; Tel.: +49-2461-612100; Fax: +49-2461-612023

† These authors contributed equally to this work.

Received: 4 September 2017; Accepted: 4 October 2017; Published: 10 October 2017

Abstract: Alzheimer's disease (AD) is a progressive neurodegenerative disorder that is associated with the aggregation of the amyloid β protein (Aβ). Aβ oligomers are currently thought to be the major neurotoxic agent responsible for disease development and progression. Thus, their elimination is highly desirable for therapy development. Our therapeutic approach aims at specific and direct elimination of toxic Aβ oligomers by stabilizing Aβ monomers in an aggregation-incompetent conformation. We have proven that our lead compound "D3", an all D-enantiomeric-peptide, specifically eliminates Aβ oligomers in vitro. In vivo, D3 enhances cognition and reduces plaque load in several transgenic AD mouse models. Here, we performed a large-scale oral proof of concept efficacy study, in which we directly compared four of the most promising D3-derivatives in transgenic mice expressing human amyloid precursor protein with Swedish and London mutations (APP_{SL}), transgenic mice, to identify the most effective compound. RD2 and D3D3, both derived from D3 by rational design, were discovered to be the most effective derivatives in improving cognition in the Morris water maze. The performance of RD2- and D3D3-treated mice within the Morris water maze was significantly better than placebo-treated mice and, importantly, nearly as good as those of non-transgenic littermates, suggesting a complete reversal of the cognitive deficit of APP_{SL} mice.

Keywords: Alzheimer's disease; amyloid β; Aβ oligomers; oral treatment; transgenic mice; D-enantiomeric peptides; large-scale; cognition

1. Introduction

Alzheimer's disease (AD) is known to be the most common form of dementia worldwide. Although the detailed reasons for the development of the disease are still not fully understood, major pathological hallmarks of this disease are extracellular amyloid β protein (Aβ) accumulations (plaques), neurofibrillary tangles of the hyperphosphorylated protein tau, neuroinflammation, and neurodegeneration, all together resulting in cognitive decline of the affected patients. Over decades, it was thought that insoluble Aβ plaques are the main cause of cognitive decline. Nowadays, soluble Aβ

oligomers are suggested to be the main toxic agent that is responsible for the development and progression of AD [1,2]. Therefore, elimination of those toxic Aβ oligomers appears to be a promising strategy for finding a curative and disease modifying therapy against AD [2,3]. Antibodies that claim to be specific for Aβ oligomers may potentially bind them, without directly destroying them and without relying on the immune system or parts thereof.

Within our group, we focus on a therapeutic strategy to specifically and directly eliminate toxic Aβ oligomers, by ligand-mediated stabilisation of Aβ monomers in an aggregation-incompetent conformation. This is supposed to shift any equilibrium between Aβ species towards Aβ monomers and away from toxic Aβ oligomers. For this purpose, we developed different peptides that solely consist of D-enantiomeric amino acid residues (D-peptides), by mirror image phage display [4,5]. Based on this, our lead compound "D3" arose. In various studies, it has been proven that D3 specifically eliminates Aβ oligomers in vitro, inhibits Aβ fibril formation, and reduces Aβ-mediated cytotoxicity. In vivo, D3 is able to reduce plaque load and enhance cognition in several transgenic AD mouse models, even after oral administration [6–9]. With the intention to improve the oligomer-eliminating efficacy of D3 in vitro, we systematically identified different derivatives of D3 [10–12]. In addition, we pursued a different approach by rationally designing new D3-derivatives to increase knowledge in regard to essential sequence motifs and to increase efficacy. In this context, we identified four compounds with very promising in vitro properties, especially regarding their efficiency in Aβ oligomer elimination. Those include "RD2", which consists of exactly the same amino acid residues as D3 but in a re-arranged sequence; "D3D3" and "RD2RD2", the head-to-tail linear connected homodimers of the lead compounds D3 and RD2, respectively; as well as the head-to-tail linear connected heterodimer of RD2 and D3, termed "RD2D3". In vitro, all these newly designed D-peptides were able to eliminate toxic Aβ oligomers more efficiently than the lead compound D3 [8]. For D3D3, it could be additionally shown that it improved cognitive performance of transgenic APP-Swedish, Dutch, Iowa (Tg-SwDI) mice and reduced Aβ plaque load within the hippocampus and cortex [8]. Pharmacokinetic studies—which were performed with D3, RD2, D3D3, and RD2D3—have shown that all compounds efficiently cross the blood–brain barrier with brain–plasma ratios close to one after three to six hours after application and long half-lives in plasma and brain [13–15].

In the current report, we performed a large-scale oral proof of concept study with a total of 88 mice, in which we directly compared the efficacy of the four most promising D3-derivatives—RD2, RD2RD2, RD2D3, and D3D3—in the transgenic mouse model APP-Swedish, London (APP_{SL}). RD2 and D3D3 were found to be the most effective derivatives based on the significantly improved cognitive performance in the Morris water maze (MWM) compared to placebo-treated mice. Most importantly, the cognitive deficit of APP_{SL} mice was completely reversed and learning abilities of both treatment groups were similar to those of non-transgenic littermates.

2. Results

2.1. D3-Derivatives Eliminated Aβ Oligomers in the QIAD Assay and Significantly Reduced Aβ-Induced Cell Toxicity

Previously, we have already proven that RD2 and D3D3 were able to eliminate Aβ(1–42) oligomers significantly more efficiently than the lead compound D3 [8,16]. In this study, the potency of the D3-derivatives RD2RD2 and RD2D3 regarding their Aβ oligomer eliminating abilities was investigated in vitro by performance of a quantitative determination of interference with the Aβ aggregate size distribution (Aβ QIAD) assay. Findings of this analysis demonstrate that RD2RD2 and RD2D3 also significantly and efficiently eliminated toxic Aβ(1–42) oligomers (Figure 1A).

Furthermore, the outcome of the 3-(4,5-dimethylthiazol-2-yl)-2,5-diphenyl-tetrazolium bromide (MTT) cell viability assay with PC-12 cells revealed that all compounds were capable of significantly reversing the cellular toxicity exerted by 1 μM preincubated Aβ(1–42) (Figure 1B and [7,16]), without negative impact on cell viability on their own.

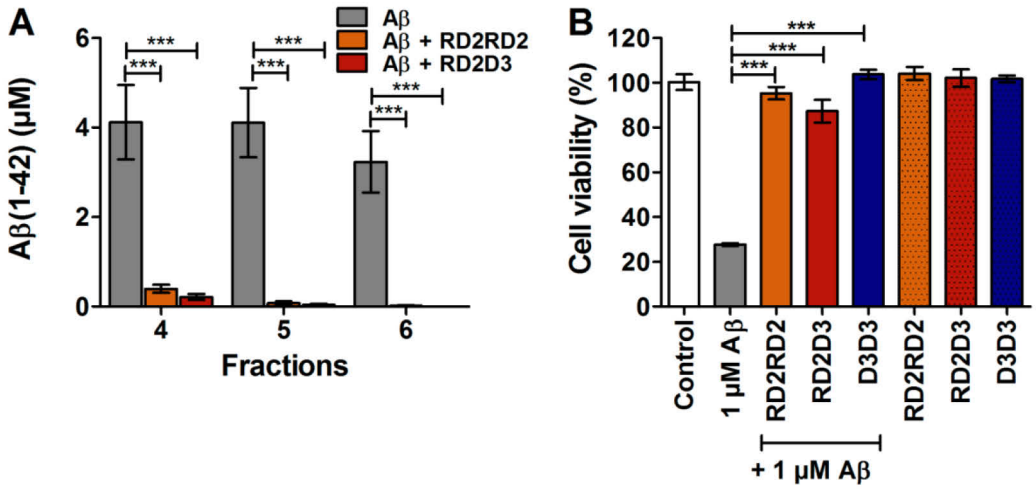

Figure 1. RD2RD2 and RD2D3 eliminated toxic amyloid β protein (Aβ) oligomers and reduced Aβ induced cell toxicity. Potency of RD2RD2 and RD2D3 to reduce toxic Aβ oligomers was demonstrated in vitro by the QIAD assay (**A**). Both compounds were able to reduce the toxic Aβ oligomers present in fractions 4–6. Cell viability was assessed by MTT (3-(4,5-dimethylthiazol-2-yl)-2,5-diphenyl-tetrazolium bromide) after incubation of PC-12 cells (**B**) with 1 μM Aβ(1–42) co-incubated with 1 μM RD2RD2 (orange), 1 μM RD2D3 (red), or 1 μM D3D3 (blue). All compounds significantly increase the cell viability after co-incubation with Aβ(1–42), without having negative impact on cell viability when incubated alone (patterned bars). Data is represented as mean ± SD (standard deviation), one-way ANOVA (analysis of variance) with Fisher post hoc analysis, *** $p \leq 0.001$.

2.2. RD2 and D3D3 Treated Mice Exhibited Improved Cognitive Performance

Oral treatment of 75 APP_{SL} mice with either placebo, RD2, RD2RD2, RD2D3, or D3D3 did not result in significant gain or loss of body weight before vs. after treatment or in any change of general conditions of the mice compared to placebo-treated mice or non-transgenic littermates (ntg) (body weight before vs. after treatment: placebo 23.8 g vs. 23.8 g; RD2 23.5 g vs. 23.7 g; RD2RD2 23.9 g vs. 23.7 g; RD2D3 24.6 g vs. 23.8 g; RD2D3 24.7 g vs. 24.5 g; ntg 25.6 g vs. 25.7 g).

The Morris water maze (MWM) was performed to explore whether treatment with the compounds RD2, RD2RD2, RD2D3, or D3D3 results in cognitive improvement. The results were compared to the performance of placebo-treated mice and non-transgenic littermates. As demonstrated in Figure 2, treatment with RD2 (Figure 2B) and D3D3 (Figure 2C) achieved a significant improvement of cognition during the acquisition phase of the MWM (two-way RM ANOVA, Fisher post hoc analysis: placebo vs. ntg $p = 0.039$, placebo vs. RD2 $p = 0.02$, placebo vs. D3D3 $p = 0.006$), which was similar to those of non-transgenic littermates. Treatment with RD2RD2, the head-to-tail tandem compound of RD2, did not show a significant improvement in cognition, nor did RD2D3 (two-way RM ANOVA, Fisher post hoc analysis: placebo vs. RD2RD2 or RD2D3 non-significant (n.s.)), a combination of the compounds RD2 and D3. There was no significant difference determined between the swimming speed and the covered path length of all analyzed groups.

The probe trial testing memory-retrieval did not reveal significant differences between the tested groups (one-way ANOVA, n.s. all groups, Figure 2D), although there is a clear tendency of RD2- and D3D3-treated mice just as non-transgenic littermates for abidance in the target quadrant.

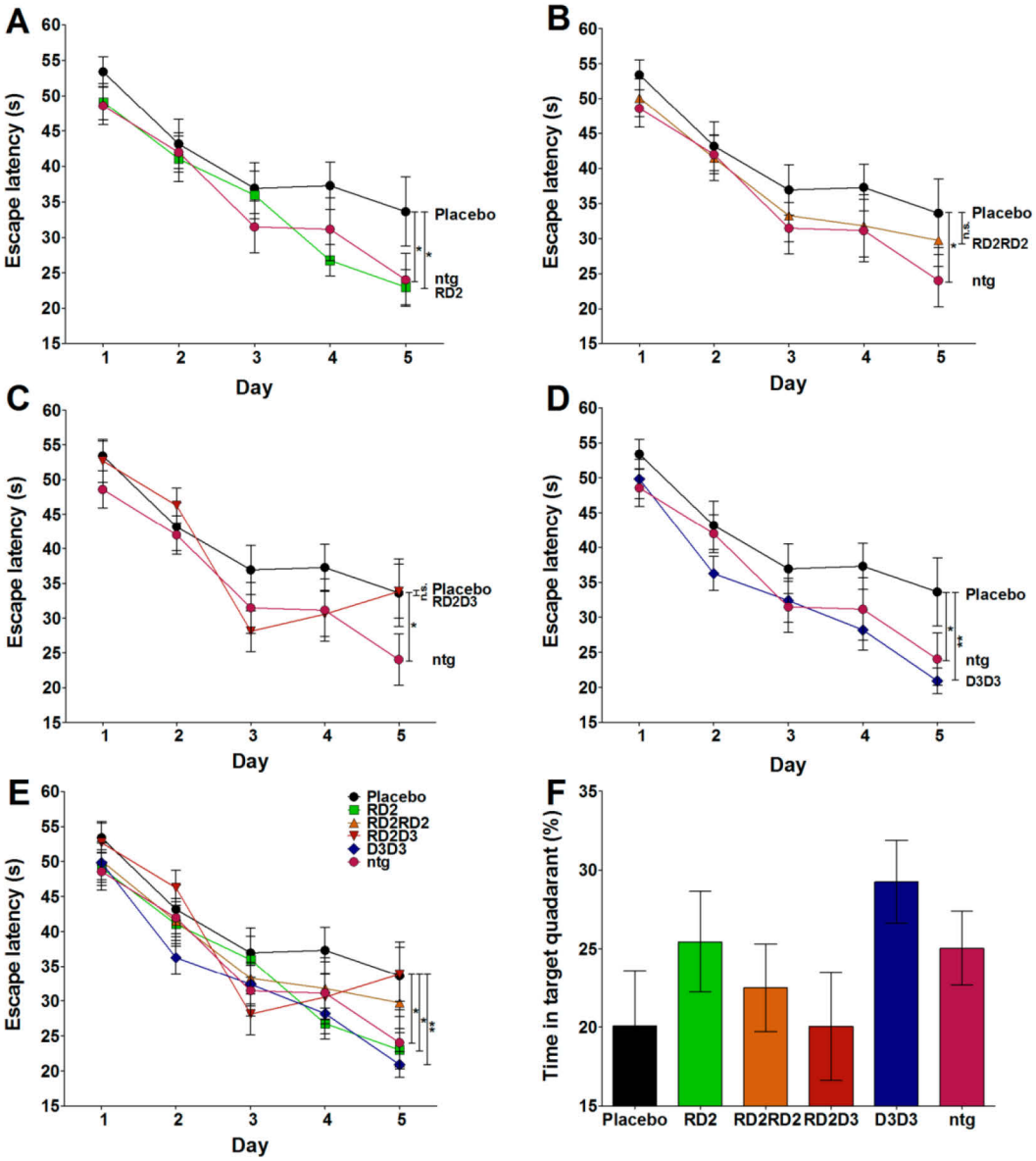

Figure 2. Treatment with RD2 and D3D3 improved cognitive performance as shown in the Morris water maze (MWM). During the acquisition phase of the MWM, RD2- (green, (**A**,**E**)) and D3D3- (blue, (**D**,**E**)) treated mice showed significantly improved learning behaviors compared to those of placebo- (black) treated mice (two-way repeated measurements (RM) ANOVA, Fisher post hoc analysis, * $p < 0.05$, ** $p < 0.001$) (**A**–**C**,**E**). The improved cognitive performance is indistinguishable to that of non-transgenic littermates (ntg, pink) ((**A**–**C**)). Neither RD2RD2- (orange (**B**,**E**)) nor RD2D3- (red, (**C**,**E**)) treated mice showed improved cognitive performance compared to the behavior of placebo-treated mice. (**E**) is a combination of (**A**) to (**D**) for direct comparison of all four tested compounds. The probe trial did not reveal significant differences between the groups, but showed the tendency of RD2- and D3D3-treated mice to spend more time in the target quadrant **F**.

2.3. RD2 and D3D3 Improved Cognitive Performance without Influencing Aβ Pathology or Inflammation

To investigate whether treatment with the four D3-derivatives has any influence on Aβ deposits or neuroinflammation in APP_{SL} transgenic mice, different staining procedures on histological brain sections were performed (Figure 3) and stained areas were analyzed within the hippocampus and

cortex. Staining with 6E10 antibody against transgenic human Aβ was performed to visualize Aβ deposits in the hippocampus and cortex. There were no significant differences in the stained area in both regions analyzed of all treated groups compared to placebo-treated mice, but there was a tendency of lowering Aβ deposits within the cortex by treatment with RD2 (6E10 IR area (%): RD2 7.4 ± 0.4 vs. placebo 8.4 ± 0.6, one-way ANOVA, $p = 0.22$).

By analysis of two populations of glia cells—glial fibrillary acidic protein (GFAP)-expressing astrocytes and CD11b-expressing reactive microglia—no significant effect of RD2, RD2RD2, RD2D3, or D3D3 treatment was achieved compared to placebo-treated mice, suggesting that there is no change within the neuroinflammatory status of the treated mice (Figure 3A–E).

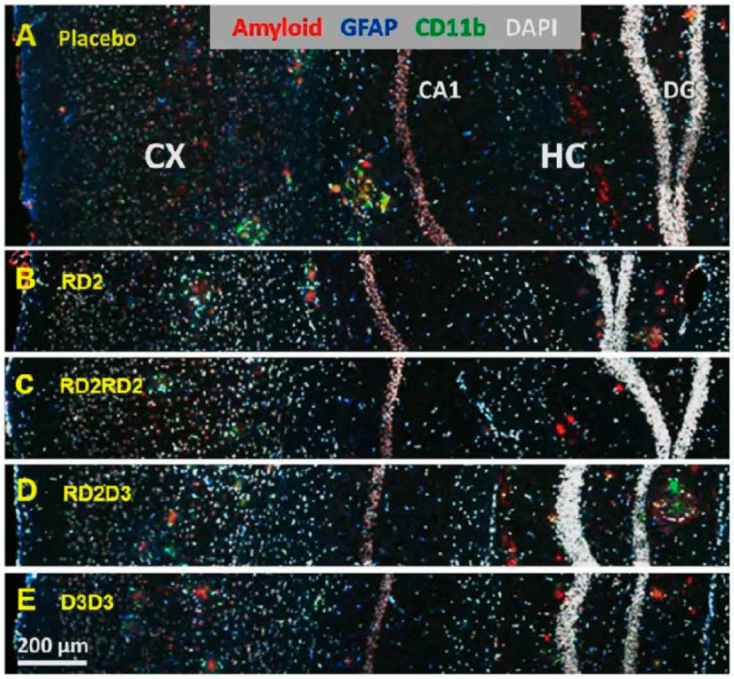

Figure 3. Immunofluorescent labeling of amyloid and glia cells. The images show exemplary immunofluorescent labeling of amyloid (antibody 6E10, red), astrocytes (GFAP (glial fibrillary acidic protein), blue), and activated microglia (CD11b, green) in mice of all groups (**A**–**E**). Nuclei are labeled with DAPI (white) to provide the requested comparison between the different groups. Abbreviations: CX, Cortex; CA1, *cornu Ammonis* area 1; HC, hippocampus; DG, dentate gyrus.

3. Discussion

One of the major challenges of the current century is finding a curative and disease-modifying treatment for Alzheimer's disease, a devastating neurodegenerative disorder. Despite intensive research, approved medications are by now not able to slow down disease progression, but are only able to treat symptoms in a very limited way, often combined with unattractive side effects. Over the past years, we developed all-D-enantiomeric peptides for direct and specific elimination of toxic Aβ oligomers as an attractive treatment strategy for AD. The lead compound D3 specifically eliminates toxic Aβ oligomers in vitro [8]. Eight weeks of oral treatment of four-months-old APP/PS1 mice with moderate doses of D3 significantly improved cognition compared to untreated mice, as tested in the Morris water maze. Additionally, Aβ plaque load in hippocampus and frontal cortex, as well as plaque-related inflammation, was significantly reduced in D3-treated versus untreated mice [9]. In the present study, we compared in vivo efficiencies of the D3-derivatives RD2, RD2RD2, RD2D3, and D3D3, which were the most efficient compounds in vitro. The direct comparison of the influence of RD2 vs. D3 or D3D3 vs. D3 on Aβ oligomer elimination efficiencies, as measured by the QIAD assay, revealed that

all tested peptides significantly reduced the amount of Aβ oligomers; however, RD2 and D3D3 performed significantly better than D3 (RD2 71%, D3D3 96%, and D3 51% oligomer reduction) [8,16]. In vivo in the current study, it was demonstrated that RD2 and D3D3 improved cognitive performances of APP_{SL} mice by oral application of moderate doses over six weeks. The hereby described comparison is based on the same single dose for each compound. Dose–response curves for the most promising compounds might give an even more quantitative basis for future comparisons. The cognitive behavior of both treated groups was similar to the behavior of non-transgenic littermates, suggesting a reversal of the cognitive impaired phenotype. In contrast, RD2RD2 and RD2D3 did not yield significant improvement of cognitive performance within this study, as neither compound changed the amyloid load or neuroinflammatory pathology within the therapeutic time frame.

The finding that cognitive improvement was achieved by treatment with RD2 and D3D3 without significantly changing the typical plaque pathology underlines the hypothesis that plaque pathology is not directly correlated to cognitive deficits. Thus, more and more evidence is given that, instead of Aβ assemblies in senile plaques, soluble Aβ oligomers are the main cause of cognitive decline [17–20]. Also, in patients, several studies demonstrated that Aβ plaque load is not directly correlated with cognitive decline [21,22].

Based on the in vitro findings, we suggest for our compounds the specific and direct elimination of toxic oligomers by stabilizing Aβ monomers in an aggregation-incompetent conformation as a possible mode of action. This shifts any equilibrium between Aβ species towards Aβ monomers and away from Aβ oligomers, leading to the elimination of toxic Aβ oligomers [8,9]. Taking advantage of this strategy, our compounds do not recognize any distinct Aβ oligomer species, thus avoiding any danger of resistance development. In addition, they not only readily prevent Aβ oligomer formation but also eliminate oligomers that are already formed. We conjecture, sustained by our in vitro results, that this mode of action eventuates in vivo, too. Within this study, a reversal of cognitive deficits by treatment with RD2 and D3D3, most likely by a specific elimination of toxic Aβ oligomers and without reducing senile plaques, was demonstrated. As described in the literature [1], the reduction of Aβ oligomers results in improved synaptic function, resulting in improved cognitive performance. Irrespective of that, the observations made in this study strengthen the hypothesis that there is no crucial link between plaque pathology and cognition. Based on our hypothesis of shifted Aβ equilibrium by treatment with our compounds, long-term therapy of several months may casually also result in reduced plaque load, as previously demonstrated for D3 [7].

In conclusion, RD2 and D3D3 were both able to significantly enhance the cognitive abilities of APP_{SL} mice. In consequence, both are predicted to be promising drug candidates for anti-amyloid treatment. Nevertheless, findings of pharmacokinetic studies, conducted with RD2 and D3D3, indicate that RD2 has more favorable properties in comparison to D3D3, especially concerning the terminal half-life and oral bioavailability [14,15], so that an accurate therapeutic regimen with once daily administration is feasible. This is of great advantage to enable a suitable compliance of orally administered drugs, especially for a drug intended to be given to patients with dementia.

4. Materials and Methods

4.1. Ethics Statement

All animal experiments conformed to the Austrian guidelines for the care and use of laboratory animals and were approved by the Styrian Government, Amt der Steiermärkischen Landesregierung Abteilung 13-Umwelt und Raumordnung, Austria (Project ID: ABT13-78Jo142-2014, date of approval: 18 June 2014).

4.2. Peptides

All peptides—RD2, RD2RD2, RD2D3, and D3D3—were C-terminally amidated and purchased from Cambridge Peptides (Cambridge Peptides, Birmingham, UK) and Peptides and Elephants (Peptides & Elephants, Henningsdorf, Germany) as lyophilized powder with a minimal purity of 97% (Table 1).

Table 1. Amino acid sequences of the applied D-enantiomeric peptides.

Peptide	Sequence (All D-Enantiomeric)
RD2	ptlhthnrrrrr
RD2RD2	ptlhthnrrrrrptlhthnrrrrr
RD2D3	ptlhthnrrrrrrprtrlhthrnr
D3D3	rprtrlhthrnrrprtrlhthrnr

4.3. QIAD Assay

To investigate the Aβ oligomer elimination properties of RD2RD2 and RD2D3 in vitro, a QIAD assay (quantitative determination of interference with Aβ aggregate size distribution) was performed according to Brener et al. [6]. In short, 10 µM of the D3-derivatives RD2RD2 or RD2D3 were added to pre-incubated 80 µM Aβ(1–42) solution. Afterwards, samples were fractionated on a 5–50% (*w*/*v*) iodixanol gradient (OptiPrep, Axis-Shield, Norway) and ultracentrifuged for 3 h at 4 °C and 259.000× g (Optima TL-100, Beckman Coulter, Brea, CA, USA). Subsequently, the resulting 14 fractions, each 140 µL, were taken top to bottom from the gradient. Obtainment of the 15th fraction was performed by boiling the pellet for 10 min after mixing with 60 µL of 6 M guanidine hydrochloride. The oligomer containing fractions 4 to 6 was analyzed by analytical reversed phase-high performance liquid chromatography (RP-HPLC) and ultraviolet absorbance was detected at 214 nm. The Aβ oligomer elimination properties of RD2 and D3D3 were previously published [8,16].

4.4. Cell Viability Test

Examination of Aβ(1–42)-induced cell toxicity in the presence or absence of the D3-derivatives RD2RD2, RD2D3, and D3D3 was conducted by use of a MTT-based cell viability assay as described previously (e.g., [11,12]). For this purpose, PC-12 phaeochromocytoma cells (DSMZ, Braunschweig, Germany) were cultured in DMEM medium supplemented with 10% fetal calf serum, 1% antibiotics (Penicillin/Streptomycin) (all Sigma-Aldrich, St. Louis, MO, USA), and 5% horse serum (PAA Laboratories GmbH, Cölbe, Germany) on collagen A-coated (Biochrom GmbH, Berlin, Germany) tissue culture flasks (SPL Life Sciences Co., Naechon-Myeon, Korea). Cells were allowed to grow in a humidified incubator with 5% CO_2 at 37 °C and a maximum of 12 passages, whereby the medium was changed every two days. Cells were passaged according to their confluence.

In accordance with the manufacturer's protocol, an MTT test was performed (CellProliferation Kit I; Roche, Basel, Switzerland). After the cells were seeded in clear, collagen-coated 96-well flat bottom microwell plates (Life Technologies Inc., Carlsbad, CA, USA) in a volume of 100 µL per well at a density of 1×10^4 cells, they were incubated for 24 h. On the next day, compounds were prepared in the following manner: after incubation of 51 µM Aβ(1-42) for 4.5 h at 37 °C shaking at 600 rpm, 25 µM RD2RD2, RD2D3, or D3D3 were added and incubated for another 40 min. During the test, cells were exposed to 1 µM Aβ with or without 0.5 µM RD2RD2, RD2D3, or D3D3. All experiments were conducted as a fivefold determination in three independent experiments. The arithmetic mean of all measurements per approach was calculated. Data is represented as the percentage of MTT reduction, assuming that the absorbance of control cells was 100%.

4.5. Mice

Female 8 months ± 2 weeks-old APP_{SL} mice were used in the present study. Mice were bred hemizygous for the transgene on a C57BL/6 background. Behavioral and pathological characteristics

of the used mouse model are previously described [23,24]. Mice were group-housed in individually ventilated cages on standard rodent bedding (Rosenberg, Germany) in the AAALAC-accredited animal facility of QPS Austria GmbH, Grambach, Austria) with a 12/12 h light dark cycle, 21 °C room temperature, 40–70% humidity and food and water ad libitum. Only mice in good health condition were included in the study. Randomization of group allocation was done per cage. All mice of a cage were randomly assigned to a treatment group. Mice were assigned to different starting groups (cohorts) comprising mice of all treatment groups. The number of mice in a starting group was limited to ensure same age and uniform handling.

4.6. Treatment

Female APP_{SL} mice, aged 32 ± 2 weeks, were orally treated once daily for six weeks. Administration was performed by gavage with 200 µL of test compound diluted in 0.9% NaCl or placebo with 20 mg/kg of either RD2 (n = 15), RD2RD2 (n = 15), RD2D3 (n = 15), D3D3 (n = 14), or 0.9% NaCl as control group (placebo). The administered dose in this study (20 mg/kg) was derived from a previous D3 treatment study [9]. In this study, mice with a body weight of approximately 25 g were orally treated with 0.5–1 mg D3 daily. This corresponds to a daily administered dose of 20 mg/kg. The administered doses were derived from the therapeutic efficient dosage from the first oral D3 treatment study [9]. For the validation of the Morris water maze, a group of non-transgenic littermates was used as control. In total, 74 transgenic and 14 non-transgenic mice were used in the present study.

4.7. Morris Water Maze

The MWM was performed to assess spatial learning and memory performance of all groups described above. The used water maze consisted of a circular pool (diameter 100 cm) filled with opaque made water (24 ± 1°C) to a depth of 20 cm, with a hidden but fixed platform, located 0.5 cm beneath the water surface. During all trials, the platform was located in the target quadrant (northeast, NE) of the pool. The used protocol was adopted and modified from Morris et al., 1982 [25]. The acquisition phase of the MWM was performed over five consecutive days. Mice had to swim on each day four trails with a maximum length of 60 s from predefined positions. If the mice did not find the hidden platform within the 60 s, they were guided to the target and were allowed to orientate themselves for 10–15 s. The escape latency was analyzed in s, the time mice needed to escape on the hidden platform. On the sixth day, 24 h after the last day of the acquisition phase, the probe trial was performed. Thereby, the platform was removed from the pool and all mice had to swim for 60 s. The abidance of mice in the target quadrant was analyzed. Mice were observed with a camera driven tracking system, Viewer III (Biobserve GmbH, Bonn, Germany).

4.8. Tissue Collection

After the behavioral assessments, the mice were sacrificed to obtain brain samples. The mice were anesthetized intraperitoneally by sodium pentobarbital injection (600 mg/kg). When the mice reached the appropriate anesthesia stage, they were transcardially perfused with 0.9% saline. Subsequently, the brains were removed and the left hemispheres were frozen in dry ice and stored at −80 °C. The right hemispheres were used for immunohistochemical analyses: hemispheres were fixed in freshly prepared 4% paraformaldehyde in phosphate buffer (pH 7.4) for one h at room temperature (RT). Afterwards, hemispheres were transferred into a 15% sucrose solution for cryoprotection. On the next day, the fixed hemispheres were frozen in isopentane and stored at −80 °C until further processing.

4.9. Immunohistology

Immunohistochemical analysis was performed with six animals per treatment group. Sagittal cryosections (10 µm) were generated on a Leica CM 1950 cryostat (Leica Biosystems, Nussloch, Germany). In brief, five cyrosections per mouse were allowed to air-dry for 45 min at RT and washed with phosphate buffered saline (PBS) for 10 min. After incubation in sodium borohydrate solution for

4 min, cyrosections were washed two times with PBS for 10 min, permeabilized with 1% TritonX-100 in PBS for 10 min, and again washed three times in PBS for 5 min. Subsequently, after blocking of unspecific bindings with 10% horse serum in PBS for 30 min at RT, cryosections were incubated with CD11b antibody (Bio-Rad Laboratories, Puchheim, Germany; dilution 1:1000) for 60 min at RT in a humid chamber. After another washing step in PBS, cyrosections were incubated with donkey anti-rat DyLight650 (Abcam, Cambridge, UK; dilution 1:500) for 60 min at RT in a humid chamber in the dark. Following a further washing step and blocking of unspecific bindings with a mouse-on-mouse (MOM) blocking reagent (MOM-kit, Vector, Burlingame, CA, USA) for 30 min at RT in the dark, cryosections were incubated for 60 min with GFAP (Dako, Agilent technologies, Santa Clara, CA, USA; dilution 1:500) and 6E10 (BioLegend, San Diego, CA, USA; dilution 1:1000) for 30 min at RT in a light protected humid chamber. Subsequently, cryosections were incubate with donkey anti-rabbit DyLight488 (Abcam, dilution 1:500) and donkey anti-mouse AlexaFluor555 (Abcam, dilution 1:500) for 60 min at RT in a light protected humid chamber. After the washing step in PBS, cryosections were incubated with 4′,6-diamidino-2-phenylindole for 15 min and differentiated two times with 80% ethanol for 2 min. Cryosections were mounted and cover-slipped. All sections were stained in equal volumes to avoid differences in staining intensity.

4.10. Quantification

All sections were acquired in one microscopy session to avoid changes in light exposure, which might affect measurements. Visualization of sections was conducted by use of a Zeiss Axio Imager Z1 microscope (Zeiss, Jena, Germany) with a high aperture lens (10× lens, numerical aperture 0.90, 1× optocoupler), equipped with a Zeiss AxioCam MRm camera and Zeiss AxioVision 4.8 software (Zeiss, Jena, Germany). Quantification was performed with ImageProPlus software (Media Cybernetics, Inc., Rockville, MD, USA).

4.11. Statistics

All statistical calculations were conducted by SigmaPlot Version 11 (Systat Software, Erkrath, Germany). Data is represented as mean ± SD (in vitro results) or SEM (in vivo results). Data was analyzed using one-way ANOVA with Fisher LSD post hoc analysis. Repeated measurements (RM) were analyzed by use of two-way RM ANOVA with Fisher LSD post hoc analysis. Significant results of the MWM were confirmed by use of Friedman Repeated Measures ANOVA on Ranks.

Acknowledgments: Financial support of D.W. was provided by "Portfolio Technology and Medicine", the Helmholtz-Validierungsfonds of the Impuls and Vernetzungs-Fonds der Helmholtzgemeinschaft. D.W. was supported by the "Portfolio Drug Research" of the Impuls and Vernetzungs-Fonds der Helmholtzgemeinschaft.

Author Contributions: J.K. planned the study in agreement with D.J. and D.W. All experiments were performed from QPS, Austria, under control of J.N., R.R. and B.H.-P. Evaluation and statistics were conducted by J.K., A.W. and, S.S. J.K., S.S. and D.W. wrote, whereas all other authors reviewed the manuscript.

Conflicts of Interest: The authors declare no conflict of interest.

References

1. Ferreira, S.T.; Lourenco, M.V.; Oliveira, M.M.; de Felice, F. Soluble amyloid-β oligomers as synaptotoxins leading to cognitive impairment in Alzheimer's disease. *Front. Cell. Neurosci.* **2015**, *9*, 191. [CrossRef] [PubMed]
2. Selkoe, D.J.; Hardy, J. The amyloid hypothesis of Alzheimer's disease at 25 years. *EMBO Mol. Med.* **2016**, *8*, 595–608. [CrossRef] [PubMed]
3. Salahuddin, P.; Fatima, M.T.; Abdelhameed, A.S.; Nusrat, S.; Khan, R.H. Structure of amyloid oligomers and their mechanisms of toxicities: Targeting amyloid oligomers using novel therapeutic approaches. *Eur. J. Med. Chem.* **2016**, *114*, 41–58. [CrossRef] [PubMed]

4. Wiesehan, K.; Buder, K.; Linke, R.P.; Patt, S.; Stold, M.; Unger, E.; Schmitt, B.; Bucci, E.; Willbold, D. Selection of D-amino-acid peptides that bind to Alzheimer's disease amyloid peptide Aβ1–42 by mirror image phage display. *Chembiochem* **2003**, *4*, 748–753. [CrossRef] [PubMed]
5. Schumacher, T.N.; Mayr, L.M.; Minor, D.L., Jr.; Milhollen, M.A.; Burgess, M.W.; Kim, P.S. Identification of D-peptide ligands through mirror-image phage display. *Science* **1996**, *271*, 1854–1857. [CrossRef] [PubMed]
6. Van Groen, T.; Kadish, I.; Funke, A.S.; Bartnik, D.; Willbold, D. Treatment with Aβ42 Binding D-Amino Acid Peptides Reduce Amyloid Deposition and Inflammation in APP/PS1 Double Transgenic Mice. *Adv. Protein Chem. Struct. Biol.* **2012**, *88*, 133–152. [PubMed]
7. Van Groen, T.; Wiesenhan, K.; Funke, S.A.; Kadish, I.; Nagel-Steger, L.; Willbold, D. Reduction of Alzheimer's disease amyloid plaque load in transgenic mice by D3, A D-enantiomeric peptide identified by mirror image phage display. *ChemMedChem* **2008**, *3*, 1848–1852. [CrossRef] [PubMed]
8. Brener, O.; Dunkelmann, T.; Gremer, L.; van Groen, T.; Mirecka, E.A.; Kadish, I.; Willuweit, A.; Kutzsche, J.; Jürgens, D.; Rudolph, S.; et al. QIAD assay for quantitating a compound's efficacy in elimination of toxic Aβ oligomers. *Sci. Rep.* **2015**, *5*, 13222. [CrossRef] [PubMed]
9. Funke, A.S.; van Groen, T.; Kadish, I.; Bartnik, D.; Nagel-Steger, L.; Brener, O.; Sehl, T.; Batra-Safferling, R.; Moriscot, C.; Schoehn, G.; et al. Oral treatment with the D-enantiomeric peptide D3 improves the pathology and behavior of Alzheimer's Disease transgenic mice. *ACS Chem. Neurosci.* **2010**, *1*, 639–648. [CrossRef] [PubMed]
10. Klein, A.N.; Ziehm, T.; Tusche, M.; Buitenhuis, J.; Bartnik, D.; Boeddrich, A.; Wiglenda, T.; Wanker, E.; Funke, S.A.; Brener, O.; et al. Optimization of the All-D Peptide D3 for Aβ Oligomer Elimination. *PLoS ONE* **2016**, *11*, e0153035. [CrossRef] [PubMed]
11. Klein, A.N.; Ziehm, T.; van Groen, T.; Kadish, I.; Elfgen, A.; Tusche, M.; Thomaier, M.; Reiss, K.; Brener, O.; Gremer, L.; et al. Optimization of D-peptides for Aβ monomer binding specificity enhances their potential to eliminate toxic Aβ oligomers. *ACS Chem. Neurosci.* **2017**, *8*, 1889–1900. [CrossRef] [PubMed]
12. Ziehm, T.; Brener, O.; van Groen, T.; Kadish, I.; Frenzel, D.; Tusche, M.; Kutzsche, J.; Reiss, K.; Gremer, L.; Nagel-Steger, L.; et al. Increase ofpPositive net charge and conformational rigidity enhances the efficacy of D-enantiomeric peptides designed to eliminate cytotoxic Aβ species. *ACS Chem. Neurosci.* **2016**, *7*, 1088–1096. [CrossRef] [PubMed]
13. Jiang, N.; Leithold, L.H.E.; Post, J.; Ziehm, T.; Mauler, J.; Gremer, L.; Cremer, M.; Schartmann, E.; Shah, N.J.; Kutzsche, J.; et al. Preclinical pharmacokinetic studies of the tritium labelled D-Enantiomeric peptide D3 developed for the treatment of Alzheimer s disease. *PLoS ONE* **2015**, *10*, e0128553. [CrossRef] [PubMed]
14. Leithold, L.H.; Jiang, N.; Post, J.; Niemietz, N.; Schartmann, E.; Ziehm, T.; Kutzsche, J.; Shah, N.J.; Breitkreutz, J.; Langen, K.-J.; et al. Pharmacokinetic properties of tandem D-peptides designed for treatment of Alzheimer's disease. *Eur. J. Pharm. Sci.* **2016**, *89*, 31–38. [CrossRef] [PubMed]
15. Leithold, L.H.; Jiang, N.; Post, J.; Ziehm, T.; Schartmann, E.; Kutzsche, J.; Shah, N.J.; Breitkreutz, J.; Langen, K.-J.; Willuweit, A.; et al. Pharmacokinetic properties of a novel D-Peptide developed to be therapeutically active against toxic β-amyloid oligomers. *Pharm. Res.* **2016**, *33*, 328–336. [CrossRef] [PubMed]
16. Van Groen, T.; Schemmert, S.; Brener, O.; Gremer, L.; Ziehm, T.; Tusche, M.; Nagel-Steger, L.; Kadish, I.; Schartmann, E.; Elfgen, A.; et al. The Aβ oligomer eliminating D-enantiomeric peptide RD2 improves cognition without changing plaque pathology. *Sci. Rep.* **2017**. under review.
17. Wang, Z.X.; Tan, L.; Liu, J.; Yu, J.T. The essential role of soluble Aβ oligomers in Alzheimer's disease. *Mol. Neurobiol.* **2016**, *53*, 1905–1924. [CrossRef] [PubMed]
18. Haass, C.; Selkoe, D.J. Soluble protein oligomers in neurodegeneration: lessons from the Alzheimer's amyloid β-peptide. *Nat. Rev. Mol. Cell Biol.* **2007**, *8*, 101–112. [CrossRef] [PubMed]
19. Larson, M.E.; Lesne, S.E. Soluble Aβ oligomer production and toxicity. *J. Neurochem.* **2012**, *120* (Suppl. 1), 125–139. [CrossRef] [PubMed]
20. Ferreira, S.T.; Klein, W.L. The Aβ oligomer hypothesis for synapse failure and memory loss in Alzheimer's disease. *Neurobiol. Learn. Mem.* **2011**, *96*, 529–543. [CrossRef] [PubMed]
21. Jagust, W. Is amyloid-β harmful to the brain? Insights from human imaging studies. *Brain* **2016**, *139*, 23–30. [CrossRef] [PubMed]
22. Rosenblum, W.I. Why Alzheimer trials fail: Removing soluble oligomeric β amyloid is essential, inconsistent, and difficult. *Neurobiol. Aging* **2014**, *35*, 969–974. [CrossRef] [PubMed]

23. Loffler, T.; Flunkert, S.; Havas, D.; Schweinzer, C.; Uger, M.; Windisch, M.; Steyrer, E.; Hutter-Paier, B. Neuroinflammation and related neuropathologies in APPSL mice: Further value of this in vivo model of Alzheimer's disease. *J. Neuroinflamm.* **2014**, *11*, 84. [CrossRef] [PubMed]
24. Havas, D.; Hutter-Paier, B.; Ubhi, K.; Rockenstein, E.; Crailsheim, K.; Masliah, E.; Windisch, M. A longitudinal study of behavioral deficits in an AβPP transgenic mouse model of Alzheimer's disease. *J. Alzheimers Dis.* **2011**, *25*, 231–243. [PubMed]
25. Morris, R.G.M.; Garrud, P.; Rawlins, J.A.; O'Keefe, J. Place navigation impaired in rats with hippocampal lesions. *Nature* **1982**, *297*, 681–683. [CrossRef] [PubMed]

Sample Availability: Samples of the compounds are not available from the authors.

3.2 The Aβ oligomer eliminating D-enantiomeric peptide RD2 improves cognition without changing plaque pathology

Autoren:	van Groen T., **Schemmert S.**, Brener O., Gremer L., Ziehm T., Tusche M, Nagel-Steger L., Kadish I., Schartmann E., Elfgen A., Juergens D., Willuweit A., Kutzsche J, Willbold D.
Journal:	Scientific Reports (2017), veröffentlicht am 24. November 2017
DOI:	10.1038/s41598-017-16565-1
Impact Factor:	4,259 (2016)
Beitrag:	Auswertung und Darstellung der Daten
	Anfertigung aller Abbildungen
	statistische Auswertung
	Hauptverfasserin des Manuskriptes

www.nature.com/scientificreports

SCIENTIFIC REPORTS

OPEN

The Aβ oligomer eliminating D-enantiomeric peptide RD2 improves cognition without changing plaque pathology

Received: 18 July 2017
Accepted: 15 November 2017
Published online: 24 November 2017

Thomas van Groen[1], Sarah Schemmert[2], Oleksandr Brener[2,3], Lothar Gremer[2,3], Tamar Ziehm[2], Markus Tusche[2], Luitgard Nagel-Steger[2,3], Inga Kadish[1], Elena Schartmann[2], Anne Elfgen[2], Dagmar Jürgens[2], Antje Willuweit[4], Janine Kutzsche[2] & Dieter Willbold[2,3]

While amyloid-β protein (Aβ) aggregation into insoluble plaques is one of the pathological hallmarks of Alzheimer's disease (AD), soluble oligomeric Aβ has been hypothesized to be responsible for synapse damage, neurodegeneration, learning, and memory deficits in AD. Here, we investigate the *in vitro* and *in vivo* efficacy of the D-enantiomeric peptide RD2, a rationally designed derivative of the previously described lead compound D3, which has been developed to efficiently eliminate toxic Aβ42 oligomers as a promising treatment strategy for AD. Besides the detailed *in vitro* characterization of RD2, we also report the results of a treatment study of APP/PS1 mice with RD2. After 28 days of treatment we observed enhancement of cognition and learning behaviour. Analysis on brain plaque load did not reveal significant changes, but a significant reduction of insoluble Aβ42. Our findings demonstrate that RD2 was significantly more efficient in Aβ oligomer elimination *in vitro* compared to D3. Enhanced cognition without reduction of plaque pathology in parallel suggests that synaptic malfunction due to Aβ oligomers rather than plaque pathology is decisive for disease development and progression. Thus, Aβ oligomer elimination by RD2 treatment may be also beneficial for AD patients.

Alzheimer's disease (AD) is the most common form of dementia in the elderly[1]. The main characteristic pathological hallmarks of AD are neurodegeneration, neurofibrillary tangles (NFTs), and neuritic plaques in the brain[2]. Intracellular neurofibrillary tangles consist of hyperphosphorylated, twisted filaments of the cytoskeletal protein tau, whereas extracellular plaques are primarily made up of amyloid-β (Aβ)[3], a 39 to 43 amino acid long peptide derived from the proteolytic processing of the amyloid protein precursor (APP)[4]. When APP is cleaved by β- and γ-secretases, the resulting breakdown product is Aβ[5].

Most cases of AD are sporadic, while a small percentage of AD cases are familial[6,7]. These cases are related to mutations in the genes coding for APP, presenilin 1 and 2 (PS1 and PS2)[7]. In general, the mutations influence APP metabolism such that the ratio of Aβ42/Aβ40 is often shifted to higher values[8,9]. Further, it has been shown that duplication of the APP gene[10,11] also results in early AD. Finally, a recent study has demonstrated that a novel mutation in the APP gene protects against the development of AD[12]. Together, these findings imply a central role for APP and its processing for the pathological changes occurring during AD[13,14].

The original amyloid cascade hypothesis[15] postulated that overproduction of Aβ would lead to Aβ deposition in neuritic plaques, which were supposed to be the cause of cognitive deficits. Nowadays, it is thought that soluble Aβ oligomers are the main etiologic agent for pathology and cognitive decline in AD[16–18]. The Aβ oligomers are hypothesized to cause a series of molecular events centring on disrupting the maintenance of synapse structure and function and thus leading to dysfunctional synapses, which are associated with memory loss[19,20].

[1]Department of Cell, Developmental and Integrative Biology, University of Alabama at Birmingham, Birmingham, AL, 35294, USA. [2]Institute of Complex Systems (ICS-6), Structural Biochemistry, Forschungszentrum Jülich GmbH, 52425, Jülich, Germany. [3]Institut für Physikalische Biologie, Heinrich-Heine-Universität Düsseldorf, 40225, Düsseldorf, Germany. [4]Institute of Neuroscience and Medicine (INM-4), Medical Imaging Physics, Forschungszentrum Jülich GmbH, 52425, Jülich, Germany. Correspondence and requests for materials should be addressed to T.G. (email: vangroen@uab.edu) or D.W. (email: d.willbold@fz-juelich.de)

Nowadays, the inhibition of the formation of Aβ oligomers and the elimination of already present Aβ oligomers is thought to be one of the most promising strategies to modify disease progression according to the modified amyloid cascade hypothesis. Currently registered drugs can only ameliorate symptoms and cannot slow down disease progression. Previously, we have reported about a D-enantiomeric peptide, named "D3", which was identified by mirror image phage display and solely consists of D-enantiomeric amino acid residues[21,22]. D3 inhibits the formation of regular Aβ fibrils, eliminates directly and specifically Aβ oligomers and reduces Aβ cytotoxicity *in vitro*[23,24]. *In vivo*, D3 binds to amyloid plaques[25], reduces Aβ plaque load, decreases inflammation and enhances cognition in various transgenic AD mouse models even after oral administration[24,26–28]. In order to enhance D3's potential to remove Aβ oligomers, we have used systematic approaches to identify derivatives with increased Aβ monomer binding activity and increased Aβ oligomer elimination properties[23,29–31]. In parallel, we also tried an additional rational approach to identify more efficient derivatives of D3 and learn more about important sequence motifs. We have identified a compound within this rational design series by the rearrangement of the amino acid residue sequence that showed very promising properties, termed "RD2" (abbreviation for "rational design 2"). In previous studies, we examined the pharmacokinetic characteristics of D3 and RD2[32,33]. These analyses have revealed a higher bioavailability of RD2 compared to D3, indicating improved pharmacokinetic characteristics.

In this study, we examined the *in vitro* profile of RD2 by various analyses to prove our hypothesis whether the rational design enhances the potential of our compound to remove Aβ oligomers. Moreover, we intraperitoneally treated APP/PS1 transgenic mice for only 28 days with RD2 compared to placebo and examined the treatment's influence on cognitive deficits at the end of the treatment period.

Material and Methods

Ethics statement. All experiments were carried out in compliance with the USPHS Guide for Care and Use of Laboratory Animals and approved by the Institutional Animal Care and Use Committee (IACUC; approval number 09457).

Peptides. The compounds D3 (rprtrlhthrnr) and RD2 (ptlhthnrrrrr) with amidated C-termini were purchased as lyophilized powder with >95% purity from JPT Peptide Technologies (JPT, Germany) and Cambridge peptides (Cambridge peptides, United Kingdom), respectively.

Synthetic and recombinant Aβ(1-42) with >95% purity was purchased as lyophilized powder from Bachem (Germany) and Isoloid (Germany), respectively. Biotinylated Aβ(1-42) was also purchased from Bachem (Germany).

Preparation of Aβ(1-42) stock solutions. Lyophilized Aβ(1-42) was dissolved overnight in HFIP (1,1,1,3,3,3-hexafluoro-2-propanol, Sigma-Aldrich, Germany). Aliquots were stored at −20 °C until further processing. Before usage, Aβ(1-42) was lyophilized and dissolved in 10 mM sodium phosphate buffer, pH 7.4.

Surface plasmon resonance measurements. The dissociation constants (K_D) of the compounds binding to Aβ(1-42) were determined by surface plasmon resonance (SPR) measurements using a T200 device (Biacore, GE Healthcare, Sweden). Because of the aggregation tendency of Aβ, especially under the binding assay conditions at neutral pH, Aβ was used solely as a ligand rather than as an analyte. Also, in order to avoid blockage of the microfluidic channels of the SPR device, we have refrained from using larger Aβ assemblies or fibrils as ligands or analytes. Immobilization was performed as described by Frenzel *et al.*[34] with minor modifications. 8 µM N-terminally biotinylated Aβ(1-42) was dissolved in 10 mM sodium phosphate buffer and monomers were separated via density gradient centrifugation as described in the QIAD section. The gradient was fractionated into 14 fractions à 140 µl. Aβ(1-42) monomers from fraction 1 were directly immobilized onto a series S sensor chip SA (Biacore, GE Healthcare, Sweden) by biotin-streptavidin coupling to a final level of 600 RU. The ligand flow cell and a reference flow cell were quenched with 10 µg/ml biotin for 7 min. For affinity determination of RD2 and D3, single cycle kinetic experiments were applied at 25 °C and 30 µl/min flow rate. 0.6 µM, 1.9 µM, 5.6 µM, 16.7 µM, and 50 µM of RD2 or D3 were diluted in 20 mM sodium phosphate buffer including 50 mM sodium chloride, pH 7.4 and injected over the flow cells for 180 s. The reference flow cell and buffer cycles were used for double referencing of the sensorgrams. For evaluation, the sensorgrams were fitted applying the steady state Langmuir 1:1 fit model of the Biacore T200 Evaluation Software 2.0 and the offset was constantly set to zero.

Quantitative determination of interference with Aβ aggregate size distribution (QIAD). For the evaluation of Aβ oligomer elimination of RD2, a QIAD assay (quantitative determination of interference with Aβ aggregate size distribution) was performed according to Brener *et al.*[23]. Briefly, 80 µM Aβ(1-42) was pre-incubated for 4.5 h to enrich Aβ oligomers. Then either RD2 or D3 were added to the pre-incubated solution with the resulting concentration of 20 µM RD2 or D3 and co-incubated for further 40 min. The samples were loaded on top of a density gradient containing 5 to 50% (w/v) iodixanol (OptiPrep, Axis-Shield, Norway) and centrifuged for 3 h at 4 °C and 259.000 × g (Optima TL-100, Beckman Coulter, USA). After centrifugation, 14 fractions à 140 µl were harvested by upward displacement. Fraction 1 from the top of the gradient was the least dense fraction while fraction 14 from just above the bottom was the densest fraction. The pellet of each tube was mixed with 60 µl of a 6 M guanidine hydrochloride solution and boiled for 10 min. The resulting solution represents fraction 15. All fractions were analysed with respect to their Aβ(1-42) content by analytical RP-HPLC (reversed phase-high performance liquid chromatography) and UV absorbance detection at 214 nm. The data for the D3 values and the Aβ(1-42) controls without compounds were already previously used in Brener *et al.*[23]. Analyses were done at least in quadruplicates (D3 and RD2 n = 4, Aβ(1-42) n = 11).

In a second experiment we investigated, whether RD2 eliminates Aβ(1-42) oligomers in a dose-dependent manner. Therefore, the QIAD assay was performed with minor modifications. Instead of 15 single fractions the

fractions 1 to 3, 4 to 6, 7 to 9, 10 to 11 and 12 to 14 have been pooled resulting in a total of six fractions. RD2 was added to 80 µM Aβ(1-42) after the 4.5 h incubation step at 1 µM, 5 µM, 10 µM, 20 µM, 30 µM, and 40 µM final concentrations. As described already above for the QIAD, the resulting mixtures were incubated for further 40 min before being applied to density gradient centrifugation. The half-maximal inhibitory concentration (IC_{50}) resulted from the compound concentration at the inflection point obtained by a logistic fit of the data (OriginPro 8.5 G, OriginLab, USA) obtained for fraction 2 (pooled fractions 4 to 6 of the above described QIAD), which contains the pooled oligomers of interest. The experiment has been performed in triplicate (n = 3).

Thioflavin T assay. The Thioflavin T (ThT) assay is a commonly used assay to visualize and quantify the fibrilisation of Aβ, since this dye binds to amyloidogenic cross-β-sheet structures. While Aβ aggregates into fibrils, the ThT fluorescence intensities increase until a saturation level is accomplished. Within this test, we analysed the inhibitory function of RD2 on the Aβ(1-42) fibril formation. 20 µM Aβ(1-42) was incubated with 5 µM ThT and different concentrations of RD2 (serial dilution from 80 µM till 1.25 µM) for IC_{50} calculation. ThT fluorescence was monitored over 21 h every 5 min at $\lambda_{ex} = 440$ nm and $\lambda_{em} = 490$ nm in a fluorescence plate reader (Polarstar Optima, Germany) at 37 °C. Correction was done using all supplements without Aβ. For data evaluation, the fibril masses were determined by subtracting the baseline fluorescence intensities from the top and normalised to the Aβ control to calculate the inhibition in percent. The IC_{50} resulted from the compound concentration at the inflection point obtained by a logistic fit of the data (OriginPro 8.5 G, OriginLab, USA).

Seeding assay. A seeding assay with RD2 was performed to investigate whether RD2 can inhibit the potential of preformed Aβ(1-42) seeds to accelerate the aggregation of monomeric Aβ(1-42). The seeds were prepared by incubating 200 µM monomeric Aβ(1-42) in 10 mM sodium phosphate buffer, pH 7.4, for three days at 37 °C with slight shaking. Afterwards, the sample was centrifuged at 14,000 × g at 4 °C for 45 min. The supernatant was discarded and the loose pellet, which contained the insoluble fibrils, was resuspended in buffer. The sample was sonicated for 2 min in an ultrasonic bath to disperse large Aβ aggregates. The concentration of Aβ seeds according to the monomers was determined by RP-HPLC[23]. The seeds were incubated with or without RD2 in a molar ratio of 1:1 for 24 h at 37 °C with slight shaking. The samples were sonicated again for 2 min. Lyophyllised monomeric Aβ(1-42) was dissolved at a concentration of 15 µM in buffer immediately before the measurement and was mixed with 1.9 µM seeds (molar ratio of 8:1 monomers:seeds) or 1.9 µM seed-RD2-mix (molar ratio of 8:1:1 of monomers:seeds:RD2). As a control, monomeric Aβ without seeds was used. Every sample was mixed with 20 µM ThT to monitor Aβ aggregation. The ThT fluorescence was monitored for 24 h at 24 °C. Samples were measured in triplicate. The resulting ThT fluorescence intensities were fitted with 5-parametrical logistic fits and the amplitude as well as the half-life was calculated in each case. The amplitude of the fluorescence intensities of the Aβ aggregation alone was set to 100% and the amplitude of the seeded Aβ aggregation with and without RD2 was normalised to it. The measurements were performed in three independent experiments (n = 9).

Cell viability assay (MTT test). MTT (3-(4,5-Dimethylthiazol-2-yl)-2,5-diphenyl-tetrazolium bromide) based cell viability assays were accomplished to examine the cytotoxicity of Aβ(1-42) in the presence of RD2 on two different cell lines, PC-12 (rat pheochromocytoma cell line), and SH-SY5Y (human neuroblastoma cell line) cells[35].

PC-12 cells (DSMZ, Germany) were cultured in DMEM medium supplemented with 10% fetal calf serum, 1% antibiotics (Penicillin/Streptomycin) (all Sigma-Aldrich, USA), and 5% horse serum (PAA Laboratories GmbH, Germany) on collagen A-coated (Biochrom GmbH, Germany) tissue culture flasks (SPL Life Sciences Co., Korea). SH-SY5Y cells (DSMZ, Germany) were cultured in DMEM medium supplemented with 20% fetal calf serum and 1% antibiotics (Penicillin/Streptomycin) (all Sigma-Aldrich, USA) on tissue culture flasks (SPL Life Sciences Co., Korea). Cells were allowed to grow in a humidified incubator with 5% CO_2 at 37 °C and a maximum of 12 (PC-12 cells) or 21 (SH-SY5Y cells) passages. Medium was changed every two days and cells were passaged every three to five days, according to their confluence.

MTT test was performed according to the manufacturer's protocol (CellProliferation Kit I; Roche, Switzerland). PC-12 or SHSY-5Y cells were seeded in clear, collagen-coated 96-well flat bottom microwell plates (Life Technologies Inc., USA) at a density of 1×10^4 cells in a volume of 100 µl per well and incubated for 24 h. For both cell lines, compounds were prepared in the following way as a fivefold determination in three independent experiments. 51 µM Aβ(1-42) was incubated for 4.5 h at 37 °C shaking at 600 rpm. Afterwards, 255 µM RD2 was added and incubated for another 40 min. Throughout the test, cells were exposed to 1 µM Aβ with or without 5 µM RD2. The arithmetic mean of all measurements per approach was calculated. Results are represented as the percentage of MTT reduction, assuming that the absorbance of control cells was 100%.

Animals. For this study, 21 APP/PS1 double transgenic mice (APPSwedish/PS1ΔE9)[36] were used. The very well characterized APP/PS1 mouse model develops cognition deficits and abundant Aβ deposits already at early age. The original mice were purchased from JAX (The Jackson Laboratory, USA) and maintained in our own colony at the University of Alabama in Birmingham. Before treatment, the mice were housed in a controlled environment (humidity 50–60%, temperature 22 °C, light from 06:00 a.m. to 6:00 p.m.) with 4 animals per cage in our facility with food and water available *ad libitum*. After the implantation of the Alzet minipumps the mice were housed individually.

Treatment of APP/PS1 mice. In this study, we treated seven months old female APP/PS1 mice intraperitoneally by use of Alzet osmotic minipumps (Alzet osmotic mini pumps, model #1004, Alzet, USA). Mice were either treated with 5.3 mg/kg/day RD2 (n = 11) or placebo (0.9% sodium chloride solution) (n = 10) as control group. The Alzet minipumps were soaked in sterile 0.9% sodium chloride solution for 24 h before implantation. The next day, the pumps were filled with the appropriate solution and implanted intraperitoneally. In short, mice

were anesthetised with isoflurane, the skin and the muscle layer below were cut in the midline and the pump was inserted in the abdominal cavity. Following placement of the pump, the wound was sutured. Three weeks after the implantations, the mice were tested in different behavioural set ups. 28 days after the implantations, the mice were sacrificed for histopathological analysis. All mice of both groups were included in the experiments described below.

Behavioural tests. The mice were tested at the end of the treatment period in different behavioural tests.

Open field test. The open field test was performed to evaluate the activity and anxiety behaviour of the mice. The arena (42 cm × 42 cm surrounded with clear Plexiglass sides (20 cm high)) was subdivided into two areas: border and centre. The mice were observed with a camera driven tracker system (Ethovision XT10, Noldus, The Netherlands) for 4 min. Time spent in both areas was analysed. After each testing day and in between the mice, the apparatus was wiped out with chlorhexidine and 70% ethanol and allowed to air-dry.

Zero maze. Similar to the open field test, the zero maze was used to assess the anxiety behaviour of the mice. The maze consisted of a circular arena (65 cm diameter) that is raised 40 cm above the table. The maze was separated into four equal parts, with two parts with 15 cm high walls of opaque material and two only 0.5 cm high walls. Therefore, it consisted of two open and two closed areas. The mice were put into the circle and observed for 4 min with a camera driven tracker system (Ethovision XT10, Noldus, The Netherlands). Analysed was the time mice spent in the open and closed arms. After each testing day and in between mice, the apparatus was wiped out with chlorhexidine solution and 70% ethanol and allowed to air-dry.

Morris water maze (MWM). The mice were tested daily for one week in a water maze. Our version of the Morris water maze consists of a blue circular tank (120 cm diameter) filled with clear water (22 °C ± 1 °C). In short, the mice were placed into the water at the edge of the pool and allowed to swim in order to find a hidden but fixed escape platform (0.5 cm below the water surface) by orientating themselves with the help of extramaze cues. The mice were allowed to swim freely for a maximum of 60 s to re-find the hidden platform (or until they climbed onto the hidden platform). If they had not found it, they were placed on the platform for 20 s. Each mouse was tested for three trials per day with inter-trial intervals of 60 s and varying starting positions in a pseudo random order. The platform was placed in the middle of one of the quadrants (south-east) of the pool approximately 30 cm from the edge of the pool. The task of the mice throughout the experiment was to find and escape on the hidden platform. Once the mouse had learned the task (day 6, trial 18), a probe trial was performed immediately following the last trial of acquisition on day 6. In the probe trial (i.e. trial 19), the platform was removed from the pool and animals were allowed to swim for 60 s. Mice were recorded with a camera driven tracker system (Ethovision XT10, Noldus, The Netherlands). It was analysed the time the mice needed to escape to the hidden platform (escape latency) and the time they spent in the target quadrant (probe trial).

Histopathology. In short, mice were anesthetized, transcardially perfused with ice-cold saline and the brains were removed. The brain was cut in half through the midline. One hemisphere was frozen for biochemical analysis and the other half was fixed overnight in 4% paraformaldehyde. Following overnight postfixation and cryoprotection in 30% sucrose, six series (1 in 6) of coronal sections were cut through the brain. One half of the first series of sections was mounted unstained, the other half was stained for Aβ using the W0-2 antibody (mouse anti-human Aβ4-10, Merck, Germany), as described in detail below. The second series was stained immunohistochemically according to published protocols[37]. One half of the second series was stained for GFAP (mouse anti-GFAP; Sigma-Aldrich, USA), a marker for astrocytes, whereas the other half was stained for Iba-1 (rabbit anti-Iba-1; WAKO, USA), a marker for microglia. Some of the stained sections were double stained with either Congo red, Thioflavin S or Thiazine red. The other three series were stored at −20 °C in antifreeze for future analyses.

The sections from the first series which had been destined for Aβ staining were pre-treated for 30 min with hot citrate buffer (85 °C). The series of sections was transferred into a tris-buffered saline (TBS) solution containing 0.5% Triton X-100 (TBS-T) and the primary antibody. 18 h after incubation in this solution at room temperature (20 °C) on a shaker table in the dark, the sections were rinsed three times with TBS-T and transferred into a solution with the secondary antibody (goat anti-mouse*biotin (Sigma-Aldrich, Germany), or sheep anti-rat Ig*biotin (Biorad, USA)) and incubated for two hours. Then, the sections were rinsed three times with TBS-T and transferred into a solution with mouse ExtrAvidin (Sigma-Aldrich, Germany). Following rinsing, the sections were incubated for approximately 3 min with a 3,3′-Diaminobenzidine (DAB) solution enhanced with a saturated nickel ammonium sulphate solution. All stained sections were mounted on slides and coverslipped.

Plaque quantification. The plaque load of the appropriate areas (dorsal hippocampus and parietal cortex) of the brains was determined as described previously[28].

Biochemistry. Diluted brain samples were assayed for Aβ(x-40) and Aβ(x-42) as described previously[24,26,28].

Statistics. All statistical calculations were performed using GraphPad Prism 5 (GraphPad Software, Inc., USA) or SigmaPlot Version 11 (Systat Software, Germany). Data is represented as mean ± SD (SPR, QIAD, ThT assay, seeding assay, MTT test) or SEM (behavioural tests, histochemical and biochemical analysis), $p > 0.05$ was considered as not significant (n.s.). Normal distribution of data was either tested by use of Shapiro-Wilk normality test or by use of a normal probability plot (InVivoStat, Version 3.4.0.0, UK)[38]. Normal distributed data was analysed with one-way ANOVA with Bonferroni post hoc analysis (QIAD assay, seeding assay, MTT test). Two-way ANOVA with Bonferroni post hoc analysis was used to analyse the results of the *in vivo* study (open

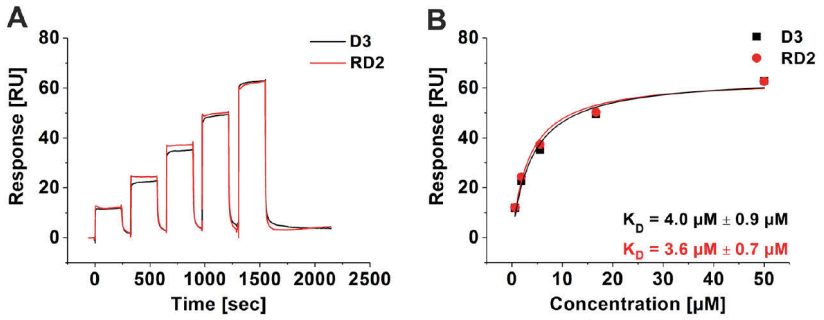

Figure 1. Affinity determination of D3 and RD2 by SPR. N-terminally biotinylated Aβ(1-42) was immobilised on a streptavidin sensor chip and the binding of different D3 (black) and RD2 (red) concentrations was analysed in a single cycle (**A**). For evaluation, the steady-state binding signals were plotted over the concentrations and fitted using a Langmuir 1:1 binding model (**B**). Data is represented as values ± errors of the fit.

field test, zero maze, probe trial Morris water maze, ELISA). Escape latency to the platform within the Morris water maze was considered as not normally distributed and therefore analysed by Friedman Repeated Measures ANOVA on Ranks with Dunn's post hoc analysis.

Results

RD2 and D3 bound to Aβ(1-42) with similar affinities. Binding affinities of D3 and RD2 were determined using surface plasmon resonance (SPR). Monomeric N-terminally biotinylated Aβ(1-42) was immobilized on the surface and concentration dependent series with the respective compound were injected (Fig. 1A). Steady-state analysis of the data revealed similar dissociation constants (K_D) for both peptides which were 4.0 µM ± 0.9 µM for D3 and 3.6 µM ± 0.7 µM for RD2 (Fig. 1B).

RD2 eliminated Aβ oligomers. *In vitro*, the influence of RD2 and D3 on the Aβ aggregate size distribution was tested by the assay for quantitative determination of interference with Aβ aggregate size distribution (Aβ QIAD)[23] (Fig. 2A). Aβ species located in fractions 4 to 6 of the density gradient were efficiently eliminated by RD2 and D3 (Fig. 2B). Aβ species located in these fractions are Aβ oligomers, which were previously characterised in detail[23]. They have a molecular weight of about 100 kDa, corresponding to about 23 monomeric units. Both, RD2 and D3 significantly reduced the amount of Aβ oligomers in fractions 4 to 6 by 71% and 51%, respectively (Fig. 2B, one-way ANOVA, $p \leq 0.001$, Bonferroni post hoc analysis, Aβ(1-42) vs. D3 or RD2 in fractions 4–6, $p \leq 0.001$, fraction 4 D3 vs RD2, $p = 0.019$, fraction 5 D3 vs RD2, $p = 0.025$, fraction 6 D3 vs RD2, $p = 0.045$) without causing a significant change of the Aβ monomer amount in the first fractions of the density gradient (one-way ANOVA, $p = 0.19$). Although RD2 and D3 have the same qualitative effect on Aβ oligomers, RD2 was found to be significantly more efficient in Aβ oligomer elimination (Fig. 2B). Furthermore, a QIAD assay for Aβ(1-42) size distributions was performed in dependence of different RD2 concentration (Fig. 2C). Based on the results of the performed assay it could be shown that RD2 eliminates Aβ(1-42) oligomers in a dose-dependent manner with a resulting half-maximal inhibition concentration (IC_{50}) of 8.4 µM (Fig. 2D).

Aβ fibril formation was inhibited by RD2 in a dose-dependent manner. Investigation of the functional effect of RD2 on Aβ(1-42) fibril formation was accomplished by Thioflavin T (ThT). As demonstrated in Fig. 3A, RD2 inhibited the formation of Aβ(1-42) fibrils in a dose-dependent manner and a half-maximal inhibition concentration (IC_{50}) of 7.7 µM was determined (Fig. 3B). Thus, the IC_{50} value is in very good agreement with the K_D value obtained by SPR, indicating that the binding event is responsible for the inhibitory function of RD2.

RD2 reduced the catalytic effect of preformed seeds on Aβ aggregation. To investigate whether RD2 can inhibit the seeding potential of Aβ, a seeding assay was performed. The aggregation of monomeric Aβ(1-42) alone or together with preformed Aβ(1-42) seeds incubated with and without RD2 was monitored. The resulting intensities were fitted and the amplitude and the half-life ($t_{1/2}$) were calculated. For monomeric Aβ(1-42) without seeds $t_{1/2}$ was 11.6 h, whereas the aggregation of seeded monomeric Aβ(1-42) was significantly ($p \leq 0.001$) accelerated to a half-life of 1 h (one-way ANOVA with Bonferroni post hoc analysis) (Fig. 4A). 24 h incubation of RD2 with seeds decelerated the aggregation of monomeric Aβ significantly ($p \leq 0.001$) by factor of 5 (4.6 h) compared to seeded Aβ without RD2. This indicates that RD2 lowers the catalytic effect of the seeds on Aβ aggregation *in vitro*. The amplitude of seeded Aβ was not affected by the pre-treatment of the seeds with RD2 (Fig. 4B). This observation supports the hypothesis that the observed effect in Fig. 4A was indeed due to the potential of RD2 to reduce the seeding potential of the seeds during the pre-treatment rather than due to any remaining free RD2, which would reduce also the overall fibril formation as shown in Fig. 3A.

Increased cell viability after pre-incubation of Aβ(1-42) assemblies with RD2. The MTT cell viability test was performed to survey the effects of RD2 co-incubated with Aβ(1-42) on PC-12 and SH-SY5Y cells. PC-12 cells are extensively used to study Aβ induced neurotoxicity, because this cell type is vulnerable to Aβ. Additionally, we have used SH-SY5Y cells in addition to study the effects on a more appropriate neuronal cell

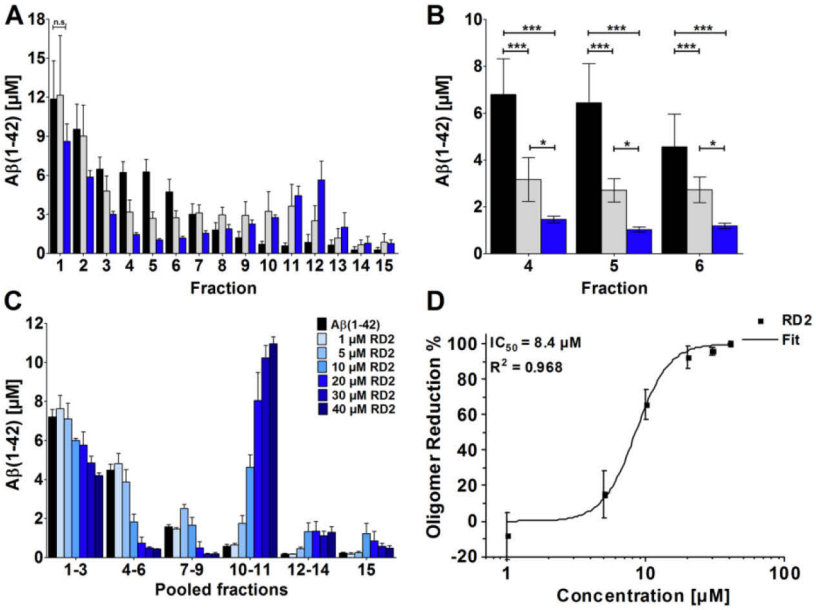

Figure 2. RD2 eliminated Aβ(1-42) oligomers in a concentration dependent manner. Aβ(1-42) size distributions without D-peptide (black in **A**–**C**) and in the presence of compounds were analysed by density gradient centrifugation. Aβ(1-42) concentrations for each fraction were determined by UV absorption during RP-HPLC. Aβ(1-42) oligomers of interest are located in fractions 4 to 6 (**A**–**C**). Comparison of 20 µM D3 (grey) and 20 µM RD2 (blue) (**A**,**B**) revealed the superior oligomer elimination efficacy of RD2. In (**C**) the QIAD assay for Aβ(1-42) size distributions in dependence of different RD2 concentrations (0 µM black, 1 µM till 40 µM, from light to dark blue) are shown. Graphical representation of the measured decrease in oligomer concentration in % of the amount of oligomers found in the control with 0 µM RD2 in dependence of the different RD2 concentration. The curve was fitted according to a logistic fit function yielding an IC_{50} value (**D**). In each experiment, data is represented as mean ± SD; A: one-way ANOVA, with Bonferroni post hoc analysis, Aβ(1-42) vs. D3 or RD2 in fractions 4–6, ***$p \leq 0.001$, fraction 4 D3 vs RD2, *$p = 0.019$, fraction 5 D3 vs RD2, *$p = 0.025$, fraction 6 D3 vs RD2, *$p = 0.045$. Data of Aβ(1-42) and D3 were taken from Brener *et al.*[23].

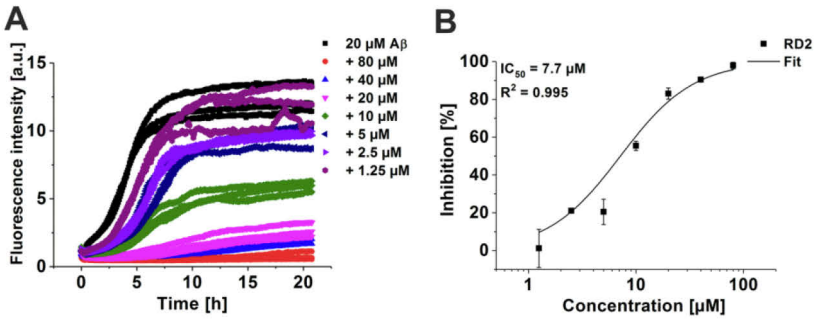

Figure 3. Inhibitory function of RD2 for Aβ(1-42) fibril formation. Aβ(1-42) fibril formation was monitored by Thioflavin T (ThT) in the absence or presence of different RD2 concentrations (0 µM black, 80 µM red, 40 µM light blue, 20 µM pink, 10 µM green, 5 µM blue, 2.5 µM lilac, 1.25 µM purple) (**A**). Fibril mass was normalised to the Aβ control and the inhibition in % was calculated. The curve was fitted according to a logistic fit function yielding an IC_{50} value (**B**). The data represent three replicates.

type. We incubated Aβ(1-42), at a final concentration of 1 µM, with and without 5 µM RD2 on PC-12 or SH-SY5Y cells. We found a significant increase of cell viability of PC-12 and SH-SY5Y cells after pre-incubation of Aβ with RD2 from 25% to 76% (Fig. 5A) and 65% to 94% (Fig. 5B), respectively (both: one-way ANOVA, $p \leq 0.001$ with

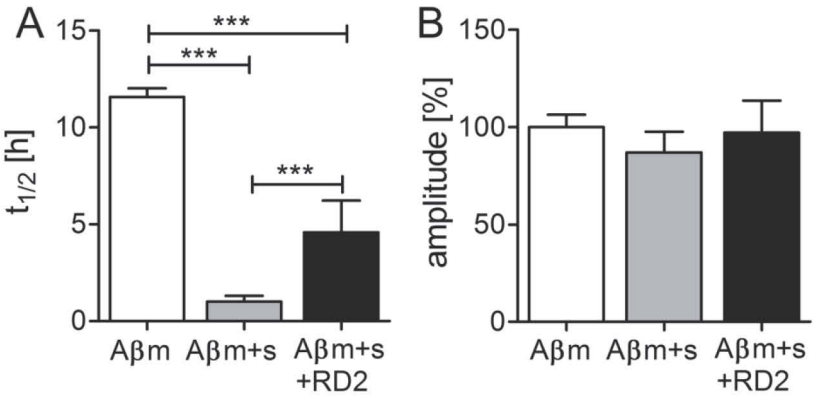

Figure 4. Influence of RD2 on the seeded Aβ(1-42) aggregation. The aggregation of monomeric Aβ without (m, white), and with preformed seeds (s, grey) incubated with or without RD2 (black) was monitored and the half-life ($t_{1/2}$) (**A**) as well as the amplitude (**B**) of the aggregation was determined. In (**B**) the amplitude of monomeric Aβ without seeds was set to be 100% and the amplitudes of the other samples were normalized accordingly. Data is represented as mean ± SD, one-way ANOVA with Bonferroni post hoc analysis, ***$p \leq 0.001$.

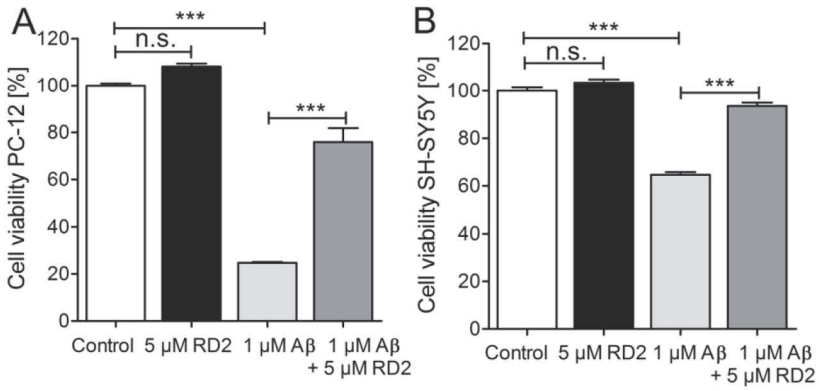

Figure 5. RD2 reduced the negative impact of Aβ(1-42) on cell viability in PC-12 and SH-SY5Y cells. Cell viability was assessed by MTT after incubation of PC-12 (**A**) or SH-SY5Y (**B**) cells with 1 μM Aβ(1-42) (light grey) or 1 μM Aβ(1-42) co-incubated with 5 μM RD2 (grey), respectively. Data confirms the efficacy of RD2 to significantly increase the cell viability after co-incubation with Aβ(1-42) on both cell lines compared to Aβ(1-42) alone. Data is represented as mean ± SD, one-way ANOVA with Bonferroni post hoc analysis, ***$p \leq 0.001$.

Bonferroni post hoc analysis: $p \leq 0.001$). In order to demonstrate that RD2 alone did not influence cell viability, 5 μM RD2 were incubated with both cells lines, which did not result in any change of cell viability compared to buffer control (one-way ANOVA: n.s., $p = 0.4$, Fig. 5A and B).

Treatment with RD2 improved cognition without showing any influence on activity or anxiety. Implantation of Alzet osmotic minipumps filled with RD2 solution or saline (placebo) into APP/PS1 mice neither changed any obvious physiological parameters (e.g. growth as measured by body weight (placebo: 25.7 ± 0.9 g vs RD2: 26.8 ± 0.8 g) or general health, i.e. look of fur, posture, and motor activity) in the implanted mice, nor caused any noticeable discomfort. None of the mice developed any health or motor problems.

After three weeks of placebo or RD2 treatment of APP/PS1 mice, both groups were tested in the open field and zero maze tests. As demonstrated in Fig. 6, there were no significant differences in activity or anxiety levels between the two groups of mice (Fig. 6A; total distance moved in the open field: 2143 ± 217 cm vs 2121 ± 163 cm, respectively, both two-way ANOVA with Bonferroni post hoc analysis, $p = 1$). Speeds in the open field was 8.9 ± 0.9 cm/s vs 8.8 ± 0.7 cm/s, respectively, while in the zero maze the average speed of movement was 5.0 ± 0.6 vs 4.8 ± 0.4 cm/s, respectively (Fig. 6A and B). In the following week, the mice were tested in the Morris water maze. There was no difference in the swimming speed between the groups of mice (placebo: 19.0 ± 1 cm/s and RD2: 18.8 ± 1 cm/s). RD2 treated mice did significantly improve their performance during the week of training

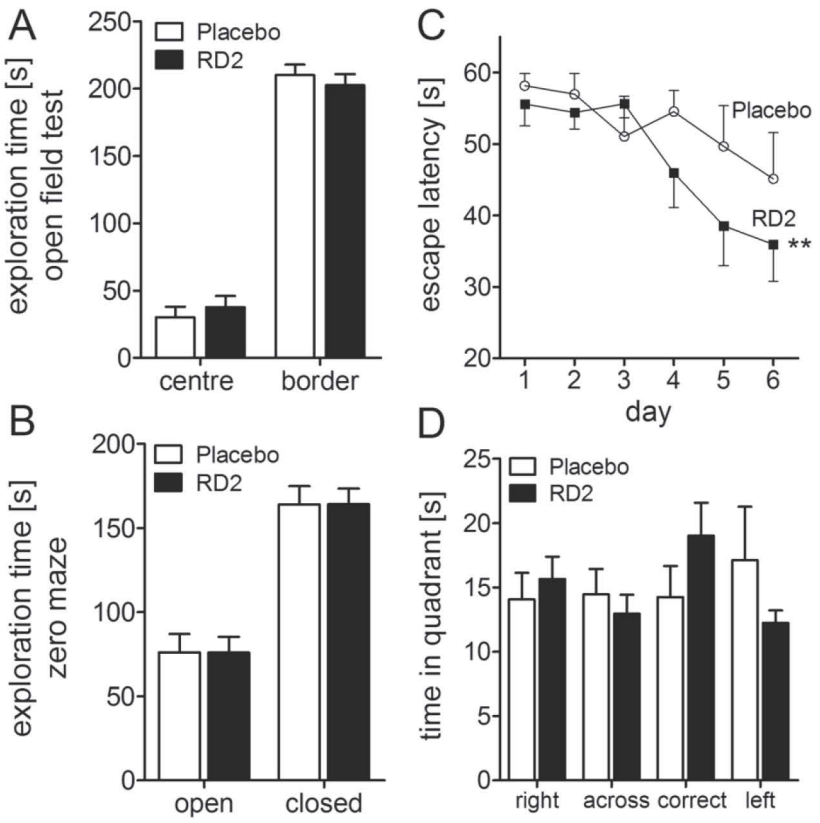

Figure 6. Effects of RD2 on cognition and evaluation of activity and anxiety. Four graphs showing the behaviour of placebo and RD2 treated mice. Assessment of the open field test (**A**) and zero maze (**B**) exhibits no difference of activity or anxiety of RD2 and placebo treated mice. Performance in the water maze showed a significantly improved cognition of RD2 treated mice in contrast to the performance of placebo treated mice (**C**). The RD2 treated group showed a preference for the correct quadrant in the probe trial which followed the last training trial (**D**). Data is represented as mean ± SEM, Friedman Repeated Measures ANOVA on Ranks, (**C**) $^{**}p = 0.003$.

in the Morris water maze compared to the placebo treated mice (escape latency, Friedman RM ANOVA, RD2 treated mice $p = 0.003$, Dunn's post hoc analysis $p \leq 0.05$, placebo treated mice $p = 0.13$, Fig. 6C). Furthermore, the RD2 group showed a preference for the correct quadrant in the probe trial, which followed the last training trial (Fig. 6D). After completion of the behavioural testing, the animals were sacrificed and the brains were removed for further analysis.

The Aβ load was measured in the dorsal hippocampus and parietal cortex by immunohistochemical staining for human Aβ(4-10) (W0-2 antibody). Treatment with RD2 did not reveal any reduction of the Aβ plaque load in the hippocampus or in the cortex compared to the placebo treated mice (% area covered, Fig. 7A–F). Furthermore, analysis of the sections that were stained for activated astrocytes (GFAP) or microglia (Iba-1) revealed that the magnitude of inflammation surrounding Aβ deposits did not differ between the two treatment groups of mice. Neither did RD2 treatment significantly reduce the amount of plaque related microglial inflammation (Iba-1; average density 40.5 ± 2.0 vs 40.7 ± 1.5, respectively; Fig. 7G–I) compared to the placebo treated mice. Nor did treatment with RD2 significantly change the amount of plaque-related activated astrocytes (GFAP; average density 34.6 ± 1.4 vs 36.7 ± 1.7, Fig. 7J–L) compared to the placebo treated mice within the hippocampus. Double staining for microglia and astrocytes confirmed that in the surroundings of all labelled plaques both glial cell types were activated.

The biochemical analysis by ELISA measurements demonstrated that Aβ(x-40) levels did not differ significantly between RD2 and placebo treated mice (insoluble Aβ(x-40): 142.5 ± 3.9 pg/g vs 148.1 ± 3.0 pg/g; soluble Aβ(x-40): 38.9 ± 5.2 pg/g vs 47.8 ± 7.4 pg/g, respectively, Fig. 8A). However, a significant decrease of insoluble Aβ(x-42) levels was detected in the hippocampus of RD2 treated mice in contrast to the placebo treated mice (insoluble Aβ(x-42): 168.8 ± 19.2 pg/g vs 219.4 ± 15.3 pg/g; soluble Aβ(x-42): 15.5 ± 2.6 pg/g vs 23.5 ± 5.1 pg/g respectively, two-way ANOVA, $p = 0.027$ with Bonferroni post hoc analysis, $p = 0.048$, Fig. 8B). Furthermore,

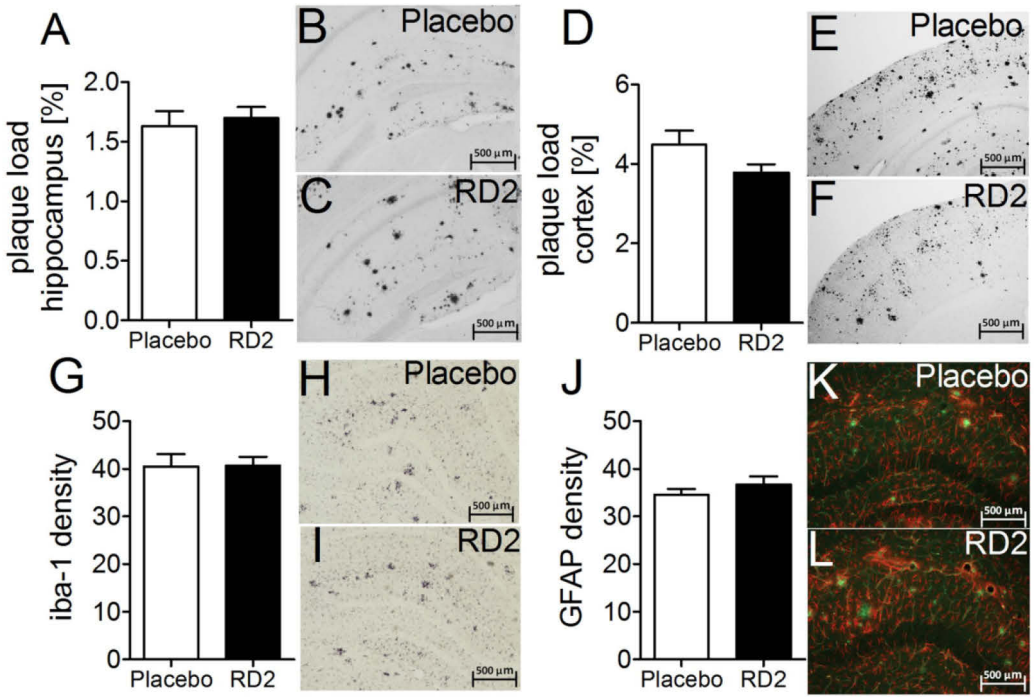

Figure 7. Histopathological analysis of AD pathology in hippocampus revealed no change after intraperitoneal treatment with RD2. Aβ load measured in hippocampus and parietal cortex (**A**–**F**), microglia (**G**–**I**) and activated astrocytes (**J**,**K**) were analysed after the behavioural tests. Data indicates that there is no change in AD typical pathology after 28 days of intraperitoneal treatment with RD2 compared to the pathology of placebo treated mice. Data is represented as mean ± SEM.

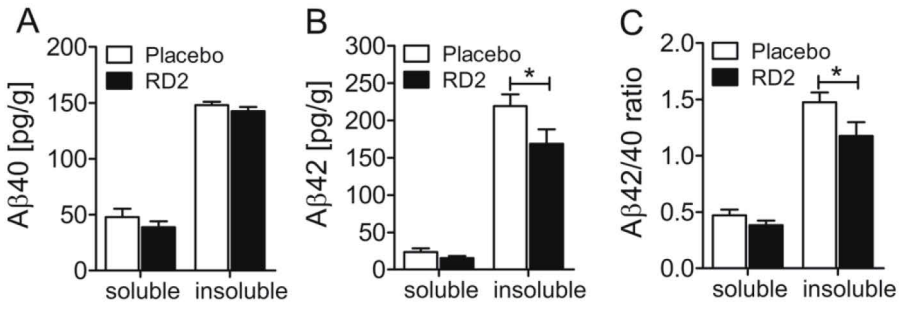

Figure 8. Treatment with RD2 significantly reduced the level of insoluble Aβ(x-42). Levels of Aβ(x-40) (**A**) and Aβ(x-42) (**B**) were analysed in soluble and insoluble fractions of hippocampus by ELISA. Treatment with RD2 exhibited a significant decrease of insoluble Aβ(x-42) level in the hippocampus and significantly lowered the Aβ42/40 ratio (**C**). Data is represented as mean ± SEM, two-way ANOVA with Bonferroni post hoc analysis, (**B**) *p = 0.027, (**C**) *p = 0.026.

treatment with RD2 lowered significantly the ratio of insoluble Aβ42/40 (insoluble Aβ42/40: RD2 1.2 ± 0.1 vs placebo 1.5 ± 0.1; soluble Aβ42/40: RD2 0.4 ± 0.1 vs placebo 0.5 ± 0.1, respectively: two-way ANOVA, p = 0.026 with Bonferroni post hoc analysis, p = 0.047, Fig. 8C).

Discussion

Finding a curative and disease modifying treatment for AD is one of the major challenges of the 21st century. Despite the fact of increasing prevalence of AD, current treatment options are only symptomatic[39], a situation that is considered inacceptable. Today, soluble Aβ oligomers are postulated to be the disease causing

agent and consequently, their elimination is a promising target for therapy. Within the last years, we developed D-enantiomeric peptides, solely consisting of D-enantiomeric amino acid residues, for stabilisation of Aβ monomers in an aggregation incompetent conformation, leading to the specific and direct elimination of Aβ oligomers[23,26].

Here, we characterised our all-D-enantiomeric amino acid residue compound RD2. RD2 is a derivative of the lead compound D3, which was characterised before[24,27,40]. Based on steady state analysis, both compounds, D3 and RD2, showed similar binding affinities to Aβ(1-42) monomers with an equilibrium dissociation constant in the micromolar range, which was shown previously and validated within this study[41]. However, the potential of RD2 to eliminate Aβ oligomers is significantly increased in comparison to D3. Moreover, RD2 eliminates Aβ(1-42) oligomers in a dose-dependent manner with an IC_{50} of 8.4 µM. Additionally, RD2 significantly reduced the cytotoxic potential of Aβ(1-42), shown by the enhanced cell viability in PC-12 and SHSY-5Y cells after co-incubation of Aβ(1-42) with RD2 and inhibited the Aβ(1-42) fibril formation with an IC_{50} of 7.7 µM. This is in very good agreement with the results of the QIAD assay. In accordance with the Aβ oligomer eliminating properties of RD2, RD2 also inhibited the seeding potential of Aβ aggregates.

Investigation of the *in vivo* efficacy of RD2 was carried out in an intraperitoneal treatment study with APP/PS1 transgenic mice. Thereby we could prove our hypothesis that RD2 showed a similar or increased efficacy compared to D3. Short term treatment with RD2 improved cognitive performance significantly after three weeks compared to the placebo control group. Treatment with RD2 did not lead to a significant reduction in the amount of Aβ deposits in the hippocampus. As it is expected that there is an equilibrium between soluble and plaque Aβ, longer treatment periods could have possibly led to a significant reduction of Aβ pathology. Furthermore, analysis of the microglia and astrocytes did not show significant reduction in activated microglia and astrocytes in RD2 treated mice compared to the placebo treated mice. Consequently, improved cognitive performance was not related to a decrease in plaque pathology. Since RD2 significantly reduced the amount of Aβ oligomers *in vitro*, a more likely explanation is that RD2 decreases synaptic toxicity and pathology by reducing the amount of Aβ oligomers *in vivo*, even without significantly changing the Aβ plaque load.

RD2 significantly reduced levels of insoluble Aβ(x-42) in the hippocampus, but did not show any significant reduction of Aβ(x-40) levels. This ultimately led to a decrease of the Aβ42/Aβ40 ratio, without affecting total Aβ levels. What that actually means remains to be elucidated. We hypothesize that the Aβ oligomer eliminating activity of RD2 is based on its binding to Aβ monomers and their stabilisation in an aggregation-incompetent conformation, thereby shifting the equilibrium between monomeric and oligomeric Aβ away from Aβ oligomers, ultimately leading to the elimination of Aβ oligomers. It certainly increases the need to further investigate the underlying mechanism of RD2 based on the improvement of cognitive performance. Irrespective of that, these observations strengthen the potential role of RD2 as a disease-modifying agent for AD treatment. Besides that, the outcome of this study supports the finding that there is not a necessarily dependence between plaque pathology and cognition. Compared with other drugs targeting Aβ oligomers (e.g. antibodies) our compound RD2 does not only interact with Aβ oligomers but directly destroys them without relying on the contribution of components of the immune system. Future treatment studies with RD2 in other transgenic AD mouse models will further elucidate the compound's mechanism of action and its future potential.

Conclusion

Summarised, the identified derivative of the lead compound D3, named RD2, was significantly more efficient in elimination of Aβ oligomers than D3. RD2 improved cognitive performance of APP/PS1 mice already after a short, three weeks, treatment and reduced insoluble Aβ(x-42) levels in the brain without a negative impact on activity or anxiety. Based on this, RD2 is a promising compound to be further developed as a drug candidate for therapy of AD.

References

1. Hirtz, D. *et al.* How common are the "common" neurologic disorders? *Neurology* **68**, 326–337, https://doi.org/10.1212/01.wnl.0000252807.38124.a3 (2007).
2. Montine, T. J. *et al.* National Institute on Aging-Alzheimer's Association guidelines for the neuropathologic assessment of Alzheimer's disease: a practical approach. *Acta neuropathologica* **123**, 1–11, https://doi.org/10.1007/s00401-011-0910-3 (2012).
3. Ballard, C. *et al.* Alzheimer's disease. *Lancet* **377**, 1019–1031, https://doi.org/10.1016/S0140-6736(10)61349-9 (2011).
4. O'Brien, R. J. & Wong, P. C. Amyloid precursor protein processing and Alzheimer's disease. *Annual review of neuroscience* **34**, 185–204, https://doi.org/10.1146/annurev-neuro-061010-113613 (2011).
5. Selkoe, D. J. & Hardy, J. The amyloid hypothesis of Alzheimer's disease at 25 years. *EMBO molecular medicine* **8**, 595–608, https://doi.org/10.15252/emmm.201606210 (2016).
6. Bertram, L. & Tanzi, R. E. Alzheimer's disease: one disorder, too many genes? *Human molecular genetics* **13**(Spec No 1), R135–141, https://doi.org/10.1093/hmg/ddh077 (2004).
7. Bertram, L., Lill, C. M. & Tanzi, R. E. The genetics of Alzheimer disease: back to the future. *Neuron* **68**, 270–281, https://doi.org/10.1016/j.neuron.2010.10.013 (2010).
8. Van Broeck, B., Van Broeckhoven, C. & Kumar-Singh, S. Current insights into molecular mechanisms of Alzheimer disease and their implications for therapeutic approaches. *Neurodegenerative Diseases.* **4**, 349–365 (2007).
9. Pauwels, K. *et al.* Structural basis for increased toxicity of pathologicalabeta42: abeta40 ratios in Alzheimer disease. *The Journal of biological chemistry* **287**, 5650–5660, https://doi.org/10.1074/jbc.M111.264473 (2012).
10. Rovelet-Lecrux, A. *et al.* APP locus duplication causes autosomal dominant early-onset Alzheimer disease with cerebral amyloid angiopathy. *Nature genetics* **38**, 24–26, https://doi.org/10.1038/ng1718 (2006).
11. Sleegers, K. *et al.* APP duplication is sufficient to cause early onset Alzheimer's dementia with cerebral amyloid angiopathy. *Brain: a journal of neurology* **129**, 2977–2983, https://doi.org/10.1093/brain/awl203 (2006).
12. Jonsson, T. *et al.* A mutation in APP protects against Alzheimer's disease and age-related cognitive decline. *Nature* **488**, 96–99, https://doi.org/10.1038/nature11283 (2012).
13. Braak, H. & Braak, E. Neuropathological stageing of Alzheimer-related changes. *Acta neuropathologica* **82**, 239–259 (1991).

14. Braak, H. & Braak, E. Staging of Alzheimer's disease-related neurofibrillary changes. *Neurobiology of aging* **16**, 271–278; discussion 278–284 (1995).
15. Hardy, J. A. 'anatomical cascade hypothesis' for Alzheimer's disease. *Trends in Neurosciences* **15**, 200–201 (1992).
16. Crews, L. & Masliah, E. Molecular mechanisms of neurodegeneration in Alzheimer's disease. *Human molecular genetics* **19**, R12–20, https://doi.org/10.1093/hmg/ddq160 (2010).
17. Larson, M. E. & Lesne, S. E. Soluble Abeta oligomer production and toxicity. *Journal of neurochemistry* **120**(Suppl 1), 125–139, https://doi.org/10.1111/j.1471-4159.2011.07478.x (2012).
18. Ferreira, S. T., Lourenco, M. V., Oliveira, M. M. & De Felice, F. G. Soluble amyloid-beta oligomers as synaptotoxins leading to cognitive impairment in Alzheimer's disease. *Frontiers in cellular neuroscience* **9**, 191, https://doi.org/10.3389/fncel.2015.00191 (2015).
19. Ferreira, S. T. & Klein, W. L. The Abeta oligomer hypothesis for synapse failure and memory loss in Alzheimer's disease. *Neurobiology of learning and memory* **96**, 529–543, https://doi.org/10.1016/j.nlm.2011.08.003 (2011).
20. Wilcox, K. C., Lacor, P. N., Pitt, J. & Klein, W. L. Abeta oligomer-induced synapse degeneration in Alzheimer's disease. *Cellular and molecular neurobiology* **31**, 939–948, https://doi.org/10.1007/s10571-011-9691-4 (2011).
21. Schumacher, T. N. *et al.* Identification of D-peptide ligands through mirror-image phage display. *Science* **271**, 1854–1857 (1996).
22. Wiesehan, K. *et al.* Selection of D-amino-acid peptides that bind to Alzheimer's disease amyloid peptide abeta1-42 by mirror image phage display. *Chembiochem: a European journal of chemical biology* **4**, 748–753, https://doi.org/10.1002/cbic.200300631 (2003).
23. Brener, O. *et al.* QIAD assay for quantitating a compound's efficacy in elimination of toxic Abeta oligomers. *Scientific reports* **5**, 13222, https://doi.org/10.1038/srep13222 (2015).
24. van Groen, T. *et al.* Reduction of Alzheimer's disease amyloid plaque load in transgenic mice by D3, A D-enantiomeric peptide identified by mirror image phage display. *ChemMedChem* **3**, 1848–1852, https://doi.org/10.1002/cmdc.200800273 (2008).
25. van Groen, T., Kadish, I., Wiesehan, K., Funke, S. A. & Willbold, D. *In vitro* and *in vivo* staining characteristics of small, fluorescent, Abeta42-binding D-enantiomeric peptides in transgenic AD mouse models. *ChemMedChem* **4**, 276–282, https://doi.org/10.1002/cmdc.200800289 (2009).
26. Funke, S. A. *et al.* Oral Treatment with the d-Enantiomeric Peptide D3 Improves the Pathology and Behavior of Alzheimer's Disease Transgenic Mice. *ACS chemical neuroscience* **1**, 639–648, https://doi.org/10.1021/cn100057j (2010).
27. van Groen, T., Kadish, I., Funke, A. S., Bartnik, D. & Willbold, D. Treatment with Aβ42 Binding d-Amino Acid Peptides Reduce Amyloid Deposition and Inflammation in APP/PS1 Double Transgenic Mice. *Advances in Protein Chemistry and Structural Biology* **88**, 133–152 (2012).
28. van Groen, T., Kadish, I., Funke, S. A., Bartnik, D. & Willbold, D. Treatment with D3 removes amyloid deposits, reduces inflammation, and improves cognition in aged AbetaPP/PS1 double transgenic mice. *Journal of Alzheimer's disease: JAD* **34**, 609–620, https://doi.org/10.3233/JAD-121792 (2013).
29. Klein, A. N. *et al.* Optimization of the All-D Peptide D3 for Abeta Oligomer Elimination. *PloS one* **11**, e0153035, https://doi.org/10.1371/journal.pone.0153035 (2016).
30. Ziehm, T. *et al.* Increase of Positive Net Charge and Conformational Rigidity Enhances the Efficacy of d-Enantiomeric Peptides Designed to Eliminate Cytotoxic Abeta Species. *ACS chemical neuroscience*, https://doi.org/10.1021/acschemneuro.6b00047 (2016).
31. Klein, A. N. *et al.* Optimization of D-peptides for Abeta monomer binding specificity enhances their potential to eliminate toxic Abeta oligomers. *ACS chemical neuroscience*, https://doi.org/10.1021/acschemneuro.7b00045 (2017).
32. Jiang, N. *et al.* Preclinical Pharmacokinetic Studies of the Tritium Labelled D-Enantiomeric Peptide D3 Developed for the Treatment of Alzheimer s Disease. *PloS one* **10**, e0128553, https://doi.org/10.1371/journal.pone.0128553 (2015).
33. Leithold, L. H. *et al.* Pharmacokinetic Properties of a Novel D-Peptide Developed to be Therapeutically Active Against Toxic beta-Amyloid Oligomers. *Pharmaceutical research* **33**, 328–336, https://doi.org/10.1007/s11095-015-1791-2 (2016).
34. Frenzel, D. *et al.* Immobilization of homogeneous monomeric, oligomeric and fibrillar Abeta species for reliable SPR measurements. *PloS one* **9**, e89490, https://doi.org/10.1371/journal.pone.0089490 (2014).
35. Biedler, J. L., Roffler-Tarlov, S., Schachner, M. & Freedman, L. S. Multiple neurotransmitter synthesis by human neuroblastoma cell lines and clones. *Cancer research* **38**, 3751–3757 (1978).
36. Jankowsky, J. L. *et al.* Co-expression of multiple transgenes in mouse CNS: a comparison of strategies. *Biomolecular engineering* **17**, 157–165 (2001).
37. van Groen, T., Kiliaan, A. J. & Kadish, I. Deposition of mouse amyloid beta in human APP/PS1 double and single AD model transgenic mice. *Neurobiology of disease* **23**, 653–662, https://doi.org/10.1016/j.nbd.2006.05.010 (2006).
38. Clark, R. A., Shoaib, M., Hewitt, K. N., Stanford, S. C. & Bate, S. T. A comparison of *InVivo*Stat with other statistical software packages for analysis of data generated from animal experiments. *Journal of psychopharmacology* **26**, 1136–1142, https://doi.org/10.1177/0269881111420313 (2012).
39. Briggs, R., Kennelly, S. P. & O'Neill, D. Drug treatments in Alzheimer's disease. *Clinical Medicine* **16**, 247–253 (2016).
40. Funke, A. S. *et al.* Oral treatment with the d-enantiomeric peptide D3 improves the pathology and behavior of Alzheimer's Disease transgenic mice. *ACS chemical neuroscience* **1**, 639–648, https://doi.org/10.1021/cn100057j (2010).
41. Olubiyi, O. O. *et al.* Amyloid aggregation inhibitory mechanism of arginine-rich D-peptides. *Current medicinal chemistry* **21**, 1448–1457 (2014).

Acknowledgements

Financial support of D.W. was provided by "Portfolio Technology and Medicine", the Helmholtz-Validierungsfonds of the Impuls and Vernetzungs-Fonds der Helmholtzgemeinschaft. D.W. was supported by the "Portfolio Drug Research" of the Impuls and Vernetzungs-Fonds der Helmholtzgemeinschaft. T.V.G. was partially supported by P30 NS47466.

Author Contributions

D.W., T.v.G., and I.K. designed and planned the study. SPR and ThT experiments were performed by T.Z. O.B. and L.G. designed the QIAD assay, O.B. and L.N.-S. performed the QIAD assays. M.T. conducted the MTT tests and A.E. the seeding assay. The *in vivo* study and all associated experiments were performed by T.V.G. and I.K. Statistical analysis was largely done by S.S. T.V.G., S.S. and D.W. wrote the manuscript, whereas all other authors (E.S., D.J., A.W., J.K.) reviewed and contributed to the manuscript.

Additional Information

Competing Interests: The authors declare that they have no competing interests.

Publisher's note: Springer Nature remains neutral with regard to jurisdictional claims in published maps and institutional affiliations.

3.3 Development and validation of an UHPLC-ESI-QTOF-MS method for quantification of the highly hydrophilic amyloid-β oligomer eliminating all-D-enantiomeric peptide RD2 in mouse plasma

Autoren:	Hupert M., Elfgen A., Schartmann E., **Schemmert S**., Buscher B., Kutzsche J., Willbold D., Santiago-Schübel B.
Journal:	Journal of Chromatography B (2017), veröffentlicht am 08. Dezember 2017
DOI:	10.1016/j.jchromb.2017.12.009
Impact Factor:	2,603 (2016)
Beitrag:	RD2-Behandlung der Mäuse
	Vorbereitung der murinen Plasmaproben
	Erstellung Kalibrierreihen zur Erprobung der Methode
	Mitverfassung und Prüfung des Manuskriptes

Journal of Chromatography B 1073 (2018) 123–129

Contents lists available at ScienceDirect

Journal of Chromatography B

journal homepage: www.elsevier.com/locate/jchromb

Development and validation of an UHPLC-ESI-QTOF-MS method for quantification of the highly hydrophilic amyloid-β oligomer eliminating all-D-enantiomeric peptide RD2 in mouse plasma

Michelle Hupert[a,1], Anne Elfgen[b,1], Elena Schartmann[b], Sarah Schemmert[b], Brigitte Buscher[c], Janine Kutzsche[b], Dieter Willbold[b,d,*], Beatrix Santiago-Schübel[a,*]

[a] Forschungszentrum Jülich GmbH, Central Institute for Engineering, Analytics (ZEA-3), Jülich, Germany
[b] Forschungszentrum Jülich GmbH, Institute of Complex Systems, Structural Biochemistry (ICS-6), Jülich, Germany
[c] Triskelion B.V., Zeist, The Netherlands
[d] Institut für Physikalische Biologie, Heinrich-Heine-Universität Düsseldorf, Düsseldorf, Germany

ARTICLE INFO

Keywords:
UHPLC-ESI-QTOF-MS
Mouse plasma
D-peptide
Amyloid-β peptide
Therapeutic compound
Alzheimer's disease

ABSTRACT

During preclinical drug development, a method for quantification of unlabeled compounds in blood plasma samples from treatment or pharmacokinetic studies in mice is required. In the current work, a rapid, specific, sensitive and validated liquid chromatography mass-spectrometric UHPLC-ESI-QTOF-MS method was developed for the quantification of the therapeutic compound RD2 in mouse plasma. RD2 is an all-D-enantiomeric peptide developed for the treatment of Alzheimer's disease, a progressive neurodegenerative disease finally leading to dementia. Due to RD2's highly hydrophilic properties, the sample preparation and the chromatographic separation and quantification were very challenging. The chromatographic separation of RD2 and its internal standard were accomplished on an Acquity UPLC BEH C18 column (2.1 × 100 mm, 1.7 µm particle size) within 6.5 min at 50 °C with a flow rate of 0.5 mL/min. Mobile phases consisted of water and acetonitrile with 1% formic acid and 0.025% heptafluorobutyric acid, respectively. Ions were generated by electrospray ionization (ESI) in the positive mode and the peptide was quantified by QTOF-MS. The developed extraction method for RD2 from mouse plasma revealed complete recovery. The linearity of the calibration curve was in the range of 5.3 ng/mL to 265 ng/mL ($r^2 > 0.999$) with a lower limit of detection (LLOD) of 2.65 ng/mL and a lower limit of quantification (LLOQ) of 5.3 ng/mL. The intra-day and inter-day accuracy and precision of RD2 in plasma ranged from −0.54% to 2.21% and from 1.97% to 8.18%, respectively. Moreover, no matrix effects were observed and RD2 remained stable in extracted mouse plasma at different conditions. Using this validated bioanalytical method, plasma samples of unlabeled RD2 or placebo treated mice were analyzed. The herein developed UHPLC-ESI-QTOF-MS method is a suitable tool for the quantitative analysis of unlabeled RD2 in plasma samples of treated mice.

1. Introduction

RD2 is an all-D-enantiomeric peptide specifically and directly targeting amyloid β peptide (Aβ) oligomers, which play a major role in the pathogenesis of Alzheimer's disease (AD), a progressive neurodegenerative disease leading to loss of memory [1]. The neuropathological cause for the development of AD is the aggregation of monomeric Aβ into Aβ oligomers and fibrils followed by the deposition of characteristic senile plaques accompanied by neuronal degeneration [2,3]. However, not the insoluble senile plaques but the soluble Aβ oligomers are currently widely believed to be the most toxic species triggering AD pathology [4–6]. The compound RD2 consists of 12 D-enantiomeric amino acid residues and has an amidated C-terminus (sequence: ptlhthnrrrrr-NH_2). It is the rationally rearranged sequence of the lead compound D3, which was previously selected by mirror image phage display against monomeric Aβ [7]. The rearrangement resulted in enhanced Aβ oligomer elimination [8,9]. *In vitro* assays also revealed that RD2 inhibits Aβ fibril formation efficiently [9]. In studies with AD transgenic mice, RD2 reduced the AD pathology in the mice's brains and showed improvement of cognition [9]. A pharmacokinetic study with the radiolabeled compound (^{3}H-RD2) revealed that RD2 has a high oral bioavailability, long blood circulation and an efficient blood brain

* Corresponding authors.
[1] These authors contributed equally to this work.

https://doi.org/10.1016/j.jchromb.2017.12.009
Received 22 September 2017; Received in revised form 30 November 2017; Accepted 6 December 2017
Available online 08 December 2017
1570-0232/

barrier permeability [10]. In these studies, it could be shown via thin layer chromatography with auto-radiographic detection that ^{3}H-RD2 remains stable after incubation in different body fluids and tissues. However, it is desirable to monitor RD2 levels also without any radioactive label in order to follow for example long-term treatment studies. Thus, as a first step, a suitable extraction method for the highly hydrophilic, arginine-rich RD2 from blood plasma followed by a rapid, sensitive and validated method for quantitative analysis of unlabeled RD2 via LC–MS has been developed for pharmacokinetic or treatment studies in this work. All validation parameters were carried out on the Guideline on bioanalytical method validation of the European Medicines Agency [11]. Using the validated method, plasma samples of RD2 or placebo treated mice were then analyzed as proof of concept.

2. Material and methods

2.1. Chemicals and reagents

UPLC-grade acetonitrile (ACN) was purchased from VWR (Langenfeld, Germany), UPLC-grade water from Merck (Darmstadt, Germany), heptafluorobutyric acid (HFBA) in LC-grade from Sigma Aldrich (Taufkirchen, Germany), formic acid (FA) in UPLC–MS grade from Biosolve (Valkenswaard, Netherlands) and trichloroacetic acid (TCA) from Sigma-Aldrich (Taufkirchen, Germany). Low binding Eppendorf tubes (Eppendorf, Hamburg, Germany) and auto-sampler vials (Agilent, Santa Clara, USA) were used because of the sticky characteristic of the peptides. Blank pooled blood plasma from healthy CD-1 mice (Innovative Grade US Origin Mouse Plasma – CD-1) was purchased from Dunn Labortechnik GmbH (Asbach, Germany). K3-EDTA served as anti-coagulator.

2.2. Peptides

The all-D-enantiomeric peptide RD2 consists of 12 amino acid residues each in D-configuration and has an amidated C-terminus (ptlhthnrrrrr-NH_2). RD2 has a monoisotopic mass of 1597.914 Da. The peptide was purchased from CBL Patras (Patras, Greece). The RD2 concentration was corrected for purity (92.3%), water content (3.7%), residual trifluoroacetic acid (TFA) (0.15%) and acetate content (25.5%). The internal standard (ISTD) has the same sequence as RD2 but with a substitution of leucine against valine at position three. It has a monoisotopic mass of 1583.898 Da. The ISTD was purchased from Peptides & Elephants GmbH (Potsdam, Germany) with a purity of 99.8%.

2.3. Stock solutions, calibration curve and quality control (QC) samples preparation

Calibration stock solutions of RD2 and ISTD were separately prepared in a water/ACN/FA (85/15/0.1%) mixture at a final concentration of 1.0 mg/mL, respectively. Dilution of 1:100 of the stock solutions in the same water/ACN/FA mixture resulted in the working solutions (10 µg/mL). Appropriate volumes of RD2 working solutions were diluted in blank mouse plasma samples to prepare the calibration standards and the QC standards. For the calibration curve, 5.30, 13.25, 26.5, 53, 132.5 and 265 ng/mL RD2 was prepared dissolving an appropriate volume of RD2 working solution. 33 ng/mL ISTD was added to correct the loss of analytes during sample preparation. For the extraction of RD2 and the ISTD, 3% TCA were added while vortexing the solution for 10 s. Precipitated proteins were removed by centrifugation at 14,000 *g* for 5 min at 4 °C. The supernatants containing the peptides were transferred to a low binding autosampler vial and stored at −20 °C. Blank plasma samples were prepared using water instead of RD2 working solution and ISTD. In addition, low quality control (LQC, 21.2 ng/mL), medium quality control (MQC, 106 ng/mL) and high quality control (HQC, 212 ng/mL) samples were prepared in the same manner. Furthermore, a quality control sample in water/ACN/FA (50 ng/mL) was prepared (QC-P) to check the performance of the method and the instrument before every series of measurements. The coefficient of determination (r^2) was used to evaluate the linearity of the calibration curve. The calibration standards were always prepared in triplicate and each extract was analyzed three times.

2.4. Chromatographic and mass spectrometry conditions

An Agilent UHPLC-ESI-QTOF-MS system was used for separation of RD2 from the ISTD and the remaining plasma components. The UHPLC (Agilent 1290 Infinity series) system consisted of a binary pump system, an autosampler, a thermostatted column compartment and a 6250 accurate-mass QTOF-MS with an electrospray ionization (ESI) interface with a resolution of 20,000. Chromatographic separation was performed on an Acquity UPLC BEH C18 column (2.1 × 100 mm, 1.7 µm particle size; Waters, Milford, USA). Column temperature was kept at 50 °C. Flow rate was 500 µL/min. The mobile phase consisted of solvent A, which was 0.025% HFBA and 1% FA in water, and solvent B, which was 0.025% HFBA and 1% FA in ACN. Sample injection volume was 20 µL. At the beginning of the run was an isocratic step of 5% B (0–2 min) followed by an increase to 22% B within 0.1 min, which was held for 0.5 min. The gradient increased from 22% to 25% B (2.6–6.5 min) in which RD2 eluted separately from the ISTD and other extracted plasma products from the column. Afterwards, the gradient increased rapidly within 0.7 min to 95% B and was held for cleaning with 95% B for 2 min. The gradient returned to 5% B within 0.1 min and equilibrated the system until 11 min. Detection was performed with the QTOF mass detector in the ESI positive ionization mode. The nebulizer pressure was set to 20 psi and the drying gas flow was set to 11 L/min. A fragmentation voltage of 215 V, a skimmer voltage of 68 V and an octopole voltage of 750 V were used. The mass range was set to *m/z* 500–600 and data acquisition rate was two spectra. Source temperature was set to 300 °C. MassHunter software LC–MS Data Acquisition B.05.01 (Agilent Technologies, Santa Clara, USA) was used to control the instrument and data acquisition. To correct the loss of analytes during sample preparation, quantification of RD2 was carried out with the ISTD. The first isotope of the three times loaded species RD2 ($(M+H^+)^{3+} = 533.649$) and ISTD ($(M+H^+)^{3+} = 528.977$) ± 8 ppm was extracted using the MassHunter software Quantitative Analysis for QTOF B.05.02 (Agilent Technologies, Santa Clara, USA). The correct isotopic ratio of RD2 and ISTD was a requirement for the identification and quantification of RD2. The advantage of this quantification method, which relies on the correct monoisotopic mass/isotopic ratio of RD2 compared to the quantification using a multiple reaction monitoring (MRM) mode, is the identification of possible metabolites of RD2 with only small modification, e.g., deamidation. We know from other studies that deamidation of RD2 sometimes occurs. In the case of deamidation of RD2, the isotope distribution ratio will be shifted to the second isotope. With an MRM method, this modification would not be detectable.

2.5. Method validation

All validation parameters were carried out on the Guideline on bioanalytical method validation of the European Medicines Agency [11].

2.5.1. Selectivity

For investigation of the method selectivity, six different blank mouse plasma matrix samples were exposed to the same extraction procedures as described before. The samples were tested for any interference peaks at retention time of RD2 or ISTD matching the chromatogram with RD2 and the ISTD spiked plasma. The assay is assured to be selective if the peak responses of tested samples were limited to ≤ 20% of the peak response of LLOQ and ≤ 5% of the ISTD.

2.5.2. Linearity, sensitivity and carry-over

Linearity and sensitivity of the suggested procedure were assessed on the basis of three individually prepared calibration curves. The calibration samples were freshly prepared and extracted with the described method. Statistical least square method was applied for the analysis of the resulting data. The % deviation for each calibrator should be ≤ 15% and for the LLOQ ≤ 20%. At least 75% of the calibration standards must fulfill this criterion. LLOQ and LLOD were calculated as a signal/noise ratio of 10 (LLOQ) or 3 (LLOD) comparing measured signals from standards of low concentrations of RD2 with those of blank samples.

Carry-over was assessed by injecting three blank plasma samples after highest calibration standard (265 ng/mL). The area response of blank samples must not exceed 20% of LLOQ and 5% of ISTD.

2.5.3. Accuracy and precision studies

Intra-day accuracy studies were carried out with the LQC, MQC and HQC samples. All samples were measured six times within one day. Additionally inter-day measurements were done in the same way in three successive days. For expression accuracy and precision of the method, the percentages error (% error) and the percentages relative standard deviation (% RSD) were used. The accuracy was determined as follows: % error = [(average measured concentration-expected concentration)/expected concentration] × 100, whereas the precision was determined as follows: % RSD = (standard deviation/average measured concentration) × 100. The acceptance criterion for accuracy was ≤ 15% of the actual values and precision should be ≤ 15%, except for LLOQ (≤ 20%) for both parameters.

2.5.4. Recovery and matrix effect

The extraction recovery was evaluated by comparing the concentrations of the extracted QC samples with the equal concentrations of RD2 spiked to plasma after extraction. Therefore, six lots of plasma were pre-treated and the extracts were spiked with RD2 concentrations corresponding to the QC samples.

The percentage of matrix effect was calculated by comparing the peak area of RD2 or ISTD spiked into blank plasma to the peak area of equal amounts of RD2 or ISTD in water/ACN/FA. The matrix factor (MF) of both RD2 and ISTD was calculated and the ISTD normalized MF was also determined. If MF is = 1, then there is no matrix effect. An MF < 1 means ion suppression and an MF > 1 means ion enhancement effects.

2.5.5. Reproducibility, performance and robustness

The QC-P sample was tested on every measurement day for one month. To show the variation within the days, the peak areas of RD2 were documented in a control chart.

2.5.6. Stability and dilution integrity

For assessing the RD2 stability in plasma matrix, the QC samples were used to perform the stability studies under different conditions. The samples were measured immediately after preparation, after 24 h at room temperature and after 72 h in the autosampler at 15 °C to assess the bench top and autosampler stability. Additionally, RD2 in plasma was measured after two weeks in the freezer (−20 °C). Moreover, the stability of the samples during three freeze-thaw-cycles was examined.

Furthermore, dilution integrity of RD2 samples was evaluated to confirm the integrity of concentrated RD2 samples that need a dilution step. Therefore, a 530 ng/mL RD2 solution was spiked into blank plasma or into water/ACN/FA to attain a concentration of two times of highest calibration standard. Then, the samples were five- or tenfold diluted with blank plasma or water/ACN/FA. Three replicates of each dilution were evaluated and the integrity of the samples was accepted when the deviation laid below 15% of the nominal values.

2.6. Applicability of the validated method for analysis of samples from a preclinical treatment study

2.6.1. Animals

Old male double transgenic APPswe/PS1ΔE9 mice [12] were purchased from The Jackson Laboratory (Sacramento, USA) and bred in-house. Water and food were available *ad libitum*. Housing rooms were maintained on a 12/12 h light–dark cycle (7:00 a.m.–7:00 p.m.) with a temperature of 22 °C and approx. 54% humidity. All animal experiments were performed in accordance with the German Law on the protection of animals and were approved by the local ethics committee (LANUV, North-Rhine-Westphalia, Germany, AZ84-02.04.2011.A359).

2.6.2. Treatment and blood collection

Treatment with RD2 or placebo was performed via intraperitoneal micro-osmotic pumps (type no. 1004) purchased from Alzet Osmotic Pumps (Cupertino, USA). The pumps were primed with 0.9% sodium chloride for 24 h at room temperature before filling with RD2 dissolved in 0.9% sodium chloride (n = 3) or 0.9% sodium chloride without peptide (placebo; n = 3). The pumps were implanted as described before [13]. In brief, for the implantation, the mice were anaesthetized intraperitoneally with 100 mg/kg ketamine (Bela-Pharm, Vechta, Germany) and 5 mg/kg medetomidine (Alfavet, Neumuenster, Germany). The skin and the muscle layer below the skin were cut in the midline and the pump was inserted into the abdominal cavity. Afterwards, the wound was sutured. The mice were treated with 40 mg/kg/day RD2 or placebo for 28 days. Subsequently, the mice were anaesthetized intraperitoneally with 100 mg/kg ketamine and 0.3 mg/kg medetomidine for blood collection via cardiac puncture. About 50 µL of 100 U/mL heparin (BD, Franklin Lakes, NJ, USA) served as anti-coagulator in the syringe.

The blood samples were centrifuged at 3,000 *g* and 4 °C for 10 min to obtain the cell free plasma. The plasma samples were frozen and stored at −20 °C.

2.6.3. Sample preparation and peptide extraction

Three RD2 and three placebo treated mice were analyzed in triplicates. The peptides were extracted from the plasma samples by the method described above. The supernatant containing the peptides RD2 and ISTD were stored at −20 °C. The samples were quantitatively analyzed in triplicate using the described method. If necessary, the samples were diluted in water/ACN/FA.

3. Results and discussion

3.1. Chromatographic separation and mass spectrometry

High resolution instruments have the ability to determine accurate mass and isotopic distribution and therefore enable high selectivity and specificity. In ESI, peptides are charged by excess of positive ions such as NH_4^+. The number of charges of each peptide depends on the experimental conditions but much more on protonable functional groups of the amino acid residues (e.g., amino groups in lysine, arginine and histidine). In addition, peptides show characteristic isotopic patterns depending on the functional groups of their amino acid composition. These two parameters were used for identification and quantification of RD2. RD2, which contains five arginine residues, has a monoisotopic mass of 1597.914 Da and was detected with two to four charges, in which > 95% was in the charge of three with a *m/z* of 533.649 $(M+H^+)^{3+}$ at all concentration levels of the calibration samples. The ISTD with a mass of 1583.898 Da was also detected > 95% via the threefold charged state with a *m/z* of 528.977 $(M+H^+)^{3+}$. As a consequence, the threefold charged state was used for quantification. The accuracy for confirmation of the extracted masses of RD2 and ISTD was within ± 8 ppm mass error showing high mass accuracy for the components' identification. The experimentally obtained isotopic pattern

was in close agreement with the theoretical isotopic pattern of RD2 and ISTD. Several parameters of mass spectrometry were optimized to obtain the highest stabilized mass response.

In addition, chromatographic conditions were adjusted. RD2 is very polar and hence difficult to chromatograph without ion pairing. We tried different additives, such as formic acid and TFA in different concentrations, but finally the combination of 1% formic acid and 0.025% HFBA improved the chromatography significantly. A run time of 7 min was capable for a good separation of ISTD (retention time: 3.5 min) and RD2 (retention time: 3.7 min) (Fig. 1).

3.2. Method validation

3.2.1. Selectivity

The developed method is specific as no interference from components of the extracted mouse plasma matrix was observed at the retention time of ISTD or RD2. ISTD and RD2 were well separated under the optimized chromatographic conditions with retention times at 3.5 min and 3.7 min, respectively (Fig. 1A).

3.2.2. Linearity, sensitivity and carry-over

The suggested method was sensitive and reliable for quantifying RD2 in mouse plasma. The linear regression analysis for the results was carried out using the least square method. The calibration curve showed linearity of RD2 concentrations between 5.3 ng/mL and 265 ng/mL with a correlation coefficient (r^2) > 0.999 in mouse plasma. The calibration curve of RD2 in plasma has a regression equation of $y = 1.01x–0.14$. The precision (RSD) of each concentration point did not exceed 7% and varied between 0.44% and 6.13%. Accuracy ranged from −4.34% to 4.79% (Table 1). The high r^2 value was indicative for the good linearity and the values of standard deviation were indicative for the significant validity of the calibration points.

Table 1
Back-calculated RD2 concentration of the calibration standards in mouse plasma.

Nominal concentration [ng/mL]	Mean [ng/mL]	Standard deviation [ng/mL]	Precision [%]	Accuracy [%]
5.30	5.07	0.18	3.60	−4.34
13.25	13.24	0.81	6.10	−0.08
26.5	27.77	0.72	2.59	4.79
53	53.22	3.26	6.13	0.42
132.5	132.72	0.58	0.44	0.55
265	269.10	16.36	6.08	1.55

No carry-over effect for RD2 or ISTD was observed in three blank plasma samples measured directly after the highest calibration standard. The peak area of blank mouse plasma revealed less than 4% of the peak area of the lowest RD2 calibration standard and less than 5% of the ISTD peak area.

The analytical measurement range started with 5.3 ng/mL as the lower limit of quantification (LLOQ). The calibration standard at 2.65 ng/mL was still detectable but was not in the linear range for quantification any more. Therefore, the lower limit of detection (LLOD) was set to 2.65 ng/mL.

3.2.3. Accuracy and precision studies

The developed method was confirmed to be reproducible using intra- and inter-day precision and accuracy of the QC samples. For expressing precision and accuracy, % RSD and % error were used. The

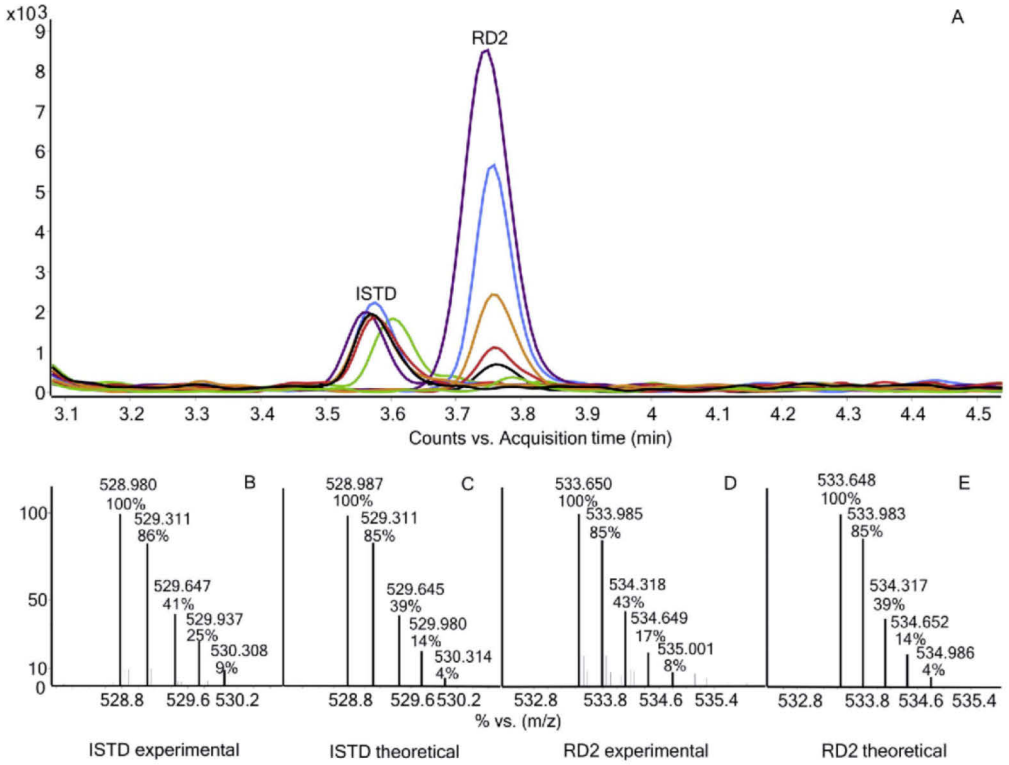

Fig. 1. Chromatographic separation and isotopic ratios of RD2 and the internal standard (ISTD). Extracted ion chromatogram (EIC) of RD2 (5.3–265 ng/mL) and ISTD (33 ng/mL) (A). Experimental (B, D) and theoretical (C, E) isotopic intensity distribution of the 3^+ charge peptide ion cluster of RD2 (D, E) and ISTD (B, C).

Table 2
Intra-day and inter-day precision and accuracy values of RD2 in mouse plasma.

	LQC [21.2 ng/mL]		MQC [106 ng/mL]		HQC [212 ng/mL]	
	Intra-day	Inter-day	Intra-day	Inter-day	Intra-day	Inter-day
Mean [ng/mL]	21.2	21.1	106.2	108.3	211.4	211.6
Standard deviation [ng/mL]	1.74	1.41	5.95	4.02	4.17	5.73
Precision [%]	8.18	6.69	5.60	3.71	1.97	2.71
Accuracy [%]	−0.24	−0.54	0.22	2.21	−0.29	−0.18

Table 3
Extraction recovery of QC samples of RD2 in mouse plasma (n = 6).

	RD2 extracted from mouse plasma			RD2 spiked to blank mouse plasma extract		
Nominal concentration [ng/mL]	21.2	106.0	212	21.2	106.0	212
Mean [ng/mL]	21.2	106.2	211.3	22.5	112.6	210.7
Recovery [%]	99.8	100.2	99.7	106.2	105.8	99.4
Standard deviation [ng/mL]	1.74	5.95	4.17	2.54	6.21	4.05
Precision [%]	8.18	5.60	1.97	11.24	5.52	1.92
Accuracy [%]	−0.24	2.83	−0.29	6.18	5.75	−0.61

values laid in the suitable range following the Guideline on bioanalytical method validation of the European Medicines Agency (2011) (Table 2).

3.2.4. Extraction recovery and matrix effect

Sample preparation for LC–MS of peptides is a critical step since peptides can undergo undesired phenomena such as adsorption to surfaces, degradation, variable recoveries or loss during transferring or drying steps. To minimize these issues, the use of a fast, simple technique such as protein precipitation with an organic solvent is preferred. To optimize the extraction of RD2 out of plasma, we used several organic solvents (ACN, methanol) and acids (HCOOH, TCA) in different ratios (varying concentrations). Finally, the extraction with 3% TCA showed best recoveries. In addition, the use of Low binding Eppendorf vials was indispensable because of the sticky character of the RD2 peptide.

Table 3 summarizes the extraction recoveries of the QC samples of RD2 in mouse plasma. The extraction recovery of RD2 was determined comparing the calculated concentration of RD2 extracted from plasma and extracted plasma spiked with corresponding amounts of RD2. The extraction efficiency was determined for the three QC samples with 99.8% (LQC), 100.2% (MQC) and 99.7% (HQC), respectively. Theoretically, the recovery rate cannot be above 100%. Due to the precision of the measurement, which was determined to be 7.1% (see 3.2.5), however, the calculations can ultimately lead to recovery rates slightly above 100%.

Table 5
Determination of RD2 in mouse plasma of intraperitoneally treated mice.

Mouse	RD2 treated			Placebo treated
	1	2	3	4–6
Mean [ng/mL]	1157.6	1554.3	1804.6	< LLOD
Standard deviation [ng/mL]	57.31	53.30	50.01	
Precision [%]	4.95	3.43	2.77	

For evaluation of the matrix effect, the peak area of RD2 or ISTD spiked into blank plasma was compared to the peak area of equal amounts of RD2 or ISTD in water/ACN/FA. The peak areas of RD2 and ISTD in water/ACN/FA and plasma samples showed that plasma has a maximal influence of 9% on the ionization of RD2 and 7% on the ionization of ISTD. The ISTD normalized MF values were 1.03 (LQC), 0.95

Table 4
RD2 stability and dilution integrity of RD2 in mouse plasma (n = 6).

	Nominal concentration [ng/mL]	Mean [ng/mL]	Recovery [%]	Precision [%]	Accuracy [%]
After extraction, 0 min	21.2	21.6	101.9	2.8	1.9
	106.0	107.7	101.5	3.6	1.5
	212.0	217.8	102.7	5.0	2.7
Room temp., after 24 h	21.2	21.4	100.9	8.3	0.9
	106.0	109.3	103.1	3.7	3.1
	212	211.0	99.5	2.8	−0.5
−20 °C, after 2 weeks	21.2	20.3	95.7	6.7	−4.2
	106.0	110.5	104.2	9.1	4.2
	212	202.1	95.3	1.7	−4.7
15 °C, 72 h	21.2	19.2	90.7	4.9	−9.3
	106.0	107.1	101.0	2.1	1.0
	212	210.7	99.4	2.0	−0.6
Three freeze-thaw-cycles	21.2	20.7	97.6	8.9	−2.4
	106.0	110.1	103.9	3.5	3.9
	212	210.4	99.3	2.5	−0.7
Dilution integrity	106.0 in plasma	114.8	108.3	4.0	8.3
	53.0 in plasma	55.4	104.6	4.6	4.6
	106.0 in water/ACN/FA	114.0	107.6	4.6	7.6
	53.0 in water/ACN/FA	55.1	104.0	3.9	4.0

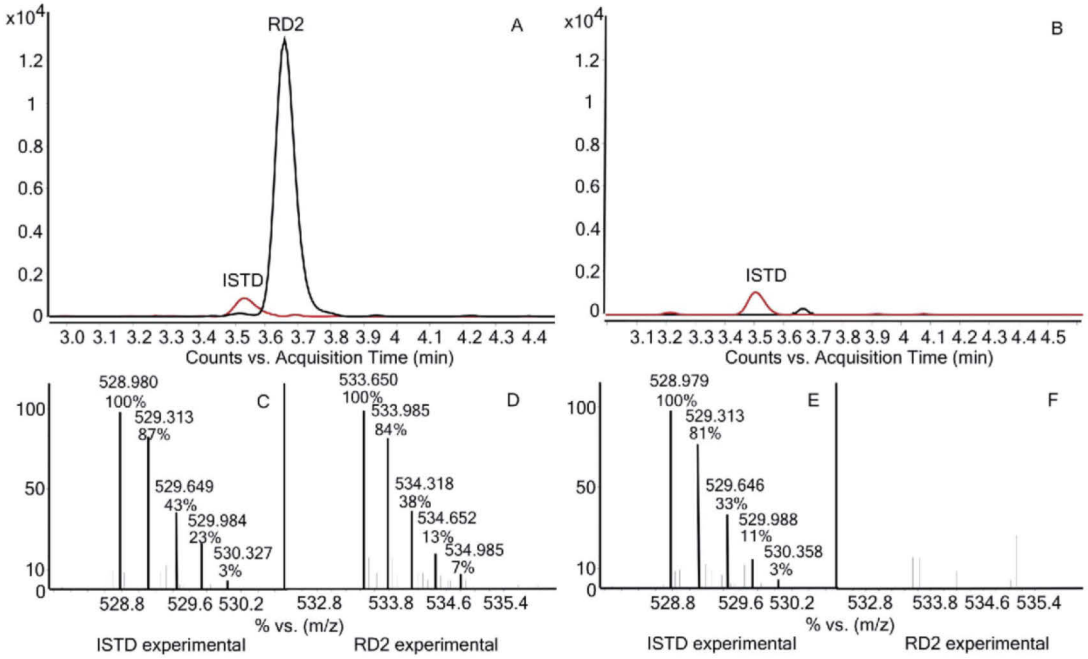

Fig. 2. Extracted ion chromatogram (EIC) of RD2 (black) and ISTD (red) of samples from RD2 treated mouse 2 (A) and placebo treated mouse 6 (B). Experimental distribution of the 3+ charged peptide ion cluster of ISTD (C, E) and RD2 (D, F). (For interpretation of the references to colour in this figure legend, the reader is referred to the web version of this article.)

(MQC) and 1.01 (HQC) respectively. This confirms matrix independency of this assay due to co-eluting matrix components.

3.2.5. *Reproducibility, performance and robustness*

The system is reproducible and robust. This was demonstrated by determination of the mean area of the QC-P standard over one month, which showed a precision of 7.1%.

3.2.6. *Stability and dilution integrity*

QC samples of RD2 were used to perform the stability studies under different conditions. The results of the stability studies are shown in Table 4. No loss of RD2 was observed during the storage at the tested conditions.

For evaluation of dilution integrity of RD2 samples, the mean recovery % and the precision % for the 1/5 and 1/10 dilution samples in plasma and in water/ACN/FA were determined. The recovery was within 104% and 108% and the precision was < 4.6%.

3.3. *Applicability of the validated method for analysis of samples from a preclinical treatment study*

To determine the applicability of the method for future treatment or pharmacokinetic studies, we analyzed plasma samples from mice after intraperitoneal treatment with 40 mg/kg/day unlabeled RD2 or with placebo (Table 5). Every mouse plasma sample was extracted in triplicate. The samples from the RD2 treated mice yielded ISTD and RD2 well separated with retention times at 3.5 and 3.7 min, respectively (Fig. 2A). The correct isotopic ratios of ISTD and RD2 were detected (Fig. 2C, D, E). In addition, no interferences from components of the extracted mouse plasma matrix were observed at the retention time of RD2 in placebo treated mice (Fig. 2F) substantiating the selectivity of the method.

Plasma of RD2 treated mice revealed an RD2 concentration of 1157.6, 1554.3 and 1804.6 ng/mL with a precision of 4.95%, 3.34% and 2.77%, respectively. As expected, RD2 has not been found in placebo treated mice (Table 5). From these results, we can conclude that the validated analytical method is reliable and suitable for the quantification of RD2 in plasma of treated mice.

4. Conclusion

Here, we describe the development and evaluation of a rapid UHPLC-ESI-QTOF-MS method for quantification of the highly hydrophilic, arginine-rich all-D-enantiomeric peptide RD2 in mouse plasma. The applied method showed a linearity range for RD2 spiked in plasma between 5.3 and 265 ng/mL with an LLOD of 2.65 ng/mL. The analysis was performed within 6.5 min with low solvent consumption. Quantifying several RD2 samples within one day as well as spread over various days demonstrated the accuracy, precision and reproducibility of the procedure. The developed method was successfully applied for the quantification of RD2 in intraperitoneally treated mice. These results provide a meaningful basis to evaluate preclinical or clinical applications of RD2.

Declaration of interest

The authors declare no competing financial or personal interests.

Acknowledgements

This work was funded by the Portfolio Technology and Medicine, the Portfolio Drug Research and the "Helmholtz-Validierungsfond" of the "Impuls- und Vernetzungsfond der Helmholtzgemeinschaft" and by the Technology Transfer Department of the Forschungszentrum Jülich.

References

[1] Alzheimer's Association, Alzheimer's disease facts and figures, Alzheimer's Dementia 12 (2016) (2016).

[2] J.A. Hardy, G.A. Higgins, Alzheimer's disease: the amyloid cascade hypothesis, Science 256 (1992) 184–185.
[3] D.J. Selkoe, J. Hardy, The amyloid hypothesis of Alzheimer's disease at 25 years, EMBO Mol. Med. 8 (2016) 595–608.
[4] S.T. Ferreira, W.L. Klein, The Abeta oligomer hypothesis for synapse failure and memory loss in Alzheimer's disease, Neurobiol. Learn. Mem. 96 (2011) 529–543.
[5] M.E. Larson, S.E. Lesne, Soluble Abeta oligomer production and toxicity, J. Neurochem. 120 (Suppl. 1) (2012) 125–139.
[6] I. Benilova, E. Karran, B. De Strooper, The toxic Abeta oligomer and Alzheimer's disease: an emperor in need of clothes, Nat. Neurosci. 15 (2012) 349–357.
[7] S.A. Funke, D. Willbold, Mirror image phage display–a method to generate D-peptide ligands for use in diagnostic or therapeutical applications, Mol. Biosyst. 5 (2009) 783–786.
[8] O.O. Olubiyi, D. Frenzel, D. Bartnik, J.M. Glück, O. Brener, L. Nagel-Steger, S.A. Funke, D. Willbold, B. Strodel, Amyloid aggregation inhibitory mechanism of arginine-rich D-peptides, Curr. Med. Chem. 21 (2014) 1448–1457.
[9] T. van Groen, S. Schemmert, O. Brener, L. Gremer, T. Ziehm, M. Tusche, L. Nagel-Steger, I. Kadish, E. Schartmann, A. Elfgen, D. Jürgens, A. Willuweit, J. Kutzsche, D. Willbold, The Aβ oligomer eliminating D-enantiomeric peptide RD2 improves cognition without changing plaque pathology, Sci. Rep. 7 (2017) 16275, http://dx.doi.org/10.1038/s41598-017-16565-1.
[10] L.H. Leithold, N. Jiang, J. Post, T. Ziehm, E. Schartmann, J. Kutzsche, N.J. Shah, J. Breitkreutz, K.J. Langen, A. Willuweit, D. Willbold, Pharmacokinetic properties of a novel D-peptide developed to be therapeutically active against toxic beta-amyloid oligomers, Pharm. Res. 33 (2016) 328–336.
[11] European Medicines Agency, Guideline on Validation of Bioanalytical Methods, Committee for Medicinal Products for Human Use, London, 2011.
[12] J.L. Jankowsky, H.H. Slunt, T. Ratovitski, N.A. Jenkins, N.G. Copeland, D.R. Borchelt, Co-expression of multiple transgenes in mouse CNS a comparison of strategies, Biomol. Eng. 17 (2001) 157–165.
[13] Alzet Osmotic Pumps, Intraperitoneal Implantation: Alzet Surgical Instuction Sheet, Alzet Osmotic Pumps, 2017.

3.4 Comparison of blood-brain barrier penetration efficiencies between linear and cyclic all-D-enantiomeric peptides developed for the treatment of Alzheimer's disease

Autoren:	Schartmann E., **Schemmert S.**, Ziehm T., Leithold L.H.E., Jiang N., Tusche M., Jon Shah N., Langen K-J., Kutzsche J., Willbold D., Willuweit A.
Journal:	European Journal of Pharmaceutical Sciences (2017), veröffentlicht am 07. Dezember 2017
DOI:	10.1016/j.ejps.2017.12.005
Impact Factor:	3,756 (2016)
Beitrag:	Gemeinsam mit Elena Schartmann: Planung der Studie und Durchführung der pharmakokinetischen Experimente Mitverfassung und Prüfung des Manuskriptes

European Journal of Pharmaceutical Sciences 114 (2018) 93–102

Contents lists available at ScienceDirect

European Journal of Pharmaceutical Sciences

journal homepage: www.elsevier.com/locate/ejps

Comparison of blood-brain barrier penetration efficiencies between linear and cyclic all-D-enantiomeric peptides developed for the treatment of Alzheimer's disease

Elena Schartmann[a], Sarah Schemmert[a], Tamar Ziehm[a], Leonie H.E. Leithold[a], Nan Jiang[a], Markus Tusche[a], N. Joni Shah[b,c,d], Karl-Josef Langen[b,e], Janine Kutzsche[a], Dieter Willbold[a,f,*], Antje Willuweit[b,**]

[a] Institute of Complex Systems, Structural Biochemistry (ICS-6), Forschungszentrum Jülich GmbH, 52425 Jülich, Germany
[b] Institute of Neuroscience and Medicine, Medical Imaging Physics (INM-4), Forschungszentrum Jülich GmbH, 52425 Jülich, Germany
[c] Department of Neurology, Faculty of Medicine, JARA, RWTH Aachen University, 52074 Aachen, Germany
[d] Department of Electrical and Computer Systems Engineering and Monash Biomedical Imaging, School of Psychological Sciences, Monash University, Melbourne, Victoria, Australia
[e] Department of Nuclear Medicine, Universitätsklinikum der RWTH Aachen, 52074 Aachen, Germany
[f] Institut für Physikalische Biologie, Heinrich-Heine-Universität Düsseldorf, 40225 Düsseldorf, Germany

ABSTRACT

Alzheimer's disease (AD), until now, is an incurable progressive neurodegenerative disease. To target toxic amyloid β oligomers in AD patients' brains and to convert them into non-toxic aggregation-incompetent species, we designed peptides consisting solely of D-enantiomeric amino acid residues. The original lead compound was named D3 and several D3 derivatives were designed to enhance beneficial properties. Here, we compare four D-peptides concerning their efficiencies to pass the blood-brain barrier (BBB). We demonstrate that the D-peptides' concentrations in murine brain directly correlate with concentrations in cerebrospinal fluid. The cyclic D-enantiomeric peptide cRD2D3 is characterized by the highest efficiency to pass the BBB. For in total three cyclic peptides we show that administration of cyclic peptides resulted in up to tenfold higher peak concentrations in brain as compared to their linear equivalents which have partially been characterized before (Jiang et al., 2015; Leithold et al., 2016a). These results suggest that cyclic peptides pass the murine BBB more efficiently than their linear equivalents. cRD2D3's proteolytic stability, oral bioavailability, long duration of action and its favorable brain/plasma ratio reveal that it may become a suitable drug for long-term AD-treatment from a pharmacokinetic point of view.

1. Introduction

More than 20 million people worldwide are currently affected by Alzheimer's disease (AD). There is clear unmet medical need to find a curative treatment for this progressive neurodegenerative disease.

Major hallmarks of AD are neurodegeneration, extracellular deposits or plaques of amyloid β (Aβ), and intracellular deposits of hyperphosphorylated tau protein. Aβ is formed constantly throughout our lifetime and is able to form soluble Aβ oligomers and insoluble Aβ fibrils that make up the plaques (Thal et al., 2006). Currently, oligomers are thought to be the most neurotoxic Aβ species (Haass and Selkoe, 2007). Both, Aβ and tau, and their formation and degradation are prominent targets in AD drug development (Anand et al., 2014).

We focused on the identification and development of substances that specifically and directly eliminate toxic Aβ oligomers. Previously, we described the properties of the compound D3 (Table 1), which is a peptide consisting of 12 D-enantiomeric amino acid residues and has been identified by mirror image phage display against Aβ monomers (Funke and Willbold, 2009; Schumacher et al., 1996; Wiesehan et al., 2003; Wiesehan et al., 2008; Wiesehan and Willbold, 2003). The lead compound D3 stabilizes Aβ monomers in an aggregation-incompetent conformation thus shifting the equilibrium between Aβ oligomers and monomers towards monomers. D3 was shown to eliminate Aβ *in vitro*, improved cognition and lowered Aβ plaque load in transgenic AD

* Correspondence to: D. Willbold, Institute of Complex Systems, Structural Biochemistry (ICS-6), Forschungszentrum Jülich GmbH, 52425 Jülich, Germany.
** Corresponding author.
E-mail addresses: d.willbold@fz-juelich.de (D. Willbold), a.willuweit@fz-juelich.de (A. Willuweit).

https://doi.org/10.1016/j.ejps.2017.12.005
Received 10 July 2017; Received in revised form 25 October 2017; Accepted 6 December 2017
Available online 07 December 2017

Table 1
Peptides' sequences and configurations.

Peptide	Amino acid residue sequence	Amino acid residue configuration
(^{3}H-)cRD2D3	ptlhthnrrrrrrprtrlhthrnr head-to-tail cyclized	All-D-enantiomeric
(^{3}H-)RD2D3	ptlhthnrrrrrrprtrlhthrnr-NH_2	All-D-enantiomeric
(^{3}H-)cD3D3	rprtrlhthrnrrprtrlhthrnr head-to-tail cyclized	All-D-enantiomeric
(^{3}H-)D3D3	rprtrlhthrnrrprtrlhthrnr-NH_2	All-D-enantiomeric
(^{3}H-)cD3r	rprtrlhthrnrr head-to-tail cyclized	All-D-enantiomeric
(^{3}H-)D3	rprtrlhthrnr-NH_2	All-D-enantiomeric
(^{3}H-)L-D3	RPRTRLHTHRNR-NH_2	All-L-enantiomeric
(^{3}H-)RD2	ptlhthnrrrrr-NH_2	All-D-enantiomeric

mouse models, and revealed promising *in vivo* properties, *e.g.* beneficial pharmacokinetic characteristics (Bartnik et al., 2010; Brener et al., 2015; Funke et al., 2010; Jiang et al., 2016; Jiang et al., 2015; Liu et al., 2010; Olubiyi et al., 2014; Olubiyi and Strodel, 2012; van Groen et al., 2012; van Groen et al., 2013; van Groen et al., 2009; van Groen et al., 2008). Derivatives of D3 with rearranged amino acid residue sequences (*e.g.* RD2, Table 1) have been developed to increase Aβ affinity and inhibition of Aβ aggregation *in vitro* (Klein et al., 2016; Kutzsche et al., 2017; Olubiyi et al., 2014). Also, linear tandem 24-mer peptides in head-to-tail arrangement (*e.g.* RD2D3, D3D3; Table 1) have been designed, pharmacokinetically investigated, and successfully tested *in vitro* as well as *in vivo* in an AD mouse model in which they improved symptoms of AD pathology (Brener et al., 2015; Leithold et al., 2016a). Another approach to increase the peptides' Aβ binding affinities and their efficiencies to eliminate toxic Aβ oligomers was head-to-tail cyclization of D3 (*e.g.* cD3r, Table 1). cD3r was shown to be more active *in vitro* and *in vivo* as compared to D3 and other non-cyclized D3 derivatives (Ziehm et al., 2016).

Here, we compared four D3 derivatives concerning their efficiencies to cross the blood-brain barrier (BBB) after intraperitoneal (i.p.) administration to C57BL/6N mice and investigated correlations between peptide concentrations in murine brain, plasma, and cerebrospinal fluid (CSF). The peptide with the highest efficiency to cross the murine BBB, cRD2D3, was pharmacokinetically further characterized, especially regarding its oral bioavailability. Finally, we investigated whether head-to-tail cyclization generally increases a peptide's efficiency to cross the murine BBB.

2. Materials and methods

2.1. Peptides

^{3}H-cRD2D3, ^{3}H-RD2D3, ^{3}H-RD2, ^{3}H-cD3r, ^{3}H-cD3D3, ^{3}H-L-D3, and ^{3}H-D3 were produced by Quotient Bioresearch (Radiochemicals) Ltd. (United Kingdom) with 1 mCi/mL and purity > 95% (Table 1). Non-^{3}H-labelled peptides were delivered by peptides & elephants GmbH (Germany). Recombinant $A\beta_{1-42}$ was obtained from Isoloid GmbH (Germany).

2.2. Animals

For *ex vivo* tests for proteolytic stability, plasma, and organ homogenates from brain, liver, and kidney were taken from a male C57BL/6N wildtype mouse (15.5 weeks). cRD2D3's pharmacokinetic profile was investigated in male C57Bl/6N mice aged 12–13 weeks, weighing about 26 g in average. These mice were ordered at Charles River (Germany) and housed at least one week under standard housing conditions (12/12 h light-dark cycle, approximately 22 °C room temperature and 54% humidity; water and food available *ad libitum*) in the animal facility of the Forschungszentrum Jülich GmbH before the experiments were carried out. All animal experiments were approved by the Animal Protection Committee of the local government (LANUV, North-Rhine-Westphalia, Germany, Az.84-02.04.2011.A356) according to the German Protection of Animals Act.

2.3. Comparison of four peptides concerning their BBB-passage efficiency

Here, we compared four D3 derivatives concerning their efficiencies to cross the murine BBB after i.p. administration to C57BL/6N mice. We investigated the linear 12-mer peptide RD2, the cyclic 13-mer peptide cD3r as well as two cyclic 24-mer tandem peptides, cRD2D3 and cD3D3. All peptides had previously shown promising *in vitro* results. Their sequences are shown in Table 1.

2.3.1. Concentration-time profiles for peptide selection

To determine the concentration-time profiles of cRD2D3, RD2, cD3r, and cD3D3 after i.p. administration (30, 60, 240, 1440 min) in murine brain, plasma, and CSF, mixed solutions of non-labelled and ^{3}H-labelled peptides were prepared. The administered solutions contained 3 mg/mL of the respective peptide including small amounts of ^{3}H-labelled peptides (1.86 µg/mL ^{3}H-cRD2D3, 0.65 µg/mL ^{3}H-RD2, 0.64 µg/mL ^{3}H-cD3r, or 1.52 µg/mL ^{3}H-cD3D3). Doses were administered by body weight with 10 mg/kg. Three to five mice were investigated per time point whereby for two time points (RD2: 240 min, cD3r: 1440 min), CSF could only be taken from two mice.

Approximately 10 min before each sampling time point, the respective animal was anesthetized with i.p. ketamine/medetomidine anesthesia. Once the mouse was deeply narcotized, the *cisterna magna* was laid free and punctuated to extract about 5 µL CSF with a small capillary as described before (Liu et al., 2012). Afterwards, blood was taken by heart puncture. Heparinized blood was centrifuged (3000*g*, 5 min, 4 °C) to get plasma, which was 1:1 diluted with PBS (phosphate-buffered saline). The right brain hemisphere was extracted, weighed, and homogenized in 500 µL PBS (Precellys Ceramic Kit 1.4 mm, Precellys 24, Bertin technologies SAS, France). 100 µL diluted plasma or brain homogenate (in triplicate each), or 5 µL CSF (single determination) were mixed with 10 mL scintillation cocktail (Ultima Gold XR, PerkinElmer, USA) and incubated overnight (100 rpm, room temperature). Quantitative measurements were carried out in a liquid scintillation counter (LSC) (Packard Tri-Carb 2100TR Liquid Scintillation Analyzer, PerkinElmer, USA). LSC results (dpm/sample) were converted into mg/mL or % injected dose (%ID)/mL for plasma and for CSF, or in mg/g or %ID/g for brain as described before (Jiang et al., 2015). Total peptide concentrations in the samples were back-calculated from the measured ^{3}H-labelled peptides' radioactivity.

The determined peptide concentrations were plotted over time to allow for comparison of all peptides' uptakes into brain, plasma, and CSF. Concentrations at 0 min were set to be 0%ID/mL or 0%ID/g. To make differences more obvious, the areas under the concentration-time curves from the first to the last measured time point (AUC_{last}) and the maximum concentrations (C_{max}) were determined by Phoenix WinNonlin (Non-Compartmental Analysis and PK/PD Modeling and Simulation, Certara).

2.3.2. Correlation of peptides' brain, CSF, and plasma concentrations

Additionally, peptide concentrations in brain, CSF, and plasma were assessed in relation to each other: brain/CSF, brain/plasma, and CSF/plasma ratios were computed and plotted over time.

2.4. Further characterization of the peptide with the highest efficiency to cross the BBB: cRD2D3

2.4.1. Proteolytic stability

Proteolytic stability was investigated by thin layer chromatography (TLC) after incubation of a ^{3}H-cRD2D3 (cyclic D-peptide, 11.76 µM) or ^{3}H-L-D3 (linear L-peptide, 9.71 µM) solution in murine plasma, brain-, liver-, and kidney-homogenate as well as in human liver microsomes

(Sigma-Aldrich, Germany) as described before (Jiang et al., 2015; Leithold et al., 2016b). ^{3}H-L-D3 served as control for enzyme functionality. In brief, ^{3}H-peptide solutions were mixed 1:3 with murine plasma, organ-homogenates, or human liver microsomes solution and incubated for 0, 4, and 24 h at 37 °C on a shaker with 300 rpm. After the respective incubation time, the enzymes in the different solutions were denatured by adding 2 µL mobile phase (10 mL 28% ammonia/34 mL pyridine/39 mL *n*-butanol/26 mL double distilled H_2O) to each 5 µL incubated solution. 2 µL of the denatured solutions were spotted on ProteoChrom HPTLC Silica gel 60 F_{254s} plates (Merck, Germany) and put into a TLC chamber with mobile phase until the solvent front reached about 5 cm. After drying, the TLC plate was developed on a Fuji Imaging Plate BAS-TR2025 20 × 25 cm (FUJIFILM, Japan) for 72 h and analyzed with a BAS reader with AIDA software (Raytest GmbH, Germany) similar to the tests for ^{3}H-RD2D3 described before (Leithold et al., 2016b).

2.4.2. Plasma protein binding

cRD2D3's plasma protein binding (PPB) to human serum albumin (HSA) and to α1-acid glycoprotein (AGP) was analyzed according to the manufacturer's protocol of TRANSIL^{XL} HSA and AGP binding kits (Sovicell GmbH, Germany). To cover a larger range of HSA and AGP concentrations, the bead concentrations in the kits were modified. For detection, a mixture of ^{3}H-cRD2D3 and non-labelled cRD2D3 (final concentration of 4.8 µM) was added to different HSA (7.4 µM to 420 µM, 9 different concentrations) or AGP concentrations (0.04 µM to 30 µM, 18 different concentrations). The amount of unbound cRD2D3 (in %) was determined using the LSC. The *Kd* as well as the free drug fraction (f_u) in human plasma were calculated as described before (Leithold et al., 2016b). The calculation is based on a cRD2D3 blood concentration of 0.29 µM, which was measured in the blood 4 h after single oral administration (10 mg/kg).

2.4.3. Pharmacokinetic profiles

To determine cRD2D3's concentration-time profiles after i.p., intravenous (i.v.) and oral (p.o.) administration in murine plasma, brain, liver, and kidney, again a mixed solution of non-labelled and ^{3}H-labelled cRD2D3 was prepared. For i.p. and p.o. administration the solution contained 3 mg/mL cRD2D3 (including 1.86 µg/mL ^{3}H-cRD2D3). For i.v. administration the solution contained 1 mg/mL (including 0.62 µg/mL ^{3}H-cRD2D3). Doses were administered per body weight (i.p. and p.o. 10 mg/kg, i.v. 3.3 mg/kg). Approximately 2 min before each organ harvesting time point, the respective animal was anesthetized with isofluran (cp-pharma, Germany) inhalation anesthesia. Organs were harvested as follows: i.p.: 10, 20, 30*, 60, 120, 180, 240*, 360, 840, 1080, 1440*, 2880, 5760 min; time points marked with * were taken from Section 2.3.1 for animal health and safety considerations; i.v.: 5, 10, 15, 30, 60, 240, 360, 840, 1080, 1440, 2880, 5760 min; p.o.: 10, 30, 60, 120, 180, 240, 360, 840, 1080, 1440, 2880, 5760 min; three mice for each time point except of one (5760 min, i.v., only two mice). Blood was taken by heart puncture. The following steps and calculations were carried out as described above (Section 2.3.1). CSF was not taken but instead about 200 mg of the liver and the right kidney were extracted and investigated similar to the right brain hemisphere. All samples were quantified in triplicate by LSC measurements. Total cRD2D3 concentrations in the samples were back-calculated from the measured ^{3}H-cRD2D3 radioactivity.

2.4.4. Pharmacokinetic parameters

To determine cRD2D3's pharmacokinetic parameters for plasma and brain, concentration-time profiles were analyzed. 0 min plasma and brain concentrations for i.p. and p.o. administration as well as 0 min brain concentrations for i.v. administration were set to be 0 mg/mL or mg/g while 0 min plasma concentrations for i.v. administration were linearly back-extrapolated based on the first two measured time points (5 min, 10 min). Non-compartmental data analysis was performed in combination of different programs as described before (Leithold et al., 2016a): the AUC_{last}, the area under the first moment curve from the first to the last measured data pair ($AUMC_{last}$), the mean residence time (MRT), and the terminal elimination rate constant (λ_z, nonlinear regression of the last three (i.p., i.v.) to five (p.o.) measured concentrations) were calculated using Phoenix WinNonlin. Further pharmacokinetic parameters were calculated with the help of the formulas listed in Table 2.

Table 2
Formulas for calculation of pharmacokinetic parameters and BBB values.

		Unit	Formula
Pharmacokinetic parameter			
$t_{1/2}$	Terminal half-life	h	$t_{1/2} = \ln(2)/\lambda_z$
D	Dose	mg/kg	
$F_{AUC_{last}}$	Bioavailability	%	$F_{AUC_{0-last}} = \frac{AUC_{last_{e.v.}} * D_{i.v.}}{AUC_{last_{i.v.}} * D_{e.v.}}$
CL	Terminal plasma clearance	mL/(min * kg)	$CL = \lambda_z * V_{last}$
BBB value			
logBB	Blood-brain equilibrium distribution	–	$\log BB = \log (AUC_{last,be}/AUC_{last,pl})$
K_{in}	Unidirectional influx rate constant	mL/(g * min)	$\frac{C_b(t)}{C_p(t)} = K_{in} * \frac{AUC_p(t)}{C_p(t)} + V_i$
V_i	Initial distribution volume	mL/g	
PS	Permeability surface-area product	mL/(g * min)	$PS = (-CBF) * \ln(1 - K_{in}/CBF)$
CBF	(Murine) cerebral blood flow	mL/(g * min)	1.07 (Muir et al., 2008)

Additionally, we determined some universally used BBB values to allow for direct comparison with other peptides (Van Dorpe et al., 2012): the blood-brain equilibrium distribution (logBB), the universal influx rate constant (K_{in}), the initial distribution volume in brain (V_i), and the permeability surface-area product (PS). The BBB values were determined based on the i.v. concentration-time profile values and pharmacokinetic parameters with formulas listed in Table 2. K_{in} and V_i were graphically determined by plotting the brain concentration to plasma concentration ratio at certain time points (C_b (t)/C_p (t) [mL/g]) on the y-axis against the exposure time (AUC_p (t)/C_p (t) [min]) on the x-axis. For both peptides, the linear range was between 0 and 240 min (R^2 (cRD2D3): 0.9216, R^2 (RD2D3): 0.9995). For calculation of the PS, the murine cerebral blood flow (CBF) was assumed to be 1.07 mL/(g * min) (Muir et al., 2008).

3. Results

3.1. Comparison of four peptides concerning their BBB-passage efficiencies

3.1.1. Concentration-time profiles for peptide selection

We compared four peptides regarding their efficiencies to enter the brain. cRD2D3's, RD2's, cD3D3's, and cD3r's concentration-time profiles in brain, plasma, and CSF after i.p. administration are shown in Fig. 1. The highest AUC_{last} as well as C_{max} in the brain was observed for cRD2D3, followed by RD2, cD3D3, and cD3r. Peptide concentrations in CSF revealed the same order as in the brain. All investigated peptides showed plasma concentration-time courses in the same range whereby initial concentrations (0.5 h after administration) were highest for the single peptides RD2 and cD3r. In plasma, C_{max} was highest for RD2 followed by cD3r, cRD2D3, and cD3D3.

3.1.2. Correlation of peptides' brain, CSF, and plasma concentrations

We further investigated whether peptides' concentrations in brain, plasma, and CSF correlated by calculating brain/plasma, CSF/plasma,

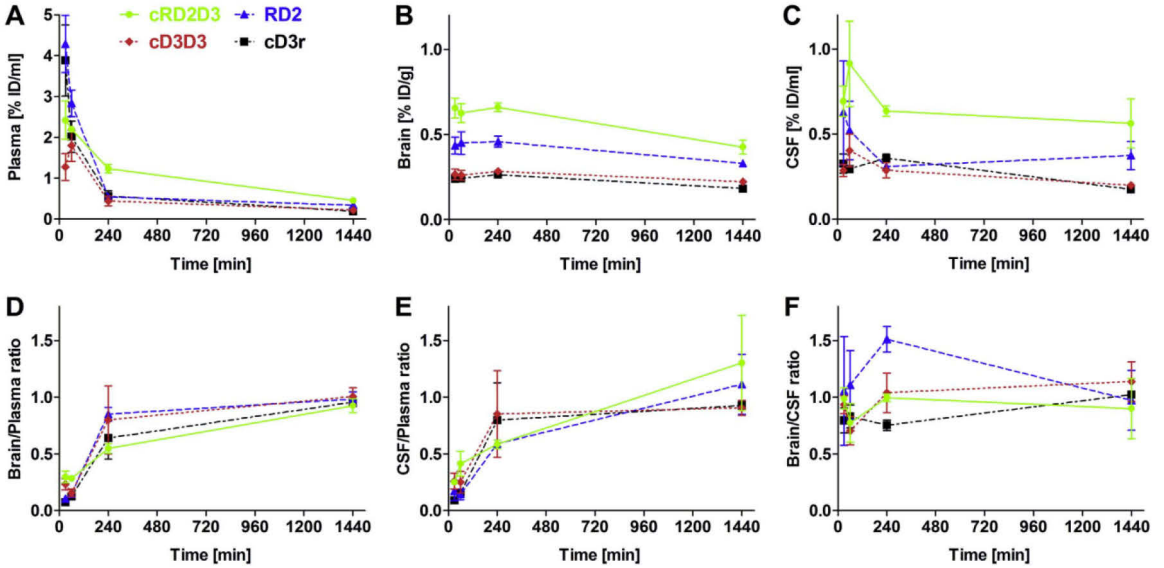

Fig. 1. Concentration-time profiles of four peptides and their ratios in murine plasma, CSF, and brain.
Mixtures of non-labelled and ^{3}H-labelled cRD2D3 (*green line, diamonds*), RD2 (*blue dashed line, triangles*), cD3D3 (*red dashed line, diamonds*), and cD3r (*black dashed line, squares*) were administered i.p. (10 mg/kg) to wildtype mice. ^{3}H-peptides' concentrations (triplicate) in plasma (A), brain (B), and CSF (C) were measured with liquid scintillation counting. Total peptide concentrations were calculated as % of the injected dose per g or mL (% ID/g for the brain; % ID/mL for plasma and CSF) and plotted over time.
Brain concentrations in % ID/g, CSF, and plasma concentrations in % ID/mL for each peptide were assessed in relation to each other. The brain/plasma (D), CSF/plasma (E), and brain/CSF (F) ratios were plotted over time to investigate correlation. (For interpretation of the references to color in this figure legend, the reader is referred to the web version of this article.)

and brain/CSF ratios (Fig. 1). Here, we showed a strong and direct correlation between all peptides' brain and CSF concentrations as the brain/CSF ratios were approx. 1 already 0.5 h after administration. In the following time course, some fluctuations were detected (4 h: ratios between 0.8 and 1.5). However, all peptides' brain/CSF ratios returned to approx. 1 24 h after administration. Brain/plasma as well as the CSF/plasma ratios time-dependently increased from low values shortly after administration (1 h: ratios between 0.1 and 0.4) to values of about 1 at 24 h after administration.

After evaluation of the concentration-time profiles (Fig. 1) cRD2D3 was selected as most promising of those four D-enantiomeric AD drug candidates regarding its efficiency to enter the brain and was subsequently characterized in more detail.

3.2. Further characterization of the peptide with the highest efficiency to cross the BBB: cRD2D3

3.2.1. Proteolytic stability

The proteolytic stability of the D-enantiomeric peptide cRD2D3 was investigated *ex vivo* in brain, liver, and kidney homogenates, in plasma, and in human liver microsomes and autoradiographically visualized *via* TLC. The TLC profile of ^{3}H-L-D3, the L-enantiomeric control peptide for enzyme activity, showed additional bands (black arrows) after incubation in brain, liver, and kidney homogenates, in plasma and human liver microsomes indicating proteolytic digestion (Fig. 2). In contrast, the TLC profile of ^{3}H-cRD2D3 did not show any additional bands even after 24 h of incubation suggesting proteolytic stability of the D-peptide.

3.2.2. Plasma protein binding

In order to estimate the plasma protein binding of cRD2D3 and thus, the unbound fraction (f_u), we investigated the dissociation constants of cRD2D3 to the two most abundant proteins in human plasma, HSA and AGP. Our results showed higher affinity of cRD2D3 to AGP (*Kd*: 1.2 μM, f_u: 6%) than to HSA (*Kd*: 33 μM, f_u: 5%) (Fig. 3). The overall predicted f_u in plasma considering binding to both investigated plasma proteins was 2.8%.

3.2.3. Pharmacokinetic profiles

Since we have shown that cRD2D3 efficiently passes the BBB, we generated a full pharmacokinetic profile of this peptide including brain, plasma, liver, and kidney concentration-time profiles and compared three different administration routes: i.p., i.v., and p.o. In general, these profiles showed the highest cRD2D3 concentrations in liver and kidney (metabolization and excretion) followed by plasma (distribution) and brain (site of action) (Fig. 4). This was especially pronounced for i.v. and i.p. administration, whereas the concentrations after oral administration were in a comparable range in all organs. The maximum concentration relative to the dose (C_{max}/D) after i.v. administration was detected immediately after the administration while the C_{max}/D for i.p. administration was detected 10 min after administration. From about 6 h after administration until 2 days after administration, the plasma concentration-time courses were very similar for all administration routes. On day 3 and 4 after administration, plasma concentrations following i.v. administration declined faster than those after i.p. and p.o. administration, finally leading to shorter terminal half-life ($t_{1/2}$) values after i.v. administration (Section 3.2.4).

The administration routes which are followed by initial high plasma concentration peaks, i.v. and i.p., were linked to much higher cRD2D3 concentrations in liver and kidney from the beginning to the last measured time point. In contrast, cRD2D3's concentration-time course in the brain was independent from the administration route (Fig. 4). These findings suggest that uptake and deposition of cRD2D3 in liver and kidney are concentration dependent whereas cRD2D3's uptake into the brain, which is of particular importance for an AD drug candidate, underlies a saturable mechanism.

3.2.4. Pharmacokinetic parameters

Despite the small initial concentration peaks after i.v. and i.p.

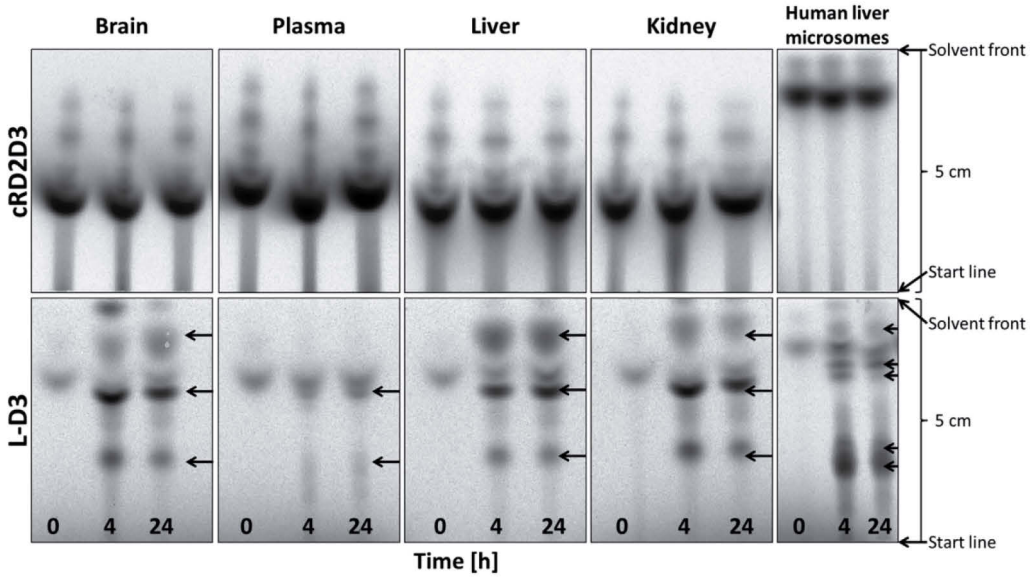

Fig. 2. Proteolytic stability.
^{3}H-cRD2D3's and ^{3}H-L-D3's (control) proteolytic stability after incubation in murine organ homogenates and plasma as well as in human liver microsomes was investigated. Samples and potential metabolites were separated *via* thin layer chromatography and bands were detected by autoradiography. Arrows highlight ^{3}H-L-D3 metabolites. As ^{3}H-cRD2D3 did not show any additional bands after incubation in the respective solutions, no metabolites were detected and cRD2D3 was considered proteolytically stable.

administration in plasma, drug exposure over time relative to the dose (AUC_{last}/D) was similar for all administration routes (approx. 0.6 (min * mg/mL)/(mg/kg)). This is also why bioavailabilities (F) for i.p. and p.o. administration were calculated to be about 100%. The mean residence time (MRT) increased from i.v. (29 h) over i.p. (34 h) to p.o. (39 h) administration. Terminal clearance (CL) was slightly lower for i.p. and p.o. than for i.v. administration while calculated $t_{1/2}$ values following i.p. and p.o. administration (58 h) were considerably longer than following i.v. administration (29 h) (Table 3). In the brain, values for C_{max}/D ranged between 0.23 and 0.28 (µg/g)/(mg/kg), and for AUC_{last}/D between 0.53 and 0.61 (min * mg/mL)/(mg/kg) indicating that both values were independent from the administration route (Table 3). Brain/plasma ratios for all administration routes increased from low ratios (i.p. 0.32, p.o. 0.57, and i.v. 0.14) early after administration to ratios around 1 which remained from 4 h after administration until the last measured time point (Fig. 5). Notably, the brain/plasma ratio after p.o. administration was higher than 1 already 1 h after administration, which was due to the lack of any plasma concentration peak after p.o. administration.

3.3. Impact of cyclization on a peptide's efficiency to cross the blood-brain barrier

We hypothesized that cyclization has a noteworthy influence on the peptide's pharmacokinetic parameters, especially raising its efficiency to pass the BBB, which is considered to be favorable for AD drugs. To proof this hypothesis, we compared cRD2D3 data to data of its linear equivalent RD2D3, which had been generated by Leithold, Jiang et al. before, using exactly the same experimental setup (Jiang et al., 2015; Leithold et al., 2016a) (Table 4). Comparing brain AUC_{0-2880}/D as well as brain concentrations (1 h after administration) of both, cyclic and linear, D-peptides after i.p. and i.v. administration, we could substantiate our hypothesis. cRD2D3's AUC_{0-2880}/D in the brain was 3.8 (i.p.) and 6.6 (i.v.) times higher than RD2D3's. One hour after administration, cRD2D3's brain concentrations were 5.9 (i.p.) and 7.1 (i.v.) times higher than RD2D3's (Table 4).

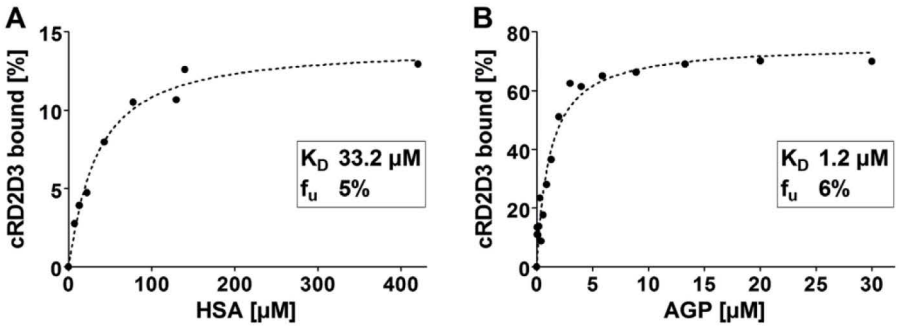

Fig. 3. Plasma protein binding to human serum albumin (HSA) and α1-acid glycoprotein (AGP).
Plasma protein binding (PPB) of a mixture of ^{3}H-cRD2D3 and cRD2D3 to HSA (A) and AGP (B) was investigated. The cRD2D3 amount (%) bound to HSA or AGP after incubation was plotted against the respective plasma protein concentration. The dissociation constants (*K*d) and fractions unbound (f_u) were determined. PPB was stronger to AGP than to HSA.

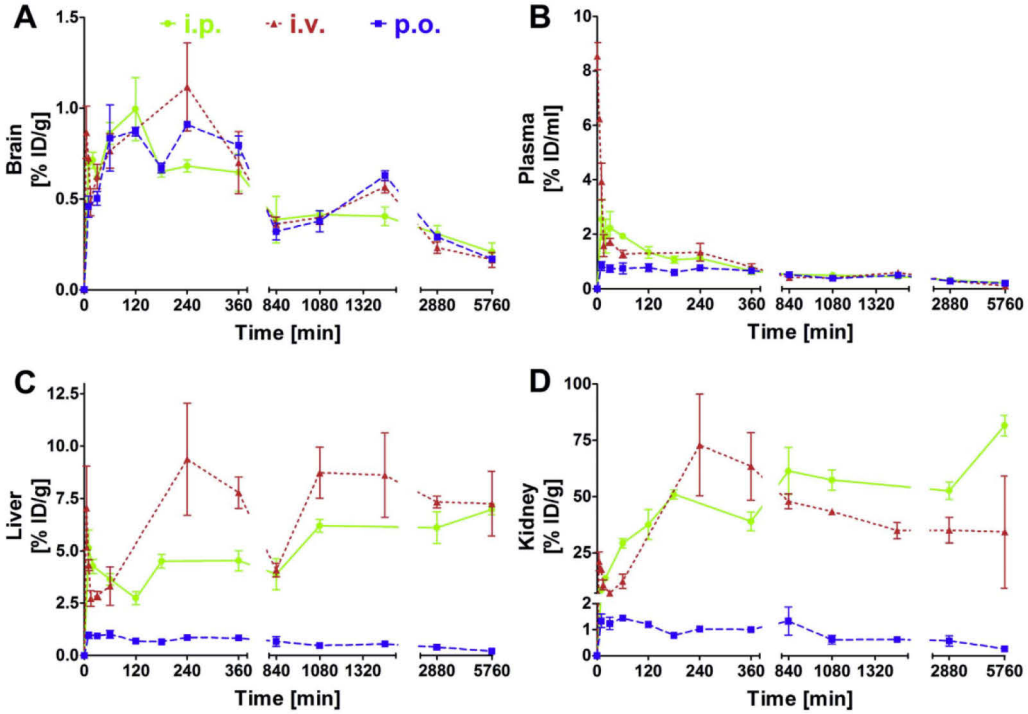

Fig. 4. Pharmacokinetic profiles of cRD2D3.
Mixtures of non-labelled and ^{3}H-labelled cRD2D3 were administered to wildtype mice: i.p. (10 mg/kg; *green line, diamonds*), i.v. (3.3 mg/kg; *red dashed line, triangles*), and p.o. (10 mg/kg; *blue dashed line, squares*). ^{3}H-cRD2D3 concentrations (triplicate) in brain (A), plasma (B), liver (C), and kidney (D) were measured with liquid scintillation counting. Total peptide concentrations were calculated as % of the injected dose per g or mL (% ID/g for brain, liver, and kidney; % ID/mL for plasma) and plotted over time. (For interpretation of the references to color in this figure legend, the reader is referred to the web version of this article.)

Table 3
Pharmacokinetic parameters for cRD2D3 in murine plasma and brain.

Parameter	Unit	i.v.	i.p.	p.o.
Plasma				
C_{max}/D	(µg/mL)/(mg/kg)	1.64	0.69	0.24
AUC_{last}/D	(min * mg/mL)/(mg/kg)	0.60	0.65	0.59
MRT	h	29	34	38
λ_z	1/min	0.0004	0.0002	0.0002
$t_{1/2}$	h	29	58	58
F (AUC_{last})	%	100[b]	108[a]	98
CL	mL/(min * kg)	1.5	1.1	1.2
Brain				
C_{max}/D	(µg/g)/(mg/kg)	0.23	0.28	0.25
AUC_{last}/D	(min * mg/g)/(mg/kg)	0.53	0.56	0.61

See list of abbreviations for explanation of pharmacokinetic parameters.
[a] Interindividual fluctuations lead to a mathematical bioavailability of 108%.
[b] By definition.

Next, we verified that higher cRD2D3 concentrations in brain resulted from cRD2D3's more efficient BBB permeation and not from higher cRD2D3 concentrations in plasma by comparing the amounts of cRD2D3 and RD2D3 found in plasma (AUC_{0-2880}/D, plasma concentrations 1 h after administration). Thereby, we showed that uptake into plasma (after i.p. administration), and clearance out of plasma (after i.p., and i.v. administration) did not notably differ between cRD2D3 and RD2D3: cRD2D3's AUC_{0-2880}/D in plasma was only 2.4 (i.p.) or 4.5 (i.v.) times higher than RD2D3's while plasma concentrations were nearly equal for cRD2D3 and RD2D3 1 h after administration (Table 4). Furthermore, the brain/plasma ratio based on the AUC_{0-2880}/D was determined. For cRD2D3, the ratio was 1.62 (i.p.) or 1.37 (i.v.) times higher than for RD2D3 (Table 4) leading to the conclusion that brain uptake across the BBB was more efficient for the cyclic peptide and independent from its uptake into plasma.

The BBB values determined for cRD2D3 and RD2D3 (RD2D3 values based on data which had been generated by Leithold, Jiang et al. before using exactly the same experimental setup (Jiang et al., 2015; Leithold et al., 2016a)) were listed in Table 4 to allow for direct comparison of the cyclic peptide and its linear equivalent. While the logBB value represents the blood-brain equilibrium distribution, the K_{in} describes the kinetics of the BBB permeability. Directly linked to determination of the K_{in} is the V_i describing the investigated peptides' fictional distribution volume in the brain shortly after administration. Here, we determined a nearly threefold higher logBB value for cRD2D3 than for RD2D3. K_{in} was nearly seven times higher for cRD2D3 than for RD2D3, and V_i was nearly four times higher for the cyclic than for the linear D-peptide. Finally, the permeability surface-area product (PS), representing uptake clearance from blood to brain, was determined. As PS values were, due to the estimated CBF of 1.07 mL/(g * min) (Muir et al., 2008), nearly the same values as the K_{in} values, the relative proportion between cRD2D3 and RD2D3 was the same as for K_{in}.

To investigate whether increased BBB penetration is a general property of cyclic peptides, we compared cD3D3 and cD3r with their linear equivalents D3D3 (Leithold et al., 2016a) and D3 (Jiang et al., 2015) after i.p. administration. Here, we could show once more that all brain concentrations of the cyclic peptides were considerably higher than those of their linear equivalents while plasma concentrations were in the same range (Fig. 6). Taking the brain/plasma ratios based on the AUC_{0-1440} into account we found factors between the cyclic and the

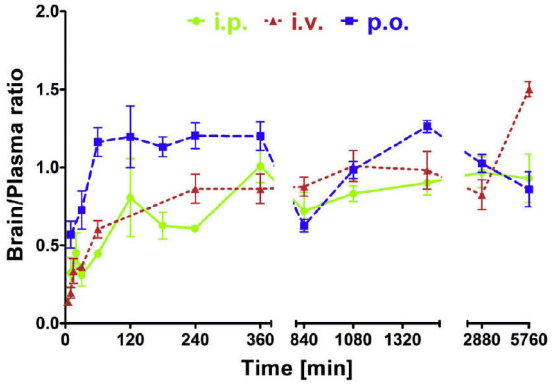

Fig. 5. Brain/Plasma ratios for different cRD2D3 administration routes.
Ratios of cRD2D3 brain concentrations divided by cRD2D3 plasma concentrations were plotted over time after administration to wildtype mice: i.p. (*green line, diamonds*), i.v. (*red dashed line, triangles*) and p.o. (*blue dashed line, squares*). Concentrations in brain and plasma equalized fastest after p.o. administration as the brain/plasma ratio was about 1 already 60 min after administration. (For interpretation of the references to color in this figure legend, the reader is referred to the web version of this article.)

Table 4
Pharmacokinetic parameters and BBB values for cRD2D3 and RD2D3* (Leithold et al., 2016a) in murine brain and plasma.

Parameter	Unit	i.v.		i.p.	
		cRD2D3	RD2D3*	cRD2D3	RD2D3*
Brain					
AUC_{0-2880}/D	(min * mg/g)/(mg/kg)	0.37	0.06	0.35	0.09
$C_{60\ min}$/D	(μg/g)/(mg/kg)	0.17	0.02	0.23	0.04
Plasma					
AUC_{0-2880}/D	(min * mg/mL)/(mg/kg)	0.45	0.10	0.43	0.18
$C_{60\ min}$/D	(μg/mL)/(mg/kg)	0.29	0.28	0.52	0.47
$t_{1/2}$	h	29	0.85	58	2.29
BBB values					
AUC_{0-2880}/D (brain)/AUC_{0-2880}/D (plasma)	–	0.82	0.60	0.81	0.50
logBB	–	−0.086	−0.222	na	na
K_{in}	mL/(g * min)	0.002	0.0003	na	na
V_{in}	mL/g	0.1955	0.0512	na	na
PS	mL/(g * min)	0.002	0.0003	na	na

linear peptides' ratios of 1.46 for the comparison between cD3r and D3, and 3.67 for the comparison between cD3D3 and D3D3.

4. Discussion

Initially, we compared four D-enantiomeric peptides concerning their efficiencies to cross the BBB. For AD drugs, passing the BBB is particularly important as the brain is the potential site of action. Considering brain, plasma, and CSF concentration-time profiles of the investigated D-peptides after i.p. administration, cRD2D3 overall achieved the highest brain and CSF concentrations (Fig. 1). Its plasma concentration-time profile was in the same range as the other peptides' profiles. These findings suggested that cRD2D3 was similarly taken up into plasma after i.p. administration but revealed an extraordinarily high drug exposure in the brain. This was not expected before since permeability for the BBB was thought to be dependent on the peptide lengths (Leithold et al., 2016a). cRD2D3 consists of twice as many amino acid residues as RD2 and cD3r and includes the same number of amino acid residues as cD3D3 (Table 1). Remarkably, comparison of brain concentrations of the linear 12-mer peptide RD2 and the cyclic 13-mer peptide cD3r disclosed that the linear peptide yielded higher brain concentrations than the cyclic one although they do consist of the same amino acid residues (except of one additional arginine in cD3r), only arranged in different sequences (Table 1). Obviously, the amino acid residue sequence of RD2 had more beneficial influence on BBB permeability than the sequence of D3 in combination with cyclization. Summarizing, cRD2D3 combined both beneficial BBB permeation properties, cyclization and the RD2 sequence, and is thus the D-peptide with the highest brain levels. As we were interested whether peptide concentrations in brain and CSF correlate, we investigated the peptides' brain/plasma, CSF/plasma, and brain/CSF ratios (Fig. 1). Brain/plasma and CSF/plasma ratios increased from values around 0.1 and 0.4 shortly after administration to values around 1 at 24 h after administration. This suggested that it took some time until the equilibrium between plasma and brain as well as plasma and CSF was reached. In contrast, there was no gradient to overcome between brain and CSF concentrations as the brain/CSF ratio was about 1 already at the first measured time point. Although a clear distinction of D-peptide penetration into CSF, across the blood-CSF barrier in the choroid plexus, and D-peptide penetration into the brain parenchyma, across the BBB, has to be made (Pardridge, 2016), correlation of D-peptide concentrations in brain parenchyma with those in CSF is reasonable. Of course, D-peptides' transport across the BBB cannot directly be reflected by their CSF concentrations as permeation of substances from CSF into the brain parenchyma is restricted by slow diffusion. Remarkably, the CSF/plasma ratio of IgG and other therapeutic antibodies is in the range of 0.2% (Pardridge, 2016) whereas the D-peptides investigated in this study reached CSF/plasma as well as brain/plasma ratios higher than 50% already 4 h after administration. Additionally, the D-peptides' brain/CSF ratios were about 100% (ratios varied between 75 and 150%) from the first (30 min) to the last (1440 min) measured time point. Summarizing, these findings speak for direct BBB permeation of the D-peptides from plasma into the brain; instead of initial blood-CSF barrier (choroid plexus) permeation from plasma into the CSF, which would then be followed by slow diffusion from CSF into the brain.

The methodology applied here does not allow for differentiation between the amount of D-peptide in brain parenchyma compared to the amount of D-peptide in and on brain capillaries. However, Jiang et al. have previously shown that the fluorescently labelled D-enantiomeric D3 (Table 3), the lead compound after which the peptides examined in this study were designed, did not bind to capillaries in the brain (Jiang et al., 2016). Furthermore, as animals were sacrificed by heart puncture, only little blood was left in the brain after finalization. Thus, we considered the residual volume of blood in the brain and bound to brain vessels as negligible.

Besides other advantages, we designed D-peptides targeting Aβ oligomers because of their high proteolytic stability. Here, we proved that cRD2D3 can be considered proteolytically stable as no additional band appeared in the TLC profile after incubation in plasma, organ homogenates, or human liver microsomes within 24 h of incubation. Of note, cRD2D3 already showed multiple bands at time point 0 h (negative control) most likely due to peptide binding to different ingredients of the respective organ homogenate or plasma solution, resulting in different retention times in the TLC. To show that degrading enzymes in the respective solutions were proteolytically active, an L-enantiomeric control peptide was also incubated and, as expected, additional bands in its TLC patterns were observed already after 4 h incubation indicating formation of metabolites. No metabolites were observed after cRD2D3 incubation. Thus, the measured ^{3}H-cRD2D3 radioactivity was anticipated to correctly reflect the total cRD2D3 concentration in the following pharmacokinetic experiments as described for other D-peptides before, where this methodology was evaluated in further detail (Jiang et al., 2015; Leithold et al., 2016a; Leithold et al., 2016b). All

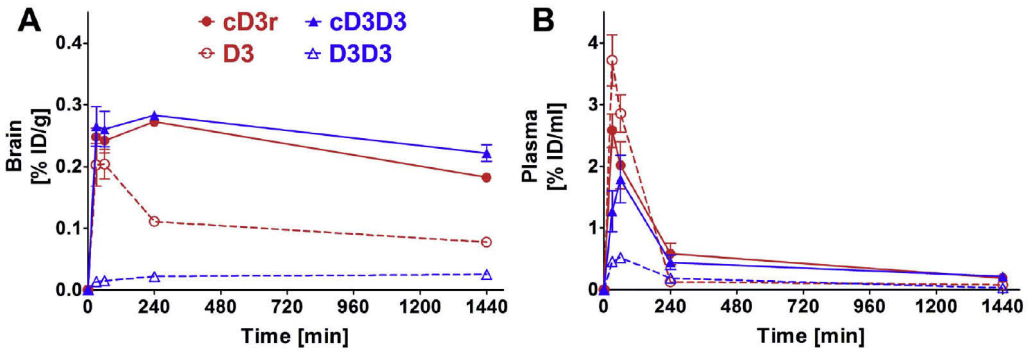

Fig. 6. Comparison of cyclic and linear peptides' brain and plasma concentration-time profiles.
Mixtures of non-labelled and ^{3}H-labelled of two cyclic D-enantiomeric peptides (cD3r: *red line, filled circles*; cD3D3: *blue line, filled triangles*) and their linear equivalents (D3: *red dashed line, open circles*; D3D3: *blue dashed line, open triangles*) were i.p. (10 mg/kg) administered to wildtype mice. ^{3}H-peptides' concentrations (triplicate) in brain (A) and plasma (B) were measured with liquid scintillation counting. Total peptide concentrations were calculated as % of the injected dose per g or mL (% ID/g for brain; % ID/mL for plasma) and plotted over time. Values for D3 were derived from Jiang et al. (Jiang et al., 2015) and values for D3D3 were derived from Leithold et al. (Leithold et al., 2016a). (For interpretation of the references to color in this figure legend, the reader is referred to the web version of this article.)

peptides were tritium-labelled in position 4 and 5 of a D-leucine amino acid residue (4,5-^{3}H-D-Leu) by tritium gassing of a precursor peptide which included 4,5-dehydro-D-leucine. As the tritium-label position is in an alkyl group, the labels were considered to be biologically stable. Any significant fraction of metabolites formed from cRD2D3 would have led to additional radioactive bands in the autoradiography of the TLC plate. In addition, recently Elfgen et al. conducted stability experiments with the lead compound D3 (Table 3), where they could show that the peptide was stable after different incubation periods in different media simulating the oral administration route (*e.g.* plasma, and human liver microsomes) using reversed phase HPLC analytics (Elfgen et al., 2017).

The stronger a drug binds to plasma proteins, the smaller is the amount of the drug freely circulating in plasma (f_u). High plasma protein binding might result in lower concentrations at the site of action but can also be advantageous because plasma proteins can work as drug releasing depot. This depot function can lead to consistent drug distribution in plasma over time. Thus, the risk of adverse side effects is lowered while longer MRTs are achieved (Gillette, 1973; Lambrinidis et al., 2015). In the most favorable case, once daily drug administration becomes possible for therapeutic regimens, which in turn is known to lead to the highest possible compliance (Eisen et al., 1990). We investigated binding to HSA which tends to bind acidic and neutral drugs rather than basic ones and to AGP which tends to bind alkaline drugs. These two proteins represent about 55% (HSA) and 1–3% (AGP) of all human plasma proteins (Lambrinidis et al., 2015). For cRD2D3, we expected stronger binding to AGP due to the high amount of basic arginines in its amino acid sequence (Table 1). This assumption was verified (*Kd* AGP: 1.2 μM; *Kd* HSA: 33 μM). Here, we calculated a total f_u of 2.8% considering influence of HSA and AGP. As > 97% of the administered drug is bound to plasma proteins, the above mentioned advantages might play a role for cRD2D3.

Having a closer look at cRD2D3's concentration-time profiles in the drug metabolization and excretion organs (liver and kidney) revealed a huge difference depending on the respective administration route (Fig. 4). The discrepancy might be explained by the initial high (i.v. and i.p.) or low (p.o.) plasma concentrations following drug administration. The more cRD2D3 was taken up directly after administration, the higher were the concentrations in liver and kidney hours after administration. This suggests that cRD2D3 may be enriched in these organs after i.v. and i.p. administration and is only slowly excreted from there. Compared to other previously examined D-peptides, the calculated CL values were quite similar within all administration routes (cRD2D3: i.v. 1.5, i.p. 1.1, p.o. 1.2 mL/(min ∗ kg); RD2D3 (Leithold et al., 2016a): i.v. 10.2, i.p. 5.4 mL/(min ∗ kg)). Nevertheless, the slightly different CL values as well as differences in λ_z and $t_{1/2}$ between intravenous and extravascular administration routes might be explained due to retarded distribution processes after extravascular administrations. As AD-treatment mainly targets elderly people and needs to be long-term, oral administration is the preferable administration route. In our experiments, low concentrations in liver and kidney were observed after oral administration. This is beneficial as strong accumulation can be a hindrance for adequate therapeutic dosing in long-term treatment. Furthermore, drugs with high oral bioavailability and long $t_{1/2}$ are of enormous benefit for long-term treatment. Thus, it additionally is of advantage that cRD2D3 is characterized by a much longer $t_{1/2}$ in plasma in contrast to its linear equivalent (Table 4). Of note, drugs with long $t_{1/2}$ are considered to be "forgiving drugs" and at the same time usually allow therapeutic regimens with once daily administration being beneficial for compliance (Eisen et al., 1990; Urquhart, 1996). Another beneficial property of cRD2D3 is a brain/plasma ratio higher than 1 already one hour after oral administration suggesting rapid uptake into the brain (Fig. 5).

In order to allow for BBB value comparison of the D-peptides examined in this study to other peptides listed in "Brainpeps: the blood-brain barrier peptide database", we determined different parameters (Table 4) (Van Dorpe et al., 2012): For cRD2D3, we calculated a nearly three times higher logBB value than for RD2D3 leading to the conclusion that the cyclic peptide enters the brain from plasma nearly three times more efficiently than the linear peptide. Nevertheless, one has to keep in mind that the logBB value depends on binding to plasma and brain tissue as well as on active transport. Graphic determination of K_{in} resulted in a nearly sevenfold higher K_{in} for cRD2D3 than for RD2D3 indicating that cRD2D3 crosses the BBB faster than RD2D3. As the calculated PS values did not notably differ from the previously determined K_{in} values, a higher uptake clearance from blood to brain for cRD2D3 than for RD2D3 is assumed. Comparison of the values determined for cRD2D3 with values of Dermorphin, a potent natural opioid consisting of five amino acid residues including one D-enantiomeric amino acid residue listed in "Brainpeps", revealed that they are in a similar range. K_{in} values determined for Dermorphin lie between 0.0002 and 0.0022 mL/(g ∗ min) while Dermorphin's V_i values were determined to be between 0.0162 and 0.0215 mL/g (Stalmans et al., 2015; Van Dorpe et al., 2010). As Dermorphin has even been suggested to be used as positive control in BBB permeability experiments (Van Dorpe et al., 2012), these results additionally underline cRD2D3's efficient BBB permeability.

As comparison of three cyclic peptides and their linear equivalents

with special attention to cRD2D3 and RD2D3 clearly indicated that cyclization has a positive impact on peptides' efficiencies to cross the BBB, it was of interest how this increased efficiency could be explained. Interestingly, brain concentrations were independent from any plasma concentration peak, which most likely suggests a saturable BBB passage mechanism. This was already reported in detail for the lead compound D3 by Jiang et al. (Jiang et al., 2016) and for the D3 derivative RD2 (Leithold et al., 2016b). D3 and RD2 have arginine-rich motifs (ARMs) and were suggested to be transported across membranes, and ultimately across the BBB, with a human deficiency virus type 1 (HIV-1) transactivator of transcription (Tat) like BBB transport mechanism (Futaki et al., 2003; Vives et al., 1997). As cRD2D3 is a cyclized version of the head-to-tail combination RD2D3, similarities in its pharmacokinetic behavior can be anticipated. However, the assumption for the underlying mechanism is also true for linear RD2D3, although the cyclic version is even more efficiently transported. We set up three hypotheses, which are partly connected to the HIV-1 Tat hypothesis, trying to explain this circumstance. According to our first hypothesis, cRD2D3 exposes the ARM with its numerous guanidinium groups more efficiently than the linear RD2D3, enabling passive transduction to a higher extent. According to the second hypothesis, cyclization downsizes the hydrodynamic radius of cRD2D3 and thus further simplifies passive transduction. Passive membrane permeability has been shown before for cyclic peptides (*e.g.* cyclosporine A) (Ahlbach et al., 2015). According to the third hypothesis, there might be a difference in cRD2D3's and RD2D3's brain efflux vulnerabilities by *e.g.* ATP binding cassette (ABC) transporters, and the Low Density Lipoprotein Receptor-related Protein 1 (LRP1) which might be more efficient for the linear RD2D3 than for the cyclic cRD2D3. Both, ABC transporters as well as LRP1 are responsible for the outward transport of peptides, *e.g.* Aβ, across the BBB from the brain back into the blood (Pahnke et al., 2014; Storck et al., 2016). As the N- and C-termini of cyclic peptides are modified, ABC transporters as well as LRP1 might not directly be able to identify the cyclic peptide, thus its transport out of the brain is decreased. Summarized, peptides' cyclization resulted in increased efficiencies to pass the murine BBB while the peptides' uptake from peritoneum into plasma, for example, was far less affected due to cyclization.

5. Conclusion

The hereby presented results suggest that concentrations of the investigated Aβ oligomer-targeting D-enantiomeric peptides in murine brain and CSF directly correlate. Furthermore, the head-to-tail cyclized D-peptide cRD2D3 was determined, out of four optimized D3 derivatives, to be the one with the highest efficiency to pass the murine BBB. Direct comparison of three cyclic D-peptides to their linear equivalents revealed an increase in the peptides' efficiencies to pass the murine BBB due to cyclization. Further experiments showed that cRD2D3 is characterized by high proteolytic stability and oral bioavailability, long duration of action and a favorable brain/plasma ratio proposing that it is a suitable drug for long-term AD-treatment from a pharmacokinetic perspective.

Abbreviations

ABC	ATP binding cassette
AD	Alzheimer's disease
ARM	arginine rich motif
AUC_p (t)	area under the curve in plasma from the first measured time point to time point t
AUC_{last}	area under the curve from the first to the last measured data pair
$AUMC_{last}$	area under the first moment curve from the first to the last measured data pair
Aβ	amyloid β
BBB	blood-brain barrier
CBF	(murine) cerebral blood flow
C_b (t)	D-peptide concentration in brain at time t
CL	clearance
C_{max}	maximum concentration
C_p (t)	D-peptide concentration in plasma at time t
CSF	cerebrospinal fluid
D	administered dose
e.v.	extravascular
f_u	free drug fraction; fraction unbound
F	bioavailability
i.p.	intraperitoneal
i.v.	intravascular
HIV-1	human deficiency virus type 1
ICS-6	Institute of Complex Systems, Structural Biochemistry
INM-4	Institute of Neuroscience and Medicine
Kd	dissociation constant
K_{in}	unidirectional influx rate constant
logBB	blood-brain equilibrium distribution
LRP1	Low Density Lipoprotein Receptor-related Protein 1
LSC	liquid scintillation counter
MRT	mean residence time
p.o.	oral
PBS	phosphate buffered saline
PPB	plasma protein binding
PS	permeability surface-area product
$t_{1/2}$	terminal half-life
Tat	transactivator of transcription
TLC	thin layer chromatography
V_i	initial distribution volume
λ_z	terminal elimination rate constant

Author contributions

A.W. and D.W. designed the overall study. D.W., A.W., J.K. and E.S. designed the experiments. E.S. and M.T. carried out preliminary experiments that were important for the final study design. E.S. and S.S. planned and carried out all pharmacokinetic experiments. E.S. calculated the pharmacokinetic parameters and implemented the proteolytic stability tests with support from L.H.E.L. and N.J. E.S. performed the plasma protein binding tests and evaluated the results with support from T.Z. E.S., A.W., J.K. and D.W. wrote the manuscript. All other authors contributed to writing.

Competing financial interest

The authors declare no competing financial interests.

Acknowledgement

D.W. and K.J.L. were supported by grants from the "Portfolio Technology and Medicine", and D.W. was additionally supported by the "Portfolio Drug Research" and the Helmholtz-Validierungsfonds of the "Impuls und Vernetzungs-Fonds der Helmholtzgemeinschaft". The study was supported by the TT-Fonds of the Technology Transfer Department of the Forschungszentrum Jülich.

References

Ahlbach, C.L., Lexa, K.W., Bockus, A.T., Chen, V., Crews, P., Jacobson, M.P., Lokey, R.S., 2015. Beyond cyclosporine A: conformation-dependent passive membrane permeabilities of cyclic peptide natural products. Future Med. Chem. 7, 2121–2130.

Anand, R., Gill, K.D., Mahdi, A.A., 2014. Therapeutics of Alzheimer's disease: past, present and future. Neuropharmacology 76 (Pt A), 27–50.

Bartnik, D., Funke, S.A., Andrei-Selmer, L.-C., Bacher, M., Dodel, R., Willbold, D., 2010. Differently selected D-enantiomeric peptides act on different Aβ species. Rejuvenation Res. 13, 202–205.

Brener, O., Dunkelmann, T., Gremer, L., van Groen, T., Mirecka, E.A., Kadish, I., Willuweit, A., Kutzsche, J., Jurgens, D., Rudolph, S., Tusche, M., Bongen, P., Pietruszka, J., Oesterhelt, F., Langen, K.J., Demuth, H.U., Janssen, A., Hoyer, W., Funke, S.A., Nagel-Steger, L., Willbold, D., 2015. QIAD assay for quantitating a compound's efficacy in elimination of toxic Abeta oligomers. Sci. Rep. 5, 13222.

Eisen, S.A., Miller, D.K., Woodward, R.S., Spitznagel, E., Przybeck, T.R., 1990. The effect of prescribed daily dose frequency on patient medication compliance. Arch. Intern. Med. 150, 1881–1884.

Elfgen, A., Santiago-Schubel, B., Gremer, L., Kutzsche, J., Willbold, D., 2017. Surprisingly high stability of the Abeta oligomer eliminating all-d-enantiomeric peptide D3 in media simulating the route of orally administered drugs. Eur. J. Pharm. Sci. 107, 203–207.

Funke, S.A., Willbold, D., 2009. Mirror image phage display—a method to generate D-peptide ligands for use in diagnostic or therapeutical applications. Mol. BioSyst. 5, 783–786.

Funke, S.A., van Groen, T., Kadish, I., Bartnik, D., Nagel-Steger, L., Brener, O., Sehl, T., Batra-Safferling, R., Moriscot, C., Schoehn, G., Horn, A.H., Muller-Schiffmann, A., Korth, C., Sticht, H., Willbold, D., 2010. Oral treatment with the D-enantiomeric peptide D3 improves the pathology and behavior of Alzheimer's disease transgenic mice. ACS Chem. Neurosci. 1, 639–648.

Futaki, S., Goto, S., Sugiura, Y., 2003. Membrane permeability commonly shared among arginine-rich peptides. J. Mol. Recognit. 16, 260–264.

Gillette, J.R., 1973. Overview of drug-protein binding. Ann. N. Y. Acad. Sci. 226, 6–17.

Haass, C., Selkoe, D.J., 2007. Soluble protein oligomers in neurodegeneration: lessons from the Alzheimer's amyloid beta-peptide. Nat. Rev. Mol. Cell Biol. 8, 101–112.

Jiang, N., Leithold, L.H., Post, J., Ziehm, T., Mauler, J., Gremer, L., Cremer, M., Schartmann, E., Shah, N.J., Kutzsche, J., Langen, K.J., Breitkreutz, J., Willbold, D., Willuweit, A., 2015. Preclinical pharmacokinetic studies of the tritium labelled D-enantiomeric peptide D3 developed for the treatment of Alzheimer's disease. PLoS One 10, e0128553.

Jiang, N., Frenzel, D., Schartmann, E., van Groen, T., Kadish, I., Shah, N.J., Langen, K.J., Willbold, D., Willuweit, A., 2016. Blood-brain barrier penetration of an Abeta-targeted, arginine-rich, D-enantiomeric peptide. Biochim. Biophys. Acta 1858, 2717–2724.

Klein, A.N., Ziehm, T., Tusche, M., Buitenhuis, J., Bartnik, D., Boeddrich, A., Wiglenda, T., Wanker, E., Funke, S.A., Brener, O., Gremer, L., Kutzsche, J., Willbold, D., 2016. Optimization of the all-D peptide D3 for Abeta oligomer elimination. PLoS One 11, e0153035.

Kutzsche, J., Schemmert, S., Tusche, M., Neddens, J., Rabl, R., Jurgens, D., Brener, O., Willuweit, A., Hutter-Paier, B., Willbold, D., 2017. Large-scale oral treatment study with the four most promising D3-derivatives for the treatment of Alzheimer's disease. Molecules (Basel, Switzerland) 22.

Lambrinidis, G., Vallianatou, T., Tsantili-Kakoulidou, A., 2015. In vitro, in silico and integrated strategies for the estimation of plasma protein binding. A review. Adv. Drug Deliv. Rev. 86, 27–45.

Leithold, L.H., Jiang, N., Post, J., Niemietz, N., Schartmann, E., Ziehm, T., Kutzsche, J., Shah, N.J., Breitkreutz, J., Langen, K.J., Willuweit, A., Willbold, D., 2016a. Pharmacokinetic properties of tandem d-peptides designed for treatment of Alzheimer's disease. Eur. J. Pharm. Sci. 89, 31–38.

Leithold, L.H., Jiang, N., Post, J., Ziehm, T., Schartmann, E., Kutzsche, J., Shah, N.J., Breitkreutz, J., Langen, K.J., Willuweit, A., Willbold, D., 2016b. Pharmacokinetic properties of a novel D-peptide developed to be therapeutically active against toxic beta-amyloid oligomers. Pharm. Res. 33, 328–336.

Liu, H., Funke, S.A., Willbold, D., 2010. Transport of Alzheimer disease amyloid-beta-binding D-amino acid peptides across an in vitro blood-brain barrier model. Rejuvenation Res. 13, 210–213.

Liu, H.N., Tjostheim, S., Dasilva, K., Taylor, D., Zhao, B., Rakhit, R., Brown, M., Chakrabartty, A., McLaurin, J., Robertson, J., 2012. Targeting of monomer/misfolded SOD1 as a therapeutic strategy for amyotrophic lateral sclerosis. J. Neurosci. 32, 8791–8799.

Muir, E.R., Shen, Q., Duong, T.Q., 2008. Cerebral blood flow MRI in mice using the cardiac-spin-labeling technique. Magn. Reson. Med. 60, 744–748.

Olubiyi, O.O., Strodel, B., 2012. Structures of the amyloid beta-peptides Abeta1-40 and Abeta1-42 as influenced by pH and a D-peptide. J. Phys. Chem. B 116, 3280–3291.

Olubiyi, O.O., Frenzel, D., Bartnik, D., Gluck, J.M., Brener, O., Nagel-Steger, L., Funke, S.A., Willbold, D., Strodel, B., 2014. Amyloid aggregation inhibitory mechanism of arginine-rich D-peptides. Curr. Med. Chem. 21, 1448–1457.

Pahnke, J., Langer, O., Krohn, M., 2014. Alzheimer's and ABC transporters—new opportunities for diagnostics and treatment. Neurobiol. Dis. 72 (Pt A), 54–60.

Pardridge, W.M., 2016. CSF, blood-brain barrier, and brain drug delivery. Expert Opin. Drug Deliv. 13, 963–975.

Schumacher, T.N.M., Mayr, L.M., Minor, D.L., Milhollen, M.A., Burgess, M.W., Kim, P.S., 1996. Identification of D-peptide ligands through mirror-image phage display. Science 271, 1854–1857.

Stalmans, S., Bracke, N., Wynendaele, E., Gevaert, B., Peremans, K., Burvenich, C., Polis, I., De Spiegeleer, B., 2015. Cell-penetrating peptides selectively cross the blood-brain barrier in vivo. PLoS One 10, e0139652.

Storck, S.E., Meister, S., Nahrath, J., Meissner, J.N., Schubert, N., Di Spiezio, A., Baches, S., Vandenbroucke, R.E., Bouter, Y., Prikulis, I., Korth, C., Weggen, S., Heimann, A., Schwaninger, M., Bayer, T.A., Pietrzik, C.U., 2016. Endothelial LRP1 transports amyloid-beta(1-42) across the blood-brain barrier. J. Clin. Invest. 126, 123–136.

Thal, D.R., Capetillo-Zarate, E., Del Tredici, K., Braak, H., 2006. The development of amyloid beta protein deposits in the aged brain. Sci. Aging Knowl. Environ. 2006 (6), re1–9.

Urquhart, J., 1996. Patient non-compliance with drug regimens: measurement, clinical correlates, economic impact. Eur. Heart J. 17 (Suppl. A), 8–15.

Van Dorpe, S., Adriaens, A., Polis, I., Peremans, K., Van Bocxlaer, J., De Spiegeleer, B., 2010. Analytical characterization and comparison of the blood-brain barrier permeability of eight opioid peptides. Peptides 31, 1390–1399.

Van Dorpe, S., Bronselaer, A., Nielandt, J., Stalmans, S., Wynendaele, E., Audenaert, K., Van De Wiele, C., Burvenich, C., Peremans, K., Hsuchou, H., De Tre, G., De Spiegeleer, B., 2012. Brainpeps: the blood-brain barrier peptide database. Brain Struct. Funct. 217, 687–718.

van Groen, T., Wiesehan, K., Funke, S.A., Kadish, I., Nagel-Steger, L., Willbold, D., 2008. Reduction of Alzheimer's disease amyloid plaque load in transgenic mice by D3, a D-enantiomeric peptide identified by mirror image phage display. ChemMedChem 3, 1848–1852.

van Groen, T., Kadish, I., Wiesehan, K., Funke, S.A., Willbold, D., 2009. In vitro and in vivo staining characteristics of small, fluorescent, Abeta42-binding D-enantiomeric peptides in transgenic AD mouse models. ChemMedChem 4, 276–282.

van Groen, T., Kadish, I., Funke, A., Bartnik, D., Willbold, D., 2012. Treatment with Abeta42 binding D-amino acid peptides reduce amyloid deposition and inflammation in APP/PS1 double transgenic mice. Adv. Protein Chem. Struct. Biol. 88, 133–152.

van Groen, T., Kadish, I., Funke, S.A., Bartnik, D., Willbold, D., 2013. Treatment with D3 removes amyloid deposits, reduces inflammation, and improves cognition in aged AbetaPP/PS1 double transgenic mice. J. Alzheimers Dis. 34, 609–620.

Vives, E., Brodin, P., Lebleu, B., 1997. A truncated HIV-1 Tat protein basic domain rapidly translocates through the plasma membrane and accumulates in the cell nucleus. J. Biol. Chem. 272, 16010–16017.

Wiesehan, K., Willbold, D., 2003. Mirror-image phage display: aiming at the mirror. Chembiochem 4, 811–815.

Wiesehan, K., Buder, K., Linke, R.P., Patt, S., Stoldt, M., Unger, E., Schmitt, B., Bucci, E., Willbold, D., 2003. Selection of D-amino-acid peptides that bind to Alzheimer's disease amyloid peptide abeta1-42 by mirror image phage display. Chembiochem 4, 748–753.

Wiesehan, K., Stohr, J., Nagel-Steger, L., van Groen, T., Riesner, D., Willbold, D., 2008. Inhibition of cytotoxicity and amyloid fibril formation by a D-amino acid peptide that specifically binds to Alzheimer's disease amyloid peptide. Protein Eng. Des. Sel. 21, 241–246.

Ziehm, T., Brener, O., van Groen, T., Kadish, I., Frenzel, D., Tusche, M., Kutzsche, J., Reiss, K., Gremer, L., Nagel-Steger, L., Willbold, D., 2016. Increase of positive net charge and conformational rigidity enhances the efficacy of D-enantiomeric peptides designed to eliminate cytotoxic Abeta species. ACS Chem. Neurosci. 7, 1088–1096.

3.5 Aβ oligomer eliminating compounds interfere successfully with pEAβ(3–42) induced motor neurodegenerative phenotype in transgenic mice

Autoren:	Dunkelmann T., Teichmann K., Ziehm T., **Schemmert S.**, Frenzel D., Tusche M. Dammers C., Jürgens D., Demuth H-U., Langen K-J., Kutzsche J., Willuweit A., Willbold D.
Journal:	Neuropeptides (2017), veröffentlicht am 26. November 2017
DOI:	10.1016/j.npep.2017.11.011
Impact Factor:	2,486 (2016)
Beitrag:	Durchführung und Analyse der Immunhistologie Anfertigung der Abbildungen (Immunhistologie) statistische Auswertung Mitverfassung und Prüfung des Manuskriptes.

ARTICLE IN PRESS

Neuropeptides xxx (xxxx) xxx–xxx

Contents lists available at ScienceDirect

Neuropeptides

journal homepage: www.elsevier.com/locate/npep

Aβ oligomer eliminating compounds interfere successfully with pEAβ(3–42) induced motor neurodegenerative phenotype in transgenic mice

Tina Dunkelmann[a,1], Kerstin Teichmann[a,2], Tamar Ziehm[a], Sarah Schemmert[a], Daniel Frenzel[a,3], Markus Tusche[a], Christina Dammers[a,4], Dagmar Jürgens[a], Karl-Josef Langen[b,c], Hans-Ulrich Demuth[d], Nadim Jon Shah[b,e,f], Janine Kutzsche[a], Antje Willuweit[b,**], Dieter Willbold[a,g,*]

[a] Institute of Complex Systems, Structural Biochemistry (ICS-6), Forschungszentrum Jülich GmbH, Wilhelm-Johnen Straße, 52425 Jülich, Germany
[b] Institute of Neuroscience and Medicine (INM-4), Medical Imaging Physics, Forschungszentrum Jülich GmbH, Wilhelm-Johnen Straße, 52425 Jülich, Germany
[c] Department of Nuclear Medicine, Faculty of Medicine, RWTH Aachen University, Pauwelsstraße 30, 52074 Aachen, Germany
[d] Fraunhofer-Institute of Cell Therapy and Immunology (IZI), Leipzig, Department of Drug Design and Target Validation (MWT), Biozentrum, Weinbergweg 22, 06120 Halle, Germany
[e] Department of Neurology, Faculty of Medicine, JARA, RWTH Aachen University, Pauwelsstraße 30, 52074 Aachen, Germany
[f] Department of Electrical and Computer Systems Engineering and Monash Biomedical Imaging, School of Psychological Sciences, Monash University, Melbourne, Victoria, Australia
[g] Institut für Physikalische Biologie, Heinrich Heine Universität Düsseldorf, Universitätsstraße 1, 40225 Düsseldorf, Germany

ARTICLE INFO

Keywords:
pEAβ(3–42)
D3
D3D3
Neurodegeneration
Alzheimer's disease
Animal model
Treatment
All-D-enantiomeric peptides
TBA2.1

ABSTRACT

Currently, there are no causative or disease modifying treatments available for Alzheimer's disease (AD). Previously, it has been shown that D3, a small, fully D-enantiomeric peptide is able to eliminate low molecular weight Aβ oligomers in vitro, enhance cognition and reduce plaque load in AD transgenic mice. To further characterise the therapeutic potential of D3 towards N-terminally truncated and pyroglutamated Aβ (pEAβ(3–42)) we tested D3 and its head-to-tail tandem derivative D3D3 both in vitro and in vivo in the new mouse model TBA2.1. These mice produce human pEAβ(3–42) leading to a strong, early onset motor neurodegenerative phenotype. In the present study, we were able to demonstrate 1) strong binding affinity of both D3 and D3D3 to pEAβ(3–42) in comparison to Aβ(1–42) and 2) increased affinity of the tandem derivative D3D3 in comparison to D3. Subsequently we tested the therapeutic potentials of both peptides in the TBA2.1 animal model. Truly therapeutic, non-preventive treatment with D3 and D3D3 clearly slowed the progression of the neurodegenerative TBA2.1 phenotype, indicating the strong therapeutic potential of both peptides against pEAβ(3–42) induced neurodegeneration.

1. Introduction

The number of patients suffering from Alzheimer's disease (AD) is expected to increase dramatically if no causal therapy becomes available (Brookmeyer et al., 2007). Major hallmarks of AD are progressive neurodegeneration, and the deposition of tau protein containing neurofibrillary tangles and amyloid β peptide (Aβ) containing extracellular plaques (Parihar and Hemnani, 2004). Aβ is produced by the cleavage of the amyloid precursor protein (APP) through β- and γ-secretases. Under pathological conditions, correlating with age, ultimately, Aβ monomers will assemble into different Aβ aggregates, e.g. the Aβ oligomers, which are thought to play an important role in the development and progression of the disease (Finder and Glockshuber, 2007). Currently, there is no causal treatment available to halt or even slow down AD progression (Bateman, 2015). Previously, the potential Aβ-binding D-enantiomeric peptide D3 has been identified by mirror image

* Correspondence to: D. Willbold, Institute of Complex Systems, Structural Biochemistry (ICS-6), Forschungszentrum Jülich GmbH, Wilhelm-Johnen Straße, 52425 Jülich, Germany.
** Corresponding author.
E-mail addresses: a.willuweit@fz-juelich.de (A. Willuweit), d.willbold@fz-juelich.de (D. Willbold).
[1] Present address: Clinical Development, Prima BioMed, Nürnberger Str. 49, 10789 Berlin, Germany.
[2] Present address: Evotec AG, Manfred Eigen Campus, Essener Bogen 7, 22419 Hamburg, Germany.
[3] Present address: European Molecular Biology Laboratory, Meyerhofstraße 1, 69117 Heidelberg, Germany.
[4] Present address: Analytical Development Biologicals, Boehringer Ingelheim Pharma GmbH & Co.KG, Birkendorfer Strasse 65, 88397 Biberach an der Riss, Germany.

https://doi.org/10.1016/j.npep.2017.11.011
Received 26 April 2017; Received in revised form 24 November 2017; Accepted 26 November 2017

Please cite this article as: Dunkelmann, T., Neuropeptides (2017), https://doi.org/10.1016/j.npep.2017.11.011

phage display (Schumacher et al., 1996) for binding to Aβ (Wiesehan and Willbold, 2003; Funke and Willbold, 2009). It has been shown that the two advantages of peptides consisting solely of D-enantiomeric amino acid residues are the lower immunogenic potential and the higher resistance to proteases as compared to L-peptides (Dintzis et al., 1993; Soto et al., 1996; Funke and Willbold, 2012; Jiang et al., 2015; Leithold et al., 2016). It was shown that D3 reduces Aβ(1–42) mediated cell toxicity, prevents further aggregation of Aβ(1–42) (van Groen et al., 2008) and converts toxic oligomers into large, non-toxic amorphous aggregates in vitro (Funke et al., 2010). Oral administration of D3 improves the spatial learning behaviour in the Morris water maze, reduces Aβ load and the inflammatory situation in transgenic APP/PS1 mice (van Groen et al., 2008; Funke et al., 2010; van Groen et al., 2013).

Animal models of AD have been successfully used to gain deeper insight into the pathogenesis of this condition and are currently without viable alternative. However, despite this utility, most of the models currently used lack the neurodegenerative pathology required to develop a curative treatment option. The transgenic TBA2.1 mouse model expresses human N-terminally truncated Aβ which is post-translationally modified to form pyroglutamate modified Aβ (pEAβ(3–42)) (Alexandru et al., 2011). pEAβ(3–42) is one of the principal components of senile plaques in human brains (Harigaya et al., 2000). Owing to its very fast aggregation and formation of toxic oligomers, pEAβ(3–42) is thought to be involved in the initiation of the amyloid cascade (Jawhar et al., 2011). Homozygous TBA2.1 mice develop a progressive motor neurodegenerative phenotype. Here, we investigated the treatment potential of D3 and its head-to-tail tandem version D3D3 in homozygous TBA2.1 mice to elucidate their potential in ameliorating pEAβ(3–42) aggregation induced pathology and neurodegeneration. This study demonstrates that a truly therapeutic, non-preventive treatment with D3 and D3D3 decelerated the progression of the pEAβ(3–42) induced neurodegenerative TBA2.1 phenotype underlining the strong therapeutic potentials of both compounds for Alzheimer's disease.

2. Material and methods

2.1. Experimental design

We determined the binding affinities of D3 and D3D3 to Aβ(1–42) and pEAβ(3–42) via SPR and tested their influence on the cytotoxicity of pEAβ(3–42) using MTT cytotoxicity analysis in cell culture. For these experiments, recombinant Aβ(1–42) was purchased from Isoloid (Germany) and recombinant pEAβ(3–42) was purified as described recently (Dammers et al., 2015). Both Aβ variants were dissolved in HFIP overnight prior to usage to destroy any existing aggregates and lyophilised to remove HFIP.

After the positive evaluation of both compounds in vitro, it was planned to determine their therapeutic properties in the TBA2.1 mouse model. Due to animal welfare we decided to use male TBA2.1 mice for phenotype characterisation and female mice for the treatment study. The phenotype assessment and the motor balance were determined longitudinally by testing ten wild type and eleven homozygous mice every four weeks starting at two months of age. For the treatment studies, four-months-old female mice were stratified into groups according to their SHIRPA score, resulting in 7 animals receiving placebo, 8 animals D3 and 8 animals D3D3. The mice were treated intraperitoneally by implanting Alzet osmotic minipumps, in order to achieve high and fast drug exposure in the brain during a short therapeutic treatment period. Additionally, the mice were tested before and after treatment in the accelerating Rotarod. All experimenters were blind to genotype or treatment and all tests were carried out at the same time of day. After the last behavioural test animals were sacrificed and brains were dissected. One hemisphere was collected for biochemical analysis and one for immunostainings. Several hemispheres were lost during processing for immunohistochemistry resulting in 4 placebo, 4 D3 and 5 D3D3 specimens. ELISA measurements were performed with samples from each animal included in the study (7 to 8 per group).

2.2. SPR spectroscopy

SPR measurements were performed using a Biacore T200 instrument (GE Healthcare, Sweden) at 25 °C with 20 mM sodium phosphate, 50 mM sodium chloride, pH 7.4 as running buffer. For preparation of the flow cells, a CM5 sensor chip (GE Healthcare, Sweden) was activated with EDC/NHS (0.2 M/0.05 M) and Aβ(1–42) (300 µg/ml) and pEAβ(3–42) (100 µg/ml), diluted in 10 mM sodium acetate pH 4.0, were immobilized to final levels of 8000 RU (pEAβ(3–42)) and 1000 RU (Aβ(1–42)). Ligand and reference flow cells were deactivated with 1 M ethanolamine-HCl. D3 and D3D3 affinity determinations were performed in multi cycle kinetics at 30 µl/min flow rate. The analytes were diluted in running buffer to the final concentrations of 100, 33.33, 11.11, 3.70, 1.23 and 0.41 µM for D3 and 10, 3.33, 1.11, 0.37, 0.12 and 0.04 µM for D3D3. Association of the peptides was recorded for 120 s, followed by a dissociation of 240 s. After each cycle, a conditional regeneration step with 2 M guanidine hydrochloride was implemented. After measurement, the sensorgrams were double referenced using the reference flow cell and a buffer cycle. Evaluation was performed by plotting the respective response levels against the applied peptide concentrations. The curves were fitted using Langmuir's 1:1 binding model (Hill function with $n = 1$, OriginPro 8.5G, OriginLab, Northampton, USA).

2.3. MTT-assay

Lyophilized pEAβ(3–42) was dissolved in 10 mM sodium phosphate buffer, pH 7.4 to a total concentration of 51 µM and the D-peptides D3 and D3D3 (molar ratio of 1:0, 1:0.1, 1:1, 1:10 for pEAβ(3–42):D3 and 1:0, 1:0.2, 1:1, 1:5 for pEAβ(3–42):D3D3) were added, respectively, and incubated at 37 °C for 5 days without shaking resulting in pEAβ(3–42) fibrils. The highest concentration of D-peptides, i.e. 510 µM (0,81 mg/ml) for D3 and 255 µM (0,81 mg/ml) for D3D3, were treated the same without co-incubation of pEAβ(3–42).

PC-12 cells (Leibniz-Institut DSMZ-Deutsche Sammlung von Mikroorganismen und Zellkulturen GmbH, Braunschweig, Germany) were cultured in Dulbecco's modified Eagle's medium (DMEM) (Sigma-Aldrich Chemie GmbH, Taufkirchen, Germany) supplemented with 10% fetal bovine serum (FCS) (Sigma-Aldrich Chemie GmbH, Taufkirchen, Germany) and 5% horse serum (HS) (Sigma-Aldrich Chemie GmbH, Taufkirchen, Germany) at 37 °C and 5% CO_2. Cells were harvested and seeded onto 96-well plates (Gibco, Life Technologies, Carlsbad, California) at 1×10^3 cells/well and incubated at 37 °C and 5% CO_2 for 24 h. The cells were treated with 1 µM incubated pEAβ(3–42) and 1 µM pEAβ(3–42) co-incubated with D3 (in molar ratios of 1:0.1, 1:1 and 1:1) or D3D3 (in molar ratios of 1:0.2, 1:1 and 1:5), respectively, as well as 10 µM D3, 10 µM D3D3 and the buffer alone (10 mM sodium phosphate, pH 7.4). The buffer containing 0.125% Triton X-100 (AppliChem, Darmstadt, Germany) was used as negative control. All samples were added five-fold in a three-fold-determination. The treated cells were incubated at 37 °C and 5% CO_2 for 24 h. MTT-assay was performed using the "Cell Proliferation Kit 1" (Roche, Mannheim, Germany) according to the manufacturer's instructions. The 96-well plate was analysed using a MicroPlate Reader (PolarStar Optima, BMG Labtech, Offenburg, Deutschland) by measuring the absorbance at 570 nm and 660 nm and background corrected.

2.4. Animals

Experiments were conducted using homozygous TBA2.1 mice and wild type littermates as control mice. Transgenic TBA2.1 mice exhibited

neuronal expression of Aβ(Q3–42) on a C57BL/6 × DBA1 background. Aβ(Q3–42) was modified by glutaminyl cyclase to pEAβ(3–42) within the secretory pathway in TBA2.1 mice (Alexandru et al., 2011). All animal procedures were performed in accordance with the German law for the protection of animals and approved by LANUV North-Rhine-Westphalia (Germany, AZ84-02.04.2011.A359). The animals were kept in a controlled environment on a 12/12-hours light/dark cycle (lights on from 7 a.m.–7 p.m.), with 54% humidity and a temperature of 22 °C. Up to four mice per cage were housed with food and water available ad libitum. Only heterozygous TBA2.1 mice were used for breeding and homozygous mice were sacrificed at five months of age to prevent suffering due to the severity of the phenotype.

2.5. Peptides

The D-enantiomeric peptides D3 (rprtrlhthrnr, all amino acids are D-enantiomers) and D3D3 (rprtrlhthrnrprtrlhthrnr, all amino acids are D-enantiomers) with ≥ 95% purity were purchased C-terminally amidated from JPT Peptide Technologies GmbH, Germany.

2.6. Phenotype assessment

For phenotype assessment the primary screen of the SHIRPA test battery was used (Rogers et al., 1997). This includes the following subtests: abnormal body carriage, alertness, abnormal gait, startle response, loss of righting reflex, touch response, pinna reflex, cornea reflex, forelimb placing reflex, hanging behaviour and pain response. Additionally, the body weight was measured. For individual observation and analysis an arena of 42.5 cm × 18 cm × 26.5 cm (L × H × W) was used. The observations were scored from 0 (similar to wild type) to 3 (extremely abnormal from wild type). The sum of all subtests per animal was used for analysis.

2.7. Accelerating Rotarod

To analyse motor coordination and motor balance TBA2.1 mice were placed on a Rotarod apparatus (Ugo Basile Srl, Italy). Testing was performed according to the previously published protocol (Alexandru et al., 2011). In the morning of the first day mice were trained to stay on the rod for at least 60 s at a constant 10 rpm. The test sessions were performed in the afternoon as well as the following morning and afternoon. Before starting the test session the mice were habituated for 30 min in single cages. In one test session the mice had to run in three trials on the beam accelerating from 4 to 40 rpm. The escape latency of running was measured. Maximum time was 10 min. For analysis the mean value of all nine trials was used.

2.8. Treatment with D3 and D3D3

Wild type and homozygous four months old TBA2.1 mice were treated intraperitoneally for four weeks with a daily dosage of 5 mg per kg peptide in PBS (pH 7.4) or vehicle (PBS, pH 7.4) using Alzet mini-osmotic pumps (model 1004, DURECT Corporation, USA). The body weight and conditions of the mice were controlled twice a week. A loss of 15% body weight and severe conspicuities were defined as exclusion criteria. No animal was affected by these exclusion criteria.

2.9. Tissue preparation

The mice were sacrificed and the brain was harvested. The right hemisphere was used for immunohistochemical analysis and the left was used for enzyme-linked immunosorbent assay (ELISA) measurements. Both hemispheres were stored at − 80 °C until further processing.

2.10. Immunofluorescence

Immunofluorescence analysis was assessed to determine the Aβ load, DAPI positive nuclei and astrocyte staining. The right hemisphere was cryosectioned sagittally into 10 µm thin sections. Six sections per animal were fixed with 4% paraformaldehyde and treated with 70% formic acid for antigen retrieval. After washing and blocking with Mouse Ig Blocking Reagent (Vector Laboratories, Inc., USA) slides were treated with either primary antibody against Aβ (6E10, Covance Inc., USA) or against activated astrocytes (GFAP, Dako Deutschland GmbH, Germany) overnight. After washing the secondary antibody (mouse anti goat 488, Life Technologies GmbH, Germany) was incubated for two hours. After washing slides were covered with 4′, 6-Diamidin-2-phenylindol (DAPI, Merck KGaA, Germany) for 10 min. Images were taken with a LMD6000 microscope (Leica Camera, Germany) with a DFC310 FX camera (Leica Camera, Germany). The number of stained Aβ aggregates (Aβ particle count) of either the whole hemisphere, or hippocampus, striatum and midbrain as well as DAPI counts and GFAP (astrocyte staining, % positive area) of the CA1 region were quantified on five to six sections per animal using ImageJ (National Institute of Health, USA).

2.11. ELISA

In brief, an Aβ ELISA (N3pE-42, IBL International GmbH, Germany) was used to quantify the pEAβ(3–42) levels. Therefore, left hemispheres were homogenised with Tris buffer (20 mM Tris pH 8.3, 250 mM NaCl, Roche EDTA free Complete Protease Inhibitor) using the PreCellys24 homogeniser (2 × 20 sec at 6500 rpm, Bertin Technologies, France). After vortexing, a 15 min sonification and additional vortexing the homogenate was then centrifuged (175,000*g*, 4 °C, 30 min). The resulting pellet was incubated and resuspended with diethanolamine (DEA) on ice and again centrifuged. The supernatant represents the DEA soluble fraction which was used for analysis. The pellet was incubated and resuspended with 70% formic acid on ice. After the final centrifugation step the interphase was taken and neutralised with 1 M Tris pH 11.3 representing the insoluble Aβ fraction. DEA soluble and insoluble Aβ fractions were subjected to the ELISA to determine the pEAβ(3–42) concentrations according to the manufacturer's protocol. The samples were normalised to their protein concentration. For the DEA-soluble fraction, the Micro BCA Protein Assay Kit (Pierce Biotechnology, USA) was used and for the insoluble fraction, the Bio-Rad Protein Assay (Bio-Rad, Germany).

2.12. Statistical analysis

To assess Gaussian distribution, all data were tested using the Shapiro-Wilk-Test or in a normality probability plot. In the case of normally distributed data the Repeated-Measures Parametric Analyses, Two- or One-Way-ANOVA with Bonferroni post hoc analysis or (paired) *t*-test were used, respectively. For the non-parametric analysis, the Friedman test or Kruskal-Wallis test were used. Multiple Comparison Tests by Dunn was used for appropriate non-parametric post hoc analysis. All data were expressed as mean with SEM. Results are considered as significantly different to $p \leq 0.05$. All statistical analyses were performed using GraphPad PRISM 5 (GraphPad Software, Inc., USA) and InVivoStat 2.5 (InVivoStat by Simon Bate and Robin Clark, United Kingdom (Clark et al., 2012).

3. Results

3.1. In vitro binding activity of D3 and D3D3 for Aβ(1–42) and pEAβ(3–42)

In order to increase the potency of D3, we chose a head-to-tail tandem version of it, D3D3, which was expected to bind with higher

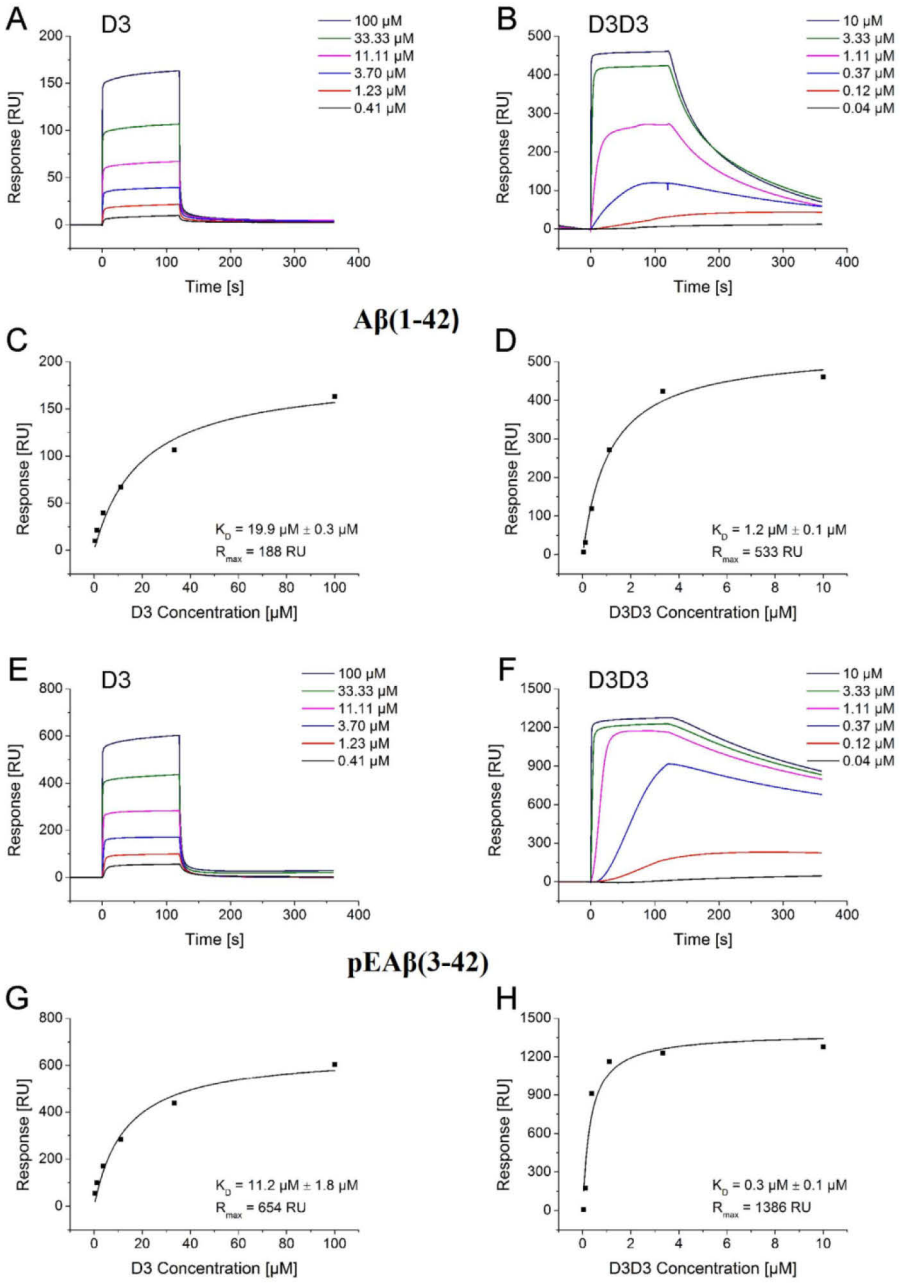

Fig. 1. Affinity determination of D3 and D3D3 to Aβ(1–42) and pEAβ(3–42) by SPR spectroscopy. (A) Sensorgrams of D3 and (B) D3D3 interaction with Aβ(1–42). (C,D) The data were fitted by plotting the response levels (RU) against applied peptide concentrations using a steady-state 1:1 binding model. Sensorgrams of (E) D3 and (F) D3D3 interaction with pEAβ(3–42) and corresponding fit results (G,H). K_D values are represented as mean with SD of two independent measurements. Representative sensorgrams and fits are shown for both measurements.

affinity to the target Aβ due to increased avidity. To validate this in vitro, equilibrium dissociation constants (K_D) of both peptides for Aβ(1–42) and pEAβ(3–42) were determined under the same assay conditions and compared with each other. As expected, D3D3 showed a higher binding affinity than D3 as indicated by lower K_D values (Fig. 1) which might be associated to increased avidity. For D3, the affinities for both Aβ species, Aβ(3–42) and pEAβ(3–42), were similar to each other with slightly higher binding affinities of D3 and D3D3 for pEAβ(3–42) as compared to Aβ(1–42) (Fig. 1).

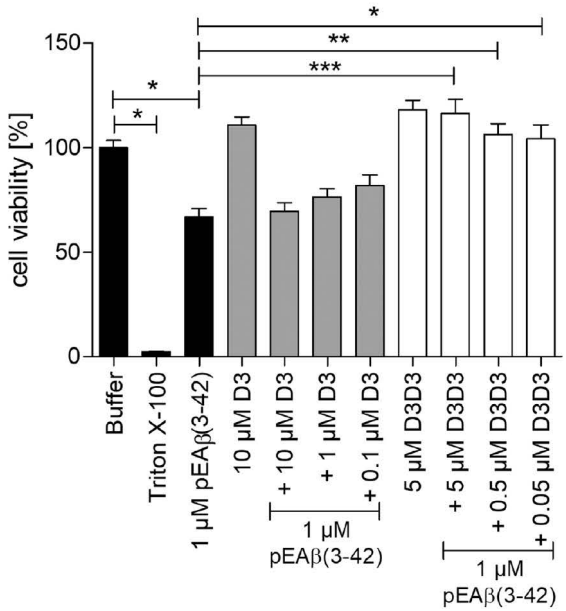

Fig. 2. MTT analysis of the interactions between D3 and D3D3 with pEAβ(3–42). MTT analysis revealed a reduced cell viability upon addition of 1 µM pEAβ(3–42). This was reversed by treatment with D3D3. Data is presented as mean with SEM; *p ≤ 0.05, **p ≤ 0.01 and ***p ≤ 0.001.

3.2. Inhibition of pEAβ(3–42) mediated toxicity by D3 and D3D3

Encouraged by the binding experiments to pEAβ(3–42), we then compared the abilities of D3 and D3D3 to neutralize the cytotoxicity of recombinant pEAβ(3–42) in PC-12 cells (Fig. 2). Already a concentration of 1 µM recombinant pEAβ(3–42) reduced the cell viability by > 30% (15 measurements per treatment in 3 tests; Kruskal-Wallis test, $p \leq 0.0001$, post hoc Buffer vs. 1 µM pEAβ(3–42)). Treatment with D3 had no significant influence on this effect (post hoc 1 µM pEAβ(3–42) vs. D3 at any concentration, not significant (ns)), although this does not mean that D3 when applied at higher concentrations would not have rescued the pEAβ(3–42) mediated reduction of cell viability. However, the addition of D3D3 at concentrations of 0.05 µM or higher resulted in a significant rescue of cell viability (post hoc 1 µM pEAβ(3–42) vs. addition of 5 µM D3D3 $p \leq 0.001$, 1 µM pEAβ(3–42) vs. addition of 0.5 µM D3D3 $p \leq 0.01$, 1 µM pEAβ(3–42) vs. addition of 0.05 µM D3D3 $p \leq 0.05$).

Thus, as expected, the increased avidity of D3D3 over D3 led to superior efficacy of D3D3 in vitro (Brener et al., 2015).

3.3. Characterisation of the motor phenotype of TBA2.1 mice

Based on the results of the SPR and cytotoxicity experiments, it was our aim to prove our hypothesis in vivo by treatment of homozygous TBA2.1 mice with D3 and D3D3 against placebo. Accordingly, we determined the motor performance and overall phenotype of transgenic TBA2.1 mice. Subsequently, we treated homozygous mice with either D3 or D3D3 for four weeks.

We characterised the motor neurodegenerative phenotype of this mouse model longitudinally using wild type (WT) and homozygous (HOM) TBA2.1 mice up to five months of age. Phenotype assessment revealed HOM TBA2.1 mice to have a significant phenotype by the age of two months (Fig. 3). Scored observations revealed HOM TBA 2.1 mice to have severely impaired sensorimotor function, which in conjunction with other deficits, rapidly resulted in a hunched body posture, wobbly and rigid gait. By two months of age HOM TBA2.1 mice had four times the score of wild type littermates, a disparity that continued to increase with time, becoming ten times greater at five months (number of animals: 10 WT and 11 HOM; Repeated-Measures-Parametric Analyses, genotype ($F_{(2,25)} = 59.01$, $p \leq 0.001$), interaction genotype with age ($F_{(6,75)} = 20.30$, $p \leq 0.001$), pairwise tests WT vs. HOM $p \leq 0.001$ at all ages, Fig. 3A). In addition, the weight gain from two to five months of age differed significantly between the groups (number of animals: 10 WT and 11 HOM; Repeated-Measures-Parametric Analyses, weight ($F_{(3,75)} = 136.19$, $p \leq 0.001$), interaction genotype with age ($F_{(6,75)} = 4.88$, $p \leq 0.001$)). More precisely, the body weight of WT TBA2.1 mice increased successively up to five months of age (pairwise tests $p \leq 0.01$), whereas in HOM TBA2.1 significant weight gain was only observed up to the fourth month of age (pairwise tests of two to four months old HOM $p \leq 0.05$ and pairwise test four to five months HOM ns) (Fig. 3C).

Analysis of the motor coordination of HOM TBA2.1 mice showed a significant deficit beginning at the age of three months which remained for all subsequent time points tested (number of animals: 10 WT and 11 HOM; Repeated-Measures-Parametric Analyses, genotype ($F_{(2,25)} = 3.59$ and $p = 0.043$), pairwise WT vs. HOM at two months ns and at three to five months $p \leq 0.05$) (Fig. 3B). Overall, these results indicated the rapid progression of the phenotype in HOM TBA2.1 mice from two to five months of age.

3.4. Treatment with D3 and D3D3

Since the motor neurodegenerative phenotype of male HOM TBA2.1 mice was highly prominent at five months of age we decided to start the treatment at four months of age over four weeks to test the truly therapeutic rather than preventive power of D3 and D3D3. Before treating female HOM and WT TBA2.1 mice, all mice were stratified into groups according to their SHIRPA score in the phenotype assessment test. Comparing the scores of WT (1.4 ± 0.22) and HOM (12.2 ± 0.71) mice clearly demonstrated that female HOM mice also developed a severe phenotype with the same baseline as the males. When comparing the outcome of the motor performance before and after treatment of female HOM TBA2.1 mice, the motor balance of placebo treated mice decreased (number of treated animals: placebo 7, D3 8, D3D3 8; Repeated-Measures-Parametric Analyses, before vs. after ($F_{(1,20)} = 2.76$, $p = 0.1122$, pairwise tests before vs. after treatment $p \leq 0.05$), indicating a progression of the phenotype over the four weeks treatment period. In contrast, treatment with D3 or D3D3 inhibited the worsening of the Rotarod performance of HOM TBA2.1 mice (Fig. 4A, pairwise tests before vs. after treatment ns). Of note, the rate of progression is the decisive factor in this model, since the phenotype can only be delayed or ideally stopped but not be reversed. Analysis of the pEAβ(3–42) concentration in the brain of HOM TBA2.1 mice showed an increase in DEA-soluble pEAβ(3–42) after the administration of D3D3 in contrast to the placebo and D3 treated groups (Fig. 4C, number of analysed samples: placebo 7, D3 8; D3D3 8; One-Way-ANOVA $p = 0.0055$, post hoc analysis placebo vs. D3 ns, placebo vs. D3D3 $p \leq 0.05$), while no significant differences were detectable between the insoluble fractions of the three groups (Fig. 4D; number of analysed samples: placebo 7, D3 8; D3D3 8; Kruskal-Wallis test $p = 0.9253$; post hoc analysis ns). The latter was confirmed by quantification of Aβ immunostaining in different brain areas in which Aβ aggregates were found (Fig. 5; 6 slices per animal, number of analysed animals: placebo 4, D3 4, D3D3 5; total brain, One-Way-ANOVA $p = 0.18$; striatum, Kruskal-Wallis test $p = 0.67$; CA1, Kruskal-Wallis test $p = 0.34$; midbrain, One-Way-ANOVA $p = 0.21$; post hoc placebo vs. D3 or D3D3 ns). To evaluate the incidence of hippocampal neurodegeneration (neuron loss and gliosis), cell nuclei and activated astrocytes in the CA1 region of D3, D3D3 and placebo-treated HOM TBA2.1 mice were stained. Quantification of stainings revealed an increasing

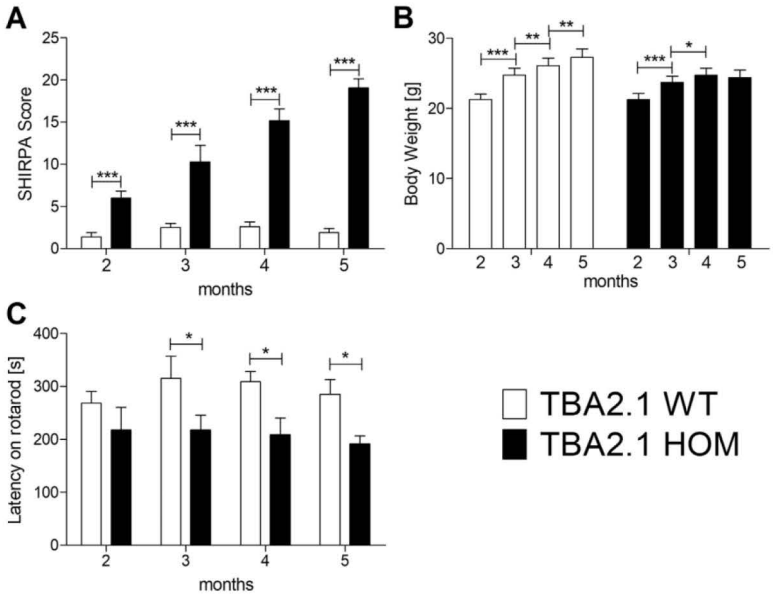

Fig. 3. Longitudinal determination of the sensorimotor phenotype of wild type (WT) and homozygous (HOM) TBA2.1 mice at 2, 3, 4 and 5 months of age. (A) Assessment using the SHIRPA test battery revealed the continuously increasing phenotype of HOM TBA2.1 mice. (B) Body weight of WT mice increased from two to five months of age, but weight gain of HOM was stable from four to five months of age. (C) Between three and five months of age the Rotarod motor performance of HOM mice was reduced when compared to control. Data are presented as mean with SEM; *p ≤ 0.05, **p ≤ 0.01 and ***p ≤ 0.001.

trend in the DAPI count and a decreasing trend in GFAP positive astrocytes of D3 or D3D3 treated animals in comparison to placebo animals, although quantification revealed no significant differences (Fig. 6; 5 to 6 slices per animal, number of analysed animals: placebo 4, D3 3, D3D3 5; GFAP: Kruskal-Wallis test, p = 0.3953, post hoc placebo vs.D3 or D3D3 ns and DAPI: Kruskal-Wallis test, p = 0.0867, post hoc placebo vs. D3 or D3D3 ns).

Additionally, WT TBA2.1 mice were treated with D3 or D3D3 to exclude unrelated effects of the compounds. No differences between these groups could be observed in the Rotarod test, indicating the effects of D3 and D3D3 were restricted to HOM TBA2.1 mice (Fig. 4B, number of treated animals: placebo 6, D3 7, D3D3 7; Friedman test p = 0.1667, post hoc analysis ns).

Overall, both D3 and D3D3 were able to inhibit the deterioration of the motor neuronal degenerative phenotype in HOM TBA2.1, and D3D3 was able to induce a concentration shift towards the DEA-soluble pEAβ(3–42) pool.

4. Discussion

The D-enantiomeric peptide D3 has been shown to be a promising lead compound for the treatment of AD. D3 was originally developed as an Aβ(1–42) monomer stabilizing ligand in order to destabilize and eliminate Aβ oligomers, which are thought to be the most toxic Aβ species and decisive for development and progression of AD. In vitro tests with D3 showed its potential to eliminate toxic Aβ(1–42) oligomers (Funke et al., 2010). The potential of D3 was further proven by inhibition of Aβ(1–42) toxicity in cell culture, the improvement of

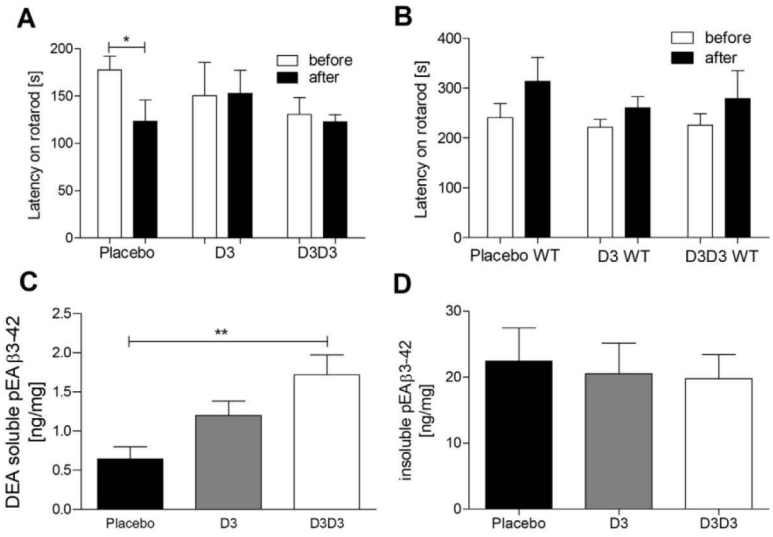

Fig. 4. Treatment of homozygous TBA2.1 mice with the D-enantiomeric peptides D3 and D3D3. Homozygous TBA2.1 (HOM) and wild-type (WT) mice were treated intraperitoneally over four weeks with vehicle (placebo) or with 5 mg per kg body weight D3 or D3D3 per day. Rotarod analysis of HOM demonstrates a worsening of the motor phenotype in placebo-treated mice whereas D3 and D3D3 administration inhibited this process. (A) Data before and after treatment per HOM mouse are shown. (B) The Rotarod performance of WT mice before and after treatment is illustrated. (C) Biochemical quantification of DEA-soluble pEAβ(3–42) in the brain of HOM revealed a significantly higher concentration in D3D3 compared to placebo treated mice. (D) Quantification of insoluble pEAβ(3–42) from the brains of HOM animals is unchanged between treatment groups. Data are presented as mean with SEM (B, C, D); *p ≤ 0.05, **p ≤ 0.01 and ***p ≤ 0.001.

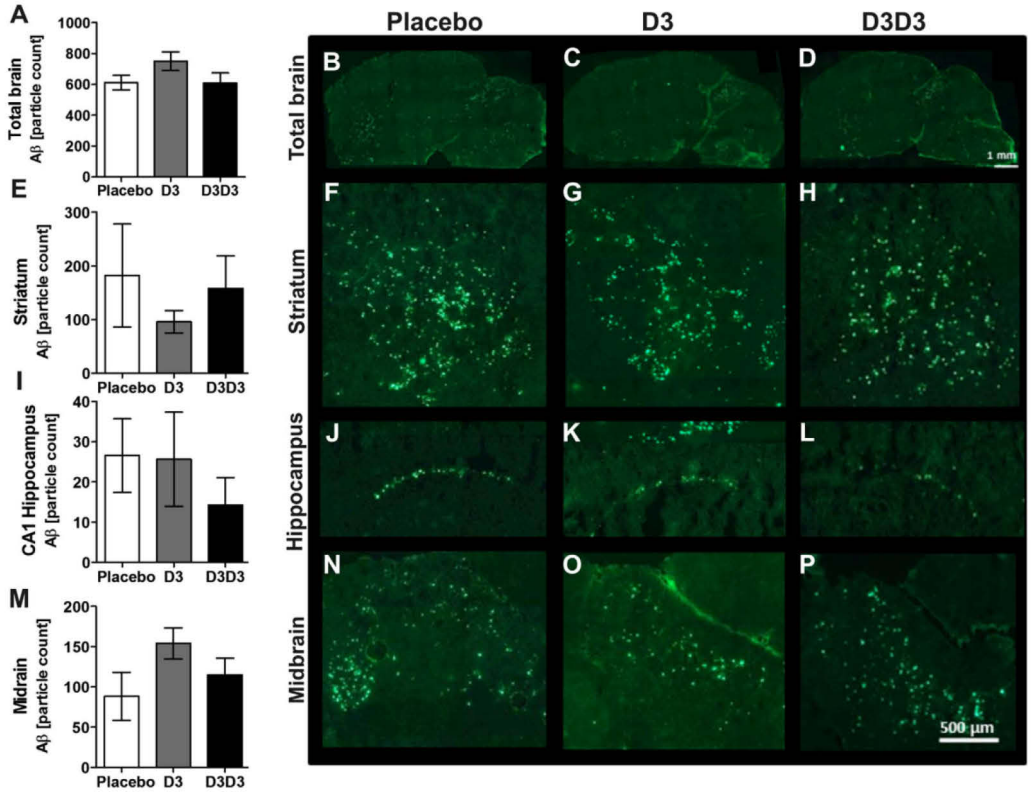

Fig. 5. Aβ immunofluorescence staining and quantification of homozygous mice treated with D3 or D3D3. After treatment, hemispheres of D3, D3D3 or placebo-treated homozygous TBA2.1 mice were harvested. Brain slices of each group were stained against Aβ (antibody 6E10). Immunofluorescence figures show the whole brain hemispheres (B–D), the striatum (F–H), the hippocampus (J–L) or midbrain (N–P) of placebo, D3 and D3D3 treated mice. Quantification of the Aβ particle count in the whole hemisphere (A), striatum (E), CA1 region of the hippocampus (I) or midbrain (M) revealed no significant differences between these groups. Data are presented as mean with SEM. Bars indicating length in (D) and (P) are representative for pictures (B–D) and (F–P), respectively.

spatial learning behaviour and the reduction of the Aβ plaque load in APP/PS1 double transgenic mice (van Groen et al., 2008; Funke et al., 2010). D3D3 was rationally designed to yield a di-valent version of D3 with increased avidity and hence increased affinity to its Aβ target species. In the present study, we have for the first time validated the higher binding affinity of the derivative D3D3 to Aβ(1–42) in comparison to D3. Furthermore, we were able to show that both peptides, and especially D3D3, show increased binding affinity to pEAβ(3–42) as compared to Aβ(1–42). We evaluated the inhibition potentials of both compounds against pEAβ(3–42) mediated toxicity in PC12 cells. Low concentrations of pEAβ(3–42) reduced cell viability, an effect blocked by minute amounts of D3D3. In contrast, D3 was unable to significantly improve cell viability at any of the concentrations tested. To validate the potentials of D3 and D3D3 in vivo, we analysed the therapeutic efficacies in the new mouse model, TBA2.1, which exhibits a motor neurodegenerative phenotype induced by the expression of human pEAβ(3–42).

From two months of age the progression of the phenotype influencing posture, gait and motor function of TBA2.1 mice was severe. Additionally, from the age of three months these mice displayed impaired motor coordination. In contrast, WT TBA2.1 mice failed to display any abnormalities over the entire period of observation. These results are in agreement with previously published observations (Alexandru et al., 2011) and confirm the strong motor neurodegenerative phenotype of HOM TBA2.1 mice.

Treatment studies with D3 or D3D3 in diseased HOM TBA2.1 over a period of four weeks with a daily dosage of 5 mg per kg of body weight showed that both compounds have strong therapeutic potential. Both compounds were able to stabilise the motor coordination of the HOM TBA 2.1 mice and to reduce phenotype progression to non-significant levels during the treatment period. In contrast, placebo-treated mice showed significant progression of their phenotype during that time. In addition, WT mice demonstrated no adverse effects caused by the treatment, which confirmed the effects of D3 and D3D3 were specific to HOM TBA2.1 mice. These findings suggest these D-enantiomeric proteins have a specific therapeutic effect against the pEAβ(3–42) induced neurodegenerative phenotype as they halted disease progression, maintaining performance to that observed at the beginning of treatment. This conclusion is also supported by Brener et al., 2015 showing D3D3 was able to delay the overall behaviour and sensorimotor progression in homozygous TBA mice. In contrast to the present report, in which both D3 and D3D3 stopped progression of the motor deficit as measured by the Rotarod test, Brener et al., 2015 demonstrated that the SHIRPA assay was able to distinguish the efficiencies of D3D3 and D3 in slowing down the progression of the motor neurodegenerative phenotype. Although this observation is in line with results of the present study demonstrating higher in vitro efficiency of D3D3 over D3, one has to keep in mind that in vitro results do not necessarily directly translate to respective in vivo efficiencies due to potentially different pharmacokinetic properties of the respective compounds. Also, the repeated Rotarod measurements for assessment of motor performance might be less sensitive than the SHIRPA derived judgements due to training

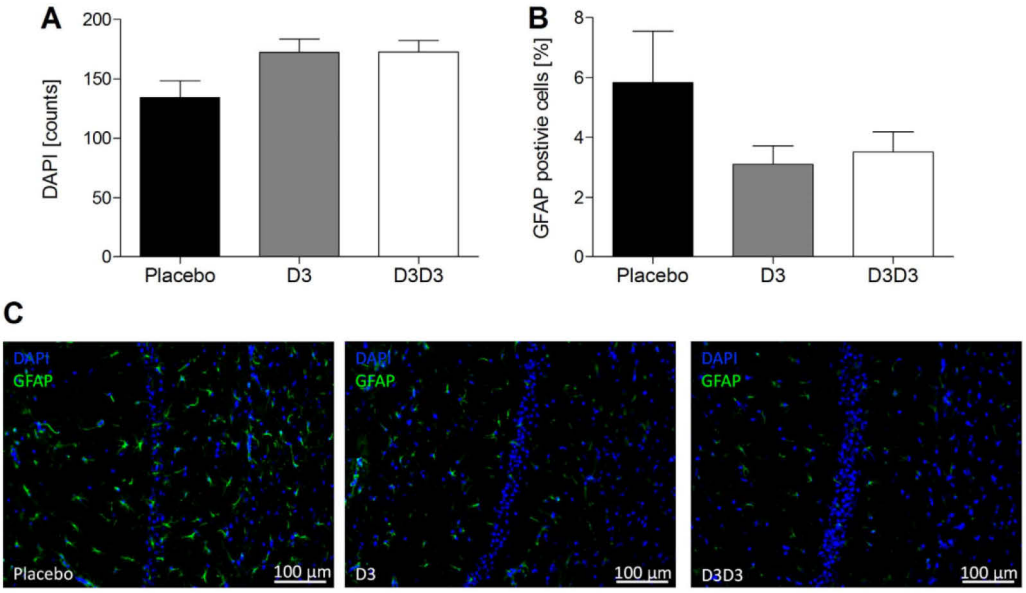

Fig. 6. DAPI and GFAP immunofluorescence stainings of homozygous mice treated with D3 and D3D3. Brain sections of D3, D3D3 or placebo-treated homozygous mice were stained for activated astrocytes with antibodies raised against GFAP and nuclei were counter stained by DAPI. DAPI positive nuclei (A) and activated astrocytes (B) were quantified in the CA1 region of the hippocampus. (C) CA1 region of merged DAPI and GFAP stainings after treatment with D3, D3D3 or placebo-treated homozygous mice. (A, B) Data are presented as mean with SEM.

effects inherently connected to the Rotarod assay. Also, by trend neuron loss was improved and correspondingly gliosis reduced in D3 and D3D3 treated HOM mice. Although statistical analyses revealed no significance of the quantification, this was most probably due to the low number of samples, which were left for this analysis. Nevertheless, it supports the hypothesis that D3 and D3D3 seem to interfere with hippocampal neurodegeneration. Besides neuronal toxicity, it is well known that oligomeric species of Aβ also interfere with neuronal function. Disturbances of synaptic transmission, either pre- or postsynaptically, synaptic loss and inhibition of synaptic plasticity via modulation of neurotransmitter receptors are discussed, which are all independent of neuronal toxicity and neuronal death (Carrillo-Mora et al., 2014). These synaptotoxic effects may also act via, or in conjunction with Tau. Recently, it was reported that oligomeric Tau exerts selective synaptotoxicity without affecting cell viability (Kaniyappan et al., 2017), and combination of oligomeric Aβ and Tau species have been shown to impair long-term-potentiation and memory (Fa et al., 2016). Thus, by reducing oligomeric Aβ D3 and D3D3 could mediate a therapeutic effect and halt in phenotype progression of TBA2.1 mice even without interfering with neurodegeneration.

The development of a disease-modifying or even curative treatment for AD is one the biggest challenges of 21st century medicine, but unfortunately most of the potential compounds that are chosen for clinical research fail. One potential reason for this is that most of the animal models used for preclinical research do not show neurodegeneration. Here we use the TBA2.1 mouse – a model exhibiting a dramatically increasing motor neurodegenerative phenotype. The principle aim of the present study was to investigate the truly therapeutic potentials of the fully D-enantiomeric peptides D3 and its derivative D3D3 in this neurodegenerative animal model. In this respect, reversal of cerebral damage and increase of motor performance cannot be expected by this kind of treatment as the animals used suffer already from distinct neurodegeneration in the brain by this age (Alexandru et al., 2011). Instead, any halt of phenotype progression has to be regarded as a treatment success. In particular, we show that the pEAβ(3–42) induced neurodegenerative phenotype of TBA2.1 mice can not only be inhibited by a preventive treatment, but arrested by a truly therapeutic treatment with D3 and D3D3, most probably by direct action against pEAβ(3–42) assemblies, e.g. pEAβ(3–42) oligomers.

Earlier in vitro studies demonstrated that these D-enantiomeric peptides are capable of binding Aβ species and convert them into non-toxic, non-fibrillar forms (Funke et al., 2010; Brener et al., 2015). In vivo, using mouse models that produce mainly Aβ(1–40) and Aβ(1–42), and develop a plaque pathology comparable to AD patients, a reduction of the Aβ load was observed after several weeks of treatment with D3 (van Groen et al., 2008; Funke et al., 2010). The exact mechanism of action in vivo has not been unraveled yet. However, all experimental data collected so far suggests the following hypothesis: By binding of D3 to Aβ monomers and oligomers the chemical equilibrium is shifted away from fibrillary species which is obviously able to result in a reduction of existing, or in prevention of newly formed plaques. In the present study, the used mouse model TBA2.1 produces aggregates consistent of Aβ and pEAβ(3–42) (Alexandru et al., 2011). Not much information is available about the chemical equilibrium of aggregates containing pEAβ(3–42), but it has been shown that those aggregates are more stable (Dammers et al., 2017). In consequence, D3 and D3D3 can probably not be expected to dissolve already formed pEAβ(3–42) aggregates or significantly prevent their formation within the short treatment window used here. Instead, we hypothesize a mechanism by which toxic oligomeric species are reduced by binding to D3 or D3D3, as has been shown for Aβ(1–42) in vitro (Brener et al., 2015). In line with our in vitro data on cell viability presented here, this may prevent neuronal cell death also in vivo resulting in the observed halt in phenotype progression in TBA2.1 mice.

We have observed a significant increase of pEAβ(3–42) in the DEA-soluble fraction upon treatment with D3D3 and a trend upon D3 treatment in the HOM TBA2.1 mice. It is not absolutely clear which Aβ species are located in the DEA fraction. Since DEA solubilizes protein complexes, one could speculate that complexes between pEAβ(3–42) and D3D3 or D3 are enriched in this fraction, which would also support our working hypothesis of shifted equilibriums, as outlined above. However, so far it is not clear whether the observed increase in the DEA

fraction is therapeutically relevant and actually does correlate with the delay in phenotype progression observed in the mice. In any case it could be a hint of target engagement by D3D3 in vivo.

TBA2.1 mice expressing pEAβ(3–42) is a very potent model delivering a highly interesting drug target. But to date, only a few compounds have been identified as targeting pEAβ(3–42). The main effects of these compounds were reducing the plaques and/or Aβ species using either active (e.g. pGlu-3 mimotope, (Schneeberger et al., 2009)) or passive immunisation (e.g. 9D5 (Wirths et al., 2010), or NT4X (Antonios et al., 2015)) in different mouse models of amyloidosis. To our knowledge these data are mostly lacking behavioural analyses or functional benefits or show preventive rather than therapeutic effects (Frost et al., 2015). Moreover, there are several challenges to overcome with these immunogenic strategies. For example, passive immunisation is deficient in bridging the blood brain barrier, which is essential to have substantial effects. The risk of active immunisation is that the immune system of AD patients might not be capable enough for the patients´ benefit. Additionally, the probability of upcoming adverse events has to be discussed (Cynis et al., 2016). Comparing these challenges to the present study, D-enantiomeric peptides are less immunogenic than L-enantiomers which seems to be an advantage (Funke and Willbold, 2012). Moreover, it is already known that D-enantiomeric peptides like D3 are passing the blood brain barrier (Jiang et al., 2015; Jiang et al., 2016). Additionally, pharmacokinetic studies showed high biological stability, long plasma half-lives and constant levels of D3 and D3D3 in the target organ brain (Jiang et al., 2015; Leithold et al., 2016).

In conclusion, D3 and D3D3 represent a potentially interesting new class of compounds with promising properties to cope with the challenge of treating Alzheimer's disease.

Funding sources

Financial support of D.W. was provided by "Portfolio Technology and Medicine", the Helmholtz-Validierungsfonds of the Impuls and Vernetzungs-Fonds der Helmholtzgemeinschaft. D.W. and K.-J.L. were supported by the "Portfolio Drug Research" of the Impuls and Vernetzungs-Fonds der Helmholtzgemeinschaft. TD was associated fellow of the graduate school "Molecules of Infection".

Conflict of interests

None.

Acknowledgements

The first breeding pairs of TBA2.1 mice were a generous gift by Probiodrug AG. We thank Elke Butzküven and Verena Graf for excellent technical assistance.

References

Alexandru, A., Jagla, W., Graubner, S., Becker, A., Bäuscher, C., Kohlmann, S., Sedlmeier, R., Raber, K., Cynis, H., Rönicke, R., Reymann, K., Petrasch-Parwez, E., Hartlage-Rübsamen, M., Waniek, A., Rossner, S., Schilling, S., Osmand, A., Demuth, H.-U., von Hörsten, S., 2011. Selective hippocampal neurodegeneration in transgenic mice expressing small amounts of truncated Aβ is induced by pyroglutamate-Aβ formation. J. Neurosci. 31 (36), 12790–12801.

Antonios, G., Borgers, H., Richard, B.C., Brauss, A., Meissner, J., Weggen, S., Pena, V., Pillot, T., Davies, S.L., Bakrania, P., Matthews, D., Brownlees, J., Bouter, Y., Bayer, T.A., 2015. Alzheimer therapy with an antibody against N-terminal Abeta 4-X and pyroglutamate Abeta 3-X. Sci. Rep. 5, 17338.

Bateman, R., 2015. Alzheimer's disease and other dementias: advances in 2014. Lancet Neurol. 14 (1), 4–6.

Brener, O., Dunkelmann, T., Gremer, L., van Groen, T., Mirecka, E.A., Kadish, I., Willuweit, A., Kutzsche, J., Jürgens, D., Rudolph, S., Tusche, M., Bongen, P., Pietruszka, J., Oesterhelt, F., Langen, K.-J., Demuth, H.-U., Janssen, A., Hoyer, W., Funke, S.A., Nagel-Steger, L., Willbold, D., 2015. QIAD assay for quantitating a compound's efficacy in elimination of toxic Abeta oligomers. Sci. Rep. 5, 13222–13234.

Brookmeyer, R., Johnson, E., Ziegler-Graham, K., Arrighi, H.M., 2007. Forecasting the global burden of Alzheimer's disease. Alzheimers Dement. 3 (3), 186–191.

Carrillo-Mora, P., Luna, R., Colín-Barenque, L., 2014. Amyloid beta: multiple mechanisms of toxicity and only some protective effects? Oxidative Med. Cell. Longev. 2014, 795375.

Clark, R.A., Shoaib, M., Hewitt, K.N., Stanford, S.C., Bate, S.T., 2012. A comparison of InVivoStat with other statistical software packages for analysis of data generated from animal experiments. J. Psychopharmacol. 26 (8), 1136–1142.

Cynis, H., Frost, J.L., Crehan, H., Lemere, C.A., 2016. Immunotherapy targeting pyroglutamate-3 Abeta: prospects and challenges. Mol. Neurodegener. 11 (1), 48.

Dammers, C., Gremer, L., Neudecker, P., Demuth, H.U., Schwarten, M., Willbold, D., 2015. Purification and characterization of recombinant N-terminally pyroglutamate-modified amyloid-beta variants and structural analysis by solution NMR spectroscopy. PLoS One 10 (10), e0139710.

Dammers, C., Reiss, K., Gremer, L., Lecher, J., Ziehm, T., Stoldt, M., Schwarten, M., Willbold, D., 2017. Pyroglutamate-modified amyloid-beta(3-42) shows alpha-helical intermediates before amyloid formation. Biophys. J. 112 (8), 1621–1633.

Dintzis, H.M., Symer, D.E., Dintzis, R.Z., Zawadzke, L.E., Berg, J.M., 1993. A comparison of the immunogenicity of a pair of enantiomeric proteins. Proteins 16 (3), 306–308.

Fa, M., Puzzo, D., Piacentini, R., Staniszewski, A., Zhang, H., Baltrons, M.A., Li Puma, D.D., Chatterjee, I., Li, J., Saeed, F., Berman, H.L., Ripoli, C., Gulisano, W., Gonzalez, J., Tian, H., Costa, J.A., Lopez, P., Davidowitz, E., Yu, W.H., Haroutunian, V., Brown, L.M., Palmeri, A., Sigurdsson, E.M., Duff, K.E., Teich, A.F., Honig, L.S., Sierks, M., Moe, J.G., D'Adamio, L., Grassi, C., Kanaan, N.M., Fraser, P.E., Arancio, O., 2016. Extracellular tau oligomers produce an immediate impairment of LTP and memory. Sci. Rep. 6, 19393.

Finder, V.H., Glockshuber, R., 2007. Amyloid-beta aggregation. Neurodegener. Dis. 4 (1), 13–27.

Frost, J.L., Liu, B., Rahfeld, J.U., Kleinschmidt, M., O'Nuallain, B., Le, K.X., Lues, I., Caldarone, B.J., Schilling, S., Demuth, H.U., Lemere, C.A., 2015. An anti-pyroglutamate-3 Abeta vaccine reduces plaques and improves cognition in APPswe/PS1DeltaE9 mice. Neurobiol. Aging 36 (12), 3187–3199.

Funke, S.A., Willbold, D., 2009. Mirror image phage display—a method to generate D-peptide ligands for use in diagnostic or therapeutical applications. Mol. BioSyst. 5 (8), 783–786.

Funke, S.A., Willbold, D., 2012. Peptides for therapy and diagnosis of Alzheimer's disease. Curr. Pharm. Des. 18 (6), 755–767.

Funke, S., van Groen, T., Kadish, I., Bartnik, D., Nagel-Steger, L., Brener, O., Sehl, T., Batra-Safferling, R., Moriscot, C., Schoehn, G., Horn, A.H., Muller-Schiffmann, A., Korth, C., Sticht, H., Willbold, D., 2010. Oral treatment with the D-enantiomeric peptide D3 improves the pathology and behavior of Alzheimer's disease transgenic mice. ACS Chem. Neurosci. 1 (9), 639–648.

van Groen, T., Wiesehan, K., Funke, S.A., Kadish, I., Nagel-Steger, L., Willbold, D., 2008. Reduction of Alzheimer's disease amyloid plaque load in transgenic mice by D3, A D-enantiomeric peptide identified by mirror image phage display. ChemMedChem 3 (12), 1848–1852.

van Groen, T., Kadish, I., Funke, S.A., Bartnik, D., Willbold, D., 2013. Treatment with D3 removes amyloid deposits, reduces inflammation, and improves cognition in aged AbetaPP/PS1 double transgenic mice. J. Alzheimers Dis. 34 (3), 609–620.

Harigaya, Y., Saido, T.C., Eckman, C.B., Prada, C.M., Shoji, M., Younkin, S.G., 2000. Amyloid beta protein starting pyroglutamate at position 3 is a major component of the amyloid deposits in the Alzheimer's disease brain. Biochem. Biophys. Res. Commun. 276 (2), 422–427.

Jawhar, S., Wirths, O., Bayer, T.A., 2011. Pyroglutamate amyloid-beta (Abeta): a hatchet man in Alzheimer disease. J. Biol. Chem. 286 (45), 38825–38832.

Jiang, N., Leithold, L.H., Post, J., Ziehm, T., Mauler, J., Gremer, L., Cremer, M., Schartmann, E., Shah, N.J., Kutzsche, J., Langen, K.J., Breitkreutz, J., Willbold, D., Willuweit, A., 2015. Preclinical pharmacokinetic studies of the tritium labelled D-enantiomeric peptide D3 developed for the treatment of Alzheimer s disease. PLoS One 10 (6), e0128553.

Jiang, N., Frenzel, D., Schartmann, E., van Groen, T., Kadish, I., Shah, N.J., Langen, K.J., Willbold, D., Willuweit, A., 2016. Blood-brain barrier penetration of an Abeta-targeted, arginine-rich, D-enantiomeric peptide. Biochim. Biophys. Acta 1858 (11), 2717–2724.

Kaniyappan, S., Chandupatla, R.R., Mandelkow, E.M., Mandelkow, E., 2017. Extracellular low-n oligomers of tau cause selective synaptotoxicity without affecting cell viability. Alzheimers Dement. 13 (11), 1270–1291.

Leithold, L.H., Jiang, N., Post, J., Niemietz, N., Schartmann, E., Ziehm, T., Kutzsche, J., Shah, N.J., Breitkreutz, J., Langen, K.J., Willuweit, A., Willbold, D., 2016. Pharmacokinetic properties of tandem d-peptides designed for treatment of Alzheimer's disease. Eur. J. Pharm. Sci. 89, 31–38.

Parihar, M.S., Hemnani, T., 2004. Alzheimer's disease pathogenesis and therapeutic interventions. J. Clin. Neurosci. 11 (5), 456–467.

Rogers, D.C., Fisher, E.M., Brown, S.D., Peters, J., Hunter, A.J., Martin, J.E., 1997. Behavioral and functional analysis of mouse phenotype: SHIRPA, a proposed protocol for comprehensive phenotype assessment. Mamm. Genome 8 (10), 711–713.

Schneeberger, A., Mandler, M., Otawa, O., Zauner, W., Mattner, F., Schmidt, W., 2009. Development of AFFITOPE vaccines for Alzheimer's disease (AD)—from concept to clinical testing. J. Nutr. Health Aging 13 (3), 264–267.

Schumacher, T.N., Mayr, L.M., Minor Jr., D.L., Milhollen, M.A., Burgess, M.W., Kim, P.S., 1996. Identification of D-peptide ligands through mirror-image phage display. Science 271 (5257), 1854–1857.

Soto, C., Kindy, M.S., Baumann, M., Frangione, B., 1996. Inhibition of Alzheimer's amyloidosis by peptides that prevent beta-sheet conformation. Biochem. Biophys. Res. Commun. 226 (3), 672–680.

Wiesehan, K., Willbold, D., 2003. Mirror-image phage display: aiming at the mirror. Chembiochem 4 (9), 811–815.

Wirths, O., Erck, C., Martens, H., Harmeier, A., Geumann, C., Jawhar, S., Kumar, S., Multhaup, G., Walter, J., Ingelsson, M., Degerman-Gunnarsson, M., Kalimo, H., Huitinga, I., Lannfelt, L., Bayer, T.A., 2010. Identification of low molecular weight pyroglutamate A{beta} oligomers in Alzheimer disease: a novel tool for therapy and diagnosis. J. Biol. Chem. 285 (53), 41517–41524.

3.6 Comprehensive characterization of the pyroglutamate Aβ induced motor neurodegenerative phenotype of TBA2.1 mice

Autoren:	Dunkelmann T.*, **Schemmert S.***, Honold D., Teichmann K., Butzküven E., Demuth H-U., Shah N. J., Langen K-J., Kutzsche J., Willbold D., Willuweit A.
	*Autoren sind gleichberechtigt
Journal:	Journal of Alzheimer's Disease, akzeptiert am 17. Januar 2018
Impact Factor:	3,731 (2016)
Beitrag:	Durchführung verschiedener Verhaltensversuche (Offenfeldtest, Murmeltest, Stangentest, Greifstärketest, Klammertest)
	Durchführung aller immunhistologischen Experimente
	Quantifizierung der immunhistologischen Ergebnisse
	Analyse der Versuche
	statistische Auswertung
	Anfertigung der Abbildungen (75% der Abbildungen)
	Verfassung und Prüfung des Manuskriptes

Journal of Alzheimer's Disease xx (20xx) x–xx
DOI 10.3233/JAD-170775
IOS Press

Comprehensive Characterization of the Pyroglutamate Amyloid-β Induced Motor Neurodegenerative Phenotype of TBA2.1 Mice

Tina Dunkelmann[a,1], Sarah Schemmert[a,1], Dominik Honold[a], Kerstin Teichmann[a], Elke Butzküven[a], Hans-Ulrich Demuth[b], Nadim Joni Shah[c,d], Karl-Josef Langen[c,e], Janine Kutzsche[a], Dieter Willbold[a,f,*] and Antje Willuweit[c,*]

[a]*Institute of Complex Systems, Structural Biochemistry, Forschungszentrum Jülich GmbH, Jülich, Germany*
[b]*Department of Drug Design and Target Validation (MWT), Fraunhofer-Institute of Cell Therapy and Immunology (IZI), Leipzig, Biozentrum, Halle, Germany*
[c]*Institute of Neuroscience and Medicine, Medical Imaging Physics, Forschungszentrum Jülich GmbH, Jülich Germany*
[d]*Department of Neurology, Faculty of Medicine, JARA, RWTH Aachen University, Aachen, Germany*
[e]*Department of Nuclear Medicine, Universitätsklinikum der RWTH Aachen, Aachen, Germany*
[f]*Institut für Physikalische Biologie, Heinrich Heine Universität Düsseldorf, Düsseldorf, Germany*

Accepted 17 January 2018

Abstract. Alzheimer's disease (AD) is the most common neurodegenerative disorder and is being intensively investigated using a broad variety of animal models. Many of these models express mutant versions of human amyloid-β protein precursor (AβPP) that are associated with amyloid-β protein (Aβ)-induced early onset familial AD. Most of these models, however, do not develop bold neurodegenerative pathology and the respective phenotypes. Nevertheless, this may well be essential for their suitability to identify therapeutically active compounds that have the potential for a curative or at least disease-modifying therapy in humans. In this study, the new transgenic mouse model TBA2.1 was explored in detail to increase knowledge about the neurodegenerative process induced by the presence of pyroglutamate modified human $A\beta_{3\text{-}42}$ ($pEA\beta_{3\text{-}42}$). Analysis of the sensorimotor phenotype, motor coordination, Aβ pathology, neurodegeneration, and gliosis revealed formation and progression of severe pathology and phenotypes including massive neuronal loss in homozygous TBA2.1 mice within a few months. In contrast, the start of a slight phenotype was observed only after 21 months in heterozygous mice. These data highlight the role of $pEA\beta_{3\text{-}42}$ in the disease development and progression of AD. Based on the findings of this study, homozygous TBA2.1 mice can be utilized to gain deeper understanding in the underlying mechanisms of $pEA\beta_{3\text{-}42}$ and might be suitable as an animal model for treatment studies targeting toxic Aβ species, complementary to the well described transgenic AβPP mouse models.

Keywords: Alzheimer's disease, behavior, motor neurons, motor phenotype, mouse model, neurodegeneration, pathology, pyroglutamate modified amyloid-$\beta_{3\text{-}42}$

[1]These authors contributed equally to this work.

*Correspondence to: Dieter Willbold, Forschungszentrum Jülich, Institute of Complex Systems, Structural Biochemistry (ICS-6), 52425 Jülich, Germany. Tel.: +49 2461 612100; Fax: +49 2461 612023; E-mail: d.willbold@fz-juelich.de and Antje Willuweit, Forschungszentrum Jülich, Institute of Neuroscience and Medicine (INM-4), 52425 Jülich, Germany. Tel.: +49 2461 6196358; Fax: +49 2461 612302; E-mail: a.willuweit@fz-juelich.de.

ISSN 1387-2877/16/$35.00

INTRODUCTION

Alzheimer's disease (AD) is the most common neurodegenerative disorder. The major postmortem pathological hallmarks of the disease are the progressive neurodegeneration, hyperphosphorylated tangles of the tau protein, and amyloid-β (Aβ) containing plaques [1, 2]. Several studies claim soluble oligomers of Aβ as the relevant pathogen for development and progression of AD [3]. Monomeric Aβ is constantly produced by cleavage of the amyloid-β protein precursor (AβPP) by β- and γ- secretase and aggregates in a series of different species from oligomers to fibrils and to the formation of plaques [4, 5]. It was suggested that the oligomerization of Aβ leads in a cascade to synaptic dysfunction, hyperphosphorylated tangles of the tau protein, neurodegeneration, and finally dementia [3]. Different Aβ species have been identified in brains of AD patients, by which $Aβ_{1-40}$ and $Aβ_{1-42}$ are the most common. Despite those isoforms, N-terminal truncated species are also dominantly found in AD brains. The most common N-terminal truncated Aβ species are pyroglutamate-modified Aβ peptides (pEAβ), which represent about 10 to 20% of total Aβ isolated from vascular amyloid deposits and up to 50% of the Aβ peptides present in purified amyloid plaque cores [6]. It is well known that $pEAβ_{3-42}$ has an enhanced oligomerization tendency and is more neurotoxic compared to $Aβ_{1-42}$ [7–9]. Moreover, it is resistant against degradation, and is able to impair long-term potentiation. Besides several potential posttranslational modifications (PTM) of Aβ, $pEAβ_{3-42}$ is the only PTM for which an immunotherapy has been developed and already tested in humans [10].

To gain deeper insight into the disease mechanisms, the use of AD animal models in research is highly relevant and thus far without alternative. However, most of the models used do not show any neurodegenerative pathology, which is certainly a major disadvantage for their use in the development of curative medications. In this study, we used the new mouse model TBA2.1, exhibiting a motor neurodegenerative phenotype induced by the neuronal presence of N-terminal truncated and pyroglutamated $Aβ_{3-42}$ ($pEAβ_{3-42}$) [11]. Several studies have shown that with the beginning of the preclinical stage of AD, humans also develop deficiencies in the motor function after first cognitive impairments [12–14]. This implies lower muscle bulks and lower muscle strength, especially the grip strength is affected, but also restrictions in motor learning. Therefore, the relation between the motor disorder and the presence of $pEAβ_{3-42}$ might also be relevant for the human disease.

The aim of the present study was to obtain further insights into the extent of the $pEAβ_{3-42}$ induced neurodegenerative process in transgenic mice. Additionally, we aimed to identify suitable experiments and behavioral tests which could be used as robust read out in future therapeutic studies. Therefore, the phenotypes of both homozygous and heterozygous TBA2.1 mice were analyzed in detail including their motoric abilities and disabilities, and cerebral pathology at different ages was compared to wild type littermates, to validate and extend the results of Alexandru et al. [11]. We have solely concentrated on the analysis of motor deficits, as motor impairment will bias standard cognition assays, like the Morris water maze, the novel object recognition test, and the Y maze, to name a few. The findings of this study extend the knowledge of the TBA2.1 mouse model as a suitable research model for treatment studies evaluating new drug candidates against AD, complementary to the AD mouse models exhibiting cognitive deficits.

MATERIAL AND METHODS

Ethics statement

All experiments were done in accordance with the German Law on the protection of animals and approved by LANUV North-Rhine-Westphalia (Germany, AZ84-02.04.2011.A359).

Animals

Heterozygous (HET) and homozygous (HOM) TBA2.1 mice exhibiting neuronal formation of $pEAβ_{3-42}$ were originally described on a C57BL/6 × DBA1 background [11] and were further crossed to C57BL/6 for more than four generations. Generation of TBA2.1 mice was described by Alexandru et al. [11]. Briefly, the chromosomal integration of the pre-pro-peptide of murine thyrotropin releasing hormone (TRH, Thyroliberin) was used, whereby the TRH was fused to the N-terminus of the modified human Aβ polypeptide Aβ(Q3–42). Thus, Aβ(Q3–42) expression was directed into the secretory pathway in neuronal tissue, based on murine Thy1.2 regulatory sequences. For final generation of $pEAβ_{3-42}$, the N-terminally truncated

Aβ species are posttranslationally modified by the endogenous glutaminyl-cyclase [11]. Wild type littermates (wild type, WT) were used as control mice. Mice were housed up to four per cage in a controlled environment on a 12/12-h light/dark cycle (lights on from 7 a.m.–7 p.m.), with 54% humidity, temperature of 22°C, and food and water *ad libitum*. For breeding, only heterozygous mice were used. Homozygous mice were sacrificed at five months of age for ethical reasons due to the severity of the disease.

Animal experimental setup

Cross-sectional characterization of male TBA2.1 mice was initially based on phenotype assessment (SHIRPA test battery) and motor balance (accelerating rotarod) from two to five months of age using heterozygous (HET), homozygous TBA2.1 (HOM) and wild type littermates (WT).

To increase the understanding of the motor phenotype progression of individual homozygous TBA2.1 mice, a longitudinal study with a different group of male, homozygous, and wild type TBA2.1 mice was performed additionally. They were tested at 3 and 5 months of age in additional motor tests including open field test, clasping behavior, marble burying behavior, grip strength, and pole test. The phenotype of old heterozygous, male mice (HET) was analyzed at 18, 21, and 24 months of age in the SHIRPA test battery, motor balance (accelerating rotarod), pole test, grip strength, and marble burying behavior compared to WT.

Except for the SHIRPA assessment, all individuals were habituated in single cages before starting the particular test. All experimenters were blind to genotype and all tests were carried out at the same time of day. For each experiment, a minimum of 5 mice per genotype and group was used. A detailed listing of the mice used per experiment is given in Table 1.

Phenotype assessment

The primary screen of the SHIRPA test battery was used to assess the phenotype [15]. This test consisted of the following subtests: abnormal body carriage, alertness, abnormal gait, startle response, loss of righting reflex, touch response, pinna reflex, cornea reflex, forelimb placing reflex, hanging behavior, and pain response. Mice were individually observed and scored in an arena of 42.5 cm × 18 cm × 26.5 cm (L × H × W). Scoring was defined from 0 (similar to WT) to 3 (extremely abnormal from WT). In every measurement, the body weight was also recorded.

Accelerating rotarod

Analysis of the motor coordination of the TBA2.1 mice was performed using a rotarod apparatus (Ugo Basile Srl, Comerio VA, Italy) and a previously published protocol [11]. The test was conducted in two days with one training and three test sessions. In the training on the first morning, the mice had to stay on the rod for at least 60 s at constant 10 rpm. In the afternoon as well as on the next day morning and afternoon, the mice had to run in three trials on the beam accelerating from 4 to 40 rpm. The total time on the beam of each trial was used for analysis and the maximum time was 10 min.

Grip strength analysis

Grip strength analysis of the forelimbs was evaluated using the Grip Strength Meter (Ugo Basile Srl, Comerio VA, Italy). Following the manufacturers protocol, TBA2.1 mice were placed with their forelimbs to a triangular grasping bar which they grip intuitively. The mice were pulled backwards until they release the holder. The peak force was measured three times in succession. The mean value of all three peak forces was used for analysis.

Modified pole test

The standard pole test evaluates basal ganglia related movement disorders [16, 17]. Owing to the severe motor phenotype of homozygous TBA2.1 mice, the following modifications were realized. The mice were placed with the head downwards instead of upwards on a vertical pole (height 50 cm, diameter 1.2 cm, rough-surfaced) and their movement downwards was rated. The runs were scored from 0 to 3 (0 continuous run, 1 part-way run, 2 slipping downwards, 3 falling down). This procedure was performed three times and the sum of all three scores was used for analysis.

Marble burying test

The marble burying test was used to assess generic and motor behavior of the mice [18]. The mice

Table 1
Overview of the used number of mice per experiment

Experiment	Age (mo)	Number of mice		
		WT	HOM	HET
Body weight, SHIRPA, Rotarod, (all cross-sectional)	2	8	8	9
	3	8	7	6
	4	10	12	11
	5	10	12	11
	18	10	7	–
	21	9	8	–
	24	6	5	–
Innate and motor behavior, open field (longitudinal)	3	8	–	7
	5	8	–	7
	18	10	8	–
	21	9	8	–
	24	6	5	–
Immunohistochemical analysis	3	–	–	6
	5	5	–	6
	18	8	6	–
	24	8	6	–
ELISA	5	5	–	5

were placed in a housing cage with 5 cm bedding, and twelve opaque, green marbles (diameter 18 mm, arranged at regular intervals). After 30 min, marbles buried to more than 75% were counted by two independent experimenters. Mean of the counts were used for analysis.

Clasping test

To characterize innate clasping behavior, the mice were lifted up by the tail for 15 s. Trembling and/or cramping of the hind limbs was observed and scored (from 0 meaning similar to wild type mice until 3 meaning extreme abnormal behavior). This procedure was performed three times and the sum of all three scores was used for analysis.

Open field test

The open field test was performed to analyze the locomotive and explorative behavior of homozygous and wild type TBA2.1 mice at an age of 3 and 5 months. After habituation, mice were placed in a square-shaped arena (44 cm × 44 cm × 44 min), imaginarily divided into two departments: center and border zone (center: 22 cm × 22 cm, border: 44 cm × 44 cm). The mice were allowed to explore the arena for 30 min. They were recorded with a camera driven tracking system, Ethovision 11 (Noldus, Wageningen, The Netherlands).

Tissue preparation

The mice were sacrificed and the brains were analyzed. The right brain hemisphere was used for immunohistological analysis and the left hemisphere for biochemical analysis. Both hemispheres were stored at –80°C until further processing.

Immunohistochemical analysis

Aβ load (antibody 6E10), neurodegeneration (antibody NeuN) and gliosis (antibodies against GFAP and CD11b) of 5 months old WT, 3 and 5 months old homozygous TBA2.1, as well as 18 and 24 months old wild type heterozygous TBA2.1 mice were assessed by immunohistochemical or immunofluorescence analysis using 20 μm thick, sagittal sections divided by a cryotome (Leica Biosystems Nussloch GmbH, Wetzlar, Germany). Five to seven brain sections per mouse were fixed and treated with 70% formic acid for antigen retrieval. The sections were washed and treated with 3% H_2O_2 in methanol for elimination of endogenous peroxidases. After a further washing step, sections were incubated with the primary antibody over night at 4°C in a humid chamber (6E10:1:1000, Bio Legend, San Diego, CA, USA; GFAP: 1:1000, DAKO, Agilent Technologies, Santa Clara, CA, USA; NeuN: 1:1000 Merck Millipore, Darmstadt, Germany, CD11b: 1:2500 Abcam, Cambridge, UK) in Tris buffered saline with 1% Triton X100 (TBST) with 1% bovine serum albumin (BSA). Afterwards, sections were incubated with a biotinylated secondary anti-mouse or anti-rabbit antibody

(both 1:1000 in TBST+1% BSA, Sigma-Aldrich, Germany). Staining was visualized by use of 3, 3'-Diaminobenzidine (DAB) enhanced with saturated nickel ammonium sulphate solution (homozygous mice, Figs. 6 and 9), or by use of secondary antibodies labeled with different fluorescence dyes (Goat anti-mouse IgG (H+L), Alexa Fluor 568, Goat anti-rabbit IgG (H+L), Alexa Fluor 488, Invitrogen, USA). Immunofluorescence sections were counterstained by DAPI (4′,6-Diamidin-2-phenylindol) (Merck, Germany). Sections were mounted with DPX Mountant (Sigma-Aldrich, Germany) after washing in an ascending alcohol series. Images were taken with a LMD6000 microscope (Leica Camera, Germany) with a DFC310 FX camera (Leica Camera, Germany). The stained area of GFAP and NeuN (motor cortex, striatum, inferior colliculus, brain stem, and hippocampal region CA1), CD11b (inferior colliculus, brain stem), and particles of Aβ in different brain regions (6E10: sensorimotor cortex, striatum, hippocampal region CA1) in homozygous TBA2.1 mice and their non-transgenic littermates were analyzed. Additionally, Aβ particles (hippocampal CA1 region, Striatum) and DAPI counts (hippocampal CA1 region) in heterozygous TBA2.1 mice and their non-transgenic littermates were analyzed. Quantification was performed using ImageJ (National Institute of Health, Bethesda, MD, USA).

Enzyme-linked immunosorbent assay (ELISA)

To quantify the cerebral $pEA\beta_{3\text{-}42}$ levels the amyloid-beta (N3pE-42) ELISA (IBL International GmbH, Hamburg, Germany) was used. For that reason, the left brain hemispheres were homogenized with Tris buffer (20 mM Tris pH 8.3, 250 mM NaCl, Roche EDTA free Complete Protease Inhibitor) in the PreCellys24 homogenizer (2 × 20 s at 6.500 rpm, Bertin Technologies, Montigny-le-Bretonneux, France). The resulting homogenate was vortexed, 15 min sonified, vortexed again and centrifuged (175.000 g, 4°C, 30 min). The pellet was incubated and resuspended with 0.2% diethanolamine on ice and centrifuged. The supernatant, the DEA soluble fraction, was used for analysis. The pellet was incubated and resuspended with 70% formic acid (FA) on ice and centrifuged. FA is used to destroy all insoluble large Aβ structures, to provide the analysis of insoluble Aβ species. The interphase was taken and neutralized with 1 M Tris pH 11.3 representing the insoluble Aβ fraction. The $pEA\beta_{3\text{-}42}$ level of the DEA soluble and the insoluble Aβ fractions were quantified in the ELISA using the manufacturer's protocol.

Statistical analysis

Gaussian distribution of all data was tested in the Shapiro-Wilk-Test. Normally distributed data were analyzed using either one- or two-way ANOVA (analysis of variance) with Fisher LSD *post hoc* analysis or *t* test. Repeated measurements (RM) were analyzed by use of one- or two-way RM ANOVA. Non-parametric data were tested using the Friedman or Kruskal-Wallis test. Appropriate non-parametric *post hoc* analysis was performed with Multiple Comparison Tests by Dunn or by Dunnet. In order to avoid the use of an insufficient number of mice in the conducted experiments, power analyses were carried out to check the appropriate group sizes to achieve a biologically relevant effect ($\alpha = 0.05$, $\beta \leq 0.2$). Power analysis was performed based on the experiments from Brener et al. and Dunkelmann et al. [19, 20]. A biologically relevant effect was set with regard to the changes between wild type and homozygous TBA2.1 mice from the recently published SHIRPA and rotarod results of Dunkelmann et al. [20]. According to the results of this study, 2 months old wild type mice revealed a mean SHIRPA score of 1.4 (SD 1.6). Assuming a biologically relevant effect of 200%, and a significance level of $\alpha = 0.05$ (5%) and $\beta \leq 0.2$ (20%), the expected power of the experiment is 80% by using 6 mice per group, or 90% by using 8 mice per group, respectively. Power analysis was performed by use of InVivoStat 2.5 (InVivoStat by Simon Bate and Robin Clark, United Kingdom, [21]). No power analysis was performed for repeated measure analysis (e.g., rotarod), as it is not accessible with simple power analysis. All data are expressed as mean ± SEM. All statistical calculations were performed using GraphPad Prism 5 (GraphPad Software, Inc., La Jolla, CA, USA), SigmaPlot Version 11 (Systat Software, Erkrath, Germany).

RESULTS

Appearance and motor coordination of transgenic TBA2.1 mice

To get a first impression of the motor neurodegenerative phenotype induced by $pEA\beta_{3\text{-}42}$, we analyzed two, three, four, and five months old heterozygous (HET) and homozygous (HOM) TBA2.1 mice and their wild type littermates (WT). They were

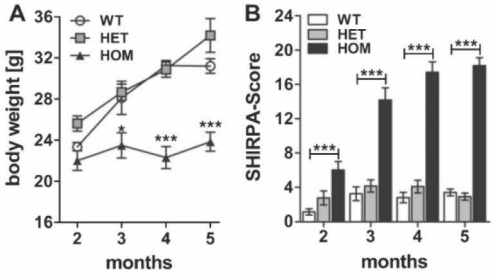

Fig. 1. Weight gain and phenotype assessment of wild type (WT), heterozygous (HET), and homozygous (HOM) TBA2.1 mice. The weight gain of HOM mice was reduced from 2 to 5 months compared to HET and WT mice (A). Phenotype assessment using the SHIRPA test battery revealed a bold phenotype of HOM TBA2.1 mice starting already at 2 months of age (B). Data is presented as mean ± SEM; *$p<0.05$ and ***$p<0.001$ versus WT.

tested cross-sectionally in the phenotype assessment test and for motor coordination using the accelerating rotarod test. First of all, we analyzed the body weight of homozygous, heterozygous, and wild type mice at different ages. Body weight gain of homozygous mice was reduced compared to wild type and heterozygous mice (two-way ANOVA, $F_{(3,95)} = 18.2$, $p<0.001$; Fisher LSD *post hoc* analyses, WT versus HOM, 2 m $p=0.39$, 3 m $p<0.01$, 4 m $p<0.001$, 5 m $p<0.001$). This means, the body weight of homozygous mice was stabilized at about 22.9 ± 0.5 g, whereas that of wild type mice increased from 23.2 ± 0.4 g to 31.2 ± 0.6 g during the period of measurements, similar to the body weight of heterozygous mice (Fig. 1A). The phenotype assessment revealed a neurological phenotype in homozygous mice already at two months of age with a five times higher score compared to wild type mice (two-way ANOVA, $F_{(2,99)} = 226.7$, $p<0.001$; Fisher LSD *post hoc* analyses, WT versus HET n.s., WT versus HOM $p<0.001$ at all ages, Fig. 1B). The score of homozygous mice, i.e., their phenotypic abnormalities, increased until five months of age. Among the phenotypic abnormalities, an impairment of lower sensorimotor functions (e.g., basic movements) in connection with the development of a kyphosis and a rigid gait could be observed. However, heterozygous mice appeared normal at this age.

Analysis of the motor coordination and motor learning of two months old mice showed similar performance regardless of the phenotype (Friedman test, not significant (n.s.)) (Fig. 2A). However, at the age of three months, the motor learning of the homozygous mice decreased when compared to the abilities of the wild type mice (Friedman test, $p=0.031$, *post hoc* analysis WT versus HET n.s., WT versus HOM $p<0.05$). A deficit in motor coordination was measurable at four and five months of age, too, although it only reached statistical significance at 5 months (Friedman test, $p=0.002$, WT versus HET n.s., WT versus HOM $p<0.001$). In contrast, motor coordination and learning of the heterozygous mice showed no significant differences in relation to the control wild type mice (Fig. 2A-D). These results indicated a proceeding phenotype in homozygous mice and no measurable abnormalities in heterozygous mice until five months of age.

Detailed investigation of the motor phenotype of homozygous TBA2.1 mice

In order to characterize the motor deficits of the homozygous mice in more detail, we performed additional tests with homozygous and wild type mice at an age of 3 and 5 months using the marble burying, clasping and pole tests, and measured their grip strength. Homozygous mice buried significantly less marbles already at an age of 3 as well as at 5 months compared to their wild type littermates (two-way RM ANOVA, $F_{(1,13)} = 33.9$, $p<0.001$, Fisher LSD *post hoc* analysis, WT versus HOM 3 m $p<0.001$, WT versus HOM 5 m $p<0.001$), with a progression of the impaired burrowing behavior of HOM TBA2.1 mice within this test from 3 to 5 months of age (two-way RM ANOVA, $F_{(1,13)} = 9.5$, $p=0.009$; Fisher LSD *post hoc* analysis, HOM 5 m versus HOM 3 m $p=0.027$) (Fig. 3A). Additionally, homozygous TBA2.1 mice showed a significantly reduced clasping score compared to the wild type littermates (two-way RM ANOVA, $F_{(1,13)} = 71.8$, $p<0.001$; Fisher LSD *post hoc* analysis, WT versus HOM 3 m $p<0.001$, WT versus HOM 5 m $p<0.001$), with a significant progression from 3 to 5 months of age (two-way RM ANOVA, $F_{(1,13)} = 63.8$, $p<0.001$; Fisher LSD *post hoc* analysis, HOM 5 m versus HOM 3 m $p<0.001$) (Fig. 3B). The grip strength of homozygous TBA2.1 mice was also significantly reduced at both ages analyzed in comparison to their wild type littermates (two-way RM ANOVA, $F_{(1,13)} = 95.2$, $p<0.001$; Fisher LSD *post hoc* analysis, WT versus HOM 3 m $p<0.001$, WT versus HOM 5 m $p<0.001$), here without a significant progression of their forelimb strength from 3 to 5 months (two-way RM ANOVA, $F_{(1,13)} = 0.01$, n.s) (Fig. 3C). Furthermore, in the pole test the mice showed similar deficits. Again, there was a significant difference in the performance of homozygous

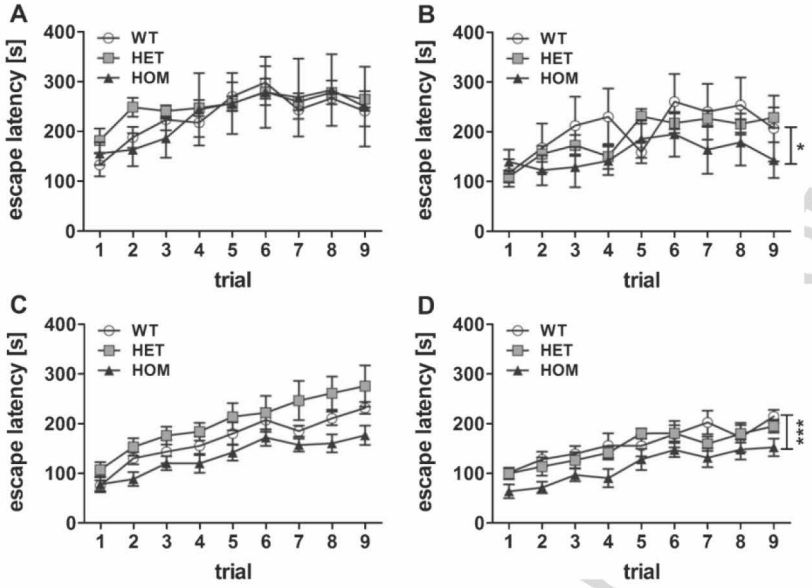

Fig. 2. Cross-sectional analysis of the motor phenotype. Motor balance was tested using rotarod apparatus with 9 trials in total in 2, 3, 4, and 5 months old transgenic TBA2.1 mice (A, B, C, D, respectively). Deterioration of motor balance of homozygous (HOM) TBA2.1 mice started with an age of 3 months and was significantly further reduced in 5 months old mice compared to wild type (WT) (B and D). No difference was observed between the performance of heterozygous (HET) TBA2.1 and WT mice. Data is represented as mean ± SEM, $*p<0.05$ and $***p<0.001$ versus WT.

TBA2.1 mice at an age of 3 and 5 months compared to wild type littermates (two-way RM ANOVA, $F_{(1,13)} = 160.9$, $p<0.001$; Fisher LSD *post hoc* analysis, WT versus HOM 3 m $p<0.001$, WT versus HOM 5 m $p<0.001$), and a significantly declined performance from 3 to 5 months of age (two-way RM ANOVA, $F_{(1,13)} = 5.3$, $p=0.035$; Fisher LSD *post hoc* analysis, HOM 5 m versus HOM 3 m $p=0.008$) (Fig. 3D).

In this study, we also performed open field tests for the assessment of the exploratory/anxiety related and locomotive behavior of 3 and 5 months old wild type and homozygous TBA2.1 mice. There was a significant difference between the times spent in border and center zones during the 30 min test for all mice at an age of 5 months but not between the groups, indicating similar anxiety related behavior of homozygous and wild type mice (two-way ANOVA, zone: $F_{(1,24)} = 240.1$, $p<0.001$, genotype: $F_{(1,24)} = 2.1 \times 10^{-13}$, n.s.) (Fig. 4A). Nevertheless, there was a significant difference between the travelled distance of wild type and homozygous TBA2.1 mice at both ages analyzed (two-way RM ANOVA, $F_{(1,24)} = 10.2$, $p=0.007$; Fisher LSD *post hoc* analysis, WT versus HOM 3 m $p=0.037$, WT versus HOM 5 m $p=0.007$) (Fig. 4B). A decline in the moved distance from 3 to 5 months of age could be observed within both analyzed genotypes, indicating a possible habituation effect (two-way ANOVA, $F_{(1,24)} = 66.4$, $p<0.001$; Fisher LSD *post hoc* analysis, both $p<0.001$) (Fig. 4B).

Phenotype assessment and motor coordination of aged heterozygous mice

Since there were no significant differences in motor coordination in young heterozygous mice compared to wild type mice of the same age, we additionally analyzed them with 18, 21, and 24 months of age. Also, at that age motor coordination was similar between heterozygous and wild type mice (Friedman test, $p<0.001$, Dunn test n.s.) (Fig. 5A). In the phenotype assessment at the age of 21 and 24 months, heterozygous mice showed a minor, but significant phenotype compared to wild type littermates at the respective age (two-way ANOVA, $F_{(1,42)} = 16.2$, $p<0.001$; Fisher LSD *post hoc* analysis, WT versus HET 18 m n.s., WT versus HET 21 m $p=0.002$, WT versus HET 24 m $p=0.032$) (Fig. 5C), which was underlined by a reduced body weight at the same age (two-way ANOVA, $F_{(1,42)} = 5.0$, $p=0.031$; Fisher

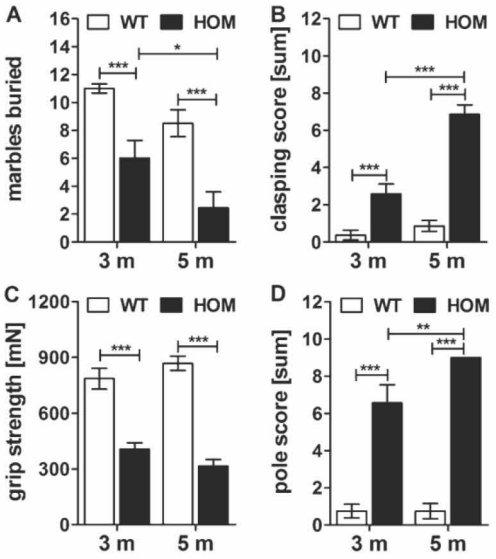

Fig. 3. Innate and motor behavior of wild type littermates (WT) and homozygous (HOM) TBA2.1 mice. Longitudinal study of WT and HOM male TBA2.1 mice. Behavior of marble burying (A), clasping (B), grip strength (C) and pole test (D) of HOM TBA2.1 mice was impaired compared to WT. Data is represented as mean ± SEM, $*p<0.05$, $**p<0.01$, and $***p<0.001$.

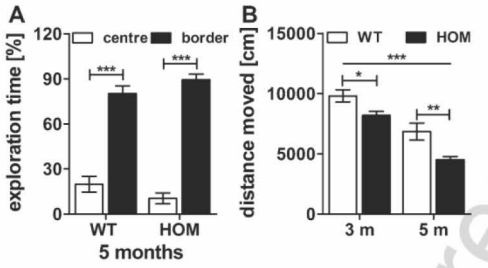

Fig. 4. Open field activity of wild type (WT) and homozygous (HOM) TBA2.1 mice. No difference in exploratory behavior of center and border zone was observed between homozygous and wild type littermates in the open field test at an age of 5 months (A). A significant difference in the travelled distance was observed between WT and HOM mice (B). Data is represented as mean ± SEM and $*p<0.5$, $**p<0.01$, and $***p<0.001$.

LSD *post hoc* analysis, WT versus HET 18 m n.s. $p=0.11$, WT versus HET 21 m $p=0.013$, WT versus HET 24 m $p=0.014$) (Fig. 5B). These minor changes are especially observable by an abnormal body carriage and gait, reduced pain response, and slightly reduced reflexes. A decreased body weight might be the result of a potential loss of muscle volume due to the reduced motor neuron innervation. The grip strength (two-way-ANOVA n.s) and the results of the pole test (two-way-ANOVA n.s.) of heterozygous mice were indistinguishable from those of the wild type mice (Fig. 5D, E). These results indicated a beginning phenotype in the heterozygous mice starting from 21 months of age but without impairment of the motor skills as measured on the rotarod.

Aβ pathology of 3 and 5 months old homozygous and aged heterozygous TBA2.1 mice

To complement our findings of the behavioral tests, we analyzed the Aβ pathology and quantified the amount of Aβ (immunohistochemistry using antibody 6E10) in different brain regions (olfactory tubercle, striatum (caudate putamen), sensorimotor area (cortex) and CA1 region (hippocampus)) and the amount of $pEA\beta_{3\text{-}42}$ protein levels with biochemical quantification (ELISA). In most of the currently used AD mouse models, Aβ deposits are described as diffuse or compact plaques of a size from about 10 μm^2 to a maximum size of 6,500 μm^2 [22]. In contrast, Aβ deposits of homozygous TBA2.1 mice are much smaller (average size 148 μm^2, maximum size 987 μm^2), and never diffuse, with more or less clear demarcation to their surrounding (Fig. 6E-P). In all analyzed regions, there was a significantly higher amount of Aβ particles in the brains of homozygous TBA2.1 mice at both ages compared to wild type littermates (cortex: one-way ANOVA $F_{(2,14)}=11.7$, $p=0.031$; Fisher LSD *post hoc* analysis, WT versus HOM 3 m $p=0.003$, WT versus HOM 5 m $p<0.001$, HOM 3 m versus HOM 5 m n.s. $p=0.26$; caudate putamen, striatum: one-way ANOVA $F_{(2,14)}=13.5$, $p<0.001$; Fisher LSD *post hoc* analysis, WT versus HOM 3 m $p<0.001$, WT versus HOM 5 m $p<0.001$, HOM 3 m versus HOM 5 m n.s. $p=1$; olfactory tubercle: one-way ANOVA $F_{(2,14)}=15.5$, $p<0.001$; Fisher LSD *post hoc* analysis, WT versus HOM 3 m $p=0.001$, WT versus HOM 5 m $p<0.001$, HOM 3 m versus HOM 5 m n.s. $p=0.16$; CA1 region hippocampus: Kruskal-Wallis one-way ANOVA on Ranks $p=0.001$; Dunn's *post hoc* analysis WT versus HOM 3 m $p<0.05$, WT versus HOM 5 m n.s., HOM 3 m versus HOM 5 m n.s.).

Quantifications of $pEA\beta_{3\text{-}42}$ protein levels in the hemispheres of homozygous TBA2.1 mice revealed a significant amount of 1.6 ± 0.2 ng/ml of DEA-soluble $pEA\beta_{3\text{-}42}$, whereas the DEA-soluble fraction of the wild type hemisphere was below detection limit (unpaired two-tailed *t* test, $p<0.001$).

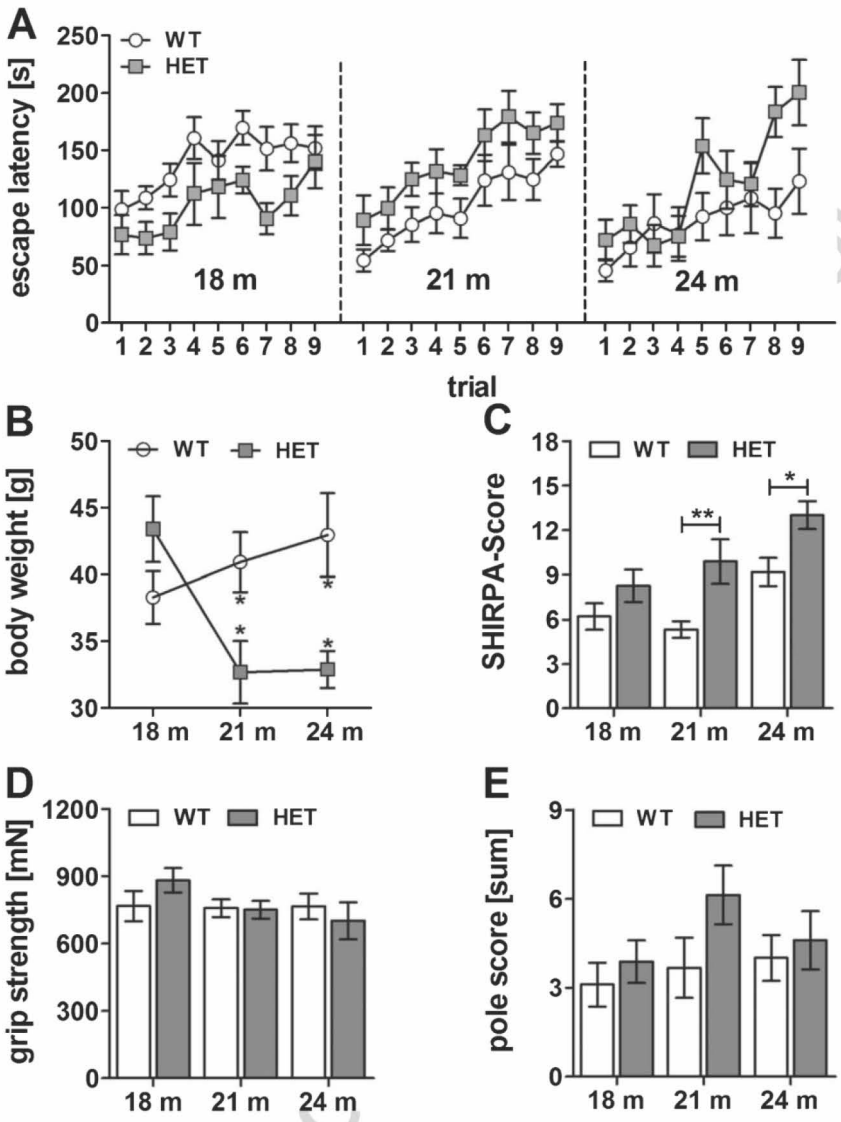

Fig. 5. Motor behavior of wild type (WT) and heterozygous (HET) mice at 18, 21, and 24 months of age. Rotarod performance was equal among WT and HET at all ages (A). Phenotype assessment using SHIRPA test battery showed a minor motor phenotype in heterozygous mice at 21 and 24 months of age (C) while the body weight was also reduced at the same age (B). The grip strength (D) and performance in the pole test (E) were not impaired at any age. Data is represented as mean ± SEM and $*p < 0.05$.

The insoluble fraction of $pEA\beta_{3\text{-}42}$ was about 32.3 ± 4.3 ng/ml insoluble $pEA\beta_{3\text{-}42}$, which was statistically significant to the insoluble $pEA\beta_{3\text{-}42}$ fraction of the wild type hemispheres (unpaired two-tailed t test, $p < 0.05$). The wild type insoluble $pEA\beta_{3\text{-}42}$ was about 12.3 ± 4.3 ng/ml representing endogenous murine $pEA\beta_{3\text{-}42}$ (Fig. 7A, B). All analyzed samples of the soluble Tris-fraction were below the detection limit.

Quantification of the amount of Aβ in the brains of 18 and 24 months old heterozygous TBA2.1 mice achieved a significant increase of Aβ in the hippocampus of 24 months old heterozygous TBA2.1 mice in comparison to wild type mice (one-way

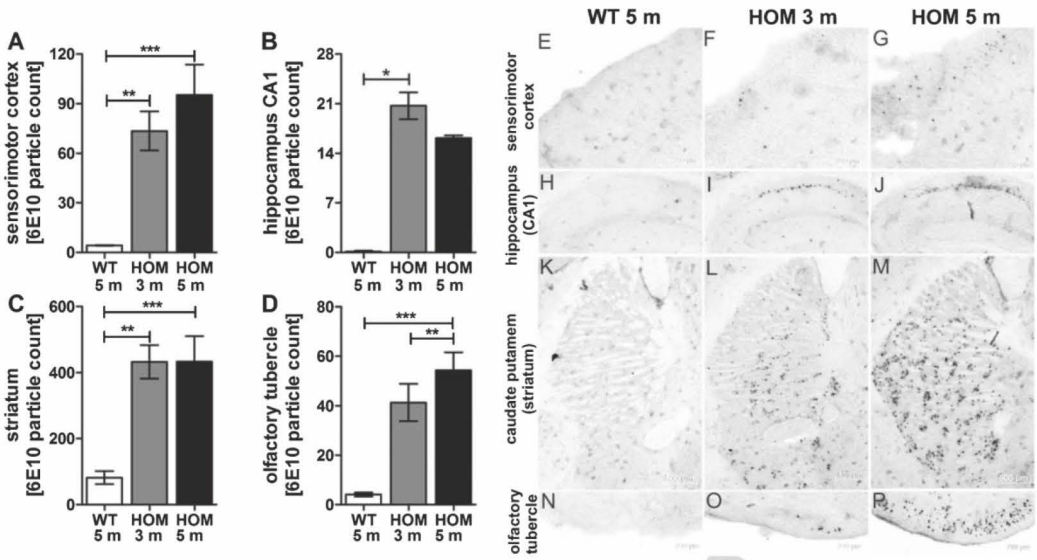

Fig. 6. Aβ aggregates in wild type (WT), and 3 and 5 months old homozygous (HOM) TBA2.1 mice. Aβ particles were visualized by 6E10 staining in wild type (WT), and 3 and 5 months old homozygous (HOM) TBA2.1 mice. Aβ particles were quantified in different brain regions (A, N-P: olfactory tubercle, B, K-M: caudate putamen (striatum), C, E-G: sensorimotor area (cortex), D, H-J: CA1 region (hippocampus)). Data is presented as mean ± SEM; $*p<0.05$, $**p<0.01$, and $***p<0.001$.

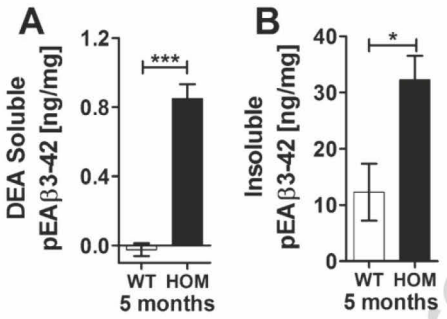

Fig. 7. Biochemical analysis of $pEA\beta_{3-42}$ of 5 months old wild type (WT) and homozygous (HOM) TBA2.1 mice. Biochemical analysis of DEA-soluble and insoluble $pEA\beta_{3-42}$ revealed a significant difference between wild type and 5 months old homozygous TBA2.1 mice. Data is represented as mean ± SEM; $*p<0.05$ and $***p<0.001$.

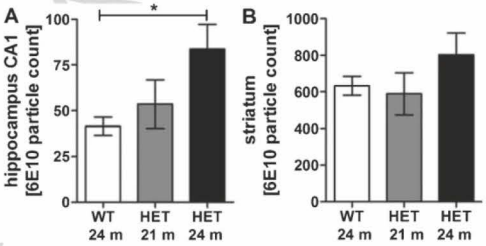

Fig. 8. Aβ aggregates in wild type (WT), and 18 and 24 months old heterozygous (HET) TBA2.1 mice. Staining of Aβ deposits in 18 and 24 months old heterozygous TBA2.1 mice compared to 24 months old wild type littermates). Aβ deposits were quantified in the striatum and CA1 hippocampal region. Data is represented as mean ± SEM; $*p<0.05$.

ANOVA $F_{(2,15)} = 3.7$, $p = 0.05$; Fisher LSD *post hoc* analysis, WT versus HET 24 m $p = 0.02$, WT versus HET 18 m n.s $p = 0.08$, HET 18 m versus HET 24 m n.s. $p = 0.46$) (Fig. 8A). There was no significant change in the amount of Aβ particles in the striatum of all analyzed ages of heterozygous TBA2.1 mice (one-way ANOVA $F_{(2,15)} = 1.3$, n.s. $p = 0.31$) (Fig. 8B).

Gliosis and neuronal loss in homozygous and aged heterozygous TBA2.1 mice

Additionally, we analyzed the neuronal loss of homozygous TBA2.1 mice in more detail. Quantification of all NeuN positive cells in the CA1 region revealed a significant decrease of neurons in homozygous mice of 3 and 5 months compared to 5 months old wild type mice (one-way ANOVA $F_{(2,13)} = 21.3$, $p < 0.001$; Fisher LSD *post hoc* analysis, WT versus HOM 3 m $p = 0.012$, WT versus HOM 5 m $p < 0.001$,

HOM 3 m versus HOM 5 m n.s. $p = 0.37$), without proceeding neuronal loss from 3 to 5 months of age (Table 2, Fig. 9). Within the striatum, no significant loss of neurons in 3 and 5 months old homozygous TBA2.1 mice was observed (one-way ANOVA $F_{(2,13)} = 21.3$, n.s. $p = 0.19$) (Table 2, Fig. 9). Furthermore, no significant decrease of neurons was detectable within the motor cortex (one-way ANOVA $F_{(2,13)} = 21.3$, n.s. $p = 0.07$).

Additionally, we analyzed activated astrocytes in and around the CA1 region, as well as in the striatum. There was no significant difference in the amount of activated astrocytes in the striatum between 5 months old wild type and 3 as well as 5 months old homozygous TBA2.1 mice (one-way ANOVA $F_{(2,13)} = 0.6$, n.s. $p = 0.59$) (Table 2, Fig. 9), but there was a significant increase of GFAP positive cells in the CA1 region of the hippocampus. Here, we observed a significant increase of the amount of GFAP positive cells in 3 months old homozygous TBA2.1 mice compared to wild type mice. Interestingly, at 5 months of age, the GFAP positive area in the CA1 region of homozygous TBA2.1 mice dropped again to levels comparable of wild type mice (one-way ANOVA $F_{(2,13)} = 21.3$, $p = 0.004$; Fisher LSD *post hoc* analysis, WT versus HOM 3 m $p = 0.002$, WT versus HOM 5 m n.s. $p = 0.66$, HOM 3 m versus HOM 5 m. $p = 0.004$) (Table 2, Fig. 9). Analysis of activated astrocytes within the motor cortex revealed a significant increase of this cell type in 3 and 5 months old homozygous TBA2.1 mice (one-way ANOVA $F_{(2,15)} = 3.86$, $p = 0.048$; Fisher LSD *post hoc* analysis, WT versus HOM 3 m $p = 0.026$, WT versus HOM 5 m n.s. $p = 0.66$, HOM 3 m versus HOM 5 m $p = 0.046$) (Table 2, Fig. 9).

To analyze the inflammatory processes in more detail, we performed additional CD11b staining to visualize and quantify activated microglia. We found CD11b positive areas in the brain stem, inferior colliculus, and a negligible amount of CD11b positive cells in parts of the thalamus and substantia nigra. Quantification revealed a significant increase of activated microglia in the brain stem of 3 as well as 5 months old homozygous TBA2.1 mice in comparison to 5 months old wild type mice (one-way ANOVA $F_{(2,15)} = 12.45$, $p < 0.001$; Fisher LSD *post hoc* analysis, WT versus HOM 3 m $p = 0.002$, WT versus HOM 5 m n.s. $p < 0.001$, HOM 3 m versus HOM 5 m n.s. $p = 0.31$, Table 2). There was no significant difference observed within the midbrain (inferior colliculus) (one-way ANOVA $F_{(2,15)} = 2.71$ n.s., $p = 0.1$, Table 2, Fig. 9).

In addition, we analyzed the possible loss of neurons within the CA1 region of 18 and 24 months old heterozygous mice compared to 18 and 24 months old wild type TBA2.1 mice. Based on the DAPI nuclear staining and quantification, we found significant loss of nuclei in 18 and 24 months old heterozygous TBA2.1 mice compared to wild type mice at the same age (two-way ANOVA $F_{(1,24)} = 26.46$, $p < 0.001$; Fisher LSD *post hoc* analysis, WT versus HET 18 m $p < 0.001$, WT versus HET 24 m. $p = 0.011$, HET 18 m versus HET 24 m. n.s. $p = 0.23$, WT 18 m versus HET 24 m. n.s. $p = 0.6$), but not between heterozygous or wild type mice with increasing age (Fig. 10).

DISCUSSION

AD has been intensively studied for more than 100 years in order to understand the underlying mechanisms for the development of neurodegeneration and to find an effective therapy to slow down or stop disease progression. In preclinical research, rodent models are frequently used and offer the possibility to verify hypotheses which are established based on experiments *in vitro*. AD is the most common neurodegenerative disorder and still, most of the animal models used do not exhibit all features of AD. While cognitive deficits, amyloid deposits or neurofibrillary tangles and some kind of inflammation are observable in many AD mouse lines, neurodegeneration is observed only in a few mouse models [23, 24]. There is an urgent need for mouse models, which develop neurodegeneration, because this is one of the major pathological hallmarks of AD in humans. To avoid further failures of AD clinical trials with Aβ-targeting drug candidates, it is advisable to test the respective compounds in animal models that develop neurodegeneration based on Aβ-aggregation mediated toxicity.

In this study, we used the TBA2.1 mouse model, which was previously introduced and described showing a $pEA\beta_{3\text{-}42}$ induced neurodegenerative phenotype [11]. As reviewed by Bayer and Wirths, $pEA\beta_{3\text{-}42}$ can be frequently found in plaques and CAA in the brains of human AD patients [25]. There, it is generated by cleavage of the first N-terminal two amino acids, aspartate and alanine, resulting in a newly formed N-terminus (glutamate at position three). Thereafter, a PTM occurs where glutamate is converted to pyroglutamate by cyclization via a glutaminyl cyclase. This PTM results in altered biochemical functions such as an enhanced oligomer-

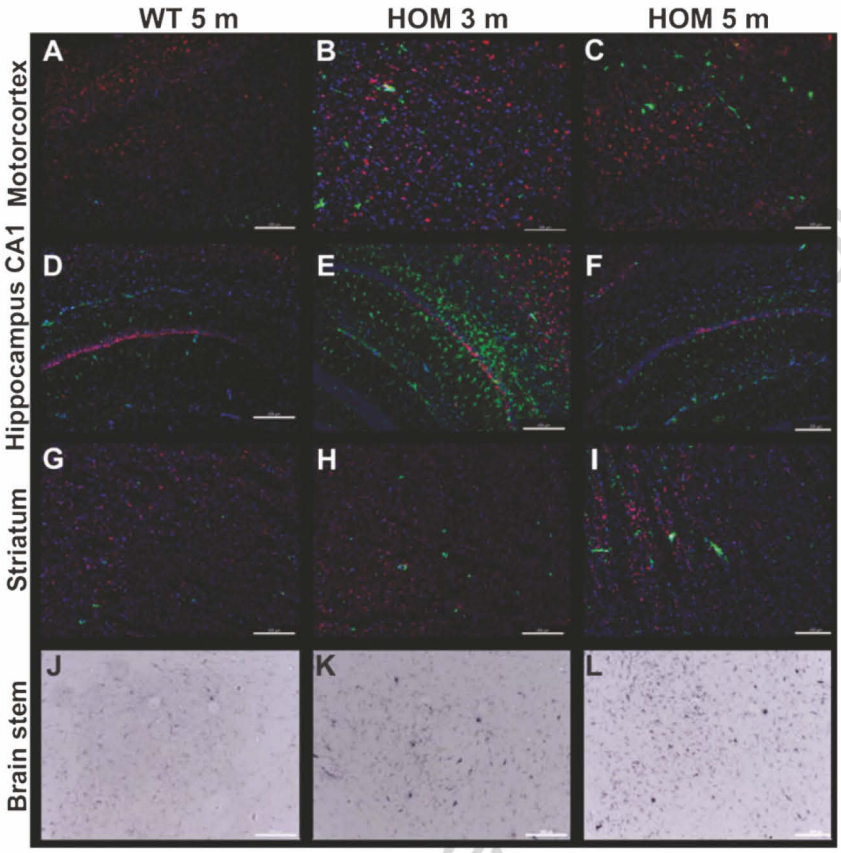

Fig. 9. Gliosis and neuronal loss in homozygous TBA2.1 mice. Representative immunofluorescence and bright field images of the motor-cortex, CA1 hippocampal region, striatum, and brain stem of a 5 months old wild type (WT), and 3 and 5 months old homozygous (HOM) mice illustrating activated astrocytes (GFAP, green, A-I), activated microglia (CD11b, bright field, J-K) and neuronal nuclei (NeuN, red, A-I). Counterstaining was performed with DAPI (A-I).

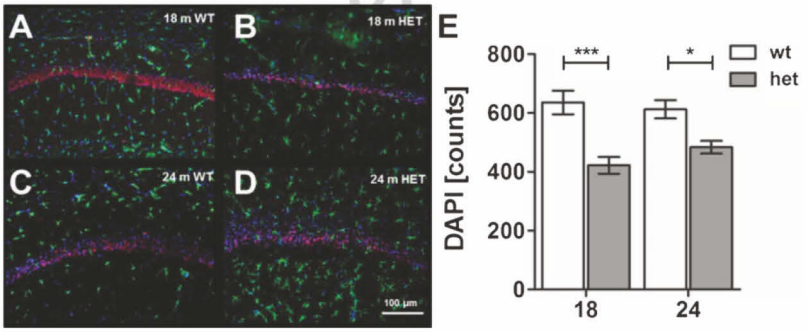

Fig. 10. Astrocytosis and neuronal loss in wild type (WT) and aged heterozygous (HET) TBA2.1 mice. Staining of activated astrocytes (GFAP) and neuronal nuclei (NeuN) in 18 and 24 months old HET TBA2.1 mice in comparison to 18 and 24 months old WT littermates (A-D). All nuclei were counter stained with DAPI. Quantification of the number of nuclei (DAPI counts) in CA1 hippocampal region revealed a significant difference between WT and HET TBA2.1 mice at both analyzed ages, but not between 24 months old HET TBA2.1 and WT mice (E). Data is represented as mean ± SEM and $*p < 0.05$ and $***p < 0.001$.

ization tendency and higher neurotoxic properties [9]. In addition, more and more evidence exists that Aβ plaques are not responsible for synaptic dysfunction, neurodegeneration, and finally dementia. According to a hypothesis by Alexandru et al., the QC-dependent generation of $pEA\beta_{x-42}$ could explain the discrepancy between healthy individuals with Aβ plaques and AD patients. To gain more knowledge about the clinical importance of pEAβ, the TBA2.1 mouse model was developed [11].

Alexandru and colleagues first described some deficits of the homozygous mice, but did not look into the phenotype of heterozygous TBA2.1 mice in detail [11]. Thus, the aim of this work was to increase knowledge about the $pEA\beta_{3-42}$ induced neurodegenerative process in AD by validating and extending the existing findings with homozygous and heterozygous TBA2.1 mice. Furthermore, we aimed at identifying additional robust motor behavioral tests which are suitable for longitudinal monitoring of homozygous TBA2.1 mice in future therapeutic studies.

Our results confirm the progressive early-onset motor neurodegenerative phenotype of the homozygous mice using the SHIRPA phenotype assessment and the accelerating rotarod test. Additional motor related tests, namely marble burying, clasping, grip strength, pole test, and open field test, revealed severe motor impairments of homozygous mice already at an age of 3 months of which some progressed further until the age of 5 months. Most of these tests picked up not only motor disabilities but also deficits in the intuitive or generic behavior and the basal ganglia of the mice [26]. All proved to be suitable for a robust measurement of the phenotype of homozygous TBA2.1 mice and thus as a useful and meaningful read out in preclinical drug testing. In particular, those tests, which were able to measure phenotype progression, i.e., SHIRPA test, marble burying, clasping, pole test, and open field test, are considered useful for a potential longitudinal monitoring of a treatment success in the homozygous mouse model, as they can be applied repeatedly with little bias by learning or habituation processes. Actually, successful monitoring of a preclinical therapeutic study with this mouse model has already been demonstrated using the SHIRPA and rotarod tests [19, 20]. The number

Table 2
Neuronal loss and gliosis in homozygous TBA2.1 mice. Staining of activated astrocytes (GFAP), activated microglia (CD11b), and neuronal nuclei (NeuN) in 3 and 5 months old homozygous TBA2.1 mice (HOM) compared to 5 months old wild type littermates (WT). Quantification was performed in different brain areas (NeuN and GFAP: motor cortex, striatum, CA1, inferior colliculus, brain stem; CD11b: inferior colliculus, brain stem), resulting in a significant decrease of neurons in the CA1 region and, by trend, a decrease of neurons in the striatum. Analysis of gliosis revealed a significant increase of activated astrocytes and microglia in different brain areas, which are known to be involved in motor function

	Brain area	WT 5 m	HOM 3 m	HOM 5 m	Statistic
NeuN (IR area [%])	Motor cortex	11.3 ± 0.4	13.7 ± 0.8	13.3 ± 0.9	n.s
	Striatum	10.0 ± 1.3	6.7 ± 0.7	4.5 ± 0.4	n.s.
	CA1	47.5 ± 3.1	30.6 ± 1.8	27.3 ± 1.7	WT versus HOM 3 m $p = 0.012$ WT versus HOM 5 m $p = 0.001$ HOM 3 m versus HOM 5 m n.s
	Inferior colliculus	2.8 ± 0.5	2.2 ± 0.5	2.4 ± 0.3	n.s.
	Brain stem	9.4 ± 1.6	7.6 ± 1.6	8.9 ± 0.6	n.s.
GFAP (IR area [%])	Motor cortex	6.6 ± 0.8	9.2 ± 0.7	8.8 ± 0.5	WT versus HOM 3 m $p = 0$ 026 WT versus HOM 5 m $p = 0.046$ HOM 3 m versus HOM 5 m n.s
	Striatum	2.2 ± 0.2	2.0 ± 0.2	2.3 ± 0.3	n.s.
	CA1	7.9 ± 1.6	18.7 ± 2.5	9.0 ± 1.7	WT versus HOM 3 m $p = 0$ 002 WT versus HOM 5 m n.s. HOM 3 m versus HOM 5 m $p = 0$ 004
	Inferior colliculus	10.4 ± 1.9	11.7 ± 1.1	12.4 ± 2.4	n.s.
	Brain stem	19.5 ± 2.6	17.4 ± 1.1	18.4 ± 1.5	n.s.
CD11b (IR area [%])	Inferior colliculus	0.7 ± 0.2	2.0 ± 0.6	3.2 ± 0.9	n.s.
	Brain stem	1.8 ± 0.7	9.7 ± 1.0	11.6 ± 1.7	WT versus HOM 3 m $p < 0.001$ WT versus. HOM 5 m $p = 0.002$ HOM 3 m versus HOM 5 m n.s

Data is presented as mean ± SEM, $^{**}p < 0.01$ and $^{***}p < 0.001$.

of mice used in the here described characterization study was based on our experience with this mouse model in these previous studies [19, 20]. This was also confirmed by statistical power analysis. In detail, the group sizes were sufficient considering an appropriate, biologically relevant effect, with regard to the changes between wild type and homozygous mice. Despite the profound phenotype in homozygous and in some parts also in heterozygous mice assessments using larger groups of mice allow for discrimination of smaller differences in certain brain regions or at younger ages and increase the statistical power. This has to be considered for planning of future treatment studies as a statistically significant effect might not be achieved with such small group sizes, especially if the treatment will not lead to complete reversal of the phenotype. Therefore, the use of larger group sizes is recommended for such preclinical therapeutic studies.

In heterozygous mice a mild, most likely starting phenotype initiating at 21 months was found in the SHIRPA phenotype assessment, which was confirmed by a drop in body weight. However, these phenotypic deficits did not have any impact on the motor abilities as tested in the rotarod test of the mice. Possible explanations are, on the one hand that the phenotype in heterozygous mice is only very slowly progressing, starting with abnormalities in the obviously very sensitive SHIRPA test and progressing further to motor disabilities. On the other hand, the number of analyzed heterozygous TBA2.1 mice was comparably low. One might speculate that by use of more mice per group a significant effect might have been achieved Nevertheless, the late-onset of phenotypic changes in heterozygous in comparison to homozygous mice suggests that the induced deficits are strongly dependent on the gene-dosage of the transgenic Aβ(Q3-42) expression, and thereby $pEA\beta_{3-42}$ level rather than a threshold for initiating neuropathological processes as suggested before [11]. This hypothesis is further underlined by the analysis of the Aβ pathology, in which we were able to find significant changes in the hippocampus of heterozygous mice only at 24 months, an age when the striatum did not show pathology yet.

Furthermore, we analyzed the neuropathological changes in the brains of homozygous TB2.1 mice in more detail. Aβ was found in form of small aggregated particles widely spread over the brain, especially in the striatum, the CA1 region of the hippocampus, brainstem, and midbrain (inferior colliculus) confirming earlier reports [11]. Moreover, we observed Aβ aggregates in the somatomotor area of the cortex and the olfactory tubercle at all analyzed ages in homozygous TBA2.1 mice. As previously described, homozygous TBA2.1 mice showed a dramatic neuronal loss in the CA1 hippocampal region already at 3 months of age. In heterozygous mice, we assessed the number of nuclei in the CA1 region to be significantly reduced at 18 and 24 months of age compared to wild type littermates of the same age. We assume that heterozygous TBA2.1 mice will develop a similar pathology compared to homozygous TBA2.1 mice, but at a very old age when there are limitations to use them for possible therapeutic studies.

To further characterize the distribution of activated astrocytes and microglia in homozygous TBA2.1 mice in more detail, we quantified the GFAP and CD11b positive area in different brain regions. There was a significant increase of CD11b positive cells in the brain stem, indicating massive inflammatory processes in a region, which is known to be involved in motor functions. There was only a negligible amount of astrocytes in the striatum without a significant alteration of GFAP positive cells in homozygous TBA2.1 mice at all analyzed ages in comparison to their wild type littermates. In contrast, the amount of GFAP positive cells in the CA1 hippocampal region was significantly higher in 3, but not in 5 months old homozygous TBA2.1 mice. Although the number of analyzed mice was relatively small, the investigated effect here is in accordance with the results published by Alexandru et al. [11]. Since massive neuronal loss was observed at 3 and 5 months of age in this hippocampal area, these finding suggests a dysfunctional chemical transmission between neurons and astrocytes or in neuronal-glial synapses at the age of 5 months [27], because within this age significantly less astrocytes were detectable in the CA1 hippocampal region compared to 3 months old homozygous TBA2.1 mice.

Depositions of Aβ aggregates in various brain areas, neuronal loss in the hippocampus and striatum in combination with severe motor deficits suggest that the basal ganglia might be affected in homozygous TBA2.1 mice. Aβ deposits and neuronal loss are found in nearly all structures of the basal ganglia organization. The connectivity of basal ganglia processes motor information about complex control loops, whereby the motor stimuli of the cortex are processed by the striatum, substantia nigra, globus pallidus, and thalamus whence the result is sent back to the cortex to give a motor output [28, 29].

Future work by us or others should pay attention on an in-depth analysis of the possibly dysfunctional basal ganglia network, since some of the accomplished motor behavioral tests reflect impairments of the basal ganglia network, which might be a further explanation for the severe motor impairments.

In contrast to the widely used APP or APP/PS expressing mouse models, for which only subtle neurodegeneration could be shown, homozygous TBA2.1 mice exhibit massive neuronal loss at very early age. A few mouse models are described in the literature expressing N-terminally truncated forms of Aβ, especially pEAβ_{3-42} and Aβ_{4-42}. Those models are characterized by neuronal loss, in particular detectable in the CA1 hippocampal region [30–34]. Moreover, they display either cognitive deficits alone or in combination with motor deficits. However, most of them develop neuronal loss or onset of the phenotype not before the age of 8 months. In contrast, the onset of the phenotype in homozygous TBA2.1 is observable already at 2 months of age and progresses rapidly [11, 20]. Due to the neuronal loss within the CA1 hippocampal region, which is a brain region involved in learning, one might expect that TBA2.1 mice will also display cognitive deficits. However, we have not addressed cognition within this study as the aim was to further characterize solely the motor phenotype. Whether there is indeed cognitive impairment has to be elucidated in future experiments. In any case, most of the behavioral tests for measuring cognitive deficits require motor skills, intact sensory function and reflexes [35, 36]. In these tests, mice are requested to explore areas (e.g., object recognition test or mazes) or react to external stimuli (e.g., passive avoidance task, fear conditioning memory test). To the best of our knowledge, dependence on intact motor and sensory function cannot be ruled out completely. Therefore, when testing homozygous TBA2.1 mice with compromised motor and reflex functions a learning effect might not be clearly detected since the neurological disorder will always bias the output. Due to this reason, tests for the evaluation of potential cognitive deficits in transgenic TBA2.1 should be selected and performed very carefully.

In summary, the findings of this study demonstrate a first evidence that the neurodegeneration in TBA2.1 mice is strongly dependent on the level of human pEAβ_{3-42} as there is a clear gene-dosage dependence of all pathological manifestations and neurodegenerative phenotypes. The behavioral set ups validated here provide a robust read out, which is able to pick up progression of the degenerative phenotype of homozygous TBA2.1 mice. A model exhibiting a clearly progressive phenotype based on neuronal loss is of advantage for preclinical treatment studies, validating therapeutic substances targeting toxic Aβ species. Even though the homozygous TBA2.1 mice exhibit rapid progression of their phenotype, they have already successfully been used for treatment studies [19, 20]. Moreover, the results of the behavioral and pathological examinations propose the TBA2.1 mouse model as an additional suitable mouse model for longitudinal studies with substances targeting Aβ, whose therapeutic efficacy was shown in an AD mouse model with cognitive deficits previously.

ACKNOWLEDGMENTS

The first breeding pairs of TBA2.1 mice were a generous gift by Probiodrug. Financial support of D.W. was provided by "Portfolio Technology and Medicine", the Helmholtz-Validierungsfonds of the Impuls and Vernetzungs-Fonds der Helmholtzgemeinschaft. D.W. and K.-J.L. were supported by the "Portfolio Drug Research" of the Impuls and Vernetzungs-Fonds der Helmholtzgemeinschaft.

Authors' disclosures available online (https://www.j-alz.com/manuscript-disclosures/17-0775r3).

REFERENCES

[1] Bloom GS (2014) Amyloid-beta and tau: The trigger and bullet in Alzheimer disease pathogenesis. *JAMA Neurol* **71**, 505-508.

[2] Parihar MS, Hemnani T (2004) Alzheimer's disease pathogenesis and therapeutic interventions. *J Clin Neurosci* **11**, 456-467.

[3] Haass C, Selkoe DJ (2007) Soluble protein oligomers in neurodegeneration: Lessons from the Alzheimer's amyloid beta-peptide. *Nat Rev Mol Cell Biol* **8**, 101-112.

[4] Zhang YW, Thompson R, Zhang H, Xu H (2011) APP processing in Alzheimer's disease. *Mol Brain* **4**, 3.

[5] Klyubin I, Cullen WK, Hu NW, Rowan MJ (2012) Alzheimer's disease Abeta assemblies mediating rapid disruption of synaptic plasticity and memory. *Mol Brain* **5**, 25.

[6] Kuo YM, Emmerling MR, Woods AS, Cotter RJ, Roher AE (1997) Isolation, chemical characterization, and quantitation of A beta 3-pyroglutamyl peptide from neuritic plaques and vascular amyloid deposits. *Biochem Biophys Res Commun* **237**, 188-191.

[7] Perez-Garmendia R, Gevorkian G (2013) Pyroglutamate-modified amyloid beta peptides: Emerging targets for Alzheimer's disease immunotherapy. *Curr Neuropharmacol* **11**, 491-498.

[8] Gunn AP, Masters CL, Cherny RA (2010) Pyroglutamate-Abeta: Role in the natural history of Alzheimer's disease. *Int J Biochem Cell Biol* **42**, 1915-1918.

[9] Jawhar S, Wirths O, Bayer TA (2011) Pyroglutamate amyloid-beta (Abeta): A hatchet man in Alzheimer disease. *J Biol Chem* **286**, 38825-38832.

[10] AlzheimerResearchForum (2017) Therapeutics, Immunotherapy (passive), N3pG-Aβ Monoclonal Antibody, LY3002813. *http://www.alzforum.org/therapeutics/ly3002813, Accessed on Octobe* **18**, 2017.

[11] Alexandru A, Jagla W, Graubner S, Becker A, Bauscher C, Kohlmann S, Sedlmeier R, Raber KA, Cynis H, Ronicke R, Reymann KG, Petrasch-Parwez E, Hartlage-Rubsamen M, Waniek A, Rossner S, Schilling S, Osmand AP, Demuth HU, von Horsten S (2011) Selective hippocampal neurodegeneration in transgenic mice expressing small amounts of truncated Abeta is induced by pyroglutamate-Abeta formation. *J Neurosci* **31**, 12790-12801.

[12] Wirths O, Bayer TA (2008) Motor impairment in Alzheimer's disease and transgenic Alzheimer's disease mouse models. *Genes Brain Behav* **7**(Suppl 1), 1-5.

[13] van Halteren-van Tilborg IA, Scherder EJ, Hulstijn W (2007) Motor-skill learning in Alzheimer's disease: A review with an eye to the clinical practice. *Neuropsychol Rev* **17**, 203-212.

[14] Buchman AS, Bennett DA (2011) Loss of motor function in preclinical Alzheimer's disease. *Expert Rev Neurother* **11**, 665-676.

[15] Rogers DC, Fisher EMC, Brown SDM, Peters J, Hunter AJ, Martin JE (1997) Behavioral and functional analysis of mouse phenotype: SHIRPA, a proposed protocol for comprehensive phenotype assessment. *Mamm Genome* **8**, 711-713.

[16] Ogawa N, Hirose Y, Ohara S, Ono T, Watanabe Y (1985) A simple quantitative bradykinesia test in MPTP-treated mice. *Res Commun Chem Pathol Pharmacol* **50**, 435-441.

[17] Meredith GE, Kang UJ (2006) Behavioral models of Parkinson's disease in rodents: A new look at an old problem. *Mov Disord* **21**, 1595-1606.

[18] Deacon RM (2006) Digging and marble burying in mice: Simple methods for in vivo identification of biological impacts. *Nat Protoc* **1**, 122-124.

[19] Brener O, Dunkelmann T, Gremer L, van Groen T, Mirecka EA, Kadish I, Willuweit A, Kutzsche J, Jurgens D, Rudolph S, Tusche M, Bongen P, Pietruszka J, Oesterhelt F, Langen KJ, Demuth HU, Janssen A, Hoyer W, Funke SA, Nagel-Steger L, Willbold D (2015) QIAD assay for quantitating a compound's efficacy in elimination of toxic Abeta oligomers. *Sci Rep* **5**, 13222.

[20] Dunkelmann T, Teichmann K, Ziehm T, Schemmert S, Frenzel D, Tusche M, Dammers C, Jurgens D, Langen KJ, Demuth HU, Shah NJ, Kutzsche J, Willuweit A, Willbold D (2018) Abeta oligomer eliminating compounds interfere successfully with pEAbeta(3-42) induced motor neurodegenerative phenotype in transgenic mice. *Neuropeptides* **67**, 27-35.

[21] Clark RA, Shoaib M, Hewitt KN, Stanford SC, Bate ST (2012) A comparison of InVivoStat with other statistical software packages for analysis of data generated from animal experiments. *J Psychopharmacol* **26**, 1136-1142.

[22] Grathwohl SA, Kalin RE, Bolmont T, Prokop S, Winkelmann G, Kaeser SA, Odenthal J, Radde R, Eldh T, Gandy S, Aguzzi A, Staufenbiel M, Mathews PM, Wolburg H, Heppner FL, Jucker M (2009) Formation and maintenance of Alzheimer's disease beta-amyloid plaques in the absence of microglia. *Nat Neurosci* **12**, 1361-1363.

[23] Hall AM, Roberson ED (2012) Mouse models of Alzheimer's disease. *Brain Res Bull* **88**, 3-12.

[24] LaFerla FM, Green KN (2012) Animal models of Alzheimer disease. *Cold Spring Harb Perspect Med* **2**, a006320.

[25] Bayer TA, Wirths O (2014) Focusing the amyloid cascade hypothesis on N-truncated Abeta peptides as drug targets against Alzheimer's disease. *Acta Neuropathol* **127**, 787-801.

[26] Glajch KE, Fleming SM, Surmeier DJ, Osten P (2012) Sensorimotor assessment of the unilateral 6-hydroxydopamine mouse model of Parkinson's disease. *Behav Brain Res* **230**, 309-316.

[27] Rodriguez JJ, Olabarria M, Chvatal A, Verkhratsky A (2009) Astroglia in dementia and Alzheimer's disease. *Cell Death Differ* **16**, 378-385.

[28] Grillner S, Robertson B, Stephenson-Jones M (2013) The evolutionary origin of the vertebrate basal ganglia and its role in action selection. *J Physiol* **591**, 5425-5431.

[29] Pappas SS, Leventhal DK, Albin RL, Dauer WT (2014) Mouse models of neurodevelopmental disease of the basal ganglia and associated circuits. *Curr Top Dev Biol* **109**, 97-169.

[30] Meissner JN, Bouter Y, Bayer TA (2015) Neuron loss and behavioral deficits in the TBA42 mouse model expressing n-truncated pyroglutamate amyloid-beta3-42. *J Alzheimers Dis* **45**, 471-482.

[31] Bouter Y, Dietrich K, Wittnam JL, Rezaei-Ghaleh N, Pillot T, Papot-Couturier S, Lefebvre T, Sprenger F, Wirths O, Zweckstetter M, Bayer TA (2013) N-truncated amyloid beta (Abeta) 4-42 forms stable aggregates and induces acute and long-lasting behavioral deficits. *Acta Neuropathol* **126**, 189-205.

[32] Wirths O, Breyhan H, Cynis H, Schilling S, Demuth HU, Bayer TA (2009) Intraneuronal pyroglutamate-Abeta 3-42 triggers neurodegeneration and lethal neurological deficits in a transgenic mouse model. *Acta Neuropathol* **118**, 487-496.

[33] Casas C, Sergeant N, Itier JM, Blanchard V, Wirths O, van der Kolk N, Vingtdeux V, van de Steeg E, Ret G, Canton T, Drobecq H, Clark A, Bonici B, Delacourte A, Benavides J, Schmitz C, Tremp G, Bayer TA, Benoit P, Pradier L (2004) Massive CA1/2 neuronal loss with intraneuronal and N-terminal truncated Abeta42 accumulation in a novel Alzheimer transgenic model. *Am J Pathol* **165**, 1289-1300.

[34] Wirths O, Bayer TA (2010) Neuron loss in transgenic mouse models of Alzheimer's disease. *Int J Alzheimers Dis* **2010**, 723782.

[35] Deacon RM (2013) Measuring motor coordination in mice. *J Vis Exp*, e2609.

[36] Ameen-Ali KE, Wharton SB, Simpson JE, Heath PR, Sharp P, Berwick J (2017) Review: Neuropathology and behavioural features of transgenic murine models of Alzheimer's disease. *Neuropathol Appl Neurobiol* **43**, 553-570.

3.7 Aβ oligomer elimination restores cognition in transgenic Alzheimer's mice with full-blown pathology

Autoren:	**Schemmert S.**, Schartmann E., Zafiu C., Kass B., Hartwig S., Lehr S., Bannach O., Langen K-J., Shah N.J., Kutzsche J., Willbold D., Willuweit A.
Journal:	EMBO Reports, eingereicht am 23.03.2018
Impact Factor:	8,568 (2016)
Beitrag:	Planung der Studie
	Durchführung und Analyse aller Verhaltensversuche (Nestbauverhalten, Murmeltest, Offenfeldtest, Morris water maze)
	Behandlung der Mäuse
	Durchführung der immunhistologischen Experimente
	Quantifizierung der immunhistologischen Ergebnisse
	Durchführung und Auswertung biochemischer Analysen
	Anfertigung aller Abbildungen
	Analyse aller Daten
	statistische Auswertung.
	Hauptverfassung und Prüfung des Manuskriptes

Title Page

Aβ oligomer elimination restores cognition in transgenic Alzheimer's mice with full-blown pathology

Sarah Schemmert[1], Elena Schartmann[1], Christian Zafiu[1], Bettina Kass[1], Sonja Hartwig[2,3], Stefan Lehr[2,3], Oliver Bannach[1], Karl-Josef Langen[4,5], Nadim Joni Shah[4,6], Janine Kutzsche[1], Antje Willuweit[4*], Dieter Willbold[1,7*]

Affiliations

[1]*Institute of Complex Systems, Structural Biochemistry (ICS-6), Forschungszentrum Jülich, Jülich, Germany*

[2]*Institute of Clinical Biochemistry and Pathobiochemistry, German Diabetes Center at the Heinrich Heine University Düsseldorf, Leibniz Centre for Diabetes Research, Düsseldorf, Germany*

[3]*German Center for Diabetes Research (DZD), Partner Düsseldorf, Germany*

[4]*Institute of Neuroscience and Medicine, Medical Imaging Physics (INM-4), Forschungszentrum Jülich, Jülich, Germany*

[5]*Clinic for Nuclear Medicine, RWTH Aachen University, Aachen, Germany*

[6]*Department of Neurology, Faculty of Medicine, JARA, RWTH Aachen University, Aachen, Germany*

[7]*Institut für Physikalische Biologie, Heinrich-Heine-Universität Düsseldorf, Düsseldorf, Germany*

*Correspondence to:

Dieter Willbold

Forschungszentrum Jülich, Institute of Complex Systems, Structural Biochemistry (ICS-6)
52425 Jülich
Germany
E-mail: d.willbold@fz-juelich.de
Phone: +49-2461-612100
Fax: +49-2461-612023

Antje Willuweit

Forschungszentrum Jülich, Institute of Neuroscience and Medicine (INM-4)
52425 Jülich
Germany
E-mail: a.willuweit@fz-juelich.de
Phone: +49-2461-6196358
Fax: +49-2461-612302

Running title: Aβ oligomer elimination restores cognition

Abstract

Oligomers of the amyloid β protein (Aβ) are suspected to be responsible for the development and progression of Alzheimer's disease. Thus, development of compounds that are able to eliminate already formed, toxic Aβ oligomers is very desirable. Here, we describe the *in vivo* efficacy of the compound RD2, which was developed to directly and specifically eliminate toxic Aβ oligomers. In a truly therapeutic, rather than preventive study, oral treatment with RD2 was able to reverse the cognitive deficits and to significantly reduce Aβ pathology in old-aged transgenic AD mice with full-blown pathology and behavioral deficits. For the first time, we demonstrate *in vivo* target engagement of RD2, in particular by showing a significant reduction of Aβ oligomers in the brains of RD2-treated compared to placebo-treated mice. The correlation of Aβ elimination *in vivo* and the reversal of cognitive deficits in old-aged transgenic mice are in support of Aβ oligomers being relevant not only for disease development and progression, but also for Aβ oligomers as a promising target for the causal treatment of Alzheimer's disease.

Keywords

Alzheimer's disease therapy, amyloid β oligomer elimination, transgenic mice, D-enantiomeric peptides, target engagement;

Introduction

The most common form of dementia worldwide is Alzheimer's disease (AD), a progressive and incurable neurodegenerative disease (Ferreira & Klein, 2011; Haass & Selkoe, 2007; Selkoe & Hardy, 2016). Presently available treatments with acetylcholinesterase inhibitors and an NMDA receptor antagonist are only able to treat some symptoms and hold the risk of unpleasant side effects (Jakob-Roetne & Jacobsen, 2009). Thus, there is an urgent need for the development of new therapeutic strategies for the causal treatment of AD (Karran et al, 2011).

The pathological hallmarks of AD are neurofibrillary tangles, consisting of hyperphosphorylated tau protein, progressive neurodegeneration and the accumulation of toxic amyloid β (Aβ) species (Karran et al, 2011; Selkoe & Hardy, 2016). The central dogma for the development of AD is the so called amyloid cascade hypothesis (Hardy, 1992; Hardy & Selkoe, 2002). It states that an imbalance between the production and clearance of Aβ in the brain of affected people is responsible for neurodegeneration and finally dementia. Monomeric Aβ, a cleavage product of the proteolytic processing of the amyloid protein precursor (APP) by a β- and a γ-secretase, aggregates into Aβ oligomers and finally into amyloid fibrils, which are found in AD plaques and were supposed to be the cause of cognitive deficits (Blennow et al, 2006). Nowadays, more and more evidence exists that instead of Aβ monomers or fibrils, small and diffusible Aβ oligomers may be the main cause for the development and progression of cognitive decline in AD (Ferreira et al, 2015; Selkoe & Hardy, 2016). Therefore, their elimination is highly desirable for therapy development and some attempts have been made in the past (Kumar et al, 2015; Rosenblum, 2014). So far, no treatment strategy based on prevention of Aβ oligomer formation with small molecule inhibitors against β- and γ-secretases has successfully completed clinical phase III. Many developments have been discontinued because of missing therapeutic benefit and side effects. In addition, therapeutic antibodies directed against monomeric or fibrillary Aβ, or both, showed so far no therapeutic efficiency in clinical phase III trials either, but suffer very often from dangerous side effects called amyloid-related imaging abnormalities (ARIA), which seems to be a consequence of an antibody-related activation of the immune system. Recent passive immunization approaches try to target Aβ oligomers more specifically by using stabilized oligomers of various size or conformation as antigens. Still, their efficacy needs to be demonstrated in clinical trials (Liu et al, 2016).

We propose a treatment strategy directed towards the specific and direct elimination of toxic Aβ oligomers, irrespective of their size and conformation, via their direct disruption without the need to rely on the immune system for their destruction. This is achieved by binding of our drug candidate to monomeric Aβ, stabilizing it in an aggregation-incompetent state, and thereby shifting the chemical equilibrium away from toxic Aβ oligomers (Cavini et al, 2018). Using this approach not only prevention of oligomer formation but also disruption of already formed Aβ oligomers is possible. Successful proof of this mode of action has been achieved for the orally available compound D3 and its derivatives *in vitro* by demonstrating removal of preformed, toxic Aβ oligomers (Brener et al, 2015). D3 has been identified by mirror image phage display and is a peptide that consists solely of D-enantiomeric amino acid residues. *In vivo* D3 has been shown to improve pathology and cognition after administration via different routes including oral application (Brener et al, 2015; Funke et al, 2010; van Groen et al, 2013;

van Groen et al, 2009; van Groen, 2012; van Groen et al, 2008). Additionally, pharmacokinetic studies have demonstrated the proteolytic stability and bioavailability of D3 (Elfgen et al, 2017; Jiang et al, 2015). The compound investigated in this study, RD2, is a derivative of D3 with a rationally repositioned amino acid sequence to enhance the Aβ oligomer elimination efficiency. Previously, we were able to demonstrate that RD2 has a higher efficacy to eliminate toxic Aβ oligomers *in vitro* by use of the Aβ-QIAD (quantitative determination of interference with Aβ aggregate size distribution) assay (Brener et al, 2015; van Groen et al, 2017). This assay is based on the fractionation of $Aβ_{(1-42)}$-assemblies (Aβ monomers, oligomers, protofibrills, larger aggregates) according to their sizes (after a predefined incubation time) by density gradient ultracentrifugation (DGC). Using this assay, it is possible to quantitatively determine the potency of a compound to reduce preformed toxic Aβ oligomers *in vitro*. According to Brener et al., the toxicity of oligomeric Aβ species is reduced after co-incubation with Aβ oligomer eliminating compounds (Brener et al, 2015). Besides oligomer removal several tests illustrate the *in vitro* efficacy of RD2 to reduce $Aβ_{(1-42)}$ fibril formation, the catalytic effect of preformed seeds on $Aβ_{(1-42)}$ aggregation and to reduce the $Aβ_{(1-42)}$ mediated cell toxicity (van Groen et al, 2017). Already in two preclinical proof of concept studies, RD2 demonstrated its efficacy by improving cognition in two different transgenic AD mouse models (Kutzsche et al, 2017; van Groen et al, 2017).

In the present study, we set out to support the suggested mode of action by demonstrating *in vivo* target engagement, which would be the reduction of the Aβ oligomer concentrations in brains of RD2-treated mice as compared to placebo-treated mice. This, however, requires an appropriate detection and quantitation method for Aβ oligomers. One of the major challenges of those attempts is to clearly distinguish between monomeric and oligomeric/aggregated Aβ species. To adequately meet this need, some attempts have been made, mostly based on ELISA techniques (Savage et al, 2014; Wang et al, 2017). One of the techniques that have been developed to quantify Aβ oligomers, is the sFIDA (surface-based fluorescence intensity distribution analysis) assay. The sFIDA assay uses a sandwich-ELISA biochemical setup using anti-Aβ-antibodies to capture all Aβ species to a glass surface, and fluorescence-labelled anti-Aβ-antibodies as probes that recognize the same, or overlapping Aβ-epitopes as the capture does, in order to avoid any contribution of Aβ monomers to the measurement. In contrast to conventional ELISAs, however, the readout is obtained by taking fluorescence micrographs from the glass surface by total internal reflection (TIRF) microscopy, which then yields single particle sensitivity. The absolute Aβ oligomer concentrations are then calculated on the basis of a suitable calibration standard (Herrmann et al, 2017a; Herrmann et al, 2017b; Hulsemann et al, 2016; Kravchenko et al, 2017; Kuhbach et al, 2016; Wang-Dietrich et al, 2013).

Besides demonstration of *in vivo* target engagement, the aim of the current study was to proof the proposed mode of action, i.e. the elimination of already formed Aβ oligomers, *in vivo* in a real therapeutic, rather than preventive setting. Therefore, we challenged the efficacy of the drug candidate RD2 by using it for the oral treatment of old-aged APP/PS1 transgenic AD mice that have developed full-blown pathology and severe cognition impairments and behavior deficits before treatment start.

Material and Methods

Ethical approval

All animal experiments were performed in accordance with the German Law on the protection of animals (TierSchG §§ 7–9) and were approved by a local ethics committee (LANUV, North-Rhine-Westphalia, Germany, reference number: 84-02.04.2011.A359).

Animals

In the present study, the double transgenic APPswe/PS1ΔE9 (APP/PS1) AD mouse model was used. The model was introduced by Jankowsky et al. in 2004 (Jankowsky et al, 2004) and its pathology and behavioral deficits are well characterized. At 6 months of age, the mice develop Aβ deposits, gliosis and cognitive deficits, especially detectable in the Morris water maze (MWM). The pathology and cognitive deficits progressively intensify with age (Garcia-Alloza et al, 2006; Jankowsky et al, 2004; Janus et al, 2015; Kamphuis et al, 2012). APP/PS1 mice were ordered by the Jackson Laboratory (Jackson Laboratory, USA) and bred in-house in a controlled environment on a light/dark cycle (12/12 h), with 54% humidity and a temperature of 22 °C. Food and water were available *ad libitum*.

Aged male APP/PS1 mice (n = 21) and their non-transgenic littermates (n = 11) were tested in the present study (average age at treatment initiation: 18 months +/- 3 weeks). During the study all mice were housed single caged.

Peptide

RD2 was purchased from CBL Patras (CBL Patras, Greece) and its amino acid residue sequence is as follows: H-ptlhthnrrrrr-NH_2.

Treatment

Mice were treated orally, every day, for 12 weeks with either RD2 (n = 11) or placebo (drinking water) (n = 10) both formulated in tailor-made jellies composed of gelatin (30% sucrose, 10% sucralose, 18.75% instant gelatin) (Dr. Oetker, Bielefeld, Germany). The mice ate each single jelly completely and voluntarily. Every week, the RD2 amount in the jellies was adjusted to the average body weights of the mice to achieve a daily dose as close as possible to 200 mg/kg. During the last weeks of treatment, for example, each jelly for the RD2 treatment group contained 6.7 mg RD2.

Behavioral assessments

In all experiments conducted the behavioral performance of RD2- and placebo-treated mice was compared to those of non-transgenic littermates, which were left untreated and assured for the quality of the behavioral assessments.

Nesting behavior and marble burying. To assess species-typical behavior, nesting behavior and marble burying were performed. Both protocols were adopted from Deacon (Deacon, 2006a; Deacon, 2006b). In short, for nesting behavior mice were placed in a new cage with a fresh nestlet (Sniff, Germany) 1 h before the dark phase of the animal house. The next morning, the built nests were

161 scored according to Deacon's scores from 0 to 5, whereby 0 represents no nest and 5 represents a
162 perfect nest (Deacon, 2006a). For marble burying, mice were placed in a new cage with 5 cm deep
163 wood chip bedding on which 12 glass marbles (diameter: 1.6 cm, weight: 5.3 g) were laid down in a
164 predefined order. After 30 min, the number of marbles buried was counted.

165 *Open field test*. The open field test is an experimental arrangement for the quantitative representation
166 of the explorative and anxiety behavior of animals (Archer, 1973). After 30 min of habituation to the
167 experiment's room, mice were placed in a square-shaped arena (45 cm x 45 cm x 45 cm). The arena
168 was imaginarily divided into two zones: center and border zone (center: 19 cm x 19 cm, border: space
169 around the center zone). Mice were allowed to observe the arena for 30 min. They were recorded with
170 a camera driven tracking system, Ethovision 11 (Noldus, Wageningen, The Netherlands). For
171 analysis, the first 25 min of the record were subdivided into five time slots (1: 0-5 min, 2: 5-10 min, 3:
172 10-15 min, 4: 15-20 min, 5: 20-25 min). The duration of stay in the center and the border zone was
173 evaluated concerning explorative and anxiety behavior in total and separately for each time slot.

174 *Morris water maze*. The Morris water maze (MWM) is a spatial learning test to investigate cognitive
175 impairments. The apparatus used consists of a circular white pool (120 cm in diameter and 60 cm in
176 height), filled with water (24 ± 1°C) to a depth of 30 cm. The water is rendered opaque by addition of a
177 non-toxic white pigment. The pool is imaginarily subdivided into four quadrants: north-east (NE, target
178 quadrant with an invisible round platform 1 cm below the surface), south-east (SE), south-west (SW)
179 and north-west (NW). The protocol was modified after Morris et al., 1982 (Morris et al, 1982). During
180 the training, the mice swam four 60 s trials daily starting from different quadrants on five consecutive
181 days. If they did not find the hidden but fixed platform within the 60 s of a trial, they were set on the
182 platform for 10 s to orient themselves before they were returned to their cages. Between each trial, the
183 mice had a recovery period of 60 s under a heating lamp to avoid a decrease in body temperature. On
184 the sixth day, the probe trial was performed in which the mice had to swim in the pool for 60 s without
185 a platform. During the trials, the mice were tracked with Ethovision 11 (Noldus, Wageningen, The
186 Netherlands). The following parameters were analyzed for the training days: escape latency to
187 platform (s), covered distance (cm), swimming speed (cm/s), and the duration in the platform quadrant
188 (s). The duration in the platform quadrant was analyzed for the probe trial, too.

189 Plasma and tissue collection

190 Mice were anesthetized with 100 mg/kg ketamine (bela-pharm, Vechta, Germany) and 0.3 mg/kg
191 medetomidine (Dormilan, alfavet, Neumünster, Germany) intraperitoneally before the final collection of
192 blood samples by terminal cardiac puncture. Brains were removed, divided into the two hemispheres
193 and snap frozen in -80 °C isopentane. The left hemispheres were used for immunohistochemistry
194 (IHC); the right hemispheres were used for biochemical analysis.

195 Immunohistochemistry and biochemical analysis

196 *Immunohistochemistry*. IHC was performed on 20 µm sagittal frozen brain sections. In brief, room
197 tempered sections were fixed in 4% paraformaldehyde (10 min, room temperature). For antigen
198 retrieval, sections were incubated in 70% formic acid (5 min, room temperature). Elimination of

endogenous peroxidases was performed with 3% H_2O_2 in methanol (15 min, room temperature). In between, the sections were washed 3 times for 5 min in 1% Triton in TBS (TBST). Sections were incubated with the primary antibody over night at 4 °C in a humid chamber (6E10: 1:2500, Bio Legend, San Diego, USA; GFAP: 1:1000, DAKO, Agilent Technologies, Santa Clara, USA; CD11b: 1:2500, Abcam, Cambridge, United Kingdom) in TBST with 1% bovine serum albumin (BSA), followed by incubation with a biotinylated secondary anti-mouse or anti-rabbit antibody (both 1:1000 in TBST + 1% BSA, Sigma-Aldrich, Darmstadt, Germany). Staining was visualized with the use of 3,3'-Diaminobenzidine (DAB) enhanced with saturated nickel ammonium sulphate solution. Sections were mounted with DPX Mountant (Sigma-Aldrich, Darmstadt, Germany) after washing in an ascending alcohol series.

To avoid differences in staining intensity and light exposure which might affect measurements, all slides were stained in one batch and acquired in one microscopy session. Sections were visualized with the use of a Zeiss SteREO Lumar V12 microscope and the according software (Zeiss AxioVision 6.4 RE) or a Leica LMD6000 microscope and the according software (LAS 4.0 software). Quantification was performed with ImageJ (National Institute of Health, Bethesda, USA). The plaque count of RD2- (n = 11) and placebo-treated (n = 8) mice was analyzed in cerebrum (8-10 slides/mouse), cortex (5-6 slides/mouse) and hippocampus (8-10 slides/mouse). Astrogliosis of RD2- (n = 8) and placebo-treated (n = 7) mice was analyzed in cortex (6 slides/mouse with 6 equally distributed pictures per slide) and hippocampus (6 slides/mouse). The activated microglia of RD2- (n = 9) and placebo-treated (n = 9) mice were analyzed in cortex (7 slides/mouse) and hippocampus (7 slides/mouse).

Aβ ELISA. For generation of three fractions (Tris-, diethanolamine (DEA)-, and formic acid (FA) fraction) the right hemispheres of RD2- (n = 10) and placebo-treated (n = 8) mice were used. To obtain the Tris-fraction, hemispheres were homogenized 2 x 20 s at 6500 rpm (Precellys® 24, Bertin Instruments, Montigny-le-Bretonneux, France) with Tris buffer (pH 8.3, 20 mM Tris, 250 mM NaCl, protease and phosphatase inhibitors (both Roche, Basel, Switzerland)). Afterwards, the homogenized samples were sonicated (5 min) and centrifuged (30 min, 175.000 x g, 4 °C). Supernatant was taken as the Tris-soluble fraction. DEA-fractions were gained after dissolving the pellet in 2% DEA, incubation (1 h on ice), and centrifugation (30 min, 175.000 x g, 4 °C). Supernatant was taken as the DEA fraction. The pellet was dissolved in 70% FA, incubated (1 h on ice), and centrifuged (30 min, 175.000 x g, 4 °C). Supernatant was taken as the FA-fraction. All fractions were snap frozen in liquid nitrogen and stored at -80 °C until further analysis.

Aβ x–40 and Aβ x–42 ELISAs were purchased from BioLegend (BioLegend, San Diego, United States) and performed according to the manufacturer's protocol with the three brain homogenate fractions described above. All samples were measured as duplicates.

Surface-based fluorescence intensity distribution analysis (sFIDA) assay

sFIDA assays were performed in 384 flat-bottom square well microplates (Sensoplate Plus, Greiner Bio-One GmbH, Frickenhausen, Germany) with a glass bottom of 170 µm thickness. The glass bottom

of the microplate was silanized with APTES (99 %; (3-Aminopropyltriethoxysilane; Sigma-Aldrich, Germany) by vapor deposition. For this procedure, a microplate was placed in a desiccator above a solution of 5% APTES in Toluene (99% Sigma-Aldrich, Germany) in an Argon atmosphere for 1 h before removing the APTES solution and drying for 2 h in a vacuum. To the wells, 2 mM succinimidyl carbonate-poly-(ethylene glycol)–carboxymethyl (MW 3400, Laysan Bio, Arab, USA) in dd H_2O was added, incubated for 4 h, and washed three times after incubation. This procedure covalently links PEG to APTES and presents carboxylic acids to the surface, which are activated by 200 mM N-(3-dimethylaminopropyl)-N′-ethylcarbodiimide hydrochloride (98%; Sigma-Aldrich, Germany), and 50 mM N-hydroxysuccinimide (98%; Sigma-Aldrich, Germany), and incubated for 30 min. After washing three times with dd H_2O, 10 µg/ml of Nab228 monoclonal antibody (Sigma-Aldrich, St. Louis, USA) in PBS was added to the wells and incubated for 1 h. After washing for three times with TBS + 0.1%Tween20 (TBST) and TBS each of the wells was blocked with Smartblock solution (Candor Bioscience, Germany) over night. The next day, samples and standards were added to the plate an incubated for 1 h. All samples were diluted tenfold in TBS. $A\beta_{(1-42)}$-SiNaPs (silica nanoparticles) with a diameter of 20 nm and approx. 30 epitopes ($A\beta_{(1-42)}$), synthesized and analyzed by methods described previously (Hulsemann et al, 2016), served as a calibration standard for Aβ oligomers. After washing the excessive sample away with TBS three times, 1.25 µg/ml mAb IC16 (epitope $A\beta_{1-8}$) (Hellmert et al, 2015), labelled with CF-633 dye, (Sigma-Aldrich, Germany) and 1.25 µg/ml Nab228 (epitope $A\beta_{1-11}$) labelled with CF-488 dye (both: Sigma-Aldrich, Germany), that were ultracentrifuged (100.000 g, 1 h, 4 °C) before adding to the wells, were incubated for 1 h. After incubation, the excessive detection antibodies were washed away three times with TBS and the plate was sealed with a plastic foil and transferred to a Leica multi-color TIRF (total internal reflection fluorescence) system (AM TIRF MC, Leica Microsystems, Wetzlar, Germany). The TIRF system operated with an automated stage and a 100 x oil immersion objective (1.47 oil CORR TIRF Leica). Images were recorded consecutively with Ex/Em = 633/705 nm and 488/525 nm with 500 ms exposure time and a gain of 800 for both color channels at a penetration depth of 200 nm. The microscope took 5 x 5 images per well in each channel, which corresponds to ca. 3% of the well surface. Each images consisted of 1000 x 1000 pixels with a lateral resolution of 116 nm (pixel to pixel) and an intensity resolution of 14 bit (grey scale).

Image analysis was performed using sFIDAta, a custom made software. After removing "out of focus" images (ca. 5%) cutoff values were calculated for each channel based on the blank. The software then applied the cutoff values to the sample results and counted pixels that were in both channels and at the same position higher than the cutoff. The number of these co-localized pixels was the sFIDA readout. Using the $A\beta_{(1-42)}$-SiNaP standards, the sFIDA readout was converted to oligomer concentration. All samples were measured in triplicate.

For all sFIDA experiments, with the expectation the one performed with the three fractions also used for ELISA, 150 µl of brain homogenate was centrifuged at 1200 g for 10 min. 100 µl supernatant of each homogenate was loaded on the top of a density gradient consisting of 5 to 50% (w/v) iodixanol (OptiPrep, Axis-Shield, Norway). After centrifugation (3 h, 259.000 x g, at 4 °C) (Optima TL-100, Beckman Coulter, USA), 14 fractions (140 µl each), were removed from top to bottom of the tubes. 10 µl of each fraction was diluted in 90 µl TBS before being applied to the sFIDA microplates.

278 Clinical Chemistry

279 Tests for the quantitative determination of lactate dehydrogenase (LDH), aspartate aminotransferase
280 (AST), alanine aminotransferase (ALT) and alkaline phosphatase (AP) were performed with plasma
281 samples from RD2- or placebo-treated mice, or their non-transgenic littermates using Roche
282 automated clinical chemistry analyzers (cobas 8000 modular analyzer series, Roche, Basel,
283 Switzerland) according to the manufacturer's protocol.

284 Cytokine assay

285 Plasma samples from RD2- or placebo-treated mice, or their non-transgenic littermates were tested
286 for interleukin 1 alpha (IL-1α), interleukin 10 (IL-10), interleukin 12p40 (IL-12p40), interleukin 13 (IL-
287 13), interleukin 17 (IL-17), granulocyte-colony stimulating factor (G-CSF), interferon gamma (IFN-γ),
288 monocyte chemoattractant protein-1 (MCP-1), macrophage inflammatory proteins alpha and beta
289 (MIP-1α and MIP-1β), regulated on activation, normal T-cell expressed and secreted (RANTES), and
290 tumor necrosis factor alpha (TNF-α) (Bio-Plex Pro Mouse Cytokine 23-plex Assay, Bio-Rad, California,
291 USA). The assay was performed following the manufacturer's protocol. Samples that were out of the
292 detection limit were excluded from analysis.

293 Statistical analysis

294 All statistical calculations were performed using GraphPad Prism 5 (GraphPad Software, Inc., La Jolla,
295 USA) or SigmaPlot Version 11 (Systat Software, Germany). All data are represented as mean ± SEM.
296 Gaussian distribution of all data was tested in the D'Agostino & Pearson omnibus normality test.
297 Normally distributed data was analyzed in the one-way analysis of variance (ANOVA) with Tukey post
298 hoc analysis (nesting behavior, probe trial MWM) or unpaired one-tailed t-test (6E10 staining). Data,
299 which were not normally distributed, was tested with Kruskal-Wallis test with Dunn's Multiple
300 Comparison Test (marble burying, open field test, cytokine assay, IHC, clinical chemistry). MWM was
301 analyzed with the use of InVivoStat 2.5 (InVivoStat by Simon Bate and Robin Clarke, United Kingdom)
302 (Clark et al, 2012) with the Repeated Measures (RM) Parametric Analysis and SigmaPlot. The escape
303 latency to the platform was considered as not normally distributed and therefore analyzed by
304 Friedman Repeated Measures ANOVA on Ranks. Distance moved and the percentage duration in the
305 platform quadrant were analyzed by a repeated measures two-way ANOVA. As the fractions
306 generated from each brain homogenate (Tris-, DEA- and FA-fraction, or DGC fractions 1 to 14) were
307 considered to be related, results from ELISA and sFIDA measurements were analyzed with a two-way
308 RM ANOVA. p-values smaller than 0.05 were considered to indicate significant statistical differences
309 in the tests.

Results

RD2 treatment resulted in improved cognition and behavior of treated mice, indistinguishable from non-transgenic mice

In the present study, three groups of mice were tested. Two groups consisted of 18 months old transgenic APP/PS1 mice. In the first group, eleven mice were orally treated with RD2. Oral treatment was carried out by giving daily one jelly containing roughly 200 mg/kg of RD2 (treatment group). In the second group, ten APP/PS1 mice were daily given a jelly without RD2 (placebo group, ten mice). The third group, consisting of eleven non-transgenic littermates, was left untreated (wild-type group) and assured for the quality of the behavioral assessments. At the end of the twelve-week treatment period, different behavioral experiments were conducted to evaluate the treatment effect. Thereafter, different immunohistochemical and biochemical experiments were performed to investigate the treatment effect on Aβ pathology, inflammation, and possible side effects.

To assess the potential consequences of long-term oral treatment with RD2 over twelve weeks on species-typical behavior and to investigate possible adverse side effects caused by the treatment, nesting behavior and marble burying, as basic behavioral tests, were performed with RD2- in comparison to placebo-treated APP/PS1 mice and their non-transgenic littermates (Fig. 1 a, b). Neither nesting behavior nor marble burying revealed any significant differences between the three groups (Fig. 1 a, b; nesting behavior score (mean ± SEM): ntg 3.3 ± 0.5, placebo 2.1 ± 0.3, RD2 2.3 ± 0.5, one-way ANOVA $F_{(2,31)} = 2.21$, n.s. $p = 0.13$; marble burying (mean ± SEM): ntg 6.6 ± 0.5, placebo 8.4 ± 0.8, RD2 7.8 ± 0.6, one-way ANOVA, $F_{(2,31)} = 1.91$, n.s. $p = 0.17$). Afterwards, an open field test was performed to assay general differences in exploratory and anxiety related behavior of treated mice and their non-transgenic littermates. Analysis of the open field test did not reveal significant differences in the analyzed parameters between RD2-treated mice and non-transgenic littermates, but did between RD2- and placebo-treated mice. This indicates that phenotypic impairments of the transgenic mice were reversed by RD2 treatment (Fig. 1 c; two-way ANOVA, $F_{(2,58)} = 0$, Tukey post hoc analysis: ntg vs. placebo n.s. $p = 0.14$, ntg vs. RD2 n.s. $p = 0.75$, placebo vs. RD2. $p = 0.03$). In detail, RD2-treated mice stayed significantly longer in the center zone than placebo-treated mice (Fig. 1 d), while the time spent in border and center zone did not significantly differ between RD2-treated mice and their non-transgenic littermates (Fig. 1 d). This suggests decreased anxiety related behavior of RD2- compared to the placebo-treated mice, again leading to reversal of the behavior of RD2-treated mice to the level of the non-transgenic littermates. Also, there was a difference in the exploratory behavior during the course of the test. RD2-treated mice and non-transgenic littermates explored the center zone significantly longer than placebo-treated mice. Thus, RD2-treated mice and non-transgenic littermates showed the typical habituation effect to the new and so far unexplored arena, while this habituation effect was not present in placebo-treated transgenic mice (Fig. 1 c; two-way RM ANOVA, $F_{(2,116)} = 4.12$, $p = 0.03$, Tukey post hoc analysis time slot 5: ntg vs. placebo $p = 0.01$, ntg vs. RD2 n.s. $p = 0.76$, placebo vs. RD2 $p = 0.001$). The presence of the habituation effect, or its absence, became especially prominent during the second half of the test, suggesting that RD2

348 treatment led to the reversal of the transgenic mouse phenotype towards the phenotype of the non-
349 transgenic littermates.

350 The Morris water maze (MWM) was conducted for the assessment of cognitive impairment, especially
351 for deficits in cognitive abilities, and in spatial learning and memory. During the five days training
352 phase of the MWM, placebo-treated transgenic mice showed impaired performance without an
353 apparent learning effect over time. In contrast, RD2-treated mice showed a significant learning effect
354 over time in the training phase of the MWM, with their performance being indistinguishable from
355 non-transgenic littermates (Fig. 1 e; Friedman repeated measure (RM) ANOVA on Ranks, RD2-
356 treated mice $p < 0.001$, non-transgenic littermates $p = 0.008$, placebo-treated mice n.s. $p = 0.1$).
357 Moreover, RD2-treated mice spent significantly more time in the target quadrant than the placebo-
358 treated mice. Also here, RD2-treated transgenic mice were indistinguishable from non-transgenic
359 littermates (Fig. 1 f; two-way RM ANOVA, $F_{(2,116)} = 4.39$, $p = 0.02$, Tukey post hoc analysis day 5, ntg
360 vs. placebo $p < 0.001$, ntg vs. RD2 n.s. $p = 0.3$, placebo vs. RD2 n.s. $p = 0.006$). Memory retrieval
361 during the probe trial on day six did not reveal significant differences in performance between RD2-
362 treated and placebo-treated mice, but did reveal differences between non-transgenic littermates and
363 placebo-treated mice. The placebo-treated mice spent significantly less time in the quadrant, where
364 the platform was located, than the non-transgenic littermates. This emphasizes the cognitive
365 impairment of the placebo-treated transgenic mice (Fig. 1 g; one-way ANOVA $F_{(2,31)} = 6.77$, $p = 0.004$,
366 Tukey post hoc analysis, non-transgenic littermates vs. placebo $p = 0.003$, non-transgenic littermates
367 vs. RD2 n.s. $p = 0.06$, placebo vs. RD2 n.s. $p = 0.4$).

368 Treatment with RD2 led to significant decrease of Aβ plaque load

369 Staining of brain tissue sections against human Aβ (6E10), activated astrocytes (GFAP), and activated
370 microglia (CD11b) was accomplished to investigate the effects of long-term oral RD2 treatment on Aβ
371 pathology and gliosis of the APP/PS1 transgenic mouse model (Garcia-Alloza et al, 2006; Kamphuis
372 et al, 2012). Fig. 2 a-c shows the results of 6E10, GFAP, and CD11b staining with subsequent
373 quantification of different brain areas (cerebrum, cortex, hippocampus). Overall, the data suggest that
374 RD2 treatment led to reduction of Aβ plaque load (Fig. 2 a). This became significant only for the Aβ
375 plaque load in the cortex (unpaired one-tailed Student's t-test, $p = 0.02$). There was no significance for
376 the Aβ plaque load reduction of the whole cerebrum or the hippocampus (unpaired one-tailed
377 Student's t-test, cerebrum n.s. $p = 0.2$, hippocampus n.s. $p = 0.1$). We observed a tendency for
378 reduction of gliosis after RD2 treatment that was close to being significant in the cortex of RD2-treated
379 mice (Fig. 2 b; GFAP staining: unpaired one-tailed Student's t-test, cortex n.s. $p = 0.064$, hippocampus
380 n.s. $p = 0.3$) (Fig 2 c; CD11b staining: unpaired one-tailed Student's t-test, cortex n.s. $p = 0.051$,
381 hippocampus n.s. $p = 0.28$).

382 Biochemical quantitation of Aβ(x–40) and Aβ(x–42) was accomplished with three fractions (Tris-
383 soluble-, DEA-soluble- and formic acid (FA)-fraction) prepared from brain homogenates of RD2-
384 treated and placebo-treated mice (Fig. 2 d-g). There were no significant differences for the contents of
385 Aβ(x–40) in any of the fractions from RD2-treated mice compared to placebo-treated mice (Fig. 2 d;
386 two-way RM ANOVA treatment, $F_{(1,32)} = 0.87$ n.s., $p = 0.365$; fractions, $F_{(2,32)} = 69.19$, $p < 0.001$;

interaction, $F_{(2,32)}$ = 0.85, n.s., p = 0.44; Tukey post hoc analysis RD2 vs. placebo, Tris-fraction n.s. p = 0.99, DEA-fraction n.s. p = 0.97, FA-fraction n.s. p = 0.12). RD2-treated mice showed a significant increase of Aβ(x–42) in the FA-fraction (Fig. 2 e; two-way RM ANOVA treatment, $F_{(1,32)}$ = 2.32 n.s., p = 0.15; fractions, $F_{(2,32)}$ = 155.58, p < 0.001; interaction, $F_{(2,32)}$ = 2.61, n.s., p = 0.089; Tukey post hoc analysis RD2 vs. placebo, Tris-fraction n.s. p = 0.94, DEA-fraction n.s. p = 0.98, FA-fraction p = 0.009). The Aβ42/40 ratio was nearly 1 in all samples, except for the Tris-fraction of placebo-treated mice that differed significantly from the Tris-fraction of RD2-treated mice (Fig. 2 f; two-way RM ANOVA treatment, $F_{(1,32)}$ = 0.026 n.s., p = 0.88; fractions, $F_{(2,32)}$ = 1.26 n.s., p = 0.3; interaction, $F_{(2,32)}$ = 3.85, n.s., p = 0.032; Tukey post hoc analysis RD2 vs. placebo, Tris-fraction p = 0.03, DEA-fraction n.s. p = 0.64, FA-fraction n.s. p = 0.146). Analysis of Aβ oligomer concentration within the Tris-, DEA-, and FA-fraction was conducted using the surface-based fluorescence intensity distribution analysis (sFIDA) assay. Results displayed a significant increase in Aβ oligomers within the DEA-fraction of RD2-treated mice compared to placebo-treated mice (Fig. 2 g; two-way RM ANOVA treatment, $F_{(1,16)}$ = 1.48 n.s., p = 0.24; fractions, $F_{(1,16)}$ = 5.68, p = 0.03; interaction, $F_{(2,32)}$ = 1.66, n.s., p = 0.22; Tukey post hoc analysis RD2 vs. placebo, Tris-fraction n.s. p = 0.73, DEA-fraction n.s. p = 0.04). The sFIDA assay is highly specific and sensitive to aggregated Aβ species and completely insensitive to monomers. All protein assemblies from the FA-solubilized pellet can be expected to be fully denatured and dissolved. Indeed, the FA-fractions yielded Aβ oligomer concentrations close to zero.

Measurement of Aβ oligomer concentrations by the sFIDA assay revealed significant reduction of Aβ oligomers in RD2 treated mice

RD2 was designed to directly and specifically eliminate Aβ oligomers. To develop a suitable method to investigate target engagement *in vivo*, an assay was developed that is able to quantitate Aβ oligomers in body liquids (e.g. cerebrospinal fluid, plasma). The assay, called sFIDA, is insensitive to Aβ monomers and achieves single particle sensitivity (Herrmann et al, 2017b; Hulsemann et al, 2016; Kuhbach et al, 2016). In the present study, we developed this technique further in order to measure Aβ oligomers in organ homogenates. Therefore, we fractionated full brain homogenates of RD2- and placebo-treated mice by density gradient centrifugation (DGC) according to particle sizes and applied each of the 14 obtained fractions to the sFIDA assay. The sFIDA assay combines the specificity of immunological assays with the sensitivity of high-resolution fluorescence microscopy, which allows a lower limit of detection, down to the single aggregate level. The selectivity for aggregated species is realized by using anti-Aβ antibodies for capturing and probing that recognize overlapping epitopes located at the N-terminus of Aβ subunits (Hellmert et al, 2015; Wang-Dietrich et al, 2013). To test for successful target engagement due to RD2 treatment, we compared DGC-fractionated brain homogenates of RD2- and placebo-treated mice. The result is shown in Figure 3 and revealed a significant decrease of Aβ oligomer levels of RD2- compared to placebo-treated mice especially in fraction 10 (Fig. 3 e; two-way RM ANOVA treatment, $F_{(1,91)}$ = 0.69 n.s., p = 0.44; fractions, $F_{(13,91)}$ = 7.3, p < 0.001; interaction, $F_{(13,91)}$ = 0.96, n.s., p = 0.49; Tukey post hoc analysis RD2 vs. placebo, Tukey post hoc analysis fraction 10 p = 0.003, fraction 1 to 9 an 11 to 14: n.s.).

426 Treatment with RD2 did not affect plasma-levels of different cytokines

427 The plasma cytokine levels of RD2- and placebo-treated mice, and their non-transgenic littermates
428 were determined using the Bio-Plex Pro Mouse Cytokine 23-plex assay (Table 1). Some values were
429 below the limit of detection (LoD) and were therefore excluded from evaluation. The only significant
430 difference found between RD2- and placebo-treated mice was the IL-1α level (Table 1, Kruskal-Wallis
431 one-way ANOVA on Ranks $p = 0.04$, ntg vs. placebo n.s., ntg vs. RD2 n.s., placebo vs. RD2 $p < 0.05$).
432 There was no significant difference between RD2-treated mice and non-transgenic littermates.
433 Additionally, a significant reduction in MIP-1α in placebo-treated mice compared to non-transgenic
434 littermates, but not between RD2- and placebo-treated mice, was observed (Table 1, Kruskal-Wallis
435 one-way ANOVA on Ranks $p = 0.008$, ntg vs. placebo $p < 0.05$, ntg vs. RD2 n.s., placebo vs. RD2
436 n.s.).

437 Adverse drug reactions have not been observed after long-term oral treatment with RD2

438 To test for any adverse or even toxic side effects of the RD2 treatment, four plasma parameters were
439 analyzed: lactate dehydrogenase (LDH), aspartate aminotransferase (AST), alanine aminotransferase
440 (ALT), and alkaline phosphatase (AP). These parameters are also analyzed in clinical routine to give
441 indications about possible drug mediated liver or heart targeted toxicity. The results did not reveal any
442 changes in these parameters (Fig. 4 a-d). Additionally, RD2 treatment did not result in significant gain
443 or loss of body weight (before vs. after treatment, mean ± SEM: RD2: 34.4 g ± 1.0 g vs. 33.5 g ± 0.9 g,
444 placebo: 34.3 g ± 0.9 g vs. 34.2 g ± 0.7 g, non-transgenic littermates 36.4 g ± 1.1 g vs. 34.1 g ± 0.8 g)
445 or a change in the general physiological or behavioral condition of the mice.

Discussion

In the present study, we examined the drug candidate RD2 for true therapeutic rather than only preventive efficacy in old-aged transgenic APP/PS1 mice. RD2 has previously proven to specifically eliminate toxic Aβ oligomers using the Aβ-QIAD assay, and to reduce formation of $A\beta_{(1\text{-}42)}$ fibrils and their seeding potential *in vitro (van Groen et al, 2017)*. *In vivo* it could be shown that RD2 has very favorable pharmacokinetic properties (Leithold et al, 2016). Additionally, intraperitoneal administration of RD2 over four weeks led to significant cognitive improvement in young APP/PS1 mice that displayed little Aβ pathology at the beginning of the treatment. This study could clearly demonstrate that RD2 is able to block progression of the disease. During a second study using the APP Swedish London mouse model it was possible to prove that also oral treatment with RD2 leads to a significant improvement of cognition and memory. Here, we decided to challenge the efficiency of RD2 by orally treating old-aged APP/PS1 mice with full-blown pathology over twelve weeks. This may closer mimic the patients´ situation at moderate and farer progressed disease stages, at least in respect to plaque pathology and cognitive deficits.

As a result of the treatment, we were able to demonstrate the curative *in vivo* efficacy of RD2. It is very well documented that APP/PS1 mice develop cognitive deficits by 7 months of age, which are clearly pronounced at the age of 18 months (Savonenko et al, 2005; Volianskis et al, 2010; Zhang et al, 2011). Because the cognitive abilities of RD2-treated mice were significantly improved over the placebo-treated mice and were indistinguishable from non-transgenic littermates, we conclude that RD2 treatment led to an overall reversal of the cognitive impairments of the transgenic mice. This is supported by the observations made in the open field test, where RD2-treated mice behaved indistinguishable from non-transgenic littermates.

RD2 treatment over 12 weeks decreased Aβ plaque load, which became significant in the cortex. We had not observed such a significant reduction in Aβ plaque load in previous RD2 treatment studies which had shorter treatment durations and used lower RD2 doses, but nevertheless yielded significant improvement in cognition (Kutzsche et al, 2017; van Groen et al, 2017). We conclude that cognitive improvement is not dependent on Aβ plaque load reduction. This is in line with the well-known fact that plaque load does not correlate with cognitive decline in humans (Aizenstein et al, 2008). The observation that cognitive improvement is achieved with shorter treatment duration and lower doses of RD2 before any reduction of plaque load becomes significant, might have implications for future clinical study designs. Therefore, one may carefully consider whether plaque load should be a primary efficacy endpoint in clinical studies for treatment of AD. As we had not observed significant plaque load reductions in the previously reported RD2 treatment studies with shorter treatment duration and lower doses, we were not surprised that there had not been a significant reduction in activated astrocytes and microglia in those studies. The significant reduction in cortex plaque load in the present study, subsequently also led to decreased gliosis, although not to a significant extent. Due to the manifested phenotype of the utilized mouse model, it is likely that the chronic inflammation could not be fully reversed during the course of the experiment and that an even longer treatment period would have been necessary to act significantly on cerebral inflammation.

485 RD2 was designed to specifically and directly eliminate toxic Aβ oligomers. Such target engagement
486 has already been shown *in vitro* using the QIAD assay (van Groen et al, 2017), where RD2 had very
487 significantly reduced the most toxic Aβ oligomers in DGC fractions 4 to 6, resembling particle sizes of
488 about 100 kDa (Brener et al, 2015). To develop an experiment that allows the investigation of target
489 engagement *in vivo*, we decided to use brain homogenates without enrichment steps for human Aβ,
490 as this could potentially lead to destruction of native Aβ oligomers and also to the formation of artificial
491 Aβ aggregates formed during Aβ precipitation steps. Because the brain homogenates contain not only
492 Aβ, but also all other brain derived components, we used the ultra-sensitive and specific sFIDA assay
493 (Herrmann et al, 2017b; Hulsemann et al, 2016; Kravchenko et al, 2017; Kuhbach et al, 2016) for
494 quantification of Aβ oligomers in the DGC-fractionated brain homogenates *ex vivo*. The most
495 significant reduction of Aβ containing particles by RD2 treatment was observed in fraction 10, which
496 corresponds to particles with a molecular weight of larger than 400 kDa (Brener et al, 2015). We
497 speculate that the elevated molecular weight of those *ex vivo* obtained particles as compared to the *in*
498 *vitro* generated Aβ oligomers of the Aβ-QIAD (Brener et al, 2015) was due to other proteins, besides
499 Aβ, that can be expected to be attached to Aβ oligomers. To the best of our knowledge, this is the first
500 time that a reduction of Aβ oligomers has been shown *in vivo* and confirms the proposed mechanism
501 of action for RD2 to be valid also in the functional brain.

502 Based on the results of additional assays probing for species typical behavior like marble burying and
503 nesting behavior (Deacon, 2006a; Deacon, 2006b; Filali & Lalonde, 2009; Torres-Lista & Gimenez-
504 Llort, 2013), we conclude that RD2 treatment did not cause any adverse side effects affecting
505 behavior. Moreover, the lack of significant changes in plasma-concentrations of enzymes like AST,
506 ALT, LDH, and AP between RD2- and placebo-treated mice as well as their non-transgenic littermates
507 further supports the absence of any adverse side effects. Otherwise, changes in plasma-
508 concentrations of these enzymes would have given indications about liver or heart targeted toxicity
509 (Ozer et al, 2008). This is particularly important, because relatively high doses of RD2 were
510 administered daily over twelve weeks.

511 In contrast to active and passive immunization against Aβ species, the postulated mechanism of
512 action of RD2 does not require components of the immune system. Therefore, one would not expect a
513 significant activation of the immune system, which would be indicated, for example, by significant
514 changes of plasma inflammation markers. Indeed, determination of various inflammation markers did
515 not yield any signs of immune system activation upon RD2 treatment. The necessity to rely on the
516 immune system might lead to a negative activation of e.g. T-cells, in the worst case resulting in
517 adverse side effects (e.g. microhemorrhages or meningoencephalitis) (Anand et al, 2014). Those
518 adverse side effects were visible occasionally during the clinical testing's of the first generation of Aβ
519 immunization, e.g. Bapineuzumab and Solanezumab (Carlson et al, 2016; Kerchner & Boxer, 2010). A
520 further advantage of RD2 in comparison to anti-Aβ-antibodies is the oral availability. Pharmacokinetic
521 profiles of RD2 and its lead compound D3 revealed high oral bioavailabilities (Jiang et al, 2015;
522 Leithold et al, 2016). Oral administration is the most attractive application method in humans and
523 usually leads to highest possible compliance.

Conclusion

Here, we describe the effects of a truly curative oral long-term treatment of old-aged APP/PS1 mice with full-blown pathology. We were able to demonstrate that RD2 reversed the cognitive and behavioral deficits in these old transgenic mice to the levels of non-transgenic littermates. Moreover, we demonstrated *in vivo* target engagement of RD2 on oligomeric Aβ species.

Even though the mice were treated with a relatively high dose this was tolerated very well, as no obvious adverse drug effects were observed. This strengthens the hypothesis that the observed improvement of cognition was due to the direct and specific reduction of oligomers, further supporting Aβ oligomer elimination as a successful therapeutic strategy against Alzheimer´s disease.

Acknowledgements

We thank Dr Carsten Korth for providing us the IC16 antibody. Moreover, we thank Dominik Honold for excellent technical support.

Author contributions

S.S., A.W., J.K. and D.W. planned and designed the study. Most parts of the experiments were performed by S.S. and E.S., with technical support. Data analysis was performed by S.S.. Cytokine assay was conducted by S.H. and S.L.. DGC was conducted and analyzed by B.K.. The sFIDA assay design, performance, analysis and interpretation were done by C.Z., O.B. and D.W.. S.S., A.W. and D.W. wrote the manuscript and E.S., C.Z., B.K. S.H., S.L., J.K., N.J.S., and K-J.L. contributed to the manuscript.

Funding

D.W. was supported by the "Portfolio Technology and Medicine" and the Helmholtz-Validierungsfonds of the Impuls and Vernetzungs-Fonds der Helmholtzgemeinschaft. D.W. and K.-J.L. were supported by the "Portfolio Drug Research" of the Impuls and Vernetzungs-Fonds der Helmholtzgemeinschaft

Conflict of Interest

The authors declare that they have no conflict of interest.

549 **References**

550 Aizenstein HJ, Nebes RD, Saxton JA, Price JC, Mathis CA, Tsopelas ND, Ziolko SK, James JA, Snitz
551 BE, Houck PR et al (2008) Frequent amyloid deposition without significant cognitive impairment
552 among the elderly. Archives of neurology 65: 1509-1517

553 Anand R, Gill KD, Mahdi AA (2014) Therapeutics of Alzheimer's disease: Past, present and future.
554 Neuropharmacology 76 Pt A: 27-50

555 Archer J (1973) Tests for emotionality in rats and mice: a review. Animal behaviour 21: 205-235

556 Blennow K, de Leon MJ, Zetterberg H (2006) Alzheimer's disease. Lancet 368: 387-403

557 Brener O, Dunkelmann T, Gremer L, van Groen T, Mirecka EA, Kadish I, Willuweit A, Kutzsche J,
558 Jurgens D, Rudolph S et al (2015) QIAD assay for quantitating a compound's efficacy in elimination of
559 toxic Abeta oligomers. Scientific reports 5: 13222

560 Carlson C, Siemers E, Hake A, Case M, Hayduk R, Suhy J, Oh J, Barakos J (2016) Amyloid-related
561 imaging abnormalities from trials of solanezumab for Alzheimer's disease. Alzheimer's & dementia 2:
562 75-85

563 Cavini IA, Munte CE, Beck Erlach M, van Groen T, Kadish I, Zhang T, Ziehm T, Nagel-Steger L,
564 Kutzsche J, Kremer W et al (2018) Inhibition of Amyloid A[small beta] Aggregation by High Pressures
565 or Specific D-Enantiomeric Peptides. Chemical Communications

566 Clark RA, Shoaib M, Hewitt KN, Stanford SC, Bate ST (2012) A comparison of InVivoStat with other
567 statistical software packages for analysis of data generated from animal experiments. Journal of
568 psychopharmacology 26: 1136-1142

569 Deacon RM (2006a) Assessing nest building in mice. Nat Protoc 1: 1117-1119

570 Deacon RM (2006b) Digging and marble burying in mice: simple methods for in vivo identification of
571 biological impacts. Nature protocols 1: 122-124

572 Elfgen A, Santiago-Schubel B, Gremer L, Kutzsche J, Willbold D (2017) Surprisingly high stability of
573 the Abeta oligomer eliminating all-d-enantiomeric peptide D3 in media simulating the route of orally
574 administered drugs. European journal of pharmaceutical sciences : official journal of the European
575 Federation for Pharmaceutical Sciences 107: 203-207

576 Ferreira ST, Klein WL (2011) The Abeta oligomer hypothesis for synapse failure and memory loss in
577 Alzheimer's disease. Neurobiology of learning and memory 96: 529-543

578 Ferreira ST, Lourenco MV, Oliveira MM, De Felice FG (2015) Soluble amyloid-beta oligomers as
579 synaptotoxins leading to cognitive impairment in Alzheimer's disease. Frontiers in cellular
580 neuroscience 9: 191

581 Filali M, Lalonde R (2009) Age-related cognitive decline and nesting behavior in an APPswe/PS1
582 bigenic model of Alzheimer's disease. Brain research 1292: 93-99

583 Funke SA, van Groen T, Kadish I, Bartnik D, Nagel-Steger L, Brener O, Sehl T, Batra-Safferling R,
584 Moriscot C, Schoehn G et al (2010) Oral treatment with the d-enantiomeric peptide D3 improves the
585 pathology and behavior of Alzheimer's Disease transgenic mice. ACS chemical neuroscience 1: 639-
586 648

587 Garcia-Alloza M, Robbins EM, Zhang-Nunes SX, Purcell SM, Betensky RA, Raju S, Prada C,
588 Greenberg SM, Bacskai BJ, Frosch MP (2006) Characterization of amyloid deposition in the
589 APPswe/PS1dE9 mouse model of Alzheimer disease. Neurobiology of disease 24: 516-524

590 Haass C, Selkoe DJ (2007) Soluble protein oligomers in neurodegeneration: lessons from the
591 Alzheimer's amyloid beta-peptide. Nature reviews Molecular cell biology 8: 101-112

592 Hardy J (1992) An 'anatomical cascade hypothesis' for Alzheimer's disease. . Trends in
593 Neurosciences 15: 200-201

Hardy J, Selkoe DJ (2002) The amyloid hypothesis of Alzheimer's disease: progress and problems on the road to therapeutics. Science 297: 353-356

Hellmert M, Muller-Schiffmann A, Peters MS, Korth C, Schrader T (2015) Hybridization of an Abeta-specific antibody fragment with aminopyrazole-based beta-sheet ligands displays striking enhancement of target affinity. Organic & biomolecular chemistry 13: 2974-2979

Herrmann Y, Bujnicki T, Zafiu C, Kulawik A, Kuhbach K, Peters L, Fabig J, Willbold J, Bannach O, Willbold D (2017a) Nanoparticle standards for immuno-based quantitation of alpha-synuclein oligomers in diagnostics of Parkinson's disease and other synucleinopathies. Clinica chimica acta; international journal of clinical chemistry 466: 152-159

Herrmann Y, Kulawik A, Kuhbach K, Hulsemann M, Peters L, Bujnicki T, Kravchenko K, Linnartz C, Willbold J, Zafiu C et al (2017b) sFIDA automation yields sub-femtomolar limit of detection for Abeta aggregates in body fluids. Clinical biochemistry 50: 244-247

Hulsemann M, Zafiu C, Kuhbach K, Luhmann N, Herrmann Y, Peters L, Linnartz C, Willbold J, Kravchenko K, Kulawik A et al (2016) Biofunctionalized Silica Nanoparticles: Standards in Amyloid-beta Oligomer-Based Diagnosis of Alzheimer's Disease. J Alzheimers Dis 54: 79-88

Jakob-Roetne R, Jacobsen H (2009) Alzheimer's disease: from pathology to therapeutic approaches. Angewandte Chemie (International ed in English) 48: 3030-3059

Jankowsky JL, Fadale DJ, Anderson J, Xu GM, Gonzales V, Jenkins NA, Copeland NG, Lee MK, Younkin LH, Wagner SL et al (2004) Mutant presenilins specifically elevate the levels of the 42 residue beta-amyloid peptide in vivo: evidence for augmentation of a 42-specific gamma secretase. Human molecular genetics 13: 159-170

Janus C, Flores AY, Xu G, Borchelt DR (2015) Behavioral abnormalities in APPSwe/PS1dE9 mouse model of AD-like pathology: comparative analysis across multiple behavioral domains. Neurobiology of aging 36: 2519-2532

Jiang N, Leithold LH, Post J, Ziehm T, Mauler J, Gremer L, Cremer M, Schartmann E, Shah NJ, Kutzsche J et al (2015) Preclinical Pharmacokinetic Studies of the Tritium Labelled D-Enantiomeric Peptide D3 Developed for the Treatment of Alzheimer s Disease. PloS one 10: e0128553

Kamphuis W, Mamber C, Moeton M, Kooijman L, Sluijs JA, Jansen AH, Verveer M, de Groot LR, Smith VD, Rangarajan S et al (2012) GFAP isoforms in adult mouse brain with a focus on neurogenic astrocytes and reactive astrogliosis in mouse models of Alzheimer disease. PloS one 7: e42823

Karran E, Mercken M, De Strooper B (2011) The amyloid cascade hypothesis for Alzheimer's disease: an appraisal for the development of therapeutics. Nature reviews Drug discovery 10: 698-712

Kerchner GA, Boxer AL (2010) Bapineuzumab. Expert opinion on biological therapy 10: 1121-1130

Kravchenko K, Kulawik A, Hulsemann M, Kuhbach K, Zafiu C, Herrmann Y, Linnartz C, Peters L, Bujnicki T, Willbold J et al (2017) Analysis of anticoagulants for blood-based quantitation of amyloid beta oligomers in the sFIDA assay. Biological chemistry 398: 465-475

Kuhbach K, Hulsemann M, Herrmann Y, Kravchenko K, Kulawik A, Linnartz C, Peters L, Wang K, Willbold J, Willbold D et al (2016) Application of an Amyloid Beta Oligomer Standard in the sFIDA Assay. Frontiers in neuroscience 10: 8

Kumar A, Singh A, Ekavali (2015) A review on Alzheimer's disease pathophysiology and its management: an update. Pharmacological reports : PR 67: 195-203

Kutzsche J, Schemmert S, Tusche M, Neddens J, Rabl R, Jurgens D, Brener O, Willuweit A, Hutter-Paier B, Willbold D (2017) Large-Scale Oral Treatment Study with the Four Most Promising D3-Derivatives for the Treatment of Alzheimer's Disease. Molecules (Basel, Switzerland) 22

Leithold LH, Jiang N, Post J, Ziehm T, Schartmann E, Kutzsche J, Shah NJ, Breitkreutz J, Langen KJ, Willuweit A et al (2016) Pharmacokinetic Properties of a Novel D-Peptide Developed to be Therapeutically Active Against Toxic beta-Amyloid Oligomers. Pharmaceutical research 33: 328-336

641 Liu J, Yang B, Ke J, Li W, Suen WC (2016) Antibody-Based Drugs and Approaches Against Amyloid-
642 beta Species for Alzheimer's Disease Immunotherapy. Drugs & aging 33: 685-697

643 Morris RG, Garrud P, Rawlins JN, O'Keefe J (1982) Place navigation impaired in rats with
644 hippocampal lesions. Nature 297: 681-683

645 Ozer J, Ratner M, Shaw M, Bailey W, Schomaker S (2008) The current state of serum biomarkers of
646 hepatotoxicity. Toxicology 245: 194-205

647 Rosenblum WI (2014) Why Alzheimer trials fail: removing soluble oligomeric beta amyloid is essential,
648 inconsistent, and difficult. Neurobiology of aging 35: 969-974

649 Savage MJ, Kalinina J, Wolfe A, Tugusheva K, Korn R, Cash-Mason T, Maxwell JW, Hatcher NG,
650 Haugabook SJ, Wu G et al (2014) A sensitive abeta oligomer assay discriminates Alzheimer's and
651 aged control cerebrospinal fluid. J Neurosci 34: 2884-2897

652 Savonenko A, Xu GM, Melnikova T, Morton JL, Gonzales V, Wong MP, Price DL, Tang F, Markowska
653 AL, Borchelt DR (2005) Episodic-like memory deficits in the APPswe/PS1dE9 mouse model of
654 Alzheimer's disease: relationships to beta-amyloid deposition and neurotransmitter abnormalities.
655 Neurobiology of disease 18: 602-617

656 Selkoe DJ, Hardy J (2016) The amyloid hypothesis of Alzheimer's disease at 25 years. EMBO
657 molecular medicine 8: 595-608

658 Torres-Lista V, Gimenez-Llort L (2013) Impairment of nesting behaviour in 3xTg-AD mice. Behavioural
659 brain research 247: 153-157

660 van Groen T, Kadish I, Funke SA, Bartnik D, Willbold D (2013) Treatment with D3 removes amyloid
661 deposits, reduces inflammation, and improves cognition in aged AbetaPP/PS1 double transgenic
662 mice. Journal of Alzheimer's disease : JAD 34: 609-620

663 van Groen T, Kadish I, Wiesehan K, Funke SA, Willbold D (2009) In vitro and in vivo staining
664 characteristics of small, fluorescent, Abeta42-binding D-enantiomeric peptides in transgenic AD
665 mouse models. ChemMedChem 4: 276-282

666 van Groen T, Kadish, I., Funke, A. S., Bartnik, D., Willbold, D. (2012) Treatment with Aβ42 Binding d-
667 Amino Acid Peptides Reduce Amyloid Deposition and Inflammation in APP/PS1 Double Transgenic
668 Mice. Advances in Protein Chemistry and Structural Biology 88: 133-152

669 van Groen T, Schemmert S, Brener O, Gremer L, Ziehm T, Tusche M, Nagel-Steger L, Kadish I,
670 Schartmann E, Elfgen A et al (2017) The Abeta oligomer eliminating D-enantiomeric peptide RD2
671 improves cognition without changing plaque pathology. Scientific reports 7: 16275

672 van Groen T, Wiesehan K, Funke SA, Kadish I, Nagel-Steger L, Willbold D (2008) Reduction of
673 Alzheimer's disease amyloid plaque load in transgenic mice by D3, A D-enantiomeric peptide
674 identified by mirror image phage display. ChemMedChem 3: 1848-1852

675 Volianskis A, Kostner R, Molgaard M, Hass S, Jensen MS (2010) Episodic memory deficits are not
676 related to altered glutamatergic synaptic transmission and plasticity in the CA1 hippocampus of the
677 APPswe/PS1deltaE9-deleted transgenic mice model of ss-amyloidosis. Neurobiology of aging 31:
678 1173-1187

679 Wang-Dietrich L, Funke SA, Kuhbach K, Wang K, Besmehn A, Willbold S, Cinar Y, Bannach O,
680 Birkmann E, Willbold D (2013) The amyloid-beta oligomer count in cerebrospinal fluid is a biomarker
681 for Alzheimer's disease. Journal of Alzheimer's disease : JAD 34: 985-994

682 Wang MJ, Yi S, Han JY, Park SY, Jang JW, Chun IK, Kim SE, Lee BS, Kim GJ, Yu JS et al (2017)
683 Oligomeric forms of amyloid-beta protein in plasma as a potential blood-based biomarker for
684 Alzheimer's disease. Alzheimer's research & therapy 9: 98

685 Zhang W, Hao J, Liu R, Zhang Z, Lei G, Su C, Miao J, Li Z (2011) Soluble Abeta levels correlate with
686 cognitive deficits in the 12-month-old APPswe/PS1dE9 mouse model of Alzheimer's disease.
687 Behavioural brain research 222: 342-350

688 **Tables**

[pg/ml]	ntg	Placebo	RD2	Statistic
IL-1α	23.54 ± 4.89	24.42 ± 2.16*	15.1 ± 2.18*	Placebo vs. ntg n.s. RD2 vs. Placebo p < 0.05 RD2 vs. ntg n.s.
IL-10	22.17 ± 5.76	39.44 ± 18.52	26.89 ± 6.78	n.s.
IL-12 (p40)	191.7 ± 19.39	187.0 ± 24.30	208.9 ± 18.22	n.s.
IL-13	147.9 ± 26.83	106.8 ± 32.31	176.2 ± 44.57	n.s.
IL-17	2.25 ± 0.42	5.03 ± 1.53	5.85 ± 1.80	n.s.
G-CSF	187.6 ± 61.63	116.2 ± 29.08	118.2 ± 19.14	n.s.
IFN-γ	16.67 ± 3.46	11.09 ± 2.19	18.38 ± 4.89	n.s.
MCP-1	131.2 ± 19.31	156.4 ± 26.47	146.0 ± 27.46	n.s.
MIP-1α	31.97 ± 3.31*	14.75 ± 2.23*	28.03 ± 6.02	Placebo vs. ntg p < 0.05 RD2 vs. Placebo n.s. RD2 vs. ntg n.s.
MIP-1β	19.72 ± 3.99	22.23 ± 4.15	30.27 ± 6.93	n.s.
RANTES	27.15 ± 10.4	16.55 ± 4.32	25.88 ± 9.57	n.s.
TNF-α	64.12 ± 7.32	87.89 ± 14.02	106.6 ± 28.51	n.s.

689 **Table 1: Cytokine assay of non-transgenic littermates, RD2- and placebo-treated mice.** For the evaluation of
690 a potential change in the amount of different cytokines, a Bio-Plex Pro Mouse Cytokine 23-plex Assay was
691 performed with heparinized plasma samples of non-transgenic littermates (ntg), RD2- and placebo-treated mice.
692 Data revealed a significant reduction in IL-1α due to RD2 treatment in comparison to placebo treatment.
693 Furthermore, significantly decreased concentrations of MIP-1α were detected in placebo-treated mice compared
694 to ntg, but no differences between RD2-treated mice and ntg were observed. Cytokine concentrations are given
695 as pg/ml. Data is represented as mean ± SEM, * < 0.05.

Figures

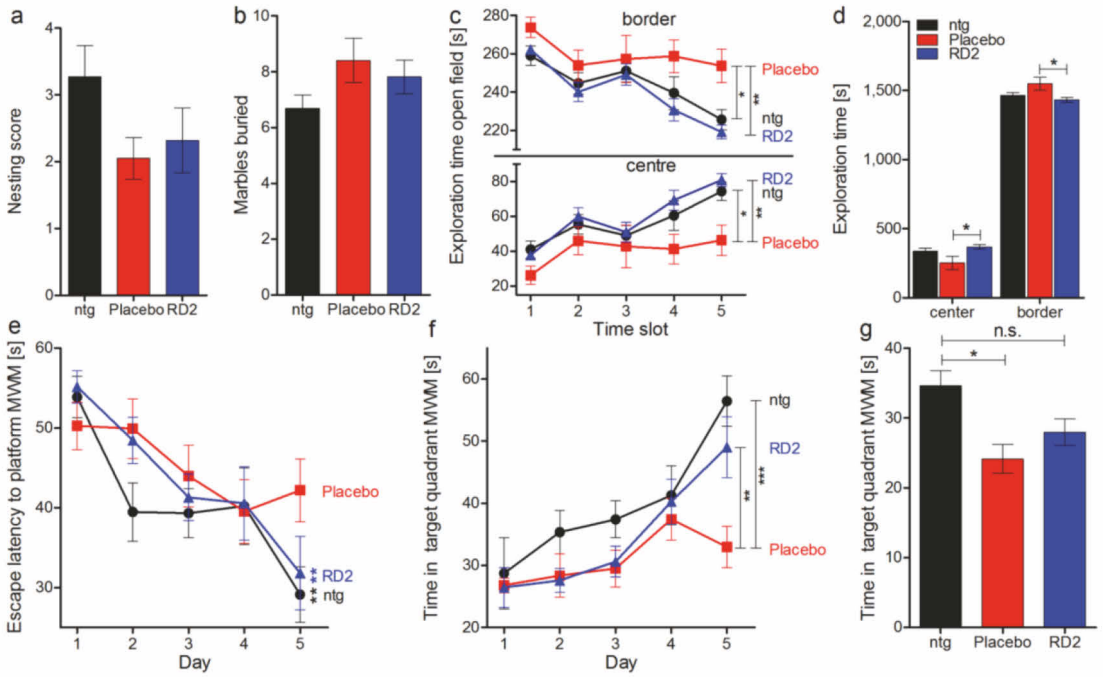

Fig. 1: RD2 treatment of old-aged APP/PS1 mice resulted in significantly improved cognitive performance. Nesting behavior (a) and marble burying (b) were examined to investigate species-typical behavior. Neither RD2 nor placebo treatment had a significant influence on the nesting behavior, nor on the marble burying results compared to non-transgenic littermates (ntg). An open field test was performed to analyze and compare the exploratory and anxiety related behavior of RD2- and placebo-treated mice, as well as their ntg (c, d). Mice were allowed to explore the arena, divided into border and center zone, for 25 min. Exploration of the center and border zone is represented as 5 different time slots (c). In contrast to placebo-treated mice, RD2-treated mice and ntg exhibited a habituation effect to the arena that significantly differs from the performance of placebo-treated mice (c). Analysis of overall exploration revealed a significant difference in the exploratory and anxiety related behavior between RD2- and placebo-treated mice but not between RD2-treated mice and ntg, indicating that RD2 treatment reversed the phenotype of the transgenic mice (d). Additionally, a Morris water maze (MWM) was conducted in which mice were trained for 5 days to find a hidden platform (e-f). Escape latencies to the platform of RD2-treated mice were significantly lower compared to placebo-treated mice indicating improved learning, similar to ntg (e). In addition, RD2 treated-mice and ntg spent significantly more time in the platform quadrant compared to placebo-treated mice on the last training day (f). Analysis of the probe trial revealed a significant difference between ntg and placebo-treated mice, but not between ntg and RD2-treated mice, respectively (g). Each behavioral performance of RD2-treated mice was similar to those of ntg, suggesting a reversed phenotype. Data is represented as mean ± SEM, RD2 n = 11, placebo n = 10, ntg n = 11.

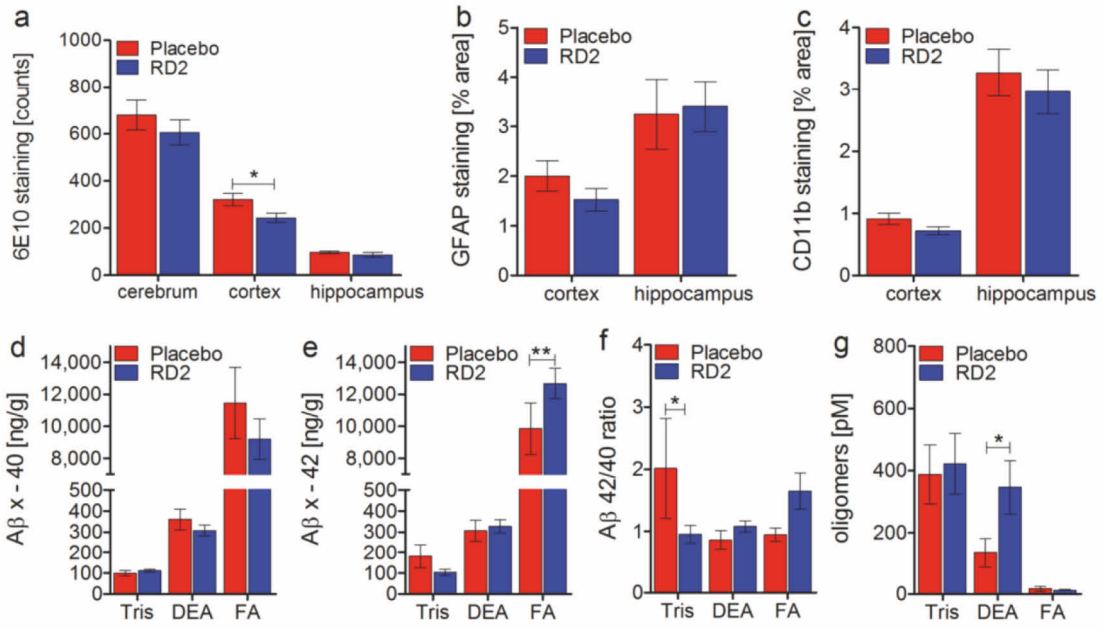

Fig. 2: Effects of RD2 treatment on Aβ pathology, gliosis, and Aβ oligomers in the brains of APP/PS1 mice. Investigations of a potential reduction in either Aβ plaque load or astrogliosis after RD2-treatment were performed using immunohistochemical analysis. Plaque count was analyzed by 6E10 staining in different areas of the brain (cerebrum, cortex, and hippocampus). Compared to placebo-treated mice, RD2-treated mice showed a decreased number of Aβ deposits in all analyzed regions being significant in the cortex (a). Activated astrocytes were quantified after GFAP staining (b) and activated microglia were quantified after CD11b staining (c). Results exhibited no significant difference in gliosis between RD2- and placebo-treated mice. Levels of Aβ x–40 (d) and Aβ x–42 (e) in the Tris-soluble (Tris), DEA-soluble (DEA) and formic acid fractions (FA) of brain homogenates of RD2- and placebo-treated mice were analyzed by ELISA, resulting in a significant increase of Aβ(x-42) in the FA-fraction of RD2-treatded mice. Concentrations were presented in ng (Aβ(x–40) or Aβ(x–42))/g (brain). Aβ 42/40 ratio is shown in (f) and yielded a significantly higher ratio in the Tris fraction of placebo-treated mice. Aβ oligomer concentrations were analyzed in the above-mentioned fractions by sFIDA assay, resulting in a significant increase in Aβ oligomers within the DEA-fraction of RD2- compared to placebo-treated mice (g). Data is represented as mean ± SEM. All: * $p > 0.05$.

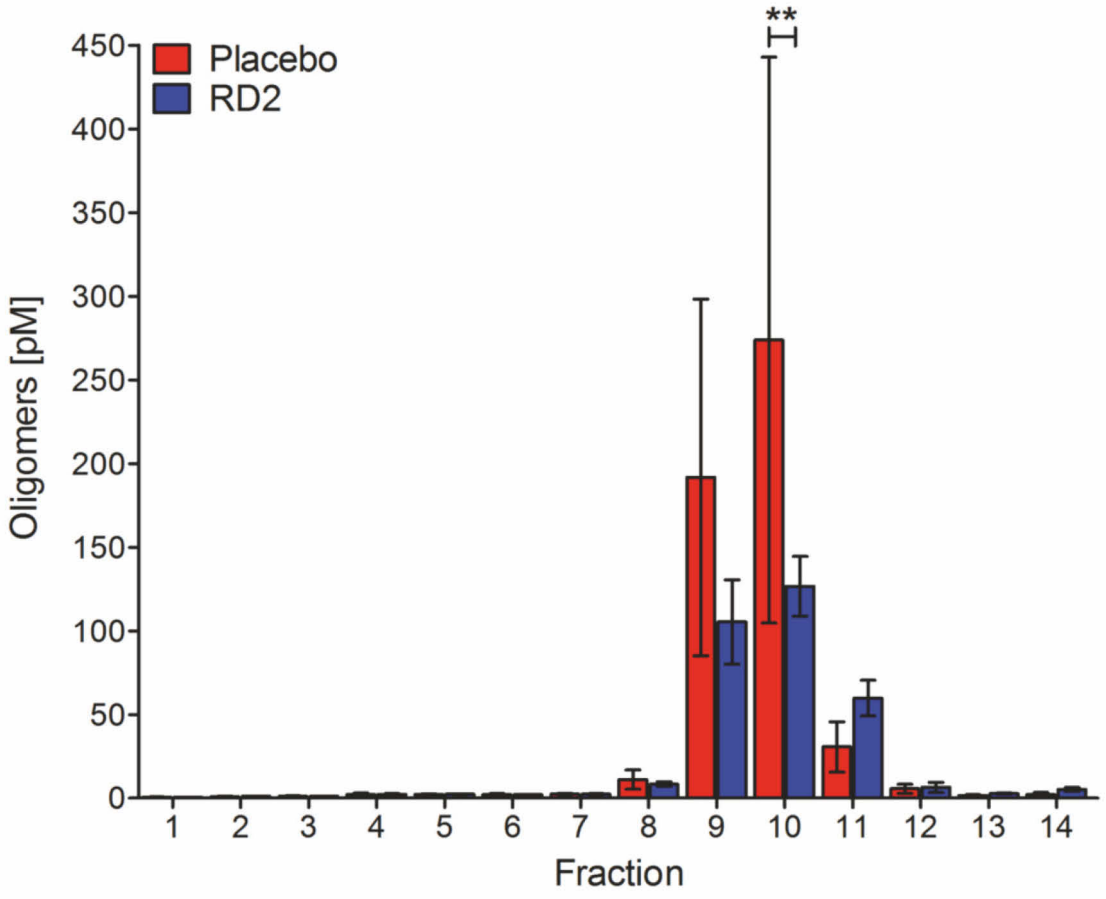

731

732 **Fig. 3: Treatment with RD2 significantly reduced oligomeric Aβ species.** Oligomeric Aβ levels in the fractions
733 of density gradient ultra-centrifuged brain homogenates of RD2- and placebo treated APP/PS1 mice were
734 analyzed by the aggregate specific and highly sensitive sFIDA assay. Results revealed a significant decrease in
735 oligomeric Aβ species in fraction 10 of RD2- compared to placebo-treated mice. sFIDA read-out was converted to
736 Aβ oligomer concentrations after calibration with $Aβ_{1-42}$-SiNaP (internal standard calibration) (silica nanoparticles).
737 Data is represented as mean ± SEM.. Placebo n = 4, RD2 n = 5. **p < 0.01.

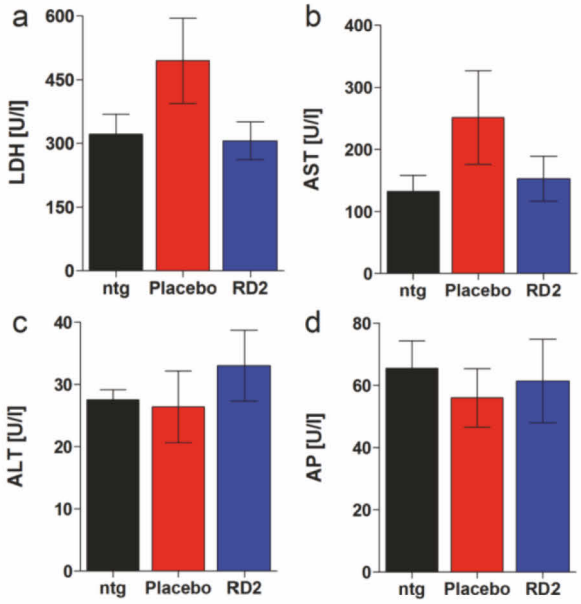

Fig. 4: Effects of long-term RD2 treatment on different plasma enzymes. Examination of lactate dehydrogenase (LDH) (a), aspartate aminotransferase (AST) (b), alanine aminotransferase (ALT) (c), and alkaline phosphatases (AP) (d). These plasma enzymes, usually analyzed to investigate whether a treatment with a new medication induces e.g. liver intoxication, indicated no toxic adverse side effects due to long-term RD2 treatment. No significant differences were detected between non-transgenic littermates (ntg), RD2- or placebo-treated APP/PS1 mice. This is particularly important based on the high administered concentration (200 mg/kg daily). Data is represented as mean ± SEM. Kruskal-Wallis one-way ANOVA on Ranks, (a): n.s. $p = 0.33$; One-way ANOVA, (b): $F_{(2,13)} = 1.42$ n.s. $p = 0.28$, (c): $F_{(2,13)} = 0.5$ n.s. $p = 0.62$, (d): $F_{(2,13)} = 0.18$ n.s. $p = 0.84$. ntg n = 4, Placebo n = 5, RD2 n = 5.

3.8 Oral treatment with an Aβ oligomer eliminating compound decelerates the neurodegenerative phenotype in pyroglutamate-Aβ accumulating transgenic mice

Autoren:	**Schemmert S**., Schartmann E., Honold D., Zafiu C., Ziehm T., Langen K-J., Shah N.J., Kutzsche J., Willuweit A., Willbold D
Journal:	Neuron, eingereicht am 09. April 2018
Impact Factor:	14,024 (2016)
Beitrag:	Planung der Studie, Durchführung aller Verhaltensversuche (SHIRPA, Rotarod, Offenfeldtest, Murmeltest, Stangentest, Greifstärketest, Klammertest)
	Behandlung der Mäuse
	Durchführung der immunhistologischen Experimente
	Quantifizierung der immunhistologischen Ergebnisse
	Durchführung und Auswertung biochemischer Analysen
	Anfertigung aller Abbildungen
	Analyse aller Daten
	statistische Auswertung.
	Hauptverfassung und Prüfung des Manuskriptes

Title Page

Oral treatment with an Aβ oligomer eliminating compound decelerates the neurodegenerative phenotype in pyroglutamate-Aβ accumulating transgenic mice

Sarah Schemmert[1], Elena Schartmann[1], Dominik Honold[1], Christian Zafiu[1], Tamar Ziehm[1], Karl-Josef Langen[2,3], Nadim Joni Shah[2,4], Janine Kutzsche[1], Antje Willuweit[2*], Dieter Willbold[1,5*]

Affiliations

[1]Institute of Complex Systems, Structural Biochemistry (ICS-6), Forschungszentrum Jülich, Jülich, Germany

[2]Institute of Neuroscience and Medicine, Medical Imaging Physics (INM-4), Forschungszentrum Jülich, Jülich, Germany

[3]Clinic for Nuclear Medicine, RWTH Aachen University, Aachen, Germany

[4]Department of Neurology, Faculty of Medicine, JARA, RWTH Aachen University, Aachen, Germany

[5]Institut für Physikalische Biologie, Heinrich-Heine-Universität, Düsseldorf, Germany

*Correspondence to:

Dieter Willbold

Forschungszentrum Jülich, Institute of Complex Systems, Structural Biochemistry (ICS-6)
52425 Jülich
Germany
E-mail: d.willbold@fz-juelich.de
Phone: +49-2461-612100
Fax: +49-2461-612023

and

Antje Willuweit

Forschungszentrum Jülich, Institute of Neuroscience and Medicine (INM-4)
52425 Jülich
Germany
E-mail: a.willuweit@fz-juelich.de
Phone: +49-2461-6196358
Fax: +49-2461-612302

Abstract

Alzheimer's disease is characterised by neurodegeneration, extracellular accumulation of amyloid-β protein (Aβ) and intracellular aggregation of hyperphosphorylated tau protein. During the last years, Aβ oligomers have been claimed to be the disease causing agent. Consequently, development of compounds disrupting already existing Aβ oligomers is highly desirable. We have developed orally available compounds that have shown high efficacy in direct and specific elimination of toxic Aβ oligomers. One of them, RD2, has already demonstrated cognition enhancement in two different transgenic AD mouse models. Here, we report on the efficacy of RD2 in the transgenic TBA2.1 mouse model, which develops pyroglutamate-$A\beta_{(3\text{-}42)}$ induced neurodegeneration. Oral treatment led to a significant deceleration of neurodegenerative phenotype.

Keywords

Alzheimer's disease, oral treatment, amyloid-β (Aβ) oligomers, D-enantiomeric peptides, motor neurodegenerative phenotype, TBA2.1

Introduction

Alzheimer's disease (AD) is still an incurable progressive neurodegenerative disorder, currently affecting more than 20 million patients as well as their relatives and care givers worldwide (Prince et al., 2015). Disease progression is characterised by neurodegeneration, finally leading to enormous cognitive and physiological impairments. The major hallmarks of the disease have been identified in the past in AD patients' brains: extracellular amyloid-β (Aβ) plaques, intracellular tau tangles, and neurodegeneration (Haass and Selkoe, 2007a; Selkoe and Hardy, 2016). As a consequence, Aβ and tau are prominent targets in drug development against AD (Godyn et al., 2016). Aβ is produced via the amyloidogenic pathway by cleavage of the amyloid protein precursor (APP) by β- and γ-secretases. Under certain circumstances, soluble Aβ monomers can aggregate to soluble Aβ oligomers, which are postulated to be the most neurotoxic Aβ species, and finally to Aβ plaques (Haass and Selkoe, 2007b; Selkoe and Hardy, 2016; Thal et al., 2006). However, the proteolytic processing of APP is a complex process resulting in a variety of different Aβ isoforms (Roher et al., 2017). Besides the C-terminal modifications of Aβ ($Aβ_{(1-40)}$ and $Aβ_{(1-42)}$), N-terminally truncated and modified Aβ species are a major component of Aβ deposits in AD patients' brains (Frost et al., 2013). In the course of this, pyroglutamate modified Aβ species (pEAβ) are of crucial importance, because they represent about 25% of total Aβ in AD patients' brains (Gunn et al., 2010). The formation of truncated Aβ for building up pEAβ is, until now, not fully understood. Apparently, the loss of the first two or ten amino acids is necessary for pEAβ formation, either by direct processing of APP by certain β-secretases or by modification of Aβ subsequently after classical β-secretase cleavage (Gunn et al., 2010). The N-terminal modification of pEAβ, starting at positon three or eleven with pyroglutamate instead of glutamate, leads to enhanced aggregation and oligomerisation tendency compared to $Aβ_{(1-42)}$ (Dammers et al., 2017a; Dammers et al., 2017b; Perez-Garmendia and Gevorkian, 2013). Moreover, pEAβ shows increased resistance against degradation, and increased neurotoxic properties, leading to impaired long-term potentiation in mice and thus, playing a potential role on AD pathogenesis (Jawhar et al., 2011; Nussbaum et al., 2012; Perez-Garmendia and Gevorkian, 2013; Schilling et al., 2006). However, so far this highly toxic Aβ-species was largely ignored as drug target.

Despite intensive research and obvious unmet medical need, no curative or disease modifying treatment for AD is available. Currently available medications only treat some of the symptoms. Therefore, the development of new treatment strategies, besides those already described, e.g. β- or γ-secretase inhibitors or anti-Aβ-immunisation, is indispensable, because none of these were successful in clinical trials yet (Kumar et al., 2015). To meet this need, we have developed D-enantiomeric peptides, solely consisting of D-enantiomeric amino acid residues. They are able to eliminate already existing toxic Aβ oligomers by a ligand mediated stabilisation of Aβ monomers in an aggregation-incompetent, amorphous conformation. By this, the equilibrium between different Aβ species is shifted away from toxic Aβ oligomers towards Aβ monomers. Thus, there is no necessity to rely on components of the immune system (e.g. for anti-Aβ-immunisation) to remove Aβ oligomers and presumably no adverse drug reaction as a consequence of a negative activation of the immune system. This mode of action was already described for the lead compound "D3". D3 eliminates toxic Aβ oligomers, as demonstrated by the Aβ-QIAD (quantitative determination of interference with the Aβ

aggregate size distribution) assay. The Aβ-QIAD assay allows analysing a potential reduction of Aβ oligomers *in vitro* (Brener et al., 2015). Moreover, D3 improves cognitive impairment, and reduces Aβ plaque load in different AD mouse models *in vivo*, even after oral administration (Brener et al., 2015; Funke et al., 2010; van Groen et al., 2013; van Groen et al., 2009; van Groen, 2012; van Groen et al., 2008). Based on a rational redesign of D3, the compound RD2 has been developed in order to enhance the Aβ oligomer elimination efficacy. It was confirmed that RD2 reveals enhanced Aβ oligomer elimination efficacy compared to D3 *in vitro* (van Groen et al., 2017a). Furthermore, RD2 has already proven its *in vivo* efficacy to ameliorate cognition in two different AD mouse models in different laboratories. In a first treatment study, RD2 improved cognition in seven months old APP/PS1 mice, without changing plaque pathology (van Groen et al., 2017a). In accordance to the promising pharmacokinetic profile of RD2, and its high oral bioavailability (Leithold et al., 2016), we challenged RD2 by oral treatment of eight months old APP_{SL} mice, verifying that RD2 is also efficacious when given orally (Kutzsche et al., 2017).

Here, we decided to additionally test the efficacy of RD2 towards pEAβ in an AD mouse model based on intraneuronal accumulation of neurotoxic $pEA\beta_{(3\text{-}42)}$, the TBA2.1 mouse model. Homozygous TBA2.1 mice develop severe motor deficits and neurodegeneration in the CA1 region of the hippocampus with a very early onset of the phenotype (Alexandru et al., 2011; Dunkelmann et al., 2018; Dunkelmann et al., 2017). Regarding the critical role of pEAβ in the development of AD and the positive validation of RD2 so far, we here investigated whether oral treatment with RD2 is able to decelerate the $pEA\beta_{(3\text{-}42)}$ induced neurodegenerative phenotype in TBA2.1 mice. Behavioural assessments revealed a significant improvement of the motor abilities of RD2- compared to placebo-treated homozygous TBA2.1 mice. Additionally, we give further evidence about our suggested mode of action, by showing a significant reduction of soluble Aβ species that include also Aβ oligomers. Additionally we confirmed that no adverse side effects were caused by RD2 treatment in homozygous TBA2.1 mice as well as in their non-transgenic littermates.

Results

RD2 bound to monomeric pEAβ$_{(3-42)}$ with micromolar affinity and inhibited pEAβ$_{(3-42)}$ fibril formation in a dose-dependent manner

In order to asses RD2 binding affinities to monomeric pEAβ$_{(3-42)}$, surface plasmon resonance (SPR) spectroscopy was conducted. Therefore, solutions containing different RD2 concentrations were injected over the sensor surface with immobilized pEAβ$_{(3-42)}$ and RD2 binding to pEAβ$_{(3-42)}$ was detected in real-time (Fig. 1 A). By plotting equilibrium responses at the end of the association phase against applied RD2 concentrations, the equilibrium dissociation constant (K_D) was determined. A K_D value of 26.6 µM was calculated for the RD2-pEAβ$_{(3-42)}$ interaction (Fig. 1 B).

The inhibitory function of pEAβ$_{(3-42)}$ fibril formation by RD2 was investigated using Thioflavin-T (ThT). ThT is a dye specifically binding β-sheets of amyloids and commonly used to monitor Aβ fibril formation. The aggregation of 5 µM pEAβ$_{(3-42)}$ was monitored for 21 h in the absence or presence of different RD2 concentrations (Fig. 1 C). RD2 inhibited pEAβ$_{(3-42)}$ fibril formation efficiently in a dose-dependent manner. Although 5 µM pEAβ$_{(3-42)}$ was used in the assay, the IC_{50} value was determined to be 707 nM suggesting substochiometric action of RD2. The Hill coefficient of 3.0 clearly suggests that the underlying mechanism is highly cooperative (Fig. 1 D).

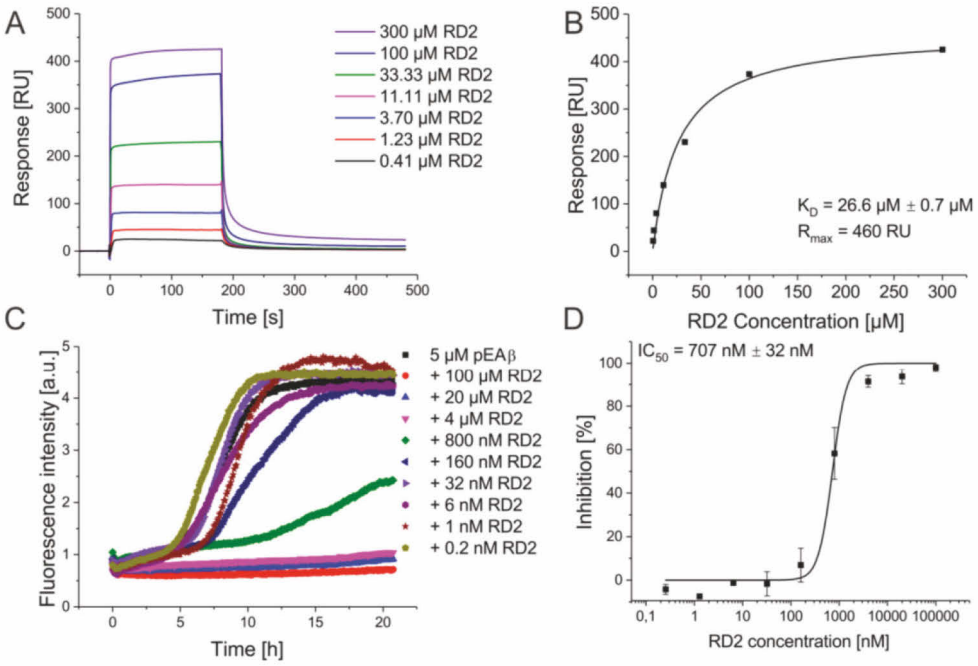

Fig. 1: Binding affinity of RD2 to pEAβ$_{(3-42)}$ and inhibitory efficacy of RD2 on pEAβ$_{(3-42)}$ fibril formation. Real-time surface plasmon resonance (SPR) sensorgrams of different RD2 concentrations binding to immobilized pEAβ$_{(3-42)}$ (A). Equilibrium dissociation constants (K_D) were determined by plotting equilibrium responses against applied RD2 concentrations and fitted using a Langmuir 1:1 binding model (B). Shown data are representative of three replicates and K_D value is presented as mean ± SD of three independent experiments. Fibril formation of 5 µM pEAβ$_{(3-42)}$ in the absence or presence of different concentrations of RD2 monitored by Thioflavin T over 21 h (C). Final fibril masses at the end of this time period were normalized to the pEAβ$_{(3-42)}$ control and plotted over RD2 concentration. The half-maximal inhibitory concentration (IC_{50}) was determined by a logistic fit of the data (D). Shown data are representative of three replicates and IC_{50} value is presented as mean ± SD of three independent experiments.

Oral treatment with RD2 improved the phenotype of homozygous TBA2.1 mice without influencing the behaviour of non-transgenic littermates

Daily, homozygous TBA2.1 mice and their non-transgenic littermates (wild type mice) were orally treated with 20 or 100 mg/kg RD2 over a period of twelve weeks. All mice were tested in different behavioural assessments, before (baseline), in the middle of the treatment (after six weeks of treatment), and at the end of the treatment period (after twelve weeks of treatment) to test the efficacy of RD2 with different concentrations on phenotype progression of homozygous TBA2.1 mice. Non-transgenic littermates were tested in parallel to assess specificity of the treatment and putative side effects. All mice were monitored closely because of the severe phenotype of the used mouse model.

RD2 treatment did not cause any loss or gain of body weight in the non-transgenic or homozygous mice in comparison to placebo treatment, irrespective of the administered RD2 concentration. Moreover, there was no detectable change in the general physiological condition or macroscopic investigations of all organs of RD2-treated non-transgenic littermates or homozygous mice, even in the group which was treated with 100 mg/kg RD2 daily.

To evaluate, whether RD2 has any influence on the progression of the neurodegenerative phenotype of homozygous TBA2.1 mice, or any impact on non-transgenic littermates, different behavioural approaches were conducted (Fig. 2).

By use of the SHIRPA test battery, it was tested whether there was a difference in the neurodegenerative phenotype of homozygous TBA2.1 mice, treated with placebo or different concentrations of RD2. At the end of the treatment period (after twelve weeks of treatment), both RD2 treatment groups were scored with significantly lower SHIRPA scores compared to placebo-treated mice (two-way RM ANOVA, $F_{(5,84)} = 54.27$, $p < 0.001$, Fisher LSD post hoc analysis placebo vs. 20 mg/kg/day $p < 0.001$, placebo vs. 100 mg/kg/day $p < 0.001$, 20 mg/kg/day vs. 100 mg/kg/day n.s. $p = 0.95$, Fig. 2 A). Moreover, daily treatment with either 20 mg/kg or 100 mg/kg RD2 slowed down the phenotype progression measured in the SHIRPA test compared to placebo-treated mice during the second half of the treatment period (two-way RM ANOVA, $F_{(5,84)} = 95.70$, $p < 0.001$, Fisher LSD post hoc analysis week six vs. week twelve of treatment placebo $p < 0.001$, 20 mg/kg/day $p = 0.002$, 100 mg/kg/day $p = 0.018$, Fig. 3 A). At each tested time point, RD2- or placebo-treated non-transgenic littermates showed no abnormalities in behaviour. They revealed SHIRPA scores around zero, indicating no change of any evaluated parameter due to treatment with different concentrations of RD2 (Fig. 2 A).

By use of the clasping test, the hind limbs of the mice were analysed (Fig. 2 B). A considerable decline in the clasping behaviour of homozygous mice (increasing clasping scores) was observed during the course of the treatment period. Although clasping behaviour of homozygous RD2-treated mice deteriorated as well, both RD2-treated groups showed significantly lower clasping scores compared to the homozygous placebo-treated group at the end of the treatment period (two-way RM ANOVA, $F_{(5,84)} = 77.05$, $p < 0.001$, Fisher LSD post hoc analysis placebo vs. 20 mg/kg/day $p < 0.001$, placebo

vs. 100 mg/kg/day p = 0.002, 20 mg/kg/day vs. 100 mg/kg/day n.s. p = 0.5, Fig. 2 B). No change in the clasping behaviour of all non-transgenic littermates was observed (Fig. 2 B).

Further investigation of RD2's influence on motor deficits was conducted by the rotarod and modified pole test. Again, a clear progression of the phenotype of homozygous mice was detected in both tests, as compared to non-transgenic littermates (Fig. 2 C-D). Analysis of the rotarod test revealed no significant difference between both homozygous RD2 treatment groups and the homozygous placebo group (two-way RM ANOVA, $F_{(2,168)} = 0.99$ n.s., p = 0.38, Fisher LSD post hoc analysis placebo vs. 20 mg/kg/day n.s. p = 0.24, placebo vs. 100 mg/kg/day n.s. p = 0.98, 20 mg/kg/day vs. 100 mg/kg/day n.s. p = 0.23, Fig. 2 D). The conducted pole test resulted in no significant difference between RD2- and placebo-treated homozygous TBA2.1 mice at the end of the treatment period (two-way RM ANOVA, $F_{(5,84)} = 43.71$, $p < 0.001$, Fisher LSD post hoc analysis week six of treatment, placebo vs. 20 mg/kg/day n.s. p = 0.10, placebo vs. 100 mg/kg/day n.s. p = 0.19, 20 mg/kg/day vs. 100 mg/kg/day n.s. p = 0.74, Fig. 2 C). However, there was a significant progression of the phenotype of placebo-treated homozygous TBA2.1 mice, but no significant (although borderline) progression was measureable within both RD2 treatment groups (two-way RM ANOVA, $F_{(5,84)} = 50.54$, $p < 0.001$, Fisher LSD post hoc analysis week six vs. end (week twelve) of treatment placebo p = 0.015, 20 mg/kg/day n.s. p = 0.054, 100 mg/kg/day n.s p = 0.054). No significant change in the performance of all non-transgenic littermates was observed in both tests (Fig. 2 C-D). Thus, RD2 treatment did not cause any adverse drug reaction influencing the behaviour of non-transgenic littermates in these tests.

The open field test was accomplished to assess changes in anxiety or exploratory behaviour. As demonstrated in Fig. 2 E RD2 treatment did not show any negative impact on anxiety or exploratory behaviour of all tested groups of mice. All treatment groups spent a significant longer time in the border zone compared to the centre zone, but no significant difference was detected between the treatment groups (two-way RM ANOVA, $F_{(5,210)} = 186.5$ $p < 0.001$, Fisher LSD post hoc analysis all centre vs. border $p < 0.001$ Fig. 2 E).

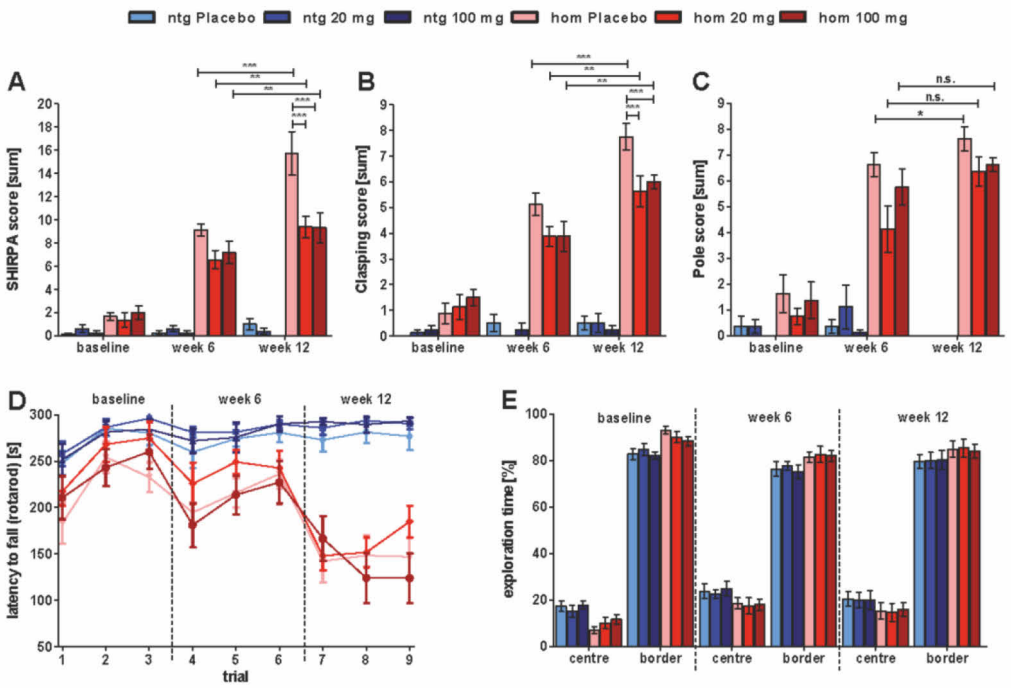

Fig. 2: Evaluation of motor, exploratory and anxiety related behaviour of RD2-treated homozygous (hom) TBA2.1 mice and their treated non-transgenic littermates (ntg). Investigation of an amelioration of the phenotype of homozygous TBA2.1 mice after RD2 treatment with 20 or 100 mg/kg/day over twelve weeks was conducted by different behavioural test. Analysis of the SHIRPA test battery (A), clasping behaviour (B), and pole test (C), did result in a significant improvement of the phenotype of both RD2 treatment groups compared to placebo-treated mice. Additionally, ntg were treated with placebo or 20 or 100 mg/kg RD2 daily to investigate possible adverse drug reactions on motor related behaviour. In each test, no difference between RD2- and placebo-treated ntg was observed (A-C). Analysis of the rotarod test did not result in a significant amelioration of the motor impaired phenotype of hom TBA2.1 mice, irrespective of the administered RD2 concentration (D). No effect regarding a negative influence of RD2 treatment on ntg was detectable (D). In total, mice complete nine trials in three sections before, after six, and after twelve weeks of treatment. Each given trial in (D) represents three completed trials of one section. There was no indication for any increased or decreased exploration or anxiety related behaviour of ntg or hom mice, either treated with placebo or RD2 in the open field test (E), suggesting that RD2 treatment has no adverse effect on anxiety or exploration. Data is represented as mean ± SEM. Statistical calculations were conducted by two-way RM ANOVA with Fisher post hoc analysis, n = 8 for all groups and each test. *p = 0.05, **p = 0.01, ***p = 0.001

Pathological analysis of RD2-treated homozygous TBA2.1 mice revealed no influence on neurodegeneration, Aβ pathology, or gliosis

Homozygous TBA2.1 mice are pathologically characterised by small aggregated, clearly distinguishable Aβ particles, especially detectable within the striatum, motor cortex, solely CA1 region of the hippocampus, and midbrain (inferior colliculus), instead of large and diffuse Aβ plaques as has been shown for other AD mouse models with APP and/or PS mutations (Alexandru et al., 2011). Investigation of RD2's possible influence on pathologic Aβ aggregates (number of Aβ aggregates as stained with antibody 6E10) was conducted by immunohistochemical analysis in different brain regions. There was no significant difference on Aβ pathology due to RD2 treatment (Fig. 3), but there was a tendency of lowered Aβ particles within the striatum of 100 mg/kg/day RD2-treated mice (Fig. 3 A).

Moreover, homozygous TBA mice show clear neurodegeneration within the hippocampal CA1 region, and gliosis distributed over different brain regions, more or less associated with Aβ particles (Alexandru et al., 2011). The correspondent immunohistochemical analysis (neurons as stained with

antibody NeuN, activated astrocytes as stained with antibody GFAP, and activated microglia, as stained with antibody CD11b) revealed no differences between all treatment groups (Tab. 1).

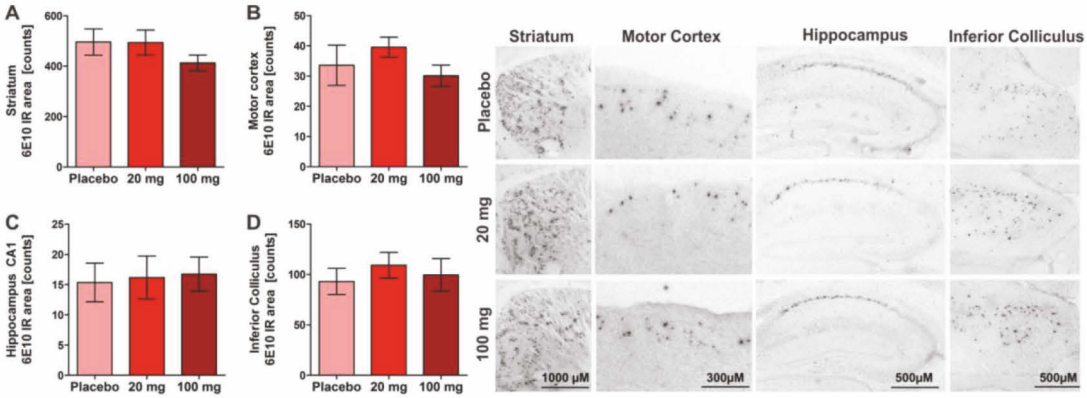

Fig. 3: Evaluation of Aβ particles of RD2-treated homozygous (hom) TBA2.1 mice in different brain regions. Treatment with 20 or 100 mg/kg RD2 daily did not significantly change Aβ deposits (staining with 6E10 antibody with subsequent quantification of Aβ particle count). By trend, a reduction of Aβ deposits was detected in the striatum of 100 mg/kg/day RD2-treated hom TBA2.1 mice in comparison to placebo treated mice. IR: immunoreactivity. Exemplary presentation of the analysed brain regions are given on the right. Data is represented as mean ± SEM, two-way ANOVA with Fisher post hoc analysis.

Besides this, the brains of placebo- and RD2-treated non-transgenic littermates were also analysed by immunohistochemistry (Tab. 1). Thereby we wanted to figure out, whether RD2 treatment caused any increase of inflammatory cells in the brains of non-transgenic littermates (wild type mice) compared to placebo-treated mice. No difference was detectable, irrespective of the analysed cell type or brain region, underpinning that RD2 treatment did not cause any adverse drug reaction (Tab. 1).

	Staining	Brain region	Placebo	20 mg/kg	100 mg/kg	Statistic
Homozygous TBA2.1	NeuN (IR [%])	Striatum	16.2 ± 0.8	14.8 ± 1.0	15.7 ± 0.7	Genotype p < 0.001; Treatment n.s. (p = 0.4)
		MC	38.3 ± 2.8	33.8 ± 2.9	37.2 ± 1.5	Genotype p < 0.001; Treatment n.s. (p = 0.5)
		CA1	10.6 ± 0.6	11.1 ± 0.5	10.1 ± 0.8	Genotype p < 0.001; Treatment n.s. (p = 0.9)
	GFAP (IR [%])	MC	22.4 ± 1.5	21.8 ± 1.6	22.8 ± 1.9	Genotype p < 0.001; Treatment n.s. (p = 0.5)
		CA1	36.2 ± 1.5	35.8 ± 1.7	38.3 ± 1.1	Genotype p < 0.001; Treatment n.s. (p = 0.1)
	CD11b (IR [%])	IC	0.86 ± 0.2	0.7 ± 0.1	1.0 ± 0.1	Genotype n.s (p = 0.14); Treatment n.s. (p = 0.6)
		Brain stem	0.2 ± 0.03	0.3 ± 0.06	0.3 ± 0.06	Genotype p < 0.001; Treatment n.s. (p = 0.5)
Non-transgenic littermates	NeuN (IR [%])	Striatum	39.6 ± 2.0	39.9 ± 1.6	41.3 ± 0.9	Genotype p < 0.001; Treatment n.s. (p = 0.4)
		MC	42.0 ± 0.4	42.5 ± 0.9	42.7 ± 0.3	Genotype p < 0.001; Treatment n.s. (p = 0.5)
		CA1	26.9 ± 5.1	27.4 ± 1.6	26.4 ± 3.9	Genotype p < 0.001; Treatment n.s. (p = 0.9)
	GFAP (IR [%])	MC	8.8 ± 1.6	6.9 ± 1.1	9.7 ± 1.5	Genotype p < 0.001; Treatment n.s. (p = 0.5)
		CA1	6.3 ± 0.7	3.1 ± 0.8	5.4 ± 0.6	Genotype p < 0.001; Treatment n.s. (p = 0.1)
	CD11b (IR [%])	IC	0.44 ± 0.3	0.77 ± 0.4	0.49 ± 0.4	Genotype n.s (p = 0.14); Treatment n.s. (p = 0.6)
		Brain stem	0.34 ± 0.2	0.12 ± 0.1	0.14 ± 0.1	Genotype p < 0.001; Treatment n.s. (p = 0.5)

Table 1: Immunohistochemical investigations of RD2 treatment on neurodegeneration, and neuroinflammation. Treatment with 20 or 100 mg/kg RD2 daily did not alleviate neurodegeneration (staining with NeuN antibody with subsequent quantification of the stained area) in the striatum, hippocampal region CA1, and motor cortex compared to placebo-treated homozygous TBA2.1 mice. Immunostaining using antibodies against GFAP and CD11b were used as markers for activated astrocytes and microglia, respectively, to analyse a possible change of inflammatory processes after treatment with RD2 in different brain regions (GFAP: motor cortex, hippocampal region CA1, inferior colliculus; CD11b inferior colliculus, brain stem). No significant difference in inflammation was detected. IC: Inferior colliculus. MC: Motor cortex. IR: immunoreactivity. Data is represented as mean ± SEM, two-way ANOVA with Fisher post hoc analysis.

Additionally, an $A\beta_{(x-42)}$ ELISA was conducted with brain homogenates, resulting in a significant decrease in $A\beta_{(x-42)}$ in the Tris-soluble fraction of RD2-treated homozygous TBA2.1 mice compared to placebo-treated mice (two-way ANOVA, $F_{(2,78)} = 3.57$ $p = 0.033$, Fisher LSD post hoc analysis placebo vs. 20 mg/kg/day $p \leq 0.001$, placebo vs. 100 mg/kg/day n.s. $p < 0.001$, 20 mg/kg/day vs. 100 mg/kg/day n.s. $p = 0.98$, Fig. 4 A). While no difference in the amount of Aβ species in the DEA-fraction was detected, a significant increase of insoluble Aβ species within the FA-fraction of both RD2 treatment groups was shown in comparison to placebo-treated mice (two-way ANOVA, $F_{(2,78)} = 3.57$ $p = 0.033$, Fisher LSD post hoc analysis placebo vs. 20 mg/kg/day $p \leq 0.001$, placebo vs. 100 mg/kg/day n.s. $p = 0.002$, 20 mg/kg/day vs. 100 mg/kg/day $p = 0.02$, Fig 4 A).

Furthermore, a $pEA\beta_{(3-42)}$ specific ELISA was accomplished to investigate, whether RD2 treatment had any influence on $pEA\beta_{(3-42)}$ concentrations in different brain homogenate fractions. The biochemical analysis revealed a significant increase of $pEA\beta_{(3-42)}$ in the DEA-soluble fraction of 20 mg/kg/day RD2-treated mice compared to placebo- and 100 mg/kg/day RD2-treated mice. This difference also has an significant impact on total $pEA\beta_{(3-42)}$ levels of 20 mg/kg/day RD2-treated mice (two-way ANOVA, $F_{(2,78)} = 15.59$, $p \leq 0.001$, Fisher LSD post hoc analysis DEA-fraction placebo vs. 20 mg/kg/day $p \leq 0.001$, placebo vs. 100 mg/kg/day n.s. $p = 0.5$, 20 mg/kg/day vs. 100 mg/kg/day $p < 0.001$, total $pEA\beta_{(3-42)}$ placebo vs. 20 mg/kg/day $p \leq 0.001$, placebo vs. 100 mg/kg/day n.s. $p = 0.5$, 20 mg/kg/day vs. 100 mg/kg/day $p < 0.001$, Fig. 3 B). Neither a difference in the Tris-soluble, nor in the FA-fraction was detected between all treatment groups (Fig. 4 B). One point worthy of note, however, is that the concentration of total $pEA\beta_{(3-42)}$, compared to all $A\beta_{(x-42)}$ species is only about 1 %.

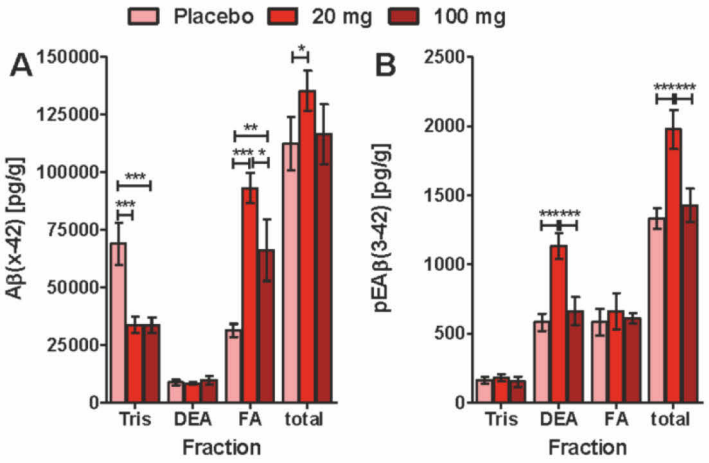

Fig. 4: Effects of RD2 treatment on $A\beta_{(x-42)}$ and $pEA\beta_{(3-42)}$ levels in brains of homozygous TBA2.1 mice. Levels of $A\beta_{(x-42)}$ and $pEA\beta_{(3-42)}$ were analysed in the Tris-, diethanolamine (DEA)-, and formic acid (FA)-fractions by ELISA of placebo- and RD2-treated homozygous TBA2.1 mice. Analysis of $A\beta_{(x-42)}$ resulted in a significant decrease of soluble $A\beta_{(x-42)}$ in the Tris-fraction of 20 and 100 mg/kg/day treated homozygous TBA2.1 mice, compared to their placebo treated littermates. Furthermore, a significant increase of insoluble $A\beta_{(x-42)}$ in the FA-fraction of 20 and 100 mg/kg/day homozygous TBA2.1 mice was demonstrated. Analysis of $pEA\beta_{(3-42)}$ revealed a significant increase in the DEA-faction of 20 mg/kg/day RD2-treated mice compared to placebo- and 100 mg/kg/day RD2-treated mice. Concentrations are given as pg $pEA\beta_{(3-42)}$/g brain. Data is represented as mean ± SEM, two-way ANOVA with Fisher post hoc analysis, *p < 0.05, **p < 0.01, ***p < 0.001.

In order to figure out, whether there is a possible relationship between the individual phenotype and the Aβ–levels in brain, we correlated the SHIRPA scores and the $A\beta_{(x-42)}$ and $pEA\beta_{(3-42)}$ concentrations with each other. A RD2-induced improvement of the phenotype correlated significantly with a decrease of soluble $A\beta_{(x-42)}$ species (p = 0.01), as well as with increased insoluble $A\beta_{(x-42)}$ (p = 0.03) (Tab. 2). No significant correlations were observed between the $pEA\beta_{(3-42)}$ concentrations in either brain fraction, or $A\beta_{(x-42)}$ in the DEA-faction and the SHIRPA scores of the mice (Tab. 2).

	$A\beta_{(x-42)}$			$pEA\beta_{(3-42)}$		
	Tris	DEA	FA	Tris	DEA	FA
SHIRPA-Score	r = 0.51 **	r = - 0.17	r = - 0.46 *	r = - 0.012	r = - 0.1	r = - 0.13

Table 2: Correlation between SHIRPA Scores and $A\beta_{(x-42)}$ or $pEA\beta_{(3-42)}$ levels.
r = Pearson correlation coefficient
*p ≤ 0.05
**p ≤ 0.01

Discussion

Convincing evidence suggests a crucial role for Aβ oligomers for the development and progression of AD (Ferreira and Klein, 2011; Ferreira et al., 2015; Haass and Selkoe, 2007a; Salahuddin et al., 2016; Selkoe and Hardy, 2016; Wang et al., 2016). Thus, compounds that eliminate Aβ oligomers are thought to be an auspicious treatment option (Rosenblum, 2014). RD2, a compound solely consisting of D-enantiomeric amino acid residues, was developed for the specific and direct elimination of toxic Aβ oligomers. In previous studies, it was demonstrated that RD2 enhanced cognition in different AD mouse models, even after oral administration (Kutzsche et al., 2017; van Groen et al., 2017a). After those successful RD2 treatment studies that had previously been conducted in transgenic AD mouse models with typical amyloid pathology and cognitive deficits (Kutzsche et al., 2017; van Groen et al., 2017b), we here decided to challenge our Aβ oligomer eliminating compound RD2 with $pEA\beta_{(3-42)}$ in homozygous TBA2.1 mice. The TBA2.1 AD mouse model develops a neurodegenerative phenotype manifested in severe motor deficits (Alexandru et al., 2011). TBA2.1 mice producing the extremely aggregation-prone Aβ species $pEA\beta_{(3-42)}$, develop small Aβ aggregates and neurodegeneration. N-terminally truncated and pE-modified Aβ isoforms are of relevance for AD, since they are suggested to play a decisive part in the pathology (Bayer and Wirths, 2014; Gunn et al., 2010). Within a previous intraperitoneal treatment study, it could be demonstrated that D-enantiomeric peptides, i.e. the lead compound D3 and its derivative D3D3, were able to significantly slow down the progression of the phenotype of homozygous TBA2.1 mice (Brener et al., 2015; Dunkelmann et al., 2017).

As described previously, RD2 binds to $A\beta_{(1-42)}$ with micromolar affinity (van Groen et al., 2017a), and inhibits the $A\beta_{(1-42)}$ fibril formation with an IC_{50} of 7.7 µm (van Groen et al., 2017a). To clarify, whether RD2 is able to bind to $pEA\beta_{(3-42)}$ and to inhibit the $pEA\beta_{(3-42)}$ aggregation *in vitro*, SPR spectroscopy and ThT-assays were conducted, resulting in a K_D of 26.6 µM and an IC_{50} value for $pEA\beta_{(3-42)}$ aggregation inhibition of 0.7 µM, which is clearly substochiometric for $pEA\beta_{(3-42)}$ and based on the Hill coefficient also highly cooperative. Compared to the results of the lead compound D3, RD2 exhibits a similar binding affinity to $pEA\beta_{(3-42)}$ as the lead compound (K_D 19.9 µM) (Dunkelmann et al., 2017). For the first time, we demonstrate here that one of our developed D-peptides is able to efficiently inhibit the $pEA\beta_{(3-42)}$ fibril formation *in vitro*.

Encouraged by the convincing *in vitro* results and the successful treatment studies in other AD mouse models, we here investigated the efficacy of RD2 treatment on the $pEA\beta_{(3-42)}$–induced neurodegenerative phenotype in homozygousTBA2.1 mice. Moreover, we examined the specificity and potential side effects by including also wildtype mice (non-transgenic littermates) into the study. Therefore, homozygous TBA2.1 mice and their non-transgenic littermates were orally treated with placebo or two different dosages of RD2 once daily for twelve weeks. Shortly before the treatment (baseline), in the middle of (after six weeks) and at the end (after twelve weeks) of the treatment period, several behavioural tests were performed to investigate RD2's influence on the neurodegenerative phenotype of the mice. By comparison of the behavioural results of placebo-treated homozygous TBA2.1 mice and non-transgenic littermates, a significant progression of the neurodegenerative phenotype in untreated mice was ensured, which was in concordance with previously published results (Alexandru et al., 2011; Dunkelmann et al., 2017).

None of the conducted behavioural assessments revealed a difference between placebo- and RD2-treated non-transgenic littermates, confirming that RD2 has no negative impact on the behaviour of wildtype mice. Consequently, it can be assumed that RD2 treatment did not cause any adverse side effects, even by administering moderate till high doses over a long treatment period. Moreover, it confirms the specificity of the compound for Aβ.

Observations regarding the behaviour of RD2-treated homozygous TBA2.1 mice in comparison to placebo-treated mice strengthen the potential therapeutic efficacy of RD2. The observed results of almost all conducted experiments revealed a significantly improved phenotype of RD2- compared to placebo-treated homozygous TBA2.1 mice at the end of the treatment period, regardless of the administered RD2 dose. Thus, RD2 treatment significantly slowed down the progression of the neurodegenerative phenotype of homozygous TBA2.1 mice, especially observable in the SHIRPA test battery.

To investigate the causal reason of the amelioration of the phenotype of homozygous TBA2.1 mice due to RD2 treatment, we performed additional immunohistochemical and biochemical analyses. Immunohistochemical investigations of neurodegeneration, Aβ pathology, and gliosis in the brains resulted in no significant difference between all tested groups in all analysed regions. By trend, a reduction of Aβ particles within the striatum of RD2-treated mice (100 mg/kg/day) was measureable. Thus, a reduction of Aβ particles and accompanied neuroinflammation in brain seemed not to be the main mode of action. This is in accordance with previous results in other AD mouse models after treatment with RD2 (Kutzsche et al., 2017; van Groen et al., 2017a).

By using an $A\beta_{(x-42)}$ specific ELISA, we were able to give further hints to the potential mode of action of RD2. We suggest that RD2 binds to monomeric $A\beta_{(1-42)}$ and $pEA\beta_{(3-42)}$, thus shifting the equilibrium from toxic Aβ oligomers away either to non-toxic Aβ monomers or other non-toxic Aβ RD2 co-assemblies, which at least under non-physiological *in vitro* conditions are high molecular weight, non-toxic, and non-amyloidogenic co-precipitates (Funke et al., 2010). Those co-precipitates, if formed *in vivo* too, can be hypothesized to be found in the formic acid-fraction of the brain homogenates. According to this hypothesis we conclude successful *in vivo* target engagement underlined by the results of the $A\beta_{(x-42)}$ specific ELISA. We were able to demonstrate a significant reduction of soluble Aβ species in the Tris-fraction, which also contains soluble Aβ oligomers, at both administered RD2 doses and an increase in the insoluble formic acid-fraction. Those observations are strengthened by a significant positive correlation of the ameliorated phenotype of RD2-treated mice and a decrease in Tris-soluble $A\beta_{(x-42)}$, and by a negative correlation of the ameliorated phenotype of RD2-treated mice and an increase of insoluble $A\beta_{(x-42)}$ species.

Total $pEA\beta_{(3-42)}$ amounts found in the brain homogenates of TBA2.1 mice were much lower in comparison to the $A\beta_{(x-42)}$ levels, which may contain mainly unconverted $A\beta_{(Q3-42)}$. This is not surprising and has already been described by Alexandru and colleagues (Alexandru et al., 2011). Results of a $pEA\beta_{(3-42)}$ ELISA yielded surprisingly significant higher amounts of $pEA\beta_{(3-42)}$ in the DEA-fraction of RD2-treated (20 mg/kg/day) mice compared to the higher RD2 dose (100 mg/kg/day) and the placebo-treated mice. Although this is hard to explain without further data at hand, one potential and

very hypothetical explanation might be that RD2 binding to $A\beta_{(x-42)}$ leads to two consequences that interfere with each other. TBA2.1 mice are expressing $A\beta_{(Q3-42)}$, which in turn is post-translationally modified to $pEA\beta_{(3-42)}$ by the enzyme glutaminyl cyclase (QC). At the lower dose (20 mg/kg), RD2 might just keep a higher fraction of $A\beta_{(Q3-42)}$ in solution making it more amenable to QC mediated conversion into $pEA\beta_{(3-42)}$. At higher doses (100 mg/kg), RD2 might bind so efficiently to $A\beta_{(Q3-42)}$ that it might either be precipitated or covered from access to QC, both leading to decreased conversion to $pEA\beta_{(3-42)}$. The obtained results in this study are well in line with the *in vivo* efficacy of RD2 published before (Kutzsche et al., 2017; van Groen et al., 2017a). In two previous treatment studies with two AD mouse models with cognitive deficits (APP/PS1 and APP_{SL}), RD2 was able to enhance cognition without changing the typical AD-associated pathology (Aβ plaque load, inflammation) (Kutzsche et al., 2017; van Groen et al., 2017b). The results presented here add a third mouse model and demonstrate *in vivo* efficacy of RD2 against $pEA\beta_{(3-42)}$ induced deficits. Growing evidence exists for Aβ oligomers as the disease causing agent of AD, responsible for progression of the disease and cognitive decline (Ferreira and Klein, 2011; Ferreira et al., 2015). Within previous studies we could demonstrate that RD2, and the lead compound D3 are capable to bind to Aβ monomers, thus eliminated toxic Aβ oligomers and converted them into non-toxic, non amyloidogenic forms (Brener et al., 2015; Funke et al., 2010). Our suggested mode of action, the direct and specific elimination of Aβ oligomers, by stabilising Aβ monomers and thus shifting away the equilibrium form Aβ oligomers to Aβ monomers in non-toxic co-precipitates, was underpinned by the results given in this study. We revealed a significant decrease of soluble and an increase of insoluble Aβ species. As a consequence of the current and previous studies one could speculate that RD2 improved the corresponding phenotypes without changing pathology. Based on the *in vitro* Aβ oligomer elimination efficacy of RD2 a likely explanation is that RD2 reduces synaptic toxicity by reducing the amount of toxic Aβ oligomers *in vivo* (Townsend et al., 2006; Walsh et al., 2002; Wang et al., 2016).

Conclusion

In this study, the *in vivo* efficacy of two different RD2 concentrations (20 and 100 mg/kg/day) on the $pEA\beta_{(3-42)}$ induced neurodegenerative motor phenotype of homozygous TBA2.1 mice was investigated. RD2 treatment led to a deceleration of phenotype progression. Furthermore, RD2 treatment of the non-transgenic littermates did not reveal any noticeable adverse drug reaction. Thus, the results of this and previous RD2 treatment studies reinforce RD2's Aβ oligomer targeting efficacy and further suggest this compound as a possible new drug candidate for a new treatment strategy against AD.

Material and Methods

Affinity determination

Binding affinity of RD2 to monomeric $pEA\beta_{(3-42)}$ using surface plasmon resonance (SPR) spectroscopy was performed as described before (Dunkelmann et al., 2017) with a concentration ranging of RD2 from 0.41 µM to 300 µM.

IC_{50} determination

Inhibitory function of $pEA\beta_{(3-42)}$ fibril formation by RD2 was assessed using Thioflavin T (ThT). $pEA\beta_{(3-42)}$ was recombinantly expressed and purified as described before (Dammers et al., 2015), dissolved in HFIP overnight to destroy any pre-existing aggregates, and lyophilized. For fibril formation, $pEA\beta_{(3-42)}$ (5 µM) was dissolved in 20 mM sodium phosphate buffer including 50 mM sodium chloride and 5 µM ThT, pH 7.4, in the presence or absence of RD2. RD2 concentrations ranged from 100 µM to 0.2 nM. The assay was conducted in non-binding 96-well plates (Greiner, Austria) under quiescent conditions. The fluorescence was monitored over 21 h every 5 min at λ_{ex} = 440 nm and λ_{em} = 490 nm in a fluorescence plate reader (Polarstar Optima, Germany) at 37 °C. For evaluation, the fibril masses at the end of this time period were normalized to the Aβ control. The IC_{50} was calculated by plotting the inhibition in % against the RD2 concentration and data were fitted using a logistic fit model (OriginPro 8.5G, OriginLab, USA). The Hill slope was calculated by using a fit model GraphPad Prism 5 (GraphPad Software, Inc., La Jolla, USA).

Ethical approval

All animal experiments were performed in accordance with the German Law on the protection of animals (TierSchG §§ 7–9) and were approved by a local ethics committee (Landesamt für Natur, Umwelt und Verbraucherschutz Nordrhein-Westfalen (LANUV), North-Rhine-Westphalia, Germany, Az: 84-02.04.2014.362 and Az: 84-02.04.2011.A359).

Mice

In this study, the TBA2.1 mouse model was used, which was first introduced by Alexandru et al. (Alexandru et al., 2011). The mice were originally described on a C57BL/6 x DBA1 background and in house further crossed to C57BL/6 background for more than four generations. As described by Alexandru et al., TBA2.1 mice express $A\beta_{(Q3-42)}$ into neuronal tissue based on murine Thy1.2 regulatory sequences. For the generation of $pEA\beta_{(3-42)}$, $A\beta_{(Q3-42)}$ is posttranslationally modified spontaneously or by the endogenous glutaminyl cyclase (Alexandru et al., 2011). The behavioural phenotype is described by severe motor deficits starting at the age of 2 months which progress further until 5 months of age, and enormous neurodegeneration, especially observable in the hippocampal CA1 region (Alexandru et al., 2011). TBA2.1 mice were a generous gift of Probiodrug and bred in-house by mating of heterozygous mice. Female two months old non-transgenic littermates and homozygous TBA2.1 mice were treated for twelve weeks in the present study.

During the study, all mice were housed with maximal four mice per cage in a controlled environment on a light/dark cycle (12/12 h), with 54% humidity and a temperature of 22 °C. Food and water were available *ad libitum*.

Peptide

RD2 was purchased as lyophilized powder with acetate as counter ion from CBL Patras (Patras, Greece). The amino acid sequence is as follows: H-ptlhthnrrrrr-NH2.

Treatment

Non-transgenic littermates and homozygous TBA2.1 mice were treated orally for twelve weeks (daily) either with placebo (n = 8) (drinking water), 20 mg/kg RD2 (n = 8) or 100 mg/kg RD2 (n = 8), all formulated in tailor-made gelatine-jellies (30% sucrose, 10% sucralose, 18.75% instant gelatine (Dr. Oetker, Bielefeld, Germany), total volume approximately 200 µl with 50 µl compound or placebo solution). The RD2 amount in the jellies was weekly adjusted to the average body weight of the mice to achieve as close as possible a daily dose of 20 or 100 mg/kg. For example, each jelly for the 20 mg/kg/day RD2 treatment group contained 0.4 mg RD2 in 50 µl in the last week of treatment. The mice ate each single jelly completely and voluntarily. Thus, it was ensured that each mouse had incorporated the appropriate amount of RD2 daily over twelve weeks.

Behavioural assessments

Each behavioural test was performed before treatment (baseline measurements and to randomise the mice), after six weeks of treatment (middle) and within the last week (after) of the twelve-week treatment period. In each test, all groups of homozygous TBA2.1 mice, and non-transgenic littermates were tested. Mice were inspected daily and body weight of each mouse was recorded weekly.

Open field test. By performance of an open field test it is possible to evaluate the locomotive and explorative behaviour of mice. Therefore, mice were placed in a square-shaped arena (44 cm x 44 cm x 44 min). For evaluation, the arena was imaginarily divided into two departments: centre and border (centre: 22 cm x 22 cm, border: 44 cm x 44 cm). The mice were allowed to explore the arena for 30 min. Recording was performed with a camera driven tracking system (Ethovision 11, Noldus, Wageningen, The Netherlands).

SHIRPA. A subset of tests from the SHIRPA (SmithKline Beecham, Harwell, Imperial College and Royal London Hospital phenotype assessment) test battery (Rogers et al., 1997) was conducted to evaluate a possible change of the phenotype of homozygous TBA2.1 mice or non-transgenic littermates due to RD2 treatment compared to the phenotype of placebo-treated mice. Following subtests and observations were chosen: body carriage, alertness, gait, startle response, righting reflex, touch response, pinna reflex, cornea reflex, forelimb placing reflex, hanging behaviour, and pain response. Each mouse was evaluated with a defined scoring system (0: no abnormalities, 3: extraordinary abnormalities), the sum was used for analysis.

Clasping test. Analysis of the innate clasping behaviour was conducted by lifting the mice up by the tail for 15 s. Trembling and/or cramping of the hind limbs was observed and scored 0: no abnormalities, 3: extraordinary abnormalities). The described procedure was performed three times and the sum of all three scores was used for analysis.

Pole test. In this study, a slightly modified version of the standard pole test was used to further evaluate the motor performance of the mice [10, 11]. Distinguished from the typical protocol, mice were placed head downwards instead of upwards on a vertical pole (height 50 cm, diameter 1.2 cm, rough-surfaced). Their movement downwards the pole was rated with a defined scoring system (0: continuous run, 1: part-way run, 2: slipping downwards, 3: falling down). This procedure was performed three times with an interval of 15 min between each run. The sum of all three scores was used for analysis.

Rotarod. Motor coordination of the treated and untreated homozygous TBA2.1 mice, as well as treated and untreated non-transgenic littermates was evaluated by use of a rotarod apparatus (Ugo Basile Srl, Comerio VA, Italy) and a previously published protocol. In brief, mice were tested on two consecutive days with one training session, and one test session on the first day, and two test sessions on the second day. During the training on the first morning, the mice had to stay on the rod for at least 60 s at constant 10 rpm. In the afternoon as well as on the next day morning and afternoon, the mice had to run in three trials on the beam accelerating from 4 to 40 rpm. The total time on the beam of each trial was used for analysis and the maximum time was 5 min.

Tissue collection.

Mice were anesthetized with isoflurane and sacrificed. Organs were assessed by visual inspection (macroscopic investigations) for any abnormalities, e.g. tumorous changes, inflammatory signs, and necrosis. Afterwards, brains were taken, cut into hemispheres and snap frozen in isopentane. Right hemispheres were used for biochemical analysis, and left hemispheres were used for immunohistochemistry (IHC).

Immunohistochemistry and biochemical analysis

Immunohistochemistry. Immunohistological analysis was performed on 20 µm sagittal frozen brain sections of homozygous and non-transgenic placebo- and RD2-treated TBA2.1 mice. In brief, the sections were thawed to room temperature and fixed in 4% paraformaldehyde for 10 min. In the following, antigen retrieval was carried out by incubation in 70% formic acid (5 min). Elimination of endogenous peroxidases was ensured by incubation in 3% H_2O_2 in methanol (15 min). In between these steps, the sections were washed three times with 1% Triton in TBS (TBST) for 5 min, respectively. Incubation with the primary antibodies (6E10: 1:2500, Bio Legend, San Diego, USA; GFAP: 1:1000, DAKO, Agilent Technologies, Santa Clara, USA, NeuN, 1:1000, Merck, Germany; CD11b 1:2500, Abcam, UK) diluted in TBST with 1% bovine serum albumin (BSA) was performed in a humid chamber at 4 °C over night. The next day, incubation with the biotinylated secondary anti-mouse- or anti-rabbit-antibody (both 1:1000 in TBST + 1% BSA, Sigma-Aldrich, Darmstadt, Germany) was performed at room temperature for 2 h. Staining was visualized by use of 3, 3'-Diaminobenzidine,

enhanced with saturated nickel ammonium sulphate solution. Finally, the sections were washed in an ascending alcohol series and mounted with DPX Mountant (Sigma-Aldrich, Darmstadt, Germany).

Quantification. All slides were stained in one staining procedure and microscope recordings were done in one microscope session to avoid differences in staining intensity and light exposure. A Zeiss SteREO Lumar V12 microscope and the according software (Zeiss AxioVision 6.4 RE) or a Leica LMD6000 microscope (LAS 4.0 software) were used for recording. Quantification was performed with ImageJ (National Institute of Health, Bethesda, USA). Aβ particles were analysed in the striatum, motor cortex, hippocampal CA1 region, and midbrain (inferior colliculus) (7 to 8 slides per mice, placebo n = 7, RD2 20 mg n = 8, RD2 100 mg n = 7). NeuN immune reactive area (percent stained area) was analysed in the striatum, motor cortex, and hippocampal CA1 region (7 to 8 slides per mice, placebo n = 8, RD2 20 mg n = 7, RD2 100 mg n = 7). GFAP immune reactive area (percent stained area) was analysed in the motor cortex, and hippocampal CA1 region (7 to 8 slides per mice, placebo n = 8, RD2 20 mg n = 8, RD2 100 mg n = 8). CD11b immune reactive area (percent stained area) was analysed in the midbrain (inferior colliculus), and brain stem (7 to 8 slides per mice, placebo n = 8, RD2 20 mg n = 7, RD2 100 mg n = 8).

ELISA. The right brain hemispheres of placebo- or RD2-treated mice were chosen for $A\beta_{(x-42)}$ and pyroglutamate Aβ ($pEA\beta_{(3-42)}$) biochemical analysis. Therefore, the hemispheres were fractionated into three fractions: Tris-, diethanolamine (DEA)-, and formic acid (FA)-fraction. At first, the hemispheres were homogenized in nine volume parts of Tris buffer (pH 8.3, containing 20 mM Tris, 250 mM NaCl, protease and phosphatase inhibitors (both Roche, Basel, Switzerland)) for 2 x 20 s at 6500 rpm. After sonification (5 min) the homogenized samples were centrifuged (30 min, 175.000 x g, 4 °C). Supernatant was collected and constitutes as Tris-fraction. To obtain the DEA-fraction, the pellet was dissolved in 2% DEA, incubated for 1 h on ice and centrifugation for 30 min at 175.000 x g at 4 °C. The supernatant constitutes as DEA-fraction and the pellet was dissolved in 70% FA. After incubation on ice (1 h) and another centrifugation step (30 min, 175.000 x g, 4 °C), the resulting supernatant constitutes the FA-fraction, which was neutralized before usage in the ELISA. All three fractions were snap frozen in liquid nitrogen and stored at -80 °C until further processing. The pyroglutamate Aβ ELISA N3pE-42 was purchased from IBL (IBL International GmbH, Germany) and the $A\beta_{(x-42)}$ ELISA was purchased from BioLegend (BioLegend, San Diego, CA, USA), and performed according to the manufacturer's protocol with the three fractions of all treatment groups (placebo n = 8, RD2 20 mg n = 8, RD2 100 mg n = 8) described above and each sample was measured in triplicate.

Statistical calculations

Descriptive statistical analysis was performed on all evaluated parameters. Data is represented as the average mean ± SD (*in vitro*), or SEM (*in vivo*). All calculations were performed by use of OriginPro 8.5G (OriginLab, USA), or SigmaPlot Version 11 (Systat Software, Germany), $p > 0.05$ was considered as not significant (n.s.). Normal distributed data was analysed with one-way ANOVA with Fisher post hoc analysis. Two-way or two-way repeated measure (RM) ANOVA with Fisher post hoc analysis was used to analyse parts of the *in vivo* study.

Data availability

The data that support the findings of this study are not available from the corresponding author upon request.

Author contributions

A.W., S.S., D.W., and J.K. planed the overall study. S.S. performed and analysed the treatment study, ELISA experiments, and immunohistochemistry with help of E.S. and D.H.. T.Z. conducted the SPR measurements and ThT assays. S.S., A.W., and D.W. wrote the initial manuscript with scientific advice of J.K., C.Z., N.J.S. and K-J.L.. All authors contributed to writing and reviewed the manuscript.

Acknowledgements

We thank Probiodrug for providing us the TBA2.1 mice. Additionally, we thank the Forschungszentrum Jülich animal facility for their excellent care.

Funding

D.W. was supported by the "Portfolio Technology and Medicine" and the Helmholtz-Validierungsfonds of the Impuls and Vernetzungs-Fonds der Helmholtzgemeinschaft. D.W. and K.-J.L. were supported by the "Portfolio Drug Research" of the Impuls and Vernetzungs-Fonds der Helmholtzgemeinschaft.

Conflict of Interest

The authors declare no competing interests.

References

Alexandru, A., Jagla, W., Graubner, S., Becker, A., Bauscher, C., Kohlmann, S., Sedlmeier, R., Raber, K.A., Cynis, H., Ronicke, R., *et al.* (2011). Selective hippocampal neurodegeneration in transgenic mice expressing small amounts of truncated Abeta is induced by pyroglutamate-Abeta formation. J Neurosci 31, 12790-12801.

Bayer, T.A., and Wirths, O. (2014). Focusing the amyloid cascade hypothesis on N-truncated Abeta peptides as drug targets against Alzheimer's disease. Acta neuropathologica 127, 787-801.

Brener, O., Dunkelmann, T., Gremer, L., van Groen, T., Mirecka, E.A., Kadish, I., Willuweit, A., Kutzsche, J., Jurgens, D., Rudolph, S., *et al.* (2015). QIAD assay for quantitating a compound's efficacy in elimination of toxic Abeta oligomers. Scientific reports 5, 13222.

Dammers, C., Gremer, L., Neudecker, P., Demuth, H.U., Schwarten, M., and Willbold, D. (2015). Purification and Characterization of Recombinant N-Terminally Pyroglutamate-Modified Amyloid-beta Variants and Structural Analysis by Solution NMR Spectroscopy. PloS one 10, e0139710.

Dammers, C., Reiss, K., Gremer, L., Lecher, J., Ziehm, T., Stoldt, M., Schwarten, M., and Willbold, D. (2017a). Pyroglutamate-Modified Amyloid-beta(3-42) Shows alpha-Helical Intermediates before Amyloid Formation. Biophysical journal 112, 1621-1633.

Dammers, C., Schwarten, M., Buell, A.K., and Willbold, D. (2017b). Pyroglutamate-modified Abeta(3-42) affects aggregation kinetics of Abeta(1-42) by accelerating primary and secondary pathways. Chemical science 8, 4996-5004.

Dunkelmann, T., Schemmert, S., Honold, D., Teichmann, K., Butzkuven, E., Demuth, H.U., Shah, N.J., Langen, K.J., Kutzsche, J., Willbold, D., and Willuweit, A. (2018). Comprehensive Characterization of the Pyroglutamate Amyloid-beta Induced Motor Neurodegenerative Phenotype of TBA2.1 Mice. Journal of Alzheimer's disease : JAD.

Dunkelmann, T., Teichmann, K., Ziehm, T., Schemmert, S., Frenzel, D., Tusche, M., Dammers, C., Jurgens, D., Langen, K.J., Demuth, H.U., *et al.* (2017). Abeta oligomer eliminating compounds interfere successfully with pEAbeta(3-42) induced motor neurodegenerative phenotype in transgenic mice. Neuropeptides.

Ferreira, S.T., and Klein, W.L. (2011). The Abeta oligomer hypothesis for synapse failure and memory loss in Alzheimer's disease. Neurobiology of learning and memory 96, 529-543.

Ferreira, S.T., Lourenco, M.V., Oliveira, M.M., and De Felice, F.G. (2015). Soluble amyloid-beta oligomers as synaptotoxins leading to cognitive impairment in Alzheimer's disease. Frontiers in cellular neuroscience 9, 191.

Frost, J.L., Le, K.X., Cynis, H., Ekpo, E., Kleinschmidt, M., Palmour, R.M., Ervin, F.R., Snigdha, S., Cotman, C.W., Saido, T.C., *et al.* (2013). Pyroglutamate-3 Amyloid-β Deposition in the Brains of Humans, Non-Human Primates, Canines, and Alzheimer Disease–Like Transgenic Mouse Models. The American journal of pathology 183, 369-381.

Funke, S.A., van Groen, T., Kadish, I., Bartnik, D., Nagel-Steger, L., Brener, O., Sehl, T., Batra-Safferling, R., Moriscot, C., Schoehn, G., *et al.* (2010). Oral treatment with the d-enantiomeric peptide D3 improves the pathology and behavior of Alzheimer's Disease transgenic mice. ACS chemical neuroscience 1, 639-648.

Godyn, J., Jonczyk, J., Panek, D., and Malawska, B. (2016). Therapeutic strategies for Alzheimer's disease in clinical trials. Pharmacological reports : PR 68, 127-138.

Gunn, A.P., Masters, C.L., and Cherny, R.A. (2010). Pyroglutamate-Abeta: role in the natural history of Alzheimer's disease. The international journal of biochemistry & cell biology 42, 1915-1918.

Haass, C., and Selkoe, D.J. (2007a). Soluble protein oligomers in neurodegeneration: lessons from the Alzheimer's amyloid beta-peptide. Nature reviews Molecular cell biology 8, 101-112.

Haass, C., and Selkoe, D.J. (2007b). Soluble protein oligomers in neurodegeneration: lessons from the Alzheimer's amyloid β peptide. Nat Rev Mol Cell Biol 8, 101-112.

Jawhar, S., Wirths, O., and Bayer, T.A. (2011). Pyroglutamate amyloid-beta (Abeta): a hatchet man in Alzheimer disease. The Journal of biological chemistry 286, 38825-38832.

Kumar, A., Singh, A., and Ekavali (2015). A review on Alzheimer's disease pathophysiology and its management: an update. Pharmacological reports : PR 67, 195-203.

Kutzsche, J., Schemmert, S., Tusche, M., Neddens, J., Rabl, R., Jurgens, D., Brener, O., Willuweit, A., Hutter-Paier, B., and Willbold, D. (2017). Large-Scale Oral Treatment Study with the Four Most Promising D3-Derivatives for the Treatment of Alzheimer's Disease. Molecules (Basel, Switzerland) 22.

Leithold, L.H., Jiang, N., Post, J., Ziehm, T., Schartmann, E., Kutzsche, J., Shah, N.J., Breitkreutz, J., Langen, K.J., Willuweit, A., and Willbold, D. (2016). Pharmacokinetic Properties of a Novel D-Peptide Developed to be Therapeutically Active Against Toxic beta-Amyloid Oligomers. Pharmaceutical research 33, 328-336.

Nussbaum, J.M., Schilling, S., Cynis, H., Silva, A., Swanson, E., Wangsanut, T., Tayler, K., Wiltgen, B., Hatami, A., Ronicke, R., *et al.* (2012). Prion-like behaviour and tau-dependent cytotoxicity of pyroglutamylated amyloid-beta. Nature 485, 651-655.

Perez-Garmendia, R., and Gevorkian, G. (2013). Pyroglutamate-Modified Amyloid Beta Peptides: Emerging Targets for Alzheimer s Disease Immunotherapy. Current neuropharmacology 11, 491-498.

Prince, M., Wimo, A., Guerchet, M., Ali, G.-M., Wu, Y.-T., and Prina, M. (2015). World Alzheimer Report 2015. The Global Impact of Dementia. An Analysis of Prevalence, Incidence, Costs and Trends. Alzheimer's Disease International.

Rogers, D.C., Fisher, E.M.C., Brown, S.D.M., Peters, J., Hunter, A.J., and Martin, J.E. (1997). Behavioral and functional analysis of mouse phenotype: SHIRPA, a proposed protocol for comprehensive phenotype assessment. Mammalian Genome 8, 711-713.

Roher, A.E., Kokjohn, T.A., Clarke, S.G., Sierks, M.R., Maarouf, C.L., Serrano, G.E., Sabbagh, M.S., and Beach, T.G. (2017). APP/Abeta structural diversity and Alzheimer's disease pathogenesis. Neurochemistry international 110, 1-13.

Rosenblum, W.I. (2014). Why Alzheimer trials fail: removing soluble oligomeric beta amyloid is essential, inconsistent, and difficult. Neurobiology of aging 35, 969-974.

Salahuddin, P., Fatima, M.T., Abdelhameed, A.S., Nusrat, S., and Khan, R.H. (2016). Structure of amyloid oligomers and their mechanisms of toxicities: Targeting amyloid oligomers using novel therapeutic approaches. European journal of medicinal chemistry 114, 41-58.

Schilling, S., Lauber, T., Schaupp, M., Manhart, S., Scheel, E., Bohm, G., and Demuth, H.U. (2006). On the seeding and oligomerization of pGlu-amyloid peptides (in vitro). Biochemistry 45, 12393-12399.

Selkoe, D.J., and Hardy, J. (2016). The amyloid hypothesis of Alzheimer's disease at 25 years. EMBO molecular medicine 8, 595-608.

Thal, D.R., Capetillo-Zarate, E., Del Tredici, K., and Braak, H. (2006). The Development of Amyloid β Protein Deposits in the Aged Brain. Sci Aging Knowl Environ.

Townsend, M., Shankar, G.M., Mehta, T., Walsh, D.M., and Selkoe, D.J. (2006). Effects of secreted oligomers of amyloid beta-protein on hippocampal synaptic plasticity: a potent role for trimers. The Journal of physiology 572, 477-492.

van Groen, T., Kadish, I., Funke, S.A., Bartnik, D., and Willbold, D. (2013). Treatment with D3 removes amyloid deposits, reduces inflammation, and improves cognition in aged AbetaPP/PS1 double transgenic mice. Journal of Alzheimer's disease : JAD 34, 609-620.

van Groen, T., Kadish, I., Wiesehan, K., Funke, S.A., and Willbold, D. (2009). In vitro and in vivo staining characteristics of small, fluorescent, Abeta42-binding D-enantiomeric peptides in transgenic AD mouse models. ChemMedChem 4, 276-282.

van Groen, T., Kadish, I., Funke, A. S., Bartnik, D., Willbold, D. (2012). Treatment with Aβ42 Binding d-Amino Acid Peptides Reduce Amyloid Deposition and Inflammation in APP/PS1 Double Transgenic Mice. Advances in Protein Chemistry and Structural Biology 88, 133-152.

van Groen, T., Schemmert, S., Brener, O., Gremer, L., Ziehm, T., Tusche, M., Nagel-Steger, L., Kadish, I., Schartmann, E., Elfgen, A., *et al.* (2017a). The Abeta oligomer eliminating D-enantiomeric peptide RD2 improves cognition without changing plaque pathology. Scientific reports 7, 16275.

van Groen, T., Schemmert, S., Brener, O., Gremer, L., Ziehm, T., Tusche, M., Nagel-Steger, L., Kadish, I., Schartmann, E., Elfgen, A., *et al.* (2017b). The Aβ oligomer eliminating D-enantiomeric peptide RD2 improves cognition without changing plaque pathology. Scientific reports.

van Groen, T., Wiesehan, K., Funke, S.A., Kadish, I., Nagel-Steger, L., and Willbold, D. (2008). Reduction of Alzheimer's disease amyloid plaque load in transgenic mice by D3, A D-enantiomeric peptide identified by mirror image phage display. ChemMedChem 3, 1848-1852.

Walsh, D.M., Klyubin, I., Fadeeva, J.V., Cullen, W.K., Anwyl, R., Wolfe, M.S., Rowan, M.J., and Selkoe, D.J. (2002). Naturally secreted oligomers of amyloid beta protein potently inhibit hippocampal long-term potentiation in vivo. Nature 416, 535-539.

Wang, Z.X., Tan, L., Liu, J., and Yu, J.T. (2016). The Essential Role of Soluble Abeta Oligomers in Alzheimer's Disease. Molecular neurobiology 53, 1905-1924.

3.9 *In vitro* potency and preclinical pharmacokinetic comparison of all-D-enantiomeric peptides developed for the treatment of Alzheimer's disease

Autoren:	Schartmann E., **Schemmert S.**, Niemietz N., Honold D., Ziehm T., Tusche M., Elfgen A., Gering I., Brener O., Shah N.J., Langen K-J., Kutzsche J., Willbold D., Willuweit A.
Journal:	Journal of Alzheimer's Disease, eingereicht am 15.02.2018
Impact Factor:	3,731 (2016)
Beitrag:	Planung der Studie gemeinsam mit Elena Schartmann
	Durchführung der pharmakokinetischen Experimente gemeinsam mit Elena Schartmann
	statistische Auswertung
	Mitverfassung und Prüfung des Manuskriptes

In vitro potency and preclinical pharmacokinetic comparison of all-D-enantiomeric peptides developed for the treatment of Alzheimer's disease

Elena Schartmann[1], Sarah Schemmert[1], Nicole Niemietz[2], Dominik Honold[1], Tamar Ziehm[1], Markus Tusche[1], Anne Elfgen[1], Ian Gering[1], Oleksandr Brener[1,3], Nadim Joni Shah[2,4], Karl-Josef Langen[2,5], Janine Kutzsche[1], Dieter Willbold[1,3,*], Antje Willuweit[2,*]

[1]*Institute of Complex Systems, Structural Biochemistry (ICS-6), Forschungszentrum Jülich GmbH, 52425 Jülich, Germany*

[2]*Institute of Neuroscience and Medicine, Medical Imaging Physics (INM-4), Forschungszentrum Jülich GmbH, 52425 Jülich, Germany*

[3]*Institut für Physikalische Biologie, Heinrich-Heine-Universität Düsseldorf, 40225 Düsseldorf, Germany*

[4]*Department of Neurology, Faculty of Medicine, JARA, RWTH Aachen University, 52074 Aachen, Germany*

[5]*Department of Nuclear Medicine, Universitätsklinikum der RWTH Aachen, 52074 Aachen, Germany*

Pharmacokinetics of D-enantiomeric peptides

*Correspondence to:

A. Willuweit, Institute of Neuroscience and Medicine, Medical Imaging Physics (INM-4), Forschungszentrum Jülich GmbH, 52425 Jülich, Germany

E-Mail: a.willuweit@fz-juelich.de

Phone: 0049 - 2461 - 6196358

D. Willbold, Institute of Complex Systems, Structural Biochemistry (ICS-6), Forschungszentrum Jülich GmbH, 52425 Jülich, Germany

E-mail: d.willbold@fz-juelich.de

Phone: 0049 - 2461 - 612100

Abstract

Diffusible amyloid-β (Aβ) oligomers are currently presumed to be the most cytotoxic Aβ assembly and held responsible to trigger the pathogenesis of Alzheimer's disease (AD). Thus, Aβ oligomers are a prominent target in AD drug development. Previously, we reported on our solely D-enantiomeric peptide D3 and its derivatives as AD drug candidates. Here, we compare one of the most promising D3 derivatives, ANK6, with its tandem version (tANK6), and its head-to-tail cyclized isoform (cANK6r). *In vitro* tests investigating the D-peptides' potencies to inhibit Aβ aggregation, eliminate Aβ oligomers, and reduce Aβ-induced cytotoxicity revealed that all three D-peptides efficiently target Aβ. Subsequent preclinical pharmacokinetic studies of the three all-D-peptides in wildtype mice showed promising blood-brain barrier permeability with cANK6r yielding the highest levels in brain. The peptides' potencies to lower Aβ toxicity and their remarkable brain/plasma ratios make them promising AD drug candidates.

Keywords

Alzheimer's disease, amyloid-β, D-enantiomeric peptides, pharmacokinetic profile

Introduction

Neurodegenerative diseases caused by the aggregation of misfolded proteins are about to become a threatening risk for our aging society and health care systems. Alzheimer's disease (AD) is one of the most intensively researched progressive neurodegenerative diseases. More than 20 million people worldwide are currently affected by AD and no curative therapy has been developed in the last 110 years since Alois Alzheimer described the disease. This circumstance manifests the extensive medical need for development of a disease modifying or even a curative treatment of AD.

AD is characterized by three major hallmarks: extracellular deposits or plaques consisting of amyloid-β protein (Aβ), intracellular deposits consisting of hyperphosphorylated tau protein, and neurodegeneration. Aβ is natively generated throughout lifetime and able to aggregate, thus forming lower molecular weight soluble Aβ oligomers or insoluble Aβ fibrils that make up the plaques [1]. Since about one decade, researchers entitle soluble oligomers to be the most neurotoxic Aβ species [2]. Both, Aβ and tau, with their formation, aggregation and degradation are prominent targets in AD drug development [3, 4].

In our lab, we identified and developed compounds that specifically and directly eliminate toxic Aβ oligomers. Previously, we described the properties of our lead compound D3 (**Table 1**). D3 consists of twelve D-enantiomeric amino acid residues and has been identified by mirror image phage display [5-9]. It stabilized Aβ monomers in an aggregation-incompetent conformation thus shifting the equilibrium between Aβ monomers and oligomers away from oligomers towards monomers. D3 eliminated Aβ oligomers *in vitro*, improved cognition and lowered Aβ plaque load in transgenic AD mouse models, and revealed promising *in vivo* properties, e.g. extraordinary high proteolytic stability and beneficial pharmacokinetic characteristics [10-22]. In an optimization approach, D3's amino acid residue sequence was systematically replaced by natural and unnatural amino acid residues, using peptide microarrays, and screened for their affinity and specificity to monomeric Aβ. The most

promising seven peptides (ANK1-ANK7) were selected and further investigated *in vitro* awarding ANK6 the most promising properties [23]. Another optimization strategy to increase the peptides' efficiency to eliminate toxic Aβ oligomers as well as to increase pharmacokinetic availability was the head-to-tail cyclization of D3 and various derivatives [24, 25]. Additionally, linear tandem 24-mer D3-derivatives in head-to-tail arrangement were designed, pharmacokinetically investigated [26], and successfully tested *in vitro* as well as *in vivo* to reduce symptoms of AD pathology, even more efficiently than the corresponding 12-mer peptides [19, 26, 27].

Here, we further investigated and characterized the most promising microarray-derived derivative ANK6 and compared it to two ANK6-variants, the head-to-tail linear tandem ANK6 (tANK6) and the head-to-tail cyclic ANK6 with an additional arginine (cANK6r) to maintain the total net charge, thus combining different peptide optimization tools. We conducted *in vitro* experiments that exhibit the D-peptides' impacts on $A\beta_{1-42}$ aggregation (Aβ aggregation assay), on Aβ oligomer elimination (QIAD assay), and on $A\beta_{1-42}$-induced cytotoxicity (cell viability assay). In another pre-*in vivo* test, the D-peptides' plasma protein binding affinities were determined. Thereby, we explored whether ANK6 and its two variants are efficient and non-toxic Aβ-targeting AD drug candidates. Afterwards, pharmacokinetic studies with intravenous (i.v.) and oral (p.o.) D-peptide administration to C57BL/6N mice were carried out to evaluate the D-peptides' eligibility for implementation in further treatment studies. Within the pharmacokinetic studies, special attention was paid to the D-peptides' uptake into the brain and their blood-brain barrier (BBB) permeability.

Materials and Methods

Peptides

Non-labelled peptides ANK6, tANK6, and cANK6r peptides were synthesized by peptides & elephants GmbH (Germany). Radio-labelled ^{3}H-ANK6, ^{3}H-tANK6, and ^{3}H-cANK6r

were produced by Cambridge Research Biochemicals (United Kingdom) with 1 mCi/mL. The peptides' sequences are shown in Table 1. Recombinant $A\beta_{1-42}$ was obtained from Isoloid GmbH (Germany). Synthetic $A\beta_{1-42}$ was obtained from Bachem AG (Switzerland).

D-peptides' *in vitro* potencies

Aβ aggregation assay

ANK6's, tANK6's, cANK6r's, and D3's potency to inhibit $A\beta_{1-42}$ aggregation was examined using Thioflavin T (ThT). For this purpose, a buffer solution composed of 20 mM sodium phosphate buffer (pH 7.4) including 50 mM sodium chloride, and 5 µM ThT was prepared. Afterwards, ANK6, tANK6, cANK6r, or D3 were diluted in this solution, respectively, to final peptide concentrations between 0.3125 and 80 µM (ANK6 and tANK6: 0.3125, 0.625, 1.25, 2.5, 5, 10, 20 µM; cANK6r: 1.25, 2.5, 5, 10, 20, 40, 80 µM; D3: 1.17, 2.34, 4.7, 9.4, 18.8, 37.5, 75 µM). The buffer solution only served as negative control (blank). Lyophilized $A\beta_{1-42}$ was dissolved in the respective peptide solution to a final concentration of 10 µM. D-peptide solutions with the highest concentration of the respective D-peptide containing all components, except of $A\beta_{1-42}$, served as negative controls. $A\beta_{1-42}$ solved in buffer solution without D-peptide served as positive control. 100 µL of each solution were transferred into the wells (triplicates) of 96 well microplates (PS, black, non-binding from Greiner Bio-One, Germany) and fluorescence signals (excitation λ 440 nm, emission λ 490 nm) were measured in a Polarstar Optima plate reader (BMG, Germany) at 37 °C every 20 min for 70 h. Afterwards, the respective blank curves were subtracted from each aggregation curve to exclude background fluorescence. The inhibition potency of each D-peptide's concentration was calculated by normalizing the final fibril mass to the positive control, which shows maximal Aβ aggregation and therefore maximal fluorescence signals (0% Aβ aggregation inhibition). The half maximal inhibitory concentration (IC_{50} value) was determined by plotting the percent inhibition against the respective D-peptides'

concentrations. Datasets were fitted by nonlinear regression (one site – specific binding with Hill slope, GraphPad Prism 5).

Cell viability assay

ANK6's, tANK6's, and cANK6r's ability to neutralize the toxicity of oligomeric $A\beta_{1-42}$ was investigated with 3-(4,5-Dimethylthiazol-2-yl)-2,5-diphenyltetrazoliumbromid (MTT). In this experiment, we used rat phaeochromocytoma cells (PC12 cells, Leibniz Institute DSMZ, Germany) cultivated in DMEM supplemented with 10 % fetal calf serum, 5 % horse serum and 1 % penicillin-streptomycin at 37 °C, 5 % CO_2 and 95 % humidity. The cells (10,000 cells/well) were incubated on collagen coated 96 well plates (Gibco, Life Technologies, # A11428-03) for growth in adherent cell culture (24 h, 37 °C). Oligomeric Aβ was generated by incubating monomeric $A\beta_{1-42}$ in sodium phosphate buffer (10 mM Na_2HPO_4/NaH_2PO_4, pH 7.4) at 21 °C and 600 rpm agitation for 4.5 h. The cell viability was investigated after the incubation with buffer only (positive control, set to 100 % cell viability), Triton X-100 (0.125 %, cytotoxic agent, negative control), $A\beta_{1-42}$ alone (1 µM), ANK6, tANK6, or cANK6r alone (15 µM each), as well as $A\beta_{1-42}$ (1 µM) in the presence of ANK6, tANK6, or cANK6r (each D-peptide in 7 different concentrations varying between 0.008 and 15 µM, in quintuplicates) (overnight, 37 °C) using the Cell Proliferation Kit I (MTT) according to the manufacturer's protocol (Roche, Switzerland). Absorbance readout was detected with a Polarstar Optima plate reader (BMG, Germany) at 570 and 660 nm. The relative cell viability [%] was calculated by normalizing the absorbance readout to the positive control (PC12 cells incubated with buffer). The IC_{50} value was determined by plotting the relative cell viability [%] against the respective D-peptides' concentrations. Datasets were fitted by nonlinear regression (logistic fit; OriginPro 9.0G).

Quantitative determination of interference with Aβ aggregate size distribution

As soluble Aβ oligomers are currently expected to be the most neurotoxic Aβ species causing AD, ANK6's, tANK6's, and cANK6r's $A\beta_{1-42}$ oligomer elimination potency was

investigated by the quantitative determination of interference with Aβ aggregate size distribution (QIAD) similar as described before [19]. In short, lyophilized $A\beta_{1-42}$ was dissolved in sodium phosphate buffer to a final concentration of 80 µM and incubated for 2.5 h (21 °C, 600 rpm) to achieve an Aβ aggregate distribution including monomers, oligomers and higher molecular aggregates. Then, sodium phosphate buffer (control), 20 µM ANK6, 20 µM tANK6, or 20 µM cANK6r were added and incubated for further 40 min (21 °C, 600 rpm). Afterwards, the samples were loaded on top of a density gradient (5 to 50% (w/v) iodixanol, OptiPrep, Axis-Shield, Norway) and ultra-centrifuged for 3 h (4 °C, 259.000 × g, Optima TL-100, Beckman Coulter, USA). In the following, 14 fractions (140 µL each) were taken from top to bottom, whereby the top fractions (1-2) contained Aβ monomers, the middle fractions (4-6) contained the Aβ oligomers of special interest, and the bottom fractions (11-14) contained high molecular weight co-precipitates. The left-over was diluted in 60 µL 6 M guanidine hydrochloride (fraction 15). Finally, the $A\beta_{1-42}$ concentrations in all fractions were determined via analytical RP-HPLC (reversed phase-high performance liquid chromatography) and UV absorbance detection at 214 nm.

Statistical calculation

Statistical analyses were performed using GraphPad Prism 5 (GraphPad Software, Inc., USA) and SigmaPlot Version 11 (Systat Software, Germany). Gaussian distribution was analyzed by use of a normal probability plot (SigmaPlot or InVivoStat by Simon Bate and Robin Clark, United Kingdom) [28]. Data is represented as mean ± SEM, $p > 0.05$ was considered to be not significant. Data was analyzed by one-way ANOVA with Bonferroni post hoc analysis.

Preclinical pharmacokinetic characterization

Plasma protein binding

ANK6's, tANK6's, and cANK6r's plasma protein binding (PPB) to human serum albumin (HSA) and α1-acid glycoprotein (AGP) was analyzed according to the manufacturer's

protocol of TRANSIL^{XL} HSA and AGP binding kits (Sovicell GmbH, Germany). To cover a larger range of HSA and AGP concentrations, the bead concentrations in the kit were modified. For detection, a mixture of ^{3}H-labelled and non-labelled ANK6, tANK6, and cANK6r (final concentrations of 5 µM) was added to different concentrations of HSA (7.4 µM to 420 µM, 10-12 different concentrations) or AGP beads (0.04 µM to 3 µM, 9-12 different concentrations). The amount of unbound ANK6, tANK6, and cANK6r (in %) to HSA or AGP, respectively, was determined by liquid scintillation counter (LSC) measurements. The dissociation constants (K_D) as well as the free drug fractions (f_u) in human plasma were calculated as described before [29]. Calculations were based on peptide concentrations detected in the blood 4 h after single oral administration of 10 mg/kg: 0.01 µM ANK6, 0.01 µM tANK6, and 0.01 µM cANK6r.

Animals

The pharmacokinetic profiles were investigated in 180 male C57Bl/6N mice aged 13-14 weeks, weighing about 27.4 g in average. Mice were ordered at Charles River (Germany) and housed at least one week under standard housing conditions (12/12 h light-dark cycle, approximately 22 °C room temperature and 54% humidity; water and food available *ad libitum*) in the animal facility of the Forschungszentrum Jülich GmbH before the experiments were carried out. All animal experiments were approved by the Animal Protection Committee of the local government according to the German Protection of Animals Act (LANUV, North-Rhine-Westphalia, Germany, Az.84-02.04.2017.A029).

Pharmacokinetic concentration-time profiles

To determine the concentration-time profiles of ANK6, tANK6, and cANK6r in murine brain, plasma, liver, kidney, and cerebrospinal fluid (CSF) after i.v. and p.o. administration, mixed solutions of non-labelled and ^{3}H-labelled peptides were prepared. The administered solutions contained 1 mg/mL (i.v.) or 3 mg/mL (p.o.) of the respective D-peptide including small amounts of ^{3}H-labelled peptides (0.54 µg/mL ^{3}H-ANK6, 1.79 µg/mL ^{3}H-tANK6, or 0.98 µg/mL

^{3}H-cANK6r). Doses were administered by body weight: i.v. 3.3 mg/kg, ANK6 & tANK6 p.o. 10 mg/kg, cANK6r p.o. 15 mg/kg. Three male C57Bl/6N mice aged 13-14 weeks were investigated per time point whereby individual outliers were excluded from further evaluation. Organs were harvested as follows: i.v. 5, 10, 30, 60, 120, 240, 360, 1080, 1440 min; p.o.: 10, 20, 30, 60, 120, 240, 360, 1080, 1440 min.

Animals whose CSF was not extracted were anesthetized with isoflurane (cp-pharma, Germany) inhalation approximately 2 min before each organ harvesting time point. Afterwards, blood was taken by cardiac puncture and the heparinized blood was centrifuged (3000 g, 5 min, 4 °C) to get plasma. The plasma in the supernatant was separated and 1:1 diluted with PBS. The right brain hemisphere, 200 mg of the big liver lobe, and the right kidney were removed, weighed, and homogenized in 500 µL PBS (Precellys Ceramic Kit 1.4 mm, Precellys 24, Bertin technologies SAS, France). 100 µL of the diluted plasma, the homogenized brain, liver, or kidney (in triplicates), or 1-5 µL (exactly determined) of the extracted CSF (extraction procedure see below, single determination) were mixed with 10 mL scintillation cocktail (Ultima Gold XR, PerkinElmer, USA). The mixture was incubated overnight (100 rpm, room temperature).

Animals whose CSF was extracted (organ harvesting time points: 60 min, 240 min, 1440 min) were i.p. anesthetized with ketamine/medetomidine approximately 20 min before each sampling time point. When the mouse was in deep narcosis, the *cisterna magna* was laid free and punctuated with a small capillary to extract about 5 µL of CSF as described before [30]. Afterwards, cardiac puncture, organ extractions, and sample preparations were performed as described above.

Quantification of the amount of ^{3}H-labelled D-peptides was performed with a LSC and the results (dpm/sample) were converted into mg/mL or % injected dose (%ID)/mL for plasma and for CSF, or in mg/g or %ID/g for brain as described before [29]. Total peptide concentrations in the samples were back-calculated from the measured ^{3}H-labelled peptides' radioactivity as described before [20, 25, 26, 29].

The determined peptide concentrations were plotted over time to allow for comparison of all peptides' uptake into brain, plasma, liver, kidney, and CSF. Concentrations at 0 min were set to 0 %ID/mL or 0 %ID/g except for plasma concentrations after i.v. administration. There, concentrations were linearly back-extrapolated based on the first two measured time points (5 min, 10 min).

Pharmacokinetic parameters

To calculate ANK6's, tANK6's, and cANK6r's pharmacokinetic parameters for plasma and brain, concentration-time profiles were analyzed. Non-compartmental data analysis was performed with Phoenix WinNonlin (Pharsight, a Certara Company; USA) to calculate the area under the curve from the first to the last measured data pair (AUC_{last}), the mean residence time (MRT), and the terminal elimination rate constant (λ_z, nonlinear regression of the last four to five measured concentrations). Further pharmacokinetic parameters were calculated with the help of the formulas listed in Table 2.

To allow for direct comparison with other peptides, four universally applied BBB parameters were determined [31]: the blood-brain equilibrium distribution (logBB), the universal influx rate constant (K_{in}), the initial distribution volume in brain (V_i), and the permeability surface-area product (PS). Based on data of the concentration-time profiles and pharmacokinetic parameters after i.v. administration, the BBB parameters were calculated with the help of the formulas listed in Table 2. Graphical determination of K_{in} and V_i was conducted by plotting the brain concentration to plasma concentration ratio at certain time points (C_b (t)/C_p (t) [mL/g]) on the y-axis against the exposure time (AUC_p (t)/C_p (t) [min]) on the x-axis. The linear range for K_{in} and V_i determination was between 0 and 240 min for ANK6 and cANK6r (R^2: 0.9970, 0.9996) and between 0 and 1440 min for tANK6 (R^2: 0.9758). PS was calculated on the basis of a murine cerebral blood flow (CBF) of 1.07 mL/(g*min) [32].

Results

D-peptides' *in vitro* potencies

The Aβ aggregation assay was performed to compare ANK6's, tANK6's, cANK6r's, with D3's potency to inhibit the formation of ThT-positive $A\beta_{1-42}$ fibrils. In Figure 1, the Aβ aggregation inhibition [%], relative to $A\beta_{1-42}$ aggregation without peptide, was plotted against different ANK6, tANK6, cANK6, or D3 concentrations (0.3125-80 µM). The data fits resulted in the following IC_{50} values: 3.6 µM ANK6, 2.1 µM tANK6, 3.7 µM cANK6r, 7.2 µM D3. Equimolar concentrations of ANK6 relative to $A\beta_{1-42}$ as well as of tANK6 relative to $A\beta_{1-42}$ reduced the aggregation amplitude by more than 97%, while cANK6r and D3 needed about 8-fold molar excess relative to $A\beta_{1-42}$ to reduce the aggregation amplitude by more than 95%.

To find out whether ANK6, tANK6, and cANK6r lowered the cytotoxic effect of $A\beta_{1-42}$ on the cell viability of PC12 cells, MTT assays were performed with various D-peptide concentrations (Figure 2). In a 1:5 ratio of Aβ:D-peptide, ANK6, tANK6, or cANK6r could hold up the cell viability to 65.3%, 75.5%, or 58% as compared to the cell viability in buffer. Previously published data revealed that D3 could hold up cell viability to about 60% in the same Aβ:D-peptide ratio [23]. For each evaluated D-peptide, we observed a significant reduction of the Aβ-induced cytotoxicity from 15 down to 5 respectively 1 µM D-peptide (ANK6: one-way ANOVA $F_{(7,39)} = 77.088$ Bonferroni post hoc analysis 1:15, 1:10, 1:5, 1:1 (Aβ:ANK6) all $p \leq 0.001$; tANK6: one-way ANOVA $F_{(7,39)} = 203.781$, Bonferroni post hoc analysis 1:15, 1:10, 1:5 (Aβ:tANK6) all $p \leq 0.001$; cANK6r: one-way ANOVA $F_{(7,39)} = 179.813$, Bonferroni post hoc analysis 1:15, 1:10, 1:5 (Aβ:cANK6r) all $p \leq 0.001$).

The D-peptides alone did not show negative influence on the cell viability. By plotting the cell viability [%] against the different ANK6, tANK6, or cANK6 concentrations, the following IC_{50} values were determined: 11 µM ANK6, 4.4 µM tANK6, 14 µM cANK6r (Figure 2).

To investigate the D-peptides' impact on Aβ oligomer elimination, a quantitative determination of interference with Aβ aggregate size distribution (QIAD) assay was

performed as described in the methods section. The results showed that ANK6, tANK6, and cANK6r significantly lowered the Aβ oligomer concentrations in fractions 4 to 6 which contain oligomeric Aβ [19] (fraction 4 one-way ANOVA $F_{(3,11)} = 176.336$, $Aβ_{1-42}$ vs. ANK6, tANK6, or cANK6r $p \leq 0.001$, fraction 5 one-way ANOVA $F_{(3,11)} = 54.555$, $Aβ_{1-42}$ vs. ANK6, tANK6, or cANK6r $p \leq 0.001$, fraction 6 one-way ANOVA $F_{(3,11)} = 356.147$, $Aβ_{1-42}$ vs. ANK6, tANK6, or cANK6r $p \leq 0.001$) (Figure 3). While cANK6r only slightly lowered Aβ concentrations in fractions 1 and 2 that contain Aβ monomers, linear ANK6 and tANK6 reduced the Aβ monomer concentrations much stronger. As a consequence, fractions 11 and 12, which contain amorphous high molecular weight Aβ co-precipitates with the respective compound, showed higher Aβ content after incubation with ANK6 and tANK6 as compared to cANK6r.

Preclinical pharmacokinetic characterization

Preclinical pharmacokinetic investigations were performed with ANK6, tANK6, and cANK6r *in vitro* and *in vivo*. First, affinity to the two most recurrent human plasma proteins, HSA and AGP, were determined in order to estimate the D-peptides' plasma protein binding (PPB) and the resulting fractions unbound (f_u) in plasma after oral administration. Results revealed about 2000 times higher affinities of all three D-peptides to AGP (K_D: ANK6 0.29 µM, tANK6 0.06 µM, cANK6r 0.28 µM) as compared to HSA (K_D: ANK6 not analyzable, tANK6 137.7 µM, cANK6r 598.6 µM) (Figure 4). The obtained affinities to HSA and AGP were used for prediction of the D-peptides' overall f_u in plasma (1.43% ANK6, 0.29% tANK6, 1.36% cANK6r).

Since we have shown that ANK6, tANK6, and cANK6r inhibit $Aβ_{1-42}$ aggregation, eliminate toxic Aβ oligomers, and lower $Aβ_{1-42}$-induced cytotoxicity, we conducted pharmacokinetic studies of these peptides via two different administration routes, intravenous (i.v.) and oral (p.o.). Concentration-time profiles of brain, plasma, liver, and kidney are presented in Figure 5 A, B, E, F while the condensed CSF concentration-time profiles for four time points are shown in Figure 5 D. The highest D-peptide concentrations relative to the injected dose per gram organ or milliliter plasma (%ID/g, %ID/mL) were detected in liver and kidney (organs of

metabolization and elimination) followed by plasma (distribution), CSF, and the brain (site of action). As i.v. administration was followed by high initial plasma concentration peaks, the amount of D-peptides detected in liver and kidney from the first to the last measured time point (AUC [min*%ID/g]) was much higher as compared to amounts detected after oral administration. From 6 h until 24 h after administration, plasma levels were in the same range independent from the administration route (0.005 to 0.02 %ID/mL). Brain levels were substantially higher after i.v. administration as compared to oral administration of the respective D-peptides at all investigated time points. Thus, higher initial plasma levels led to higher brain levels, but interestingly also for the time points when plasma levels had already equalized (>6 h). An exception from these differences for the respective administration routes, i.e. i.v. levels > p.o. levels, was observed in CSF. Here, D-peptide levels were, contrary to expectations, higher after oral administration than after i.v. administration. Extraordinary high CSF levels were observed for ANK6 about 60 min after both types of administration. 4 h after administration, CSF levels of ANK6 were again in the same range as those of tANK6 and cANK6r. Of note, the brain/plasma ratios were about one or even higher already 4 h after administration (Figure 5 C). 24 h after administration, the ratios were between 1.17 (cANK6r, p.o.) and 6.89 (tANK6, i.v.).

The maximum concentrations relative to the injected dose (C_{max}, %ID/mL) in plasma increased from tANK6 (i.v. 0.40, p.o. 0.02) over ANK6 (i.v. 3.17, p.o. 0.02) to cANK6r (i.v. 3.29, p.o. 0.05) while in the brain, the C_{max} value (%ID/g) was dependent on the administration route. After i.v. administration, C_{max} increased from tANK6 (0.06) over ANK6 (0.07) to cANK6r (0.12). After oral administration, C_{max} increased from ANK6 (0.01) to tANK6 (0.02) and cANK6r (0.02).

The pharmacokinetic parameters in plasma and brain are summarized in Table 3. In plasma, compound exposure over time relative to the dose ($AUC_{\%ID, 0\text{-}1440}$, min*%ID/mL) after i.v. administration was highest for the cyclic 13-mer cANK6r (i.v. 181) followed by the linear 12-mer ANK6 (91.7) and finally by the linear 24-mer tANK6 (26.1). After oral administration,

$AUC_{\%ID,\ 0\text{-}1440}$ was still highest for cANK6r (17.9) but tANK6 (12.9) and ANK6 (10.8) changed the order whereby differences between the three D-peptides' $AUC_{\%ID,\ 0\text{-}1440}$ were smaller after oral administration. These findings were also reflected in the terminal half-lives ($t_{1/2}$) which were determined to be longer after oral (22-31 h) than after i.v. (15-18 h) administration. Consistently, terminal clearance (CL, mL/(min*kg)) was lowest for cANK6r (i.v. 18.4), followed by ANK6 (i.v. 32.0), and tANK6 (i.v. 88.9). Oral bioavailability (F) was calculated to be 9.9% for cANK6r, 11.8% for ANK6, and 49.4% for tANK6. Interestingly, the mean residence time (MRT) had the same order within the three D-peptides (tANK6 > ANK6 > cANK6r) for both administration routes. Overall, the MRT values were higher after oral administration (9-11 h) than after i.v. administration (2-7 h).

In the brain, $AUC_{\%ID,\ 0\text{-}1440}$ (min*%ID/g) after i.v. administration for cANK6r (85.6) was higher than for tANK6 (56.6), and for ANK6 (35.8). In contrast to the plasma values after oral administration, tANK6 (22.5) showed the highest $AUC_{\%ID,\ 0\text{-}1440}$ followed by cANK6r (19.1) and ANK6 (11.0) in the brain. MRT in the brain was similar for all three D-peptides (11-14 h) independent from the respective administration route.

Calculated values of four commonly used BBB parameters, determined to allow for global comparison of any peptides' efficiencies to cross the BBB, are listed in Table 4. The logBB value describes the blood-brain equilibrium distribution: negative logBB values result from lower AUCs in the brain than in plasma, whereas positive logBB values result from higher AUCs in the brain than in plasma. K_{in} describes the BBB permeability kinetics while V_i describes a peptides' fictional (initial) distribution volume in the brain. The PS represents the uptake clearance from blood to brain. In this study, logBB values of ANK6 and cANK6r were below zero while tANK6's logBB value was greater than zero. Regarding the graphically determined K_{in} and V_i values, ANK6 and cANK6r were in the same range while the values of tANK6 were increased by around factor 10. As PS was determined in consideration of a presumed CBF of 1.07 mL/(g*min) [32], values of all three D-peptides were the same as for K_{in}.

Discussion

The approach of Aβ oligomer elimination by D-peptides clearly differs as compared to e.g. antibodies directed against Aβ, or β- or γ-secretase inhibitors that already failed in several clinical trials. As opposed to passive immunization, the D-peptides' therapeutic efficacy is independent from the individual immune system, and they are able to destroy already existing Aβ oligomers, a property which makes them superior to secretase inhibitors. The most obvious reason why numerous Aβ antibodies have failed in clinical trials is most likely that they had been either directed against Aβ fibrils or monomers, which are the wrong targets, or do bind to all forms of Aβ assemblies. In contrast, the results published so far for the Aβ oligomer targeting antibody Aducanumab are very promising and do underline the reasonability of the therapeutic approach of our Aβ oligomer eliminating D-peptides [33]. Consequently, the D-peptides could already show very promising results of therapeutic *in vivo* studies in various transgenic AD mouse models [10, 12, 15, 17, 19, 27, 34, 35].

In this study, we focused on optimizing ANK6 regarding its potency to eliminate toxic Aβ oligomers as well as its pharmacokinetic *in vivo* characteristics by designing two derivatives. To increase the D-peptide's binding avidity to Aβ, so-called tandem peptides were developed and investigated before [19, 26]. They usually are head-to-tail juxtapositions of two 12-mer D-peptides resulting in a linear 24-residue D-peptide. Thus, tANK6 was included in this study to find out whether a tandem version indeed showed enhanced Aβ-targeting potency as compared to single ANK6. Another optimization approach, which aimed to increase blood-brain barrier permeation, revealed the 13-mer cANK6r. Previously, it had been shown that cyclic isoforms of several D3-derivatives reached remarkably higher brain levels after administration to wild type mice as compared to the corresponding linear peptides [25]. Consequently, we included cANK6r in this study to find out whether cyclization had an impact on ANK6's *in vitro* potency and whether cyclization, here, also led to higher brain levels in comparison to the originally selected linear peptide although it contains six amino acid residue substitutions as compared to D3.

The comparison of *in vitro* properties of ANK6, tANK6, and cANK6r included different experimental approaches, namely Aβ aggregation, cell viability, and QIAD assays. Thereby we could validate our assumption that tANK6 has an enhanced potency as it most efficiently inhibited the $A\beta_{1-42}$ fibril formation with a resulting IC_{50} of 2.1 µM as compared to ANK6 (3.6 µM), cANK6r (3.7 µM), and D3 (7.2 µM). Additionally, one could observe that only tANK6 and ANK6 did completely inhibit $A\beta_{1-42}$ fibril formation by two-fold molar excess with regard to Aβ whereas cANK6r and D3 needed about eight-fold molar excess. Cell viability assays, which were conducted to investigate the D-peptides' efficiencies to reduce Aβ-induced cytotoxicity in PC12 cells, showed a similar trend: tANK6 was most efficient with an IC_{50} value of 4.4 µM followed by ANK6 (11 µM) and cANK6r (14 µM). PC12 cells were used for this experiment because they had originally been established by Greene and Tischler for "neurobiological and neurochemical studies" [36] and are nowadays a commonly used cell line in AD research [37, 38]. Additionally, the MTT test with PC12 cells belongs to our standard test battery for newly developed D-peptides to allow for comparison with data generated previously [10, 27]. The most meaningful *in vitro* assay QIAD awarded all three investigated D-peptides very promising oligomer eliminating characteristics as they drastically eliminated Aβ oligomers (>96% oligomer reduction in fractions 4-6). Previously published data for D3, generated in this test with exactly the same setting, show that D3 could, in the same molar ratio of Aβ:D-peptide as used in this study, reduce the Aβ oligomers by 51% [34]. Because we have developed the ANK compounds for their ability to stabilize Aβ monomers in an aggregation-incompetent conformation, one would expect to see an increase of the Aβ content in the monomer containing fractions (1 and 2), however in presence of the high µM concentrations of Aβ and compound, it is well imaginable that instead the observed high molecular weight co-precipitates were observed. In any case all three compounds were able to eliminate the Aβ oligomers and converted them into non-toxic co-precipitates as was already shown previously for the lead compound D3 [12, 24] and another D3 derivative, RD2 [34].

In the following, PPB experiments were conducted to predict the D-peptides' affinities to the most abundant human plasma proteins, HSA and AGP. If a drug strongly binds to plasma proteins, it is possible that the drug is in the organism but is not able to leave the circulation to the site of action. For AD drugs, this could mean that the drug circulates in plasma, but does not reach the brain, at least not to a very high proportion. Conversely, one can make use of PPB to a certain extent as there is always a dynamic equilibrium between drug bound and freely circulating in plasma (f_u). Thus, plasma proteins can work as kind of drug releasing depots leading to consistent drug distribution in plasma over time. This can lower the risk of adverse side effects and at the same time lead to longer MRTs [39, 40]. Slow drug release from the plasma proteins might even also allow for once daily drug administration, which is followed by the best patients' compliance [41].

ANK6, tANK6, as well as cANK6r bound to AGP (K_D between 0.06 and 0.29 µM) much stronger than to HSA (K_D of 138 µM and higher). This had been expected before as all three D-peptides have a positive net charge and AGP is known to more strongly bind positively charged molecules as compared to HSA, which is known to bind rather acidic or neutral molecules [40]. This had been observed previously for D3 in a similar manner. Jiang et al. determined a K_D of 1.8 µM for D3 to AGP while the K_D of D3 to AGP was above the detection limit of the used kit (>1.4 mM) [20]. The unbound fractions (f_u) of the three D-peptides regarding PPB to HSA and AGP were determined to be in the same range (0.29-1.43%). Results again confirmed the assumption that tANK6 (f_u 0.29%) bound strongest to AGP because it consists of twice as many basic amino acid residues as compared to ANK6 and cANK6r.

Summarizing the *in vitro* studies, cANK6r's slight inferiorities after the Aβ aggregation inhibition and cell viability tests, possibly caused by structural hindrances due to cyclization, could be balanced by cANK6r's very beneficial QIAD outcome in eliminating Aβ oligomers while not strongly affecting Aβ monomer levels. Nevertheless, tANK6 showed very promising results in all conducted *in vitro* tests especially supporting the hypothesis that our tandem

peptides do possess enhanced Aβ-targeting efficacy *in vitro*. As compared to the lead structure D3, the ANK peptides investigated in this study do show the same or, especially in the most important *in vitro* QIAD assay, even more promising results in these Aβ interaction assays. This is why we consider these D-peptides, especially tANK6 and cANK6r, very promising Aβ-targeting D-peptides which are supposed to be therapeutically active even if they reach lower brain levels than D3. One example for the importance of high efficacy, as determined *in vitro*, is the tandem D-peptide D3D3, which has demonstrated already higher efficacy than D3 *in vivo*, despite lower brain penetrance [19].

After extensive *in vitro* investigation of the three D-peptides, they were pharmacokinetically investigated in further detail. For these studies, a mixture of ^{3}H-labelled and non-labelled D-peptide was administered to C57Bl/6N wild type mice. On the one hand, we used C57Bl/6N mice as it is the gold standard to conduct pharmacokinetic experiments with new compounds in young, healthy wild type organisms, especially in rodents [42, 43]. On the other hand, we used exactly these mice at this age in order to allow for direct comparison to our results of D3 and other D3-derivatives that had been determined before using exactly the same experimental method [20, 26, 29]. As D-peptides had been proven to be extraordinary stable against proteolytic degradation and metabolites can therefore be neglected, the detected amount of ^{3}H-labelled D-peptide in the murine samples (brain, plasma, liver, and kidney) was anticipated to correctly reflect the total D-peptide concentration. This has been described and evaluated several times before [20, 25, 26, 29]. As each D-peptide's ^{3}H-label was located in a leucine alkyl group (4,5-^{3}H-D-Leu), the labels were also considered to be biologically stable [25]. Further underlining the D-peptides' stabilities, Elfgen et al. confirmed this by incubation in several media simulating the oral administration route with HPLC analyses [22]. Thus, the amount of ^{3}H-labelled D-peptide quantified in LSC measurements was used for back-calculation of the total D-peptide concentration in the respective samples and pharmacokinetic parameters were calculated subsequently.

Apparently, the pharmacokinetic profiles of liver and kidney revealed huge differences after i.v. and oral administration. The fact that i.v. administration was followed by far higher D-peptide levels in the organs responsible for metabolization and excretion could be explained by the initially higher plasma levels. After the rapid initial rise, liver and kidney levels remained quite constant throughout the observation time of 24 h. Thus, one could surmise that the D-peptides were not immediately excreted but that they accumulated in liver and kidney for some time. Although the administered dose was three times higher for oral than for i.v. administration, only relatively small amounts of the D-peptides were taken up via the gastrointestinal tract. Direct comparison to data of D3 (generated by Jiang et al. using exactly the same experimental setup before [20]), revealed that plasma levels of ANK6, tANK6, and cANK6r were considerably lower especially in plasma after oral administration. Regarding the brain, the AUCs of D3 after oral administration were 7.2 (tANK6), 7.7 (cANK6r), and 13.4 (ANK6) times higher as compared to the respective D-peptides. Thus, the notable differences in plasma and consequently also in brain levels between D3, and ANK6 and its derivative most likely derived from the different amino acid residue compositions. This assumption is substantiated by the fact that brain and plasma levels of other D3-derivatives, composed of the same amino acid residues as D3, were rather in comparable ranges to those of D3 than to those of ANK6 and its derivatives [20, 25, 26]. These pharmacokinetic findings might also partially explain why the intraperitoneal treatment study (4 weeks) with ANK6, conducted by Klein et al., only showed "a non-significant tendency for improving memory performance of tg-APPSwDI mice" [23]. Despite the fact that ANK6 and its derivatives do reach lower brain levels as compared to their lead compound D3, we still consider tANK6 and cANK6r very promising drug candidates for future therapeutic studies because of their superior Aβ interaction *in vitro* efficiencies.

Probably, huge parts of orally administered ANK6, tANK6, and cANK6r in this pharmacokinetic study were immediately excreted. Interestingly, plasma levels after i.v. and oral administration were in the same range about 6 h after administration while brain levels of

the i.v. administered D-peptides, especially those of cANK6r and tANK6, remained higher than those of the orally administered D-peptides. These findings suggested that the D-peptides' outward transport across the BBB, back into plasma, was not as fast as plasma clearance. A reason for that might have been that the D-peptides bound to structures in the murine brain or that the outward transport was limited. Either way is beneficial for an AD drug candidate as the brain is supposed to be its site of action. In this context, the cyclic peptide (cANK6r) revealed higher brain levels than its linear equivalent (ANK6) or the tandem D-peptide (tANK6) after i.v. administration, again substantiating the previously set up hypothesis that cyclization results in more efficient BBB permeation [25]. Finally regarding the C_{max} values in plasma as well as in brain for both administration routes, cANK6r always revealed the highest values suggesting and confirming high stability and enhanced abilities to cross membranes.

Regarding pharmacokinetic parameters in plasma disclosed a bigger difference within the $AUC_{\%ID,\ 0\text{-}1440}$ values after i.v. than after oral administration, most likely due to different uptake and accumulation characteristics in liver and kidney. These characteristics had more impact after i.v. administration, as plasma levels were initially higher. After oral administration, when most of the administered D-peptides had already been eliminated due to the first-pass effect, the impact of liver and kidney over time was smaller. The unexpected result that tANK6 revealed the highest oral bioavailability might be relativized by consideration that tANK6 had a relatively low plasma $AUC_{\%ID,\ 0\text{-}1440}$ after i.v. administration in contrast to the two other peptides. Thus, tANK6's oral bioavailability was higher than those of ANK6 and cANK6r despite the fact that their plasma $AUC_{\%ID,\ 0\text{-}1440}$ after oral administration were in a similar range. Conversely, cANK6r's unexpected low bioavailability was explained by the same approach. Regarding $t_{1/2}$, a therapeutic regimen with once daily dosing would be applicable as the values varied between 15 and 31 h. During a therapeutic study, the steady state levels would be attained after 3 to 6.5 days as a general rule states that the steady state is reached after five $t_{1/2}$ periods [44]. As $t_{1/2}$ for ANK6 was determined to be shorter than for tANK6 and

cANK6r, the two derivatives could be awarded being more favorable regarding $t_{1/2}$. Comparison of i.v. and oral administration generally pointed out longer $t_{1/2}$ after oral administration. These findings were in accordance with the general opinion that long-term AD-treatment in elderly people would be done best orally, not least because of the small impact on the patients' daily living.

To allow for comparability to other peptides listed in "Brainpeps: the blood-brain barrier peptide database", four characterizing BBB values were determined (Table 4) [31]. tANK6's logBB value (positive sign) reflected that the peptide's drug exposure over time was greater in the brain than in plasma whereas for ANK6 and cANK6r (negative signs) it was the other way around. Thus, tANK6r seemed to have entered the brain from plasma most efficiently. However, one may not neglect that logBB values depend on binding to plasma and brain tissue as well as on active transport. K_{in} and V_i had been graphically determined with regard to investigate the velocity of the three D-peptides' BBB passage. Remarkably, both values were tenfold greater for tANK6 than for ANK6, and cANK6r underlining that tANK6 crossed the BBB fastest. Uptake clearance from blood to brain was calculated based on K_{in} so that tANK6 here also revealed the highest PS value. To classify ANK6 and its two derivatives, their BBB parameters were compared to those of Dermorphin, a potent natural opioid consisting of seven amino acid residues including one D-enantiomeric amino acid residue. Dermorphin had been suggested as positive control [31]. Dermorphin's K_{in} values were determined to be between 0.0002 and 0.0022 mL/(g*min) while its V_i values were determined to be between 0.0162 and 0.0215 mL/g [45, 46]. By all means, especially tANK6's, but also ANK6's and cANK6r's, BBB parameters were in the same scale as Dermorphin's awarding the three D-peptides a very efficient BBB permeability.

Summarized, ANK6 and its two derivatives, tANK6 and cANK6r, showed very beneficial Aβ-targeting *in vitro* efficacies. Analyzing the results, it became obvious that both newly developed ANK6-derivatives, tANK6 and cANK6r, had superior Aβ interacting properties as compared to ANK6. As shown already for ANK6's predecessor peptide D3, i.v. administration

led to accumulation in liver and kidney, whereas p.o. administration did not [20]. Oral bioavailabilities were with about 10 % for ANK6 and cANK6r and 50 % for tANK6 very high when compared with typical oral bioavailabilities of L-enantiomeric peptides. cANK6r showed the highest drug exposure over time in the brain. All three investigated compounds revealed very high BBB penetration as indicated by typically determined BBB values (**Table 4**).

Acknowledgement

D.W. and K.J.L. were supported by grants from the "Portfolio Technology and Medicine", and D.W. was additionally supported by the "Portfolio Drug Research" and the Helmholtz-Validierungsfonds of the "Impuls und Vernetzungs-Fonds der Helmholtzgemeinschaft". The study was supported by the TT-Fonds of the Technology Transfer Department of the Forschungszentrum Jülich.

Conflict of interest

The authors have no conflict of interest to report.

Author's information

Corresponding authors

Dr. Antje Willuweit (a.willuweit@fz-juelich.de)

Prof. Dr. Dieter Willbold (d.willbold@fz-juelich.de)

Author contributions

A.W. and D.W. designed the overall study. D.W., A.W., J.K., E.S., and S.S. designed the experiments. E.S., M.T., and T.Z. carried out and evaluated the *in vitro* experiments on the

570 D-peptides' interaction with Aβ. O.B. carried out HPLC measurements for the QIAD assay. E.S. performed the plasma protein binding tests and evaluated the results with support from T.Z.. E.S. and S.S. planned and carried out all pharmacokinetic experiments with the help of N.N., and D.H.. E.S. determined the pharmacokinetic parameters and the blood-brain barrier values. A.E. and I.G. carried out preliminary experiments that were important for the final study design. E.S., A.W., J.K., N.J.S., K.J.L., and D.W. wrote the manuscript. All other authors contributed to writing.

References

[1] Thal DR, Capetillo-Zarate E, Del Tredici K, Braak H (2006) The development of amyloid beta protein deposits in the aged brain. *Sci Aging Knowledge Environ* **2006**, re1.

[2] Haass C, Selkoe DJ (2007) Soluble protein oligomers in neurodegeneration: lessons from the Alzheimer's amyloid beta-peptide. *Nat Rev Mol Cell Biol* **8**, 101-112.

[3] Anand R, Gill KD, Mahdi AA (2014) Therapeutics of Alzheimer's disease: Past, present and future. *Neuropharmacology* **76 Pt A**, 27-50.

[4] Gremer L, Scholzel D, Schenk C, Reinartz E, Labahn J, Ravelli RBG, Tusche M, Lopez-Iglesias C, Hoyer W, Heise H, Willbold D, Schroder GF (2017) Fibril structure of amyloid-beta(1-42) by cryo-electron microscopy. *Science* **358**, 116-119.

[5] Schumacher TNM, Mayr LM, Minor DL, Milhollen MA, Burgess MW, Kim PS (1996) Identification of D-peptide ligands through mirror-image phage display. *Science* **271**, 1854-1857.

[6] Wiesehan K, Willbold D (2003) Mirror-image phage display: aiming at the mirror. *Chembiochem* **4**, 811-815.

[7] Wiesehan K, Buder K, Linke RP, Patt S, Stoldt M, Unger E, Schmitt B, Bucci E, Willbold D (2003) Selection of D-amino-acid peptides that bind to Alzheimer's disease amyloid peptide abeta1-42 by mirror image phage display. *Chembiochem* **4**, 748-753.

[8] Wiesehan K, Stohr J, Nagel-Steger L, van Groen T, Riesner D, Willbold D (2008) Inhibition of cytotoxicity and amyloid fibril formation by a D-amino acid peptide that specifically binds to Alzheimer's disease amyloid peptide. *Protein Eng Des Sel* **21**, 241-246.

[9] Funke SA, Willbold D (2009) Mirror image phage display--a method to generate D-peptide ligands for use in diagnostic or therapeutical applications. *Mol Biosyst* **5**, 783-786.

[10] van Groen T, Wiesehan K, Funke SA, Kadish I, Nagel-Steger L, Willbold D (2008) Reduction of Alzheimer's disease amyloid plaque load in transgenic mice by D3, A D-enantiomeric peptide identified by mirror image phage display. *ChemMedChem* **3**, 1848-1852.

[11] van Groen T, Kadish I, Wiesehan K, Funke SA, Willbold D (2009) In vitro and in vivo staining characteristics of small, fluorescent, Abeta42-binding D-enantiomeric peptides in transgenic AD mouse models. *ChemMedChem* **4**, 276-282.

[12] Funke SA, van Groen T, Kadish I, Bartnik D, Nagel-Steger L, Brener O, Sehl T, Batra-Safferling R, Moriscot C, Schoehn G, Horn AH, Muller-Schiffmann A, Korth C, Sticht H, Willbold D (2010) Oral treatment with the d-enantiomeric peptide D3 improves the pathology and behavior of Alzheimer's Disease transgenic mice. *ACS Chem Neurosci* **1**, 639-648.

[13] Bartnik D, Funke SA, Andrei-Selmer L-C, Bacher M, Dodel R, Willbold D (2010) Diffenrently Selected D-Enantiomeric Peptides Act on Different Aβ Species. *Rejuvenation Res.* **13**, 202-205.

[14] Liu H, Funke SA, Willbold D (2010) Transport of Alzheimer disease amyloid-beta-binding D-amino acid peptides across an in vitro blood-brain barrier model. *Rejuvenation Res* **13**, 210-213.

[15] van Groen T, Kadish I, Funke A, Bartnik D, Willbold D (2012) Treatment with Abeta42 binding D-amino acid peptides reduce amyloid deposition and inflammation in APP/PS1 double transgenic mice. *Adv Protein Chem Struct Biol* **88**, 133-152.

[16] Olubiyi OO, Strodel B (2012) Structures of the amyloid beta-peptides Abeta1-40 and Abeta1-42 as influenced by pH and a D-peptide. *J Phys Chem B* **116**, 3280-3291.

[17] van Groen T, Kadish I, Funke SA, Bartnik D, Willbold D (2013) Treatment with D3 removes amyloid deposits, reduces inflammation, and improves cognition in aged AbetaPP/PS1 double transgenic mice. *J Alzheimers Dis* **34**, 609-620.

[18] Olubiyi OO, Frenzel D, Bartnik D, Gluck JM, Brener O, Nagel-Steger L, Funke SA, Willbold D, Strodel B (2014) Amyloid Aggregation Inhibitory Mechanism of Arginine-rich D-peptides. *Current Medicinal Chemistry* **21**, 1448-1457.

[19] Brener O, Dunkelmann T, Gremer L, van Groen T, Mirecka EA, Kadish I, Willuweit A, Kutzsche J, Jurgens D, Rudolph S, Tusche M, Bongen P, Pietruszka J, Oesterhelt F, Langen KJ, Demuth HU, Janssen A, Hoyer W, Funke SA, Nagel-Steger L, Willbold D (2015) QIAD assay for quantitating a compound's efficacy in elimination of toxic Abeta oligomers. *Sci Rep* **5**, 13222.

[20] Jiang N, Leithold LH, Post J, Ziehm T, Mauler J, Gremer L, Cremer M, Schartmann E, Shah NJ, Kutzsche J, Langen KJ, Breitkreutz J, Willbold D, Willuweit A (2015) Preclinical

Pharmacokinetic Studies of the Tritium Labelled D-Enantiomeric Peptide D3 Developed for the Treatment of Alzheimer s Disease. *PLoS One* **10**, e0128553.

[21] Jiang N, Frenzel D, Schartmann E, van Groen T, Kadish I, Shah NJ, Langen KJ, Willbold D, Willuweit A (2016) Blood-brain barrier penetration of an Abeta-targeted, arginine-rich, d-enantiomeric peptide. *Biochim Biophys Acta* **1858**, 2717-2724.

[22] Elfgen A, Santiago-Schubel B, Gremer L, Kutzsche J, Willbold D (2017) Surprisingly high stability of the Abeta oligomer eliminating all-d-enantiomeric peptide D3 in media simulating the route of orally administered drugs. *Eur J Pharm Sci* **107**, 203-207.

[23] Klein AN, Ziehm T, van Groen T, Kadish I, Elfgen A, Tusche M, Thomaier M, Reiss K, Brener O, Gremer L, Kutzsche J, Willbold D (2017) Optimization of D-peptides for Aβ monomer binding specificity enhances their potential to eliminate toxic Aβ oligomers. *ACS Chem Neurosci*.

[24] Ziehm T, Brener O, van Groen T, Kadish I, Frenzel D, Tusche M, Kutzsche J, Reiss K, Gremer L, Nagel-Steger L, Willbold D (2016) Increase of Positive Net Charge and Conformational Rigidity Enhances the Efficacy of d-Enantiomeric Peptides Designed to Eliminate Cytotoxic Abeta Species. *ACS Chem Neurosci* **7**, 1088-1096.

[25] Schartmann E, Schemmert S, Ziehm T, Leithold LHE, Jiang N, Tusche M, Joni Shah N, Langen KJ, Kutzsche J, Willbold D, Willuweit A (2017) Comparison of blood-brain barrier penetration efficiencies between linear and cyclic all-d-enantiomeric peptides developed for the treatment of Alzheimer's disease. *Eur J Pharm Sci* **114**, 93-102.

[26] Leithold LH, Jiang N, Post J, Niemietz N, Schartmann E, Ziehm T, Kutzsche J, Shah NJ, Breitkreutz J, Langen KJ, Willuweit A, Willbold D (2016) Pharmacokinetic properties of tandem d-peptides designed for treatment of Alzheimer's disease. *Eur J Pharm Sci* **89**, 31-38.

[27] Dunkelmann T, Teichmann K, Ziehm T, Schemmert S, Frenzel D, Tusche M, Dammers C, Jürgens D, Langen K-J, Demuth H-U, Shah NJ, Kutzsche J, Willuweit A, Willbold D (2017) Aβ oligomer eliminating compounds interfere successfully with pEAβ (3–42) induced motor neurodegenerative phenotype in transgenic mice. *Neuropeptides*.

[28] Clark RA, Shoaib M, Hewitt KN, Stanford SC, Bate ST (2012) A comparison of InVivoStat with other statistical software packages for analysis of data generated from animal experiments. *J Psychopharmacol* **26**, 1136-1142.

[29] Leithold LH, Jiang N, Post J, Ziehm T, Schartmann E, Kutzsche J, Shah NJ, Breitkreutz J, Langen KJ, Willuweit A, Willbold D (2016) Pharmacokinetic Properties of a Novel D-Peptide Developed to be Therapeutically Active Against Toxic beta-Amyloid Oligomers. *Pharm Res* **33**, 328-336.

[30] Liu HN, Tjostheim S, Dasilva K, Taylor D, Zhao B, Rakhit R, Brown M, Chakrabartty A, McLaurin J, Robertson J (2012) Targeting of monomer/misfolded SOD1 as a therapeutic strategy for amyotrophic lateral sclerosis. *J Neurosci* **32**, 8791-8799.

[31] Van Dorpe S, Bronselaer A, Nielandt J, Stalmans S, Wynendaele E, Audenaert K, Van De Wiele C, Burvenich C, Peremans K, Hsuchou H, De Tre G, De Spiegeleer B (2012) Brainpeps: the blood-brain barrier peptide database. *Brain Struct Funct* **217**, 687-718.

[32] Muir ER, Shen Q, Duong TQ (2008) Cerebral blood flow MRI in mice using the cardiac-spin-labeling technique. *Magn Reson Med* **60**, 744-748.

[33] Sevigny J, Chiao P, Bussiere T, Weinreb PH, Williams L, Maier M, Dunstan R, Salloway S, Chen T, Ling Y, O'Gorman J, Qian F, Arastu M, Li M, Chollate S, Brennan MS, Quintero-Monzon O, Scannevin RH, Arnold HM, Engber T, Rhodes K, Ferrero J, Hang Y, Mikulskis A, Grimm J, Hock C, Nitsch RM, Sandrock A (2016) The antibody aducanumab reduces Abeta plaques in Alzheimer's disease. *Nature* **537**, 50-56.

[34] van Groen T, Schemmert S, Brener O, Gremer L, Ziehm T, Tusche M, Nagel-Steger L, Kadish I, Schartmann E, Elfgen A, Jurgens D, Willuweit A, Kutzsche J, Willbold D (2017) The Abeta oligomer eliminating D-enantiomeric peptide RD2 improves cognition without changing plaque pathology. *Sci Rep* **7**, 16275.

[35] Kutzsche J, Schemmert S, Tusche M, Neddens J, Rabl R, Jurgens D, Brener O, Willuweit A, Hutter-Paier B, Willbold D (2017) Large-Scale Oral Treatment Study with the Four Most Promising D3-Derivatives for the Treatment of Alzheimer's Disease. *Molecules* **22**.

[36] Greene LA, Tischler AS (1976) Establishment of a noradrenergic clonal line of rat adrenal pheochromocytoma cells which respond to nerve growth factor. *Proc Natl Acad Sci U S A* **73**, 2424-2428.

[37] Dong H, Mao S, Wei J, Liu B, Zhang Z, Zhang Q, Yan M (2012) Tanshinone IIA protects PC12 cells from β-amyloid25–35-induced apoptosis via PI3K/Akt signaling pathway. *Molecular Biology Reports* **39**, 6495-6503.

[38] Zeng Z, Xu J, Zheng W (2017) Artemisinin protects PC12 cells against β-amyloid-induced apoptosis through activation of the ERK1/2 signaling pathway. *Redox Biol* **12**, 625-633.
[39] Gillette JR (1973) Overview of drug-protein binding. *Ann N Y Acad Sci* **226**, 6-17.
[40] Lambrinidis G, Vallianatou T, Tsantili-Kakoulidou A (2015) In vitro, in silico and integrated strategies for the estimation of plasma protein binding. A review. *Adv Drug Deliv Rev* **86**, 27-45.
[41] Eisen SA, Miller DK, Woodward RS, Spitznagel E, Przybeck TR (1990) The effect of prescribed daily dose frequency on patient medication compliance. *Arch Intern Med* **150**, 1881-1884.
[42] Beconi MG, Howland D, Park L, Lyons K, Giuliano J, Dominguez C, Munoz-Sanjuan I, Pacifici R (2012) Pharmacokinetics of memantine in rats and mice. *PLoS Curr* **3**.
[43] Chen C, Ortega F, Alameda L, Ferrer S, Simonsson US (2016) Population pharmacokinetics, optimised design and sample size determination for rifampicin, isoniazid, ethambutol and pyrazinamide in the mouse. *Eur J Pharm Sci* **93**, 319-333.
[44] Zhao W, Jacqz-Aigrain E (2011) Principles of therapeutic drug monitoring. *Handb Exp Pharmacol* **205**, 77-90.
[45] Stalmans S, Bracke N, Wynendaele E, Gevaert B, Peremans K, Burvenich C, Polis I, De Spiegeleer B (2015) Cell-Penetrating Peptides Selectively Cross the Blood-Brain Barrier In Vivo. *PLoS One* **10**, e0139652.
[46] Van Dorpe S, Adriaens A, Polis I, Peremans K, Van Bocxlaer J, De Spiegeleer B (2010) Analytical characterization and comparison of the blood-brain barrier permeability of eight opioid peptides. *Peptides* **31**, 1390-1399.

Tables

Table 1: Peptides' sequences and configurations

peptide	amino acid residue sequence	amino acid residue configuration
D3	rprtrlhthrnr-NH_2	all-D-enantiomeric
ANK6	rkrirlvtkkkr-NH_2	all-D-enantiomeric
tANK6	rkrirlvtkkkrrkrirlvtkkkr-NH_2	all-D-enantiomeric
cANK6r	rkrirlvtkkkrr head-to-tail cyclized	all-D-enantiomeric

720

Table 2: Formulas for calculation of pharmacokinetic parameters and blood-brain barrier values

pharmacokinetic parameter		unit	formula
$t_{1/2}$	terminal half-life	h	$t_{1/2} = \ln(2)/\lambda_z$
D	dose	mg/kg	
$F_{AUC_{\%ID}}$	bioavailability	%	$F_{AUC_{\%ID}} = \frac{AUC_{\%ID_{e.v.}}}{AUC_{\%ID_{i.v.}}}$
CL	terminal plasma clearance	mL/(min*kg)	$CL = \lambda_z * V_{last}$
blood-brain barrier value		**unit**	**formula**
logBB	blood-brain equilibrium distribution	-	$logBB = \log(AUC_{last,br}/AUC_{last,pl})$
K_{in}	unidirectional influx rate constant	mL/(g*min)	$\frac{C_b(t)}{C_p(t)} = K_{in} * \frac{AUC_p(t)}{C_p(t)} + V_i$
V_i	initial distribution volume	mL/g	see formula for K_{in}
PS	permeability surface-area product	mL/(g*min)	$PS = (-CBF)*\ln(1-K_{in}/CBF)$
CBF	(murine) cerebral blood flow	mL/(g*min)	1.07 [32]

Table 3: Pharmacokinetic parameters for ANK6, tANK6, and cANK6r in murine plasma and brain

PLASMA							
D-peptide		**ANK6**	**tANK6**	**cANK6r**	**ANK6**	**tANK6**	**cANK6r**
administration route		**i.v.**	**i.v.**	**i.v.**	**p.o.**	**p.o.**	**p.o.**
parameter	**unit**						
D	mg/kg	3.3	3.3	3.3	10	10	15
C_{max}	%ID/mL	3.17	0.40	3.29	0.02	0.02	0.05
t_{max}	min	0	0	0	120	240	60
$AUC_{\%ID,\ 0\text{-}1440}$	min*%ID/mL	91.7	26.1	181.0	10.8	12.9	17.9
MRT	h	3	7	2	10	11	9
λ_z	1/min	0.00077	0.00063	0.00064	0.00054	0.00038	0.00039
$t_{1/2}$	h	15	18	18	22	31	30
F ($AUC_{\%ID}$)	%	na	na	na	11.8	49.4	9.9
CL	mL/(min*kg)	32.0	88.9	18.4	174.5	113.0	135.5
BRAIN							
D-peptide		**ANK6**	**tANK6**	**cANK6r**	**ANK6**	**tANK6**	**cANK6r**
administration route		**i.v.**	**i.v.**	**i.v.**	**p.o.**	**p.o.**	**p.o.**
parameter	**unit**						
C_{max}	%ID/g	0.07	0.06	0.12	0.01	0.02	0.02
t_{max}	min	5	30	5	60	1080	360
$AUC_{\%ID,\ 0\text{-}1440}$	min*%ID/g	35.8	56.6	85.6	11.0	22.5	19.1

730 **Table 4: Blood-brain barrier values for ANK6, tANK6, and cANK6r after i.v. administration**

Parameter	Unit	ANK6	tANK6	cANK6r
logBB	-	-0.401	0.335	-0.329
K_{in}	mL/(g*min)	0.0003	0.0016	0.0003
V_{im}	mL/g	0.0575	0.5833	0.0396
PS	mL/(g*min)	0.0003	0.0016	0.0003

Figures

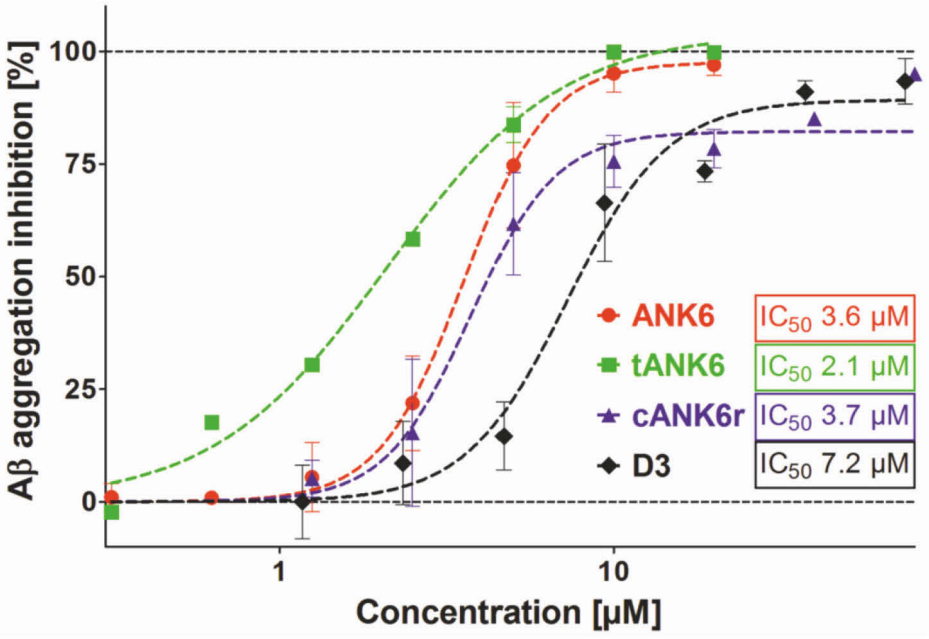

Figure 1: Aβ aggregation assay

To investigate ANK6's (red circles), tANK6's (green squares), cANK6r's (blue triangles), and D3's (black diamonds) potencies to inhibit $A\beta_{1-42}$ monomer aggregation into ThT-positive fibrils, different concentrations of the respective peptides (0.3125-80 µM) were incubated with 10 µM $A\beta_{1-42}$ each. The Aβ aggregation inhibition [%], relative to the fluorescence signal of ThT-positive $A\beta_{1-42}$ fibrils which were formed without any peptide added, was plotted against the respective D-peptides' concentrations. The IC_{50} values were determined by nonlinear regression.

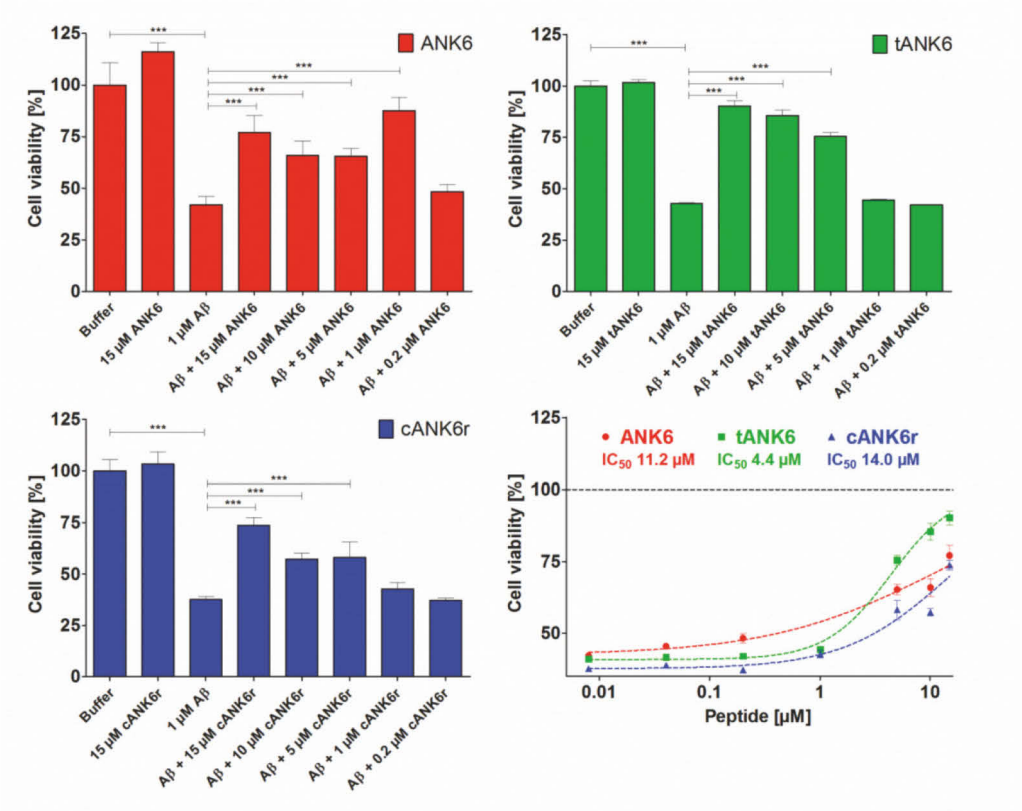

Figure 2: Cell viability assay

To investigate ANK6's (red circles), tANK6's (green squares), and cANK6r's (blue triangles) potencies to reduce the toxicity of $A\beta_{1\text{-}42}$, a cell viability assay was performed. After pre-incubation of $A\beta_{1\text{-}42}$ monomers to ensure Aβ oligomerization, solutions containing either $A\beta_{1\text{-}42}$ alone (1 µM final concentration), or $A\beta_{1\text{-}42}$ with different amounts of ANK6, tANK6, and cANK6r (final concentrations between 0.008 and 15 µM) were incubated on PC12 cells overnight. Cell viabilities [%], relative to buffer-treated cells, were plotted against the respective D-peptides' concentrations. Datasets were fitted by nonlinear regression to determine the IC_{50} values. Data is represented as mean ± SEM; one-way ANOVA, ***$p \leq 0.001$.

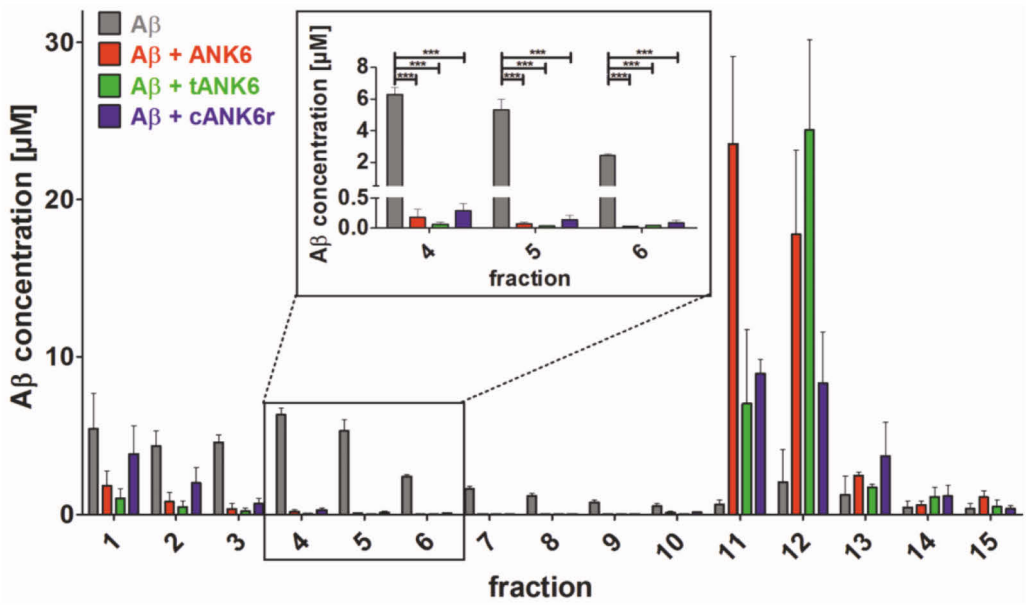

Figure 3: Quantitative determination of interference with Aβ aggregate size distribution (QIAD) assay

To investigate the D-peptides' impact on Aβ oligomer elimination, a quantitative determination of interference with Aβ aggregate size distribution (QIAD) assay was performed. $Aβ_{1-42}$ was pre-incubated to form the natural Aβ aggregate size distribution. Afterwards, sodium phosphate buffer (control, grey bars), ANK6 (red bars), tANK6 (green bars), or cANK6r (blue bars) was added. The samples were separated via density gradient centrifugation into 15 different fractions containing different Aβ particle sizes (fractions 1-2: monomers, 4-6: oligomers, 11-14: high molecular weight co-precipitates). Results revealed that ANK6, tANK6, and cANK6r significantly lowered the Aβ oligomer concentrations in fractions 4 to 6 as compared to the control (Aβ alone). Data is represented as mean ± SEM; one-way ANOVA, ***p ≤ 0.001.

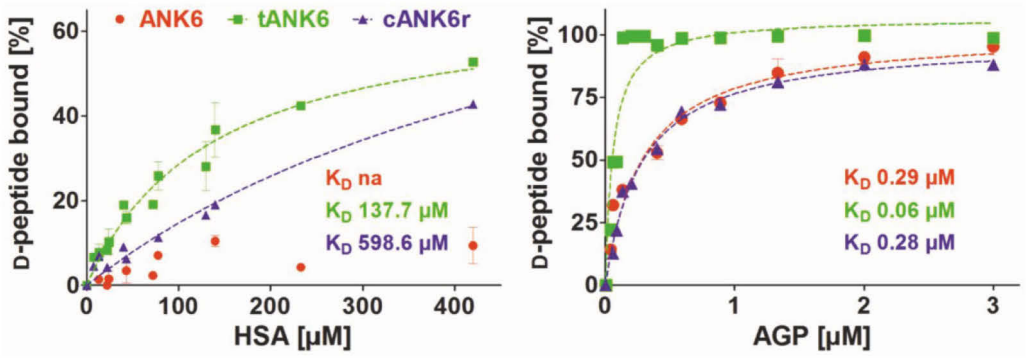

Figure 4: Binding to the plasma proteins HSA and AGP

ANK6's (red circles), tANK6's (green squares), and cANK6r's (blue triangles) binding to the plasma proteins human serum albumin (HSA) and to α1 acid glycoprotein (AGP) was analyzed. The D-peptides were applied at
770 5 µM while HSA and AGP concentrations were adjusted as follows: HSA 7.4 µM to 420 µM, AGP 0.04 µM to 3 µM. The unbound amount of ANK6, tANK6, and cANK6r (in %) to HSA or AGP respectively was plotted against the D-peptides' concentrations. Datasets were fitted by nonlinear regression to determine the K_D.

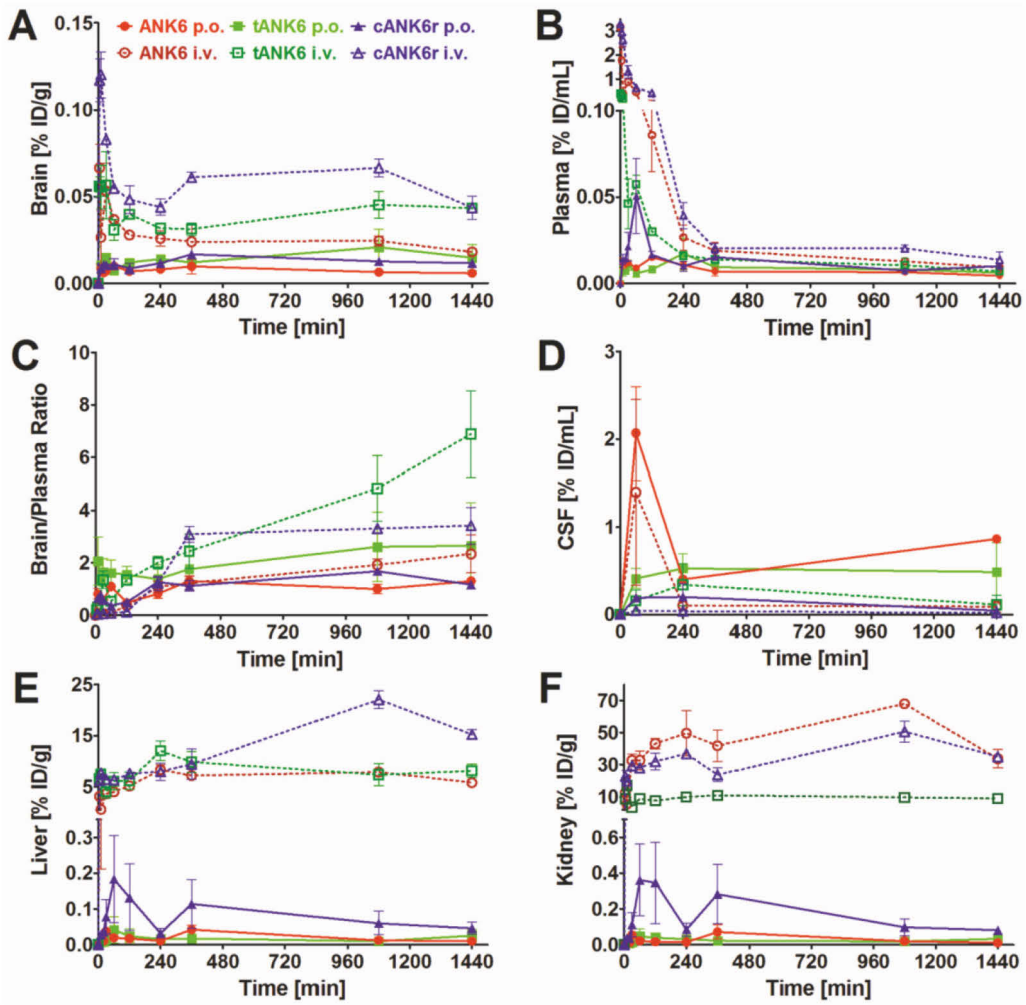

Figure 5: Pharmacokinetic concentration-time profiles of ANK6, tANK6, and cANK6r

Pharmacokinetic concentration-time profiles of ANK6 (red circles), tANK6 (green squares), and cANK6r (blue triangles) were investigated in brain (A), plasma (B), CSF (D), liver (E), and kidney (F) after i.v. (3.3 mg/kg, dotted lines) and p.o. (10 mg/kg ANK6 & tANK6, 15 mg/kg cANK6r, continuous lines) administration to wild type mice (3 mice/time point). The D-peptides were administered as a mixture of ^{3}H-labelled and non-labelled peptide in 0.9% sodium chloride solution. The ^{3}H-peptides' concentrations (triplicate) in the respective organs and plasma were measured with liquid scintillation counting. Total peptide concentrations were calculated as % of the injected dose per g or mL (% ID/g for brain, liver, kidney; % ID/mL for plasma, CSF) and plotted over time. The brain and plasma concentrations were set in relation to each other and plotted against the time as the brain/plasma ratio (C).

780

Abbreviations

Aβ	amyloid-β
AD	Alzheimer's disease
AGP	α1-acid glycoprotein
AUC_{last}	area under the curve from the first to the last measured data pair
BBB	blood-brain barrier
C	concentration
CBF	(murine) cerebral blood flow
CL	terminal plasma clearance
CSF	cerebrospinal fluid
D	administered dose
F	bioavailability
f_u	free drug fraction = fraction unbound
HSA	human serum albumin
IC_{50} value	half maximal inhibitory concentration
ID	injected dose = intravenously or orally administered dose
i.v.	intravenous
K_D	dissociation constant
K_{in}	universal influx rate constant
logBB	blood-brain equilibrium distribution
LSC	liquid scintillation counter
MRT	mean residence time
MTT	3-(4,5-Dimethylthiazol-2-yl)-2,5-diphenyltetrazoliumbromid
PC12 cells	rat phaeochromocytoma cells
p.o.	oral
PPB	plasma protein binding
PS	permeability surface-area product
QIAD	quantitative determination of interference with Aβ aggregate size distribution
RP-HPLC	reversed phase-high performance liquid chromatography
ThT	Thioflavin T
t	time
$t_{1/2}$	terminal half-life
V_i	initial distribution volume in brain
λ_z	terminal elimination rate constant

4. Zusammenfassung und Schlussfolgerung

4.1 Mausmodelle der Alzheimer'schen Demenz – Das TBA2.1 Mausmodell

Zur Erforschung der zugrundeliegenden Mechanismen der AD und zur Entwicklung neuer Medikationen ist der Nutzen von Tiermodellen mangels Alternativen zurzeit noch unerlässlich. In der Literatur werden weit über 100 Mausmodelle der AD beschrieben, die entweder durch Einbringen menschlicher, AD-relevanter Gene, oder durch intrazerebrale Injektion verschiedener (humaner) Aβ-Spezies einen AD-ähnlichen Phänotyp und die zugehörige Pathologie ausprägen. Jedoch kristallisierte sich in den letzten Jahren heraus, dass die meisten Mausmodelle nur einen Bruchteil der menschlichen AD widerspiegeln. Das Versagen vieler neuer Wirkstoffkandidaten gegen die AD wird auch darauf zurückgeführt, dass diese in zu wenigen oder nicht ausreichend diversen Mausmodellen in der Präklinik evaluiert worden sind. Aufgrund dessen ist es unerlässlich, die Entwicklung adäquater Mausmodelle voranzutreiben, die entweder ein optimiertes Modell darstellen, oder einen Zusatz zu den klassischen Mausmodellen bieten. Ein Nachteil einiger der zurzeit verfügbaren Modelle ist, dass diese keine, oder eine unzureichende Neurodegeneration aufweisen, eines der pathologischen Charakteristika der AD. Darüber hinaus ist die Pathologie der meisten Modelle der Amyloidose auf eine Überexpression der $A\beta_{(1-42)}$ zurückzuführen, ohne andere, potentiell toxischere Aβ-Spezies zu berücksichtigen.

Im Jahr 2011 wurde das TBA2.1 AD Mausmodell erstmalig von Alexandru und Kollegen vorgestellt [130]. Ein Ziel dieser Arbeit bestand darin, das Mausmodell hinsichtlich seines motorischen Phänotyps und seiner Pathologie eingehender zu charakterisieren. Homozygote Tiere des TBA2.1 Mausmodells kennzeichnen sich durch eine $pEA\beta_{(3-42)}$ Freisetzung aus, die in einem motorischen Phänotyp mit einer enormen Neurodegeneration in der CA1 Region des Hippocampus resultiert [130]. $pEA\beta_{(3-42)}$ ist neben $A\beta_{(1-42)}$ eine der aggregationsfreudigsten und toxischsten Aβ-Spezies [45]. Basierend auf der initialen Charakterisierung des Mausmodells durch Alexandru und Kollegen wurde durch Dunkelmann und Kollegen das Mausmodell weitergehend charakterisiert (Manuskripte Kapitel 3.5 und 3.6). In diesen Studien konnte, durch die Verwendung weiterer motorischer und allgemeiner Verhaltenstests, validiert werden, dass homozygote TBA2.1 Mäuse einen progressiven neuromotorischen Phänotyp aufweisen, der bereits ab einem Alter von zwei Monaten im SHIRPA- und Rotarod-Test detektierbar ist (Manuskripte Kapitel 3.5 und 3.6). Pathologisch sind die Tiere durch Aβ-Ablagerungen in der CA1-Region, dem Striatum, dem motorischen und olfaktorischen Kortex, dem Colliculus Inferior (Mittelhirn) und dem Cerebellum gekennzeichnet. Es konnte bereits durch Alexandru et al. gezeigt werden, dass homozygote TBA2.1 Mäuse in diesen Bereichen Aβ-Ablagerungen zeigen. Die in dieser

Arbeit durchgeführte Studie validiert und erweitert diese Ergebnisse, indem verschiedene Altersgruppen und Genotypen miteinander verglichen wurden und weitere Zelltypen (Neuronen, Gliazellen) quantifiziert wurden. Die Aβ-Ablagerungen der TBA2.1 Mäuse unterscheiden sind stark von Aβ-Plaques, der z.B. APP/PS1 Mäuse. Sie sind wesentlich kleiner und weniger bis gar nicht diffus mit klaren Abgrenzungen zum umliegenden Gewebe. Neben den Aβ-Ablagerungen weisen die homozygoten Tiere eine starke Neurodegeneration, vor allem in der CA1 Region auf. Generell zeigt auch dieses Mausmodell, wie z.B. auch das APP/PS1 AD-Mausmodell, eine verstärke Gliose in jenen Regionen, in denen Aβ-Ablagerungen auftreten. Auffallend ist jedoch der signifikante Rückgang reaktiver Astrozyten in der CA1 Region homozygoter Tiere im Alter von drei bis fünf Monaten (Manuskript Kapitel 3.6). Dieser Umstand ist vermutlich auf die Neurodegeneration in dieser Region zurückzuführen, da so die chemische Transmission zwischen Neuronen und Astrozyten nicht gewährleistet ist [146]. Neurone rekrutieren bei Schädigung Astrozyten und mögliche weitere inflammatorische Zellen durch die Freisetzung von verschiedensten Botenstoffen (Zytokine/Chemokine), um schädliche Einflüsse abzuwenden. Da die Zahl der Neuronen in dieser Region stark vermindert ist, können diese keine Signale aussenden, sodass in der CA1-Region fünf Monate alter homozygoter TBA2.1 Mäuse keine Entzündungszellen mehr vorzufinden sind. Die Kombination zwischen Ablagerungen der Aβ-Aggregate und der Neurodegeneration in den beschrieben Gehirnregionen legt nahe, dass die motorischen Defizite auf eine dysfunktionale Basalganglienverschaltung zurückzuführen sind [147, 148].

Im Vergleich zu den häufig genutzten APP oder APP/PS1 AD Mausmodellen weisen homozygote TBA2.1 Mäuse eine früh auftretende Neurodegeneration auf, sowie einen progressiven und manifestierten Phänotyp im frühen Alter. In der Literatur werden einige wenige weitere Mausmodelle beschrieben, die N-terminal modifizierte Aβ-Spezies ausbilden ($pEA\beta_{(3\text{-}42)}$ und $A\beta_{(4\text{-}42)}$). Jedoch zeigen diese Modelle erst relativ spät Neurodegeneration oder zeigen ausschließlich kognitive Defizite mit einem sehr schwachen motorischen Phänotyp (Tabelle 2).

Die von uns generierten Daten über das TBA2.1 Mausmodell legen nahe, dass der Phänotyp und die Pathologie der Tiere stark von der Ausbildung des humanen $pEA\beta_{(3\text{-}42)}$ und somit von der Genexpression abhängig sind. Dies wird auch anhand der Charakterisierung der heterozygoten Tiere deutlich. Diese weisen auch einen Phänotyp auf, der sich vor allem in einem erhöhten SHIRPA-Score widerspiegelt. Jedoch zeigen heterozygote TBA2.1 Mäuse diesen erst im späten Alter, mit einer deutlich geringeren Pathologie. Allerdings besteht nur die Möglichkeit, die Pathologie homo- und heterozygoter Tiere mit einem Alter von maximal 5 Monaten direkt zu vergleichen, da homozygote TBA2.1 Mäuse bedingt durch ihren schwer belasteten Phänotyps mit diesem Alter getötet werden müssen. Aufgrund dieser erzielten

Ergebnisse lässt sich die Hypothese aufstellen, dass der Phänotyp der TBA2.1 Mäuse stark von der Genexpression abhängig ist (Manuskript Kapitel 3.6).

Das genutzte Testsetup und die erzielten Ergebnisse bestätigen, dass homozygote Tiere ein geeignetes Mausmodell darstellen, um Wirkstoffe gegen AD in diesem Mausmodell zu testen, um so zu überprüfen, ob der eingesetzte Wirkstoff einen Einfluss auf den neuromotorischen Phänotyp und die Pathologie zeigt. In einer ersten Behandlungsstudie mit diesem Mausmodell konnte seine Eignung prinzipiell gezeigt werden, indem demonstriert wurde, dass D3 und eins seiner Derivate die Progression des Phänotyps verringern (Manuskript Kapitel 3.5). Der Umstand, dass an AD erkrankte Patienten nicht nur unter kognitiven Beeinträchtigungen leiden, sondern auch motorisch eingeschränkt sind [149, 150], stützt die Bedeutung dieses Mausmodells noch zusätzlich. Da dieses Modell jedoch nicht alle Aspekte der humanen AD widerspiegelt, vor allem aber bisher nicht gezeigt wurde, dass Mäuse dieser Linien einen kognitiv defizitären Phänotyp ausprägen, sollten neu entwickelte Pharmaka zunächst in einem klassischen Modell, mit kognitiven Defiziten (AD-Mausmodelle der Amyloidose, z.B. APP/PS1, tgSwDI, APP_{SL} u.v.m.), auf ihre Wirksamkeit untersucht werden.

Mausmodell	Mutation	Pathologie	Neurodegeneration	Phänotyp	Literatur
TBA2.1	$A\beta Q_{(3-42)}$	Aβ-Ablagerungen (2 M) Gliose (2 M)	√ 5 M	Motorik (2 M) ↓ Kognition k.A.	[109, 130]
Tg4-42	-	Aβ-Ablagerungen (3 M) Gliose (2 M)	√ 8 M	Motorik k.A. Kognition (8 M) ↓	[151]
Tg2576	APP_{swe}	Aβ-Ablagerungen (12 M) Gliose (10 M)	Nicht bekannt	Motorik (k.A.) Kognition (12 M) ↓	[152, 153]
5XFAD	$APP_{sweFILon}$	Aβ-Ablagerungen (1,5 M) Gliose (2 M)	√ 5 M	Motorik (k.A.) Kognition (4 M) ↓	[154]
APP/PS1	APP_{swe} PS1dE9	Aβ-Ablagerungen (6 M) Gliose (3 M)	√ 10 M	Motorik (k.A.) Kognition (12 M) ↓	[122, 124, 155]
TBA42	$A\beta Q_{(3-42)}$	Aβ-Ablagerungen (k.A.) Neurodegeneration (12 M) Gliose (k.A.)		Motorik (6 M) ↓ Kognition (12 M) ↓	[156]
TBA2	$A\beta Q_{(3-42)}$	Aβ-Ablagerungen (2 M) Neurodegeneration (12 M) Gliose (k.A.)		Motorik (k.A.) Kognition (k.A.)	[157]

Tabelle 2:Vergleich einiger AD Mausmodelle, in denen ein neuronaler Verlust beschrieben wird (k.A. keine Angabe, M Monate).

4.2 D-enantiomere Peptide zur kausalen Behandlung der Alzheimer'schen Demenz

Die Leitsubstanz D3

Der in dieser Arbeit beschriebene Ansatz für eine kausale Behandlung der AD beruht auf Peptiden, die aus mindestens 12 Aminosäureresten bestehen und in D-enantiomerer Konfiguration vorliegen. Diese wurden aus einer Peptidbibliothek mittels Spiegelbild-Phagendisplay gegen monomeres $A\beta_{(1-42)}$ selektiert [99].

Für die Leitsubstanz D3 konnte in diversen Studien der *in vitro* und *in vivo* Wirksamkeitsnachweis demonstriert werden. D3 eliminiert effizient toxische AβO im Aβ-QIAD assay [103], inhibiert die Aβ-Fibrillenbildung ($A\beta_{(1-42)}$ und $pEA\beta_{(3-42)}$) und das Nukleationsverhalten [110, 112]. Des Weiteren reduziert D3 die $A\beta_{(1-42)}$ und $pEA\beta_{(3-42)}$ induzierte Zelltoxizität [110, 158]. In mehreren *in vivo* Studien mit unterschiedlichen kognitiven AD Mausmodellen konnte belegt werden, dass D3 die kognitiven Fähigkeiten der Tiere (MWM und ORT) steigert und die AD assoziierte Pathologie reduziert (Aβ-Plaques, Gliose, lösliches und unlösliches Aβ). Zur weiteren Charakterisierung des D-Peptids D3 wurde eine intraperitoneale Behandlungsstudie am TBA2.1 Mausmodell durchgeführt (Manuskript Kapitel 3.5). In dieser konnte gezeigt werden, dass D3 die Progression des neuromotorischen Phänotyps, im direkten Vergleich zu Placebo-behandelten Mäusen, verringert. Des Weiteren bewirkte die D3-Behandlung, dass tendenziell weniger Neuronen innerhalb der CA1-Region absterben und weniger aktivierte Astrozyten in jener Region präsent sind (Manuskript Kapitel 3.5).Neben dem Wirksamkeitsnachweis wurden weitere Studien zur Untersuchung der pharmakokinetischen Eigenschaften sowie zur Stabilität von D3 durchgeführt. Diese ergaben, dass D3 eine aussichtsvolle orale Bioverfügbarkeit und terminale Halbwertszeit aufweist [107] und in verschiedenen Körperflüssigkeiten bzw. Organen über einen großen Zeitraum stabil ist [105]. Zusammenfassend legen diese Ergebnisse nahe, dass D3 ein potentieller Kandidat für eine kausale Therapie der AD wäre, jedoch zeigen einige D3-Derivate, insbesondere RD2, dessen Ergebnissen im Folgenden beschrieben werden, optimierte Eigenschaften.

Optimierungsstrategien - D3-Derivate

Trotz der vielversprechenden Eigenschaften der Leitsubstanz D3 als ein möglicher Wirkstoff zur kausalen Therapie der AD, wurde an weiteren Wirkstoffen, abgeleitet von der Leitsubstanz, geforscht, um die pharmakologischen Eigenschaften (z.B. eine höhere Effizienz zur AβO-Eliminierung, oder gesteigerte pharmakokinetische Eigenschaften) zu optimieren. Im Zuge dessen wurden, entweder durch rationales Wirkstoffdesign, z.B.

Umstrukturierung der Aminosäurereste (z.B. RD2), Zyklisierung der Peptide (z.B. cRD2D3), oder sequenzieller Austausch der D3-Aminosäureresten (ANK-Peptide) die sog. D3-Derivate entwickelt.

Das D3-Derivat RD2

Unter Verwendung eines rationalen Ansatzes zur Optimierung der Leitstruktur entstand das sog. D-Peptid RD2, welches aus exakt den gleichen Aminosäureresten besteht wie D3, nur in veränderter Reihenfolge. RD2 zeigt weiterhin das sog. Arginin-reiche-Motiv, jedoch mit einer Anreicherung der Arginine am C-Terminus. Durch die C-terminale Anhäufung der Arginine wurde angestrebt, die Bindung zu erhöhen und so effizienter AβO zu eliminieren. Pharmakokinetische Analysen des Peptides zeigten, dass es ähnlich positive Parameter aufweist wie die Leitstruktur, darüber hinaus noch eine erhöhte orale Verfügbarkeit und eine verlängerte Halbwertszeit zeigt [113].

In einer initialen Studie erfolgte die ausführliche *in vitro* Charakterisierung des D-Peptids RD2, sowie eine erste *in vivo* Studie, in der weibliche APP/PS1 transgene AD Mäuse (Alter: 7 Monate) über 28 Tage hinweg mittels einer intraperitonealen osmotischen Minipumpe kontinuierlich pro Tag mit 5,3 mg/kg RD2 behandelt worden sind. Durch das rationale Wirkstoffdesign erhöhte sich die AβO-Eliminierungseffizient. Im direkten Vergleich zu D3 eliminierte RD2 die AβO um ca. 70% (D3 ca. 50%). Darüber hinaus konnte in dieser Studie gezeigt werden, dass RD2 *in vitro* die Aβ-Fibrillenbildung dosisabhängig mit einem IC_{50} von 7,7 µM reduziert und diese unter Verwendung der höchsten eingesetzten Konzentrationen vollständig inhibiert. Des Weiteren konnte eine Bindungsaffinität von RD2 an Aβ-Monomere mit einem K_D von 3,6 µM gezeigt, sowie der Nachweis erbracht werden, dass RD2 das Nukelationspotential herabsetzt. Zudem erzielte RD2 eine Reduktion der $Aβ_{(1-42)}$-induzierten Zelltoxizität, ohne selbst ein zytotoxisches Potential aufzuweisen. Ferner bestätigten die Ergebnisse der Behandlungsstudie, dass die intraperitoneale RD2-Applikation zu einer signifikanten Steigerung der kognitiven Fähigkeiten im MWM führte, jedoch ohne einen signifikanten Einfluss auf die typische zerebrale Pathologie aufzuzeigen. Die Aβ-Plaques in Gehirnen RD2 behandelter APP/PS1 Mäuse wurden nur tendenziell verringert. Gleichwohl wurde die Konzentration unlöslicher $Aβ_{(x-42)}$ signifikant verringert. Aufgrund dessen ist anzunehmen, dass eine Steigerung der kognitiven Defizite nicht auf eine Reduktion der Aβ-Plaques beruht, sondern vielmehr auf einer Reduktion der toxischen AβO (Manuskript Kapitel 3.2, [158]).

Diese Studie lieferte einen ersten Hinweis, dass die AβO-Eliminierung ein vielversprechendes Ziel für eine AD-Therapie darstellt.

Aufgrund der vielversprechenden oralen Bioverfügbarkeit und der ersten erfolgreichen Behandlungsstudie wurde RD2, im direkten Vergleich zu weiteren D3-Derivaten (RD2RD2, RD2D3, D3D3) in einer groß angelegten oralen Behandlungsstudie getestet. In dieser wurden 32 Wochen alte weiblichen APP_{SL} Mäuse mit einer Dosierung von 20 mg/kg/Tag des jeweiligen Peptides behandelt. Es konnte der Nachweis erbracht werden, dass sowohl RD2, als auch D3D3 die kognitiven Fähigkeiten der Mäuse im MWM signifikant steigerte. Mäuse, die mit RD2RD2 oder RD2D3 behandelt wurden zeigten keine Steigerung ihrer kognitiven Leistung. In keiner der Behandlungsgruppen konnte eine Veränderung der Aβ-Pathologie oder der Gliose verzeichnet werden (Manuskript Kapitel 3.1 [159]). Sowohl in dieser Studie, als auch in der zuvor beschriebenen, konnte erwiesen werden, dass RD2 eine therapeutische Wirkung zeigt, die wegen des geringen Alters zum Zeitpunkt der Behandlung zum Teil jedoch auf einer präventiven Wirksamkeit beruhen kann.

Deshalb war es interessant herauszufinden, ob RD2 auch eine klare kurative Wirkung zeigt, da in den zuvor beschrieben Studien AD-Mausmodelle in einem Alter behandelt wurden, in dem weder die Pathologie, noch die kognitiven Defizite bereits allzu stark ausgeprägt sind (Manuskript Kapitel 3.7). Zu diesem Zweck wurden sehr alte (18 Monate ± 2 Wochen) APP/PS1 Mäuse oral behandelt. Laut der Literatur ist bekannt, dass APP/PS1 Mäuse in diesem Alter eine stark ausgeprägte AD-ähnliche Pathologie zeigten und starke kognitive Beeinträchtigungen aufweisen. Die männlichen Tiere wurden über einen Zeitraum von 12 Wochen mit 200 mg/kg/Tag RD2 oral behandelt. Im Zuge des 3R Prinzips des Tierschutzes (Reducement, Refinement, Replacement), wurden den Mäusen die Substanz nicht mittels einer üblichen Schlundsonde verabreicht, sondern in Form von neu entwickelten Gelatinedrops („Jellies“). Die orale Applikation von Substanzen über eine Schlundsonde kann, insbesondere über längere Zeiträume, zu einem vermehrten Stress für die Tiere führen sowie Verletzungen der Speiseröhre hervorrufen und im schlimmsten Fall, durch eine falsche Applikation in die Lunge, zum Tod der Versuchstiere führen. Im Menschen stellt die orale Applikation die Darreichungsform der Wahl da, da eine orale Gabe z.B. in Form von Tabletten eine hohe Therapietreue (Compliance) gewährleistet (Manuskript Kapitel 3.7).

Am Ende der zwölfwöchigen Behandlung konnte festgestellt werden, dass die RD2-Behandlung zu einer signifikanten Steigerung der kognitiven Fähigkeiten (MWM) der Tiere sowie eine Aufhebung des Phänotyps in allgemeinen Verhaltenstests (Offenfeldtest) führte. Die Analyse der AD-assoziierten Pathologie zeigte, dass die RD2-Behandlung in einer signifikanten Reduktion der Aβ-Plaques im Kortex sowie einer Reduktion löslicher $Aβ_{(x-42)}$-Spezies resultierte. Da die Tiere mit einer relativ hohen Dosis behandelt worden sind (200 mg/kg/Tag), wurden verschiedene Plasmaenzyme untersucht (Laktatdehydrogenase, Alanin-Aminotransferase, Aspartat-Aminotransferase und Alkaline-Phosphatase). Diese Parameter

werden in der Humanmedizin verwendet, um Aussagen über eine mögliche Intoxikation (Leber, Herz) durch eine zu hohe Dosierung von Wirkstoffen vorherzusagen. Eine Behandlung mit RD2 führte zu keiner Erhöhung oder Senkung der analysierten Parameter im Vergleich zu den beiden Kontrollgruppen. Da sich in der Vergangenheit gezeigt hat, dass einige potentiell kausale Therapien gegen die AD (Antikörper-basierte Therapien) verheerende Nebenwirkungen mit sich bringen, die auf einer (Über-)Aktivierung des Immunsystems beruhen, wurden in dieser Studie auch eine Vielzahl Entzündungsmarker im Plasma der Tiere analysiert (Zytokine, Chemokine). Auch hier konnte keine Erhöhung oder Senkung der analysierten Parameter im Vergleich zu den beiden Kontrollgruppen verzeichnet werden. Zusammenfassend konnte festgestellt werden, dass selbst unter Einsatz hoher Dosen RD2 keine Nebenwirkungen verursacht wurden (Manuskript Kapitel 3.7).

Eine weitere bemerkenswerte Errungenschaft dieser Studie war, dass in dieser zum ersten Mal ein sog. „Target-Engagement“ *in vivo* demonstriert werden konnte. Als Target-Engagement wird die Interaktion des Liganden (der Substanz, in diesem Fall RD2) mit der Zielstruktur beschrieben (in diesem Fall AβO). Untersuchungen des *in vivo* Target-Engagements wurden unter Verwendung des neu entwickelten diagnostischen Werkzeugs, des sFIDA-Assays (Surface-based Fluorescence Intensity Distribution Analysis), durchgeführt. Der sFIDA-Test, ursprünglich etabliert, um AβO als Biomarker aus Körperflüssigkeiten (z. B. Cerebrospinalflüssigkeit oder Plasma) zu quantifizieren, kombiniert die Spezifität eines ELISA-ähnlichen Tests mit hochauflösender Fluoreszenzmikroskopie [160-163]. Unter Verwendung des sFIDA-Tests werden Aβ-Spezies aus Körperflüssigkeiten durch einen Anti-Aβ-Antikörper (z.B. 6E10), der gegen den N-Terminus des Aβ gerichtet ist, an einer Oberfläche gebunden. Zur Diskriminierung gebundener Aβ-Monomere von AβO bzw. Aβ-Aggregaten beinhalten die verwendeten Fänger- und Detektions-Antikörper überlappende Epitope. Dadurch ist der sFIDA völlig unempfindlich für Aβ-Monomere. Um gebundene AβO und Aβ-Aggregate nachzuweisen, werden kolokalisierte Signale über einem vordefinierten Cutoff durch TIRF-Mikroskopie (Total Internal Reflection) gezählt. Anschließend wird die AβO-Konzentrationen unter Anwendung eines geeigneten Kalibrierungsstandards berechnet [160-162]. Mit dem Ziel, den sFIDA-Test auch für den Nachweis von AβO aus Hirnhomogenaten zu verwenden, wurde der sFIDA-Test mit dem Aβ-QIAD-Assay kombiniert, um Aβ-Spezies entsprechend ihrer Größe zu fraktionieren. Unter Verwendung dieser Kombination konnte eine signifikante Reduktion toxischer AβO in den Gehirnen von RD2-behandelten Mäusen gezeigt werden. Dieser Versuch ist ein weiterer Beleg für den Wirkmechanismus von RD2 – die gezielte Eliminierung toxischer AβO (Manuskript Kapitel 3.7).

Verglichen zu den anderen mit RD2 durchgeführten Studien, in denen auch AD-Modelle der Amyloidose behandelt wurden, konnte in dieser Studie, wie bereits beschrieben, ein schwacher aber signifikanter Rückgang der Aβ-Plaques im Kortex verzeichnet werden. Eine Reduktion von Aβ-Plaques ist nicht zwingend notwendig, um eine Steigerung kognitiver Fähigkeiten zu erzielen, da AβO für diese verantwortlich gemacht werden. Es ist davon auszugehen, dass in dieser Studie Aβ-Plaques reduziert worden sind, da hier die Behandlungsdauer erheblich länger war und eine zehnfach höhere Dosierung eingesetzt wurde (200 mg/kg/Tag RD2 anstatt 20 mg/kg/Tag RD2).

Wie bereits zuvor erwähnt, ist es zwingend notwendig, neue Substanzen zur potentiell kausalen Therapie der AD in mehreren AD-Mausmodellen zu evaluieren, insbesondere im Hinblick auf eine mögliche Veränderung der Neurodegeneration. Zu diesem Zweck wurde in dieser Arbeit eine weitere RD2-Behandlungsstudie mit dem TBA2.1 AD-Mausmodell durchgeführt (Manuskript Kapitel 3.8). Wie unter Kapitel 1.6 und 3.6 näher beschrieben, zeichnen sich homozygote Mäuse dieser Linie durch einen motorischen Phänotyp aus, einhergehend mit einer starken Neurodegeneration innerhalb der CA1 Region. Wie auch in der Studie mit gealterten APP/PS1 Mäusen, wurde diese Studie mit oraler Applikation (mittels Jellies) durchgeführt. Die Mäuse erhielten entweder 20 oder 100 mg/kg RD2 täglich über einen Zeitraum von 12 Wochen. Eine Besonderheit dieser Studie ist, neben dem genutzten Mausmodell, dass in dieser nicht nur transgene (homozygote) Mäuse, sondern auch nicht-transgene Geschwistertiere mit den o.g. Konzentrationen RD2 behandelt wurden. Dies diente dem Zweck, zu evaluieren, ob eine Behandlung zu möglichen unerwünschten Arzneimittelwirkungen führt, die sich auf das Verhalten der Tiere niederschlägt, und um die Spezifität der Behandlung in transgenen Mäusen zu demonstrieren. Ersteres ist insbesondere von besonderer Wichtigkeit, da in dieser Studie eine relativ hohe Dosierung gewählt wurde (100 mg/kg/Tag RD2). Die Analyse der durchgeführten motorischen und allgemeinen Verhaltenstests, die zuvor in der Charakterisierung des Mausmodell evaluiert wurden, (Manuskript Kapitel 3.6) zeigte, dass RD2 einen positiven Effekt auf die Progression des Phänotyps der homozygoten Tiere hat, indem diese in verschiedenen Tests (SHIRPA-, Stangen- und Clasping-Test) eine signifikant gesteigerte Leistung im Vergleich zu den Placebotieren zeigten. Jedoch war kein Unterschied zwischen den beiden Behandlungsgruppen mit unterschiedlicher Dosierung zu erkennen, beide zeigten eine ähnliche Verbesserung des Phänotyps. Ausgegend von einer möglichen Dosisabhängigkeit wäre zu erwarten gewesen, dass die Wirkung von 100 mg/kg/Tag RD2-Behandlung stärker ist als eine Behandlung mit 20 mg/kg/Tag. Jedoch konnte kein Unterschied zwischen den beiden RD2-Behandlungsgruppen determiniert werden. Eine mögliche Erklärung ist, dass die Dosis-Wirkungs-Kurve bereits im Sättigungsbereich liegt (Manuskript Kapitel 3.8).

Auf histologischer Ebene konnte insgesamt kein signifikanter Unterschied zwischen den Behandlungsgruppen determiniert werden. Es konnte zwar eine Tendenz für einen möglichen Rückgang der Aβ-Ablagerungen im Striatum der 100 mg/kg/Tag RD2-behandelten Tiere gezeigt werden, jedoch zeigte weder eine Analyse der Neuronen, noch der analysierten Entzündungszellen (aktivierte Mikroglia und Astrozyten) eine Änderung der Pathologie dieses AD-Mausmodells (Manuskript Kapitel 3.8).

Die behandelten Wildtypen zeigten weder Auffälligkeiten im Verhalten, noch Veränderungen auf histologischer Ebene. Dieser Umstand verstärkt die Vermutung, dass eine Behandlung mit RD2 zu keinerlei Nebenwirkungen führt. Außerdem konnte demonstriert werden, dass die mit RD2-behandelten nicht-transgenen Geschwistertiere keinerlei Abweichungen zu den Placebo-behandelten Tieren zeigten, was die Spezifität der RD2-Behandlung gegen Aβ beweist.

Durch die in dieser Arbeit erzielten Ergebnisse lässt sich schlussfolgern, dass RD2 ein äußerst vielversprechender Kandidat für eine kausale Therapie der AD sein könnte. Unabhängig vom ausgewählten Mausmodell (APP/PS1, APP_{SL}, TBA2.1) und der gewählten Applikationsart (intraperitoneal, oral), konnten immer positive Ergebnisse erzielt werden. In den drei Studien, die an kognitiven Mausmodellen der AD durchgeführt wurden, konnte jedes Mal der Wirksamkeitsnachweis erbracht werden (Manuskripte Kapitel 3.1, 3.2 und 3.7). Darüber hinaus wurde RD2 nicht nur in kognitiven Mausmodellen der AD evaluiert, sondern auch in einem Mausmodell, welches durch einen neurodegenerativen und motorischen Phänotyp gekennzeichnet ist, das TBA2.1 AD-Mausmodell. In diesem konnte demonstriert werden, dass RD2, unabhängig von der eingesetzten Dosierung, den Phänotyp signifikant verbessert, ohne dabei geringste Anzeichen möglicher unerwünschter Arzneimittelwirkungen aufzuweisen (Behandlung nicht-transgener Geschwistertiere). Im Vergleich zu vielen Studien mit anderen potentiell kausalen Therapien ist dies ein entscheidender Vorteil. Ein Versagen vieler klinischer Studien ist unter anderem darauf zurückzuführen, dass die Substanzen ausschließlich in einer Art AD-Mausmodelle getestet wurden (z.B. Modelle der Amyloidose (APP/PS1).

Die hier evaluierten Daten und die zuvor veröffentlichen pharmakokinetischen Studien zeigen, dass RD2 eine neue und geeignete Substanz für eine Therapie der AD darstellt. Nicht nur der neue Wirkmechanismus stellt eine Errungenschaft dar. Die gezielte Eliminierung von AβO, ohne auf z.B. Komponenten des Immunsystems angewiesen zu sein, ist ein entscheidender Vorteil gegenüber anderen Therapien, wie z.B. der Antikörper-basierten Therapie. In der Vergangenheit zeigte sich, dass durch die Aktivierung des Immunsystems, die zur Behandlung der Erkrankung durch diesen Therapieansatz zwingend

notwendig ist, gravierende Nebenwirkungen verzeichnet wurden. Eine mögliche Therapie mit RD2 ist nicht auf das Immunsystem angewiesen. Dies wird vor allem dadurch deutlich, dass in keiner der durchgeführten Studien eine Veränderungen (weder eine Erhöhung, noch eine Senkung) des zerebral-entzündlichen Milieus erkennbar war. Darüber hinaus zeigte sich keine Änderungen pro- und anti-inflammatorischer Zytokine, welche im Plasma RD2- und Placebo-behandelter Mäuse, sowie deren nicht-transgener Geschwistertiere analysiert wurden. Aufgrund der von Leithold et al. 2016 durchgeführten pharmakokinetischen Analysen ließ sich eine hervorragende orale Bioverfügbarkeit mit einer langen terminalen Halbwertszeit erkennen, die nahe legte, dass RD2 orale Wirksamkeit zeigt [113]. Dies wurde in dieser Arbeit mit drei Behandlungsstudien an drei Mausmodellen belegt. Die orale Verfügbarkeit und die lange terminale Halbwertszeit sind wieder ein entscheidender Vorteil gegenüber anderen Wirkstoffkandidaten, wie z.B. Antikörpern. Eine tägliche orale Darreichung bietet die beste Therapietreue und wird in der Regel von Patienten besser angenommen, als immer wiederkehrende Injektion, wie sie bei der passiven Immunisierung nötig sind.

Die D3-Derivate D3D3, cD3r, RD2D3, cRD2D3 und RD2RD2

Im Zuge der letzten Jahre wurde eine Vielzahl weiterer D3-Derivate entwickelt, von denen die effizientesten in pharmakokinetischen und/oder Behandlungsstudien analysiert worden sind. Zur Optimierung der Leitstruktur wurde nicht nur eine rationale Umstrukturierung der Aminosäurereste (RD2) vorgenommen. Daneben wurde auch versucht, durch sog. Tandempeptide (Kopf-Schwanz-Verbindung) aus zwei Kopien eines Ursprungspeptids (z.B. D3D3, RD2RD2, ANK6ANK6 (tANK6)), oder einer Kombination aus zwei Ursprungspeptiden (RD2D3) die Effizienz zur AβO-Eliminierung zu erhöhen. Weiterhin wurden zyklische Peptide aus den bekannten Strukturen entwickelt (head-to-tail-Zyklisierung; cD3r, cRD2D3). *In vitro* zeigten die von RD2 und D3 abgeleiteten Substanzen eine erhöhte Effizient zur AβO-Eliminierung im Aβ-QIAD Assay sowie eine z.T. erhöhte Bindungsaffinität an monomeres $A\beta_{(1\text{-}42)}$ (Tabelle 3). Neben den *in vitro* Untersuchungen wurden mit einigen dieser Substanzen (D3D3, cD3r, RD2RD2, RD2D3) *in vivo* Experimente in entweder einem, oder mehreren Mausmodellen der AD durchgeführt. D3D3 zeigte in zwei kognitiven Mausmodellen (tgSw-DI, APP_{SL}) (Manuskript Kapitel 3.1 [103, 159]) eine Steigerung der kognitiven Fähigkeiten im Vergleich zu den Placebo-behandelten Mäusen. Des Weiteren konnte eine Stagnation des Phänotyps im TBA2.1 Mausmodell verzeichnet werden (Manuskript 3.4 [110]). Für die D-Peptide cD3r, RD2RD2 und RD2D3 konnte bisher keine Steigerung der Kognition nach einer Behandlung nachgewiesen werden [159, 164]. Die pharmakokinetischen Eigenschaften der D-Peptide D3, cD3r, D3D3, RD2, RD2D3 und cRD2D3 wurden in diversen Studien untersucht (Manuskript 3.4 [107, 113, 165, 166]). In

diesen Studien konnte gezeigt werden, dass alle D-Peptide ihren Wirkort (das Gehirn) erreichen. Auffällig war, dass vor allem cRD2D3, trotz ähnlicher Plasmawerte, in höheren Konzentrationen im Gehirn nachzuweisen war. Aufgrund der erhobenen Daten zur Effizient der BHS-Gängigkeit [166] wurde die Hypothese erstellt, dass die Zyklisierung der D-Peptide zu erhöhten CSF- und Gehirnkonzentrationen führt. Die Analyse einiger universell einsetzbarer BHS-Parameter [167] zeigt, dass eine Zyklisierung der D-Peptide, vor allem im Vergleich von RD2D3 und cRD2D3, einen positiven Einfluss auf die Effizient der BHS-Gängigkeit hat [166] (Tabelle 3) (Manuskript 3.4 [166]). Wir postulieren, dass cRD2D3, aufgrund seiner erhöhten Effizienz der Überschreitung der BHS und somit einer erhöhten Konzentration im Zielorgan Gehirn, eine gesteigerte *in vivo* Wirksamkeit aufzeigen wird. Ein solcher Nachweis würde den endgültigen Beweis erbringen, dass die Zyklisierung der D-Peptide eine vielversprechende Optimierungsform darstellt.

Ausgehend von einer weiteren systematischen Optimierung der Leitstruktur D3 entstanden die sog. ANK1 bis ANK 7 D-Peptide. Während dieser Optimierung wurden zur Steigerung der Sequenzvariabilität neben den 18 natürlichen Aminosäuren (außer Cystein) auch 13 nicht natürlich vorkommende Aminosäuren verwendet. *In vitro* zeigten diese neuartigen Peptide eine gesteigerte Bindung an monomeres Aβ sowie eine erhöhte Aβ-Fibrilleninhibierung. Darüber hinaus zeigten die D-Peptide ANK1 bis ANK7 eine gesteigerte Effizienz zur AβO-Eliminierung [112]. Jedoch konnte in einer initialen *in vivo* Studien mit ANK6, dem vielversprechendsten der ANK D-Peptide, keine signifikante Steigerung der kognitiven Fähigkeiten im tgSw-DI Mausmodells gezeigt werden (Tabelle 3).

Zu Überprüfung der pharmakokinetischen Eigenschaften des D-Peptides ANK6 und dessen Tandem- (tANK6) und zyklisierter-Form (cANK6) wurde mit den drei ANK D-Peptiden eine ausgiebige pharmakokinetische Studie durchgeführt (Manuskript Kapitel 3.9). In dieser Studie sollte ebenfalls die aufgestellte Hypothese überprüft werden, ob die Zyklisierung des Peptides zu einer erhöhten BHS-Gängigkeit führt. Im Vergleich zu den anderen getesteten D -Peptiden zeigten die ANK6-Peptide, trotz der gesteigerten *in vitro* Qualitäten, weniger erfolgsversprechende pharmakokinetische Eigenschaften (Manuskript Kapitel 3.9). Diese könnten eine mögliche Erklärung für die nicht signifikant erfolgreiche Behandlungsstudie mit ANK6 darstellen [112].

Ein direkter Vergleich der unter Tabelle 3 aufgeführten D-Peptide zeigt, dass trotz herausragender *in vitro* Eigenschaften, wie z.B. eine erhöhte Effizienz zur AβO-Eliminierung, diese nicht direkt auf die *in vivo* Ergebnisse (Pharmakokinetik und Wirksamkeitsnachweis) übertragbar sind. Im Vergleich zu der Leitstruktur D3 und dem Derivat RD2 zeigen alle unter Tabelle 3 aufgeführten D3-Derivate eine erhöhte Effizienz zur AβO-Eliminierung, sowie z.T.

erhöhte Bindungseigenschaften (D3D3, RD2D3 und ANK6) und eine erhöhte Inhibierung der $A\beta_{(1-42)}$-Fibrillenbildung (cRD2D3, ANK-Peptide). Jedoch konnte bisher nur das D3-Derivat D3D3, neben der Leitstruktur und RD2, *in vivo* den Wirksamkeitsnachweis liefern (Manuskripte Kapitel 3.1 und 3.2 [103, 110, 159]). Die ANK6-Peptide (ANK6, tANK6, cANK6) verdeutlichen diesen Umstand. Alle zeigen im Vergleich zu den anderen unter Tabelle 3 aufgelisteten D-Peptiden die effizientere *in vitro* Eigenschaften. Jedoch konnte für ANK6 bisher kein Wirksamkeitsnachweis *in vivo* erzielt werden [112]. Darüber hinaus konnte in pharmakokinetischen Studien gezeigt werden, dass ANK6, tANK6 und cANK6, im Vergleich zu RD2, unvorteilhaftere Parameter aufweisen. Diese spiegeln sich insbesondere in einer niedrigeren terminalen Halbwertszeit, eine geringeren oralen Verfügbarkeit und einer niedrigeren maximalen Konzentration im Gehirn wider (Manuskript Kapitel 3.9). Jedoch können keine direkten Rückschlüsse von einer vielversprechenden Pharmakokinetik auf eine spätere Wirksamkeit im Tiermodell geschlossen werden. Dies wird am Beispiel des D3-Derivates D3D3 deutlich. Im Vergleich zu D3 und RD2 zeigt dieses D-Peptid unvorteilhaftere pharmakokinetische Eigenschaften [107, 113, 165], zeigte jedoch aufgrund einer deutlich höheren *in vitro* Effizienz im TBA2.1 Tiermodell eine tendenziell erhöhten Wirksamkeit als D3 (Manuskript Kapitel 3.5 [103, 110]).

Mit Referenz zu allen bis hierhin generierten Daten der D-Peptide kristallisiert sich heraus, dass RD2 das herausragendste pharmakologische Profil präsentiert. Die evaluierten Daten

1. der Wirksamkeitsnachweis in drei AD-Mausmodellen in drei verschiedenen Laboratorien,
2. die orale Verfügbarkeit, kombiniert mit einer zuverlässigen BHS-Gängigkeit und einer langen terminalen Halbwertszeit,
3. die *in vivo* erwiesene Effektivität für die Zerstörung der Zielstruktur (Eliminierung toxischer AβO in Gehirnen behandelter Mäuse),
4. keine bis zu diesem Zeitpunkt in Erscheinung getretenen unerwünschten Arzneimittelwirkungen in Mäusen, selbst nach Behandlungsstudien mit hohen Dosierungen,

sprechen für eine potentiell erste Anwendung im Menschen. RD2 stellt eine neue Substanzklasse zur kausalen Behandlung der AD dar, mit einem neuartigen Wirkmechanismus.

	D3	D3D3	cD3r	RD2	RD2RD2	RD2D3	cRD2D3	ANK6	tANK6	cANK6
AβO-Eliminierung [%]	51	96	90	71	95	98	n.D.	98	99	97
K_D Aβ$_{(1-42)}$ [µM]	4,0	1,2	2,9	3,8	n.D.	0,5	n.D.	2,3	n.D.	n.D.
K_D pEAβ$_{(3-42)}$ [µM]	11,2	0,3	n.D.	26,6	n.D.	n.D.	n.D.	n.D.	n.D.	n.D.
Inhibition Fibrillenbildung Aβ$_{(1-42)}$	√	√	√	√	n.D.	√	√*	√	√	√
IC50 ThT Aβ$_{(1-42)}$ [µM]	7,2	n.D.	n.D.	7,7	n.D.	n.D.	1,8 *	3,6	2,1	3,7
Reduktion Zelltoxizität Aβ$_{(1-42)}$ (pEAβ$_{(3-42)}$)	√ (√)	√ (√)	√	√	√	√	√	√	√	√
orale Bioverfügbarkeit [%]	58	n.D.	n.D.	77	n.D.	n.D.	98	11,8	49,4	9,9
orale terminale Halbwertszeit ($t_{1/2}$) [h]	41 h	n.D.	n.D.	58	n.D.	n.D.	58	22	31 h	30
logBB	-0,07	n.D.	n.D.	0,78	n.D.	-0,22	-0,09	-0,4	0,34	-0,33
K_D HSA [µM]	n.a.	n.a.	n.D.	n.a.	n.D.	n.a.	33,2	n.a.	137,7	598,7
K_D AGP [µM]	1,8	n.a.	n.D.	2,8	n.D.	n.a.	1,2	0,29	0,06	0,28
Kognition	↑	↑ (i.p. ORT)	k.V. (i.p. MWM)	↑ (MWM)	n.D.	k.V. (i.p. MWM)	n.D.	k.V. (i.p. MWM)	n.D.	n.D.
Kognition nach oraler Gabe	↑	↑ (MWM)	n.D.	↑ (MWM)	k.V.(MWM)	k.V.(MWM)	n.D.	n.D.	n.D.	n.D.
Motorik (TBA2.1)	k.V.(i.p.)	↑	n.D.	↑	k.V. (i.p.)*	k.V. (i.p.)*	n.D.	n.D.	n.D.	n.D.
Aβ-Plaques	↓	k.V.	k.V.	↓	k.V.	k.V.	n.D.	n.D.	n.D.	n.D.
Gliose	↓	k.V.	n.D.	k.V.	k.V.	k.V.	n.D.	n.D.	n.D.	n.D.
Biochemie (Aβ40 und 42)	↓	n.D.	n.D.	↓	n.D.	n.D.	n.D.	n.D.	n.D.	n.D.
Biochemie (pEAβ$_{(3-42)}$)	↑	↑	n.D.	↑	n.D.	n.D.	n.D.	n.D.	n.D.	n.D.
Literatur	[98, 100, 102, 103, 107]	[103, 110, 165]	[164, 166]	[113, 158, 159]	[159]	[159, 165]	[166]	[111]		

Tabelle 3: Übersicht der D-Peptide hinsichtlich ihrer *in vitro* Charakteristika, pharmakokinetischen Eigenschaften und *in vivo* Wirksamkeit. k.V. keine Veränderung; n.D. nicht determiniert; i.p. intraperitoneal; ORT object recognition test; MWM Morris water maz

5. Ausblick

Die AD stellt ein immer größer werdendes gesundheitliches und ökonomisches Problem in unserer alternden Gesellschaft dar. Für Betroffene als auch für deren Angehörige birgt die Erkrankung, nach ihren ersten erkennbaren klinischen Symptomen – dem fortschreitenden Gedächtnisverlust – progressiv fortschreitend sowohl physische, als auch starke psychische Belastungen. Aufgrund dessen ist es unerlässlich, an neuen und kausal wirkenden Wirkstoffen zu forschen, die nicht nur die Progression der Krankheit hinauszögern, sondern diese auch heilen.

In dieser Arbeit wurde eine neuartige Arzneimittelklasse für eine mögliche Behandlung der AD beschrieben. Das umfassend analysierte D-enantiomere Peptid RD2 konnte in mehreren Mausmodellen der AD eine signifikante Verbesserung des Phänotyps (Kognition, Motorik und AD-assoziierte Pathologie) bewirken. Darüber hinaus konnte bestätigt werden, dass RD2 *in vivo* eine Spezifität für seine Zielstruktur zeigt. Aufgrund dieser erhobenen Daten stellt RD2 einen vielversprechenden Kandidaten für eine mögliche Anwendung im Menschen dar. Die hervorragenden pharmakokinetischen Eigenschaften, insbesondere die hohe orale Verfügbarkeit, sowie der *in vivo* Wirksamkeitsnachweis nach oraler Applikation zeigen, dass der hier gebotene Therapieansatz einen entscheidenden Vorteil gegenüber anderen Therapien bietet. Es ist davon auszugehen, dass an AD erkrankte Patienten über mehrere Jahre, wenn nicht sogar Jahrzehnte hinweg behandelt werden müssen. Die orale Gabe bietet hier die bestmögliche Darreichungsform, da sie durch ihre Einfachheit und Praktikabilität eine hohe Therapietreue (Compliance) gewährleistet. Eine orale Darreichungsform kann nicht bei jeder neuartigen, kausalen Therapie der AD gewährleitet werden, ganz besonders wie bei Antikörper-basierten Therapieansätzen. Darüber hinaus konnte bisher kein Hinweis auf eine unerwünschte (Über-)Reaktion des Immunsystems beobachtet werden, die oft in bisherigen klinischen Studien mit Antikörper-basierten Therapieansätzen beobachtet wurden. Der hier beschriebene Therapieansatz zielt ausschließlich auf die direkte Eliminierung toxischer AβO ab. Da die bisher veröffentlichten Ergebnisse keine weiteren Wechselwirkungen mit anderen Zielstrukturen beschreiben, liegt die Vermutung nahe, dass keine Nebenwirkungen auftreten werden (On/Off-Target Effekte, die z.B. unter dem Einsatz von γ-Sekretaseinhibitoren beobachtet wurden). Jedoch bleiben, trotz der umfassend erhobenen Daten, einige Fragen offen, die es gilt in der Zukunft zu beantworten. Dazu zählt der genaue *in vivo* Wirkmechanismus – wie wird die Toxizität der AβO hinabgesetzt? Bewirkt eine Behandlung mit RD2 eine Normalisierung der synaptischen Transmission? Können Signalwege, die in der AD beeinträchtigt sind, durch eine Behandlung mit RD2 wiederhergestellt werden?

Zusätzlich besteht trotz der (präklinisch) erwiesenen Wirksamkeit von RD2 die Notwendigkeit, nach weiteren von D3 oder RD2 abgeleiteten Strukturen (Derivaten) zu forschen, um die pharmakologischen, insbesondere die pharmakokinetischen Eigenschaften noch weiter zu erhöhen. Trotz der aussichtsreichen oralen Bioverfügbarkeit kann diese durch weitere Modifikationen erhöht werden. Ein solches Derivat könnte das zyklische cRD2D3 darstellen, welches vorteilhaftere pharmakokinetische Eigenschaften aufweist. Bei gleich eingesetzten Konzentrationen gelangt cRD2D3 effizienter in das Gehirn als RD2.

Da bereits gezeigt werden konnte, dass D3 nicht nur an Aβ bindet, sondern auch einen Einfluss auf die SEVI-Fibrillen (HIV) zeigt, liegt es nahe zu untersuchen, ob D3 und seine Derivate auch einen Einfluss auf andere Proteine, die in der AD involviert sind haben (z.B. auf das Tau-Protein). Des Weiteren besteht die Möglichkeit, die Wirksamkeit von D3 und seinen Derivaten auf andere neurodegenerative Erkrankungen auszuweiten, denen ebenfalls eine Akkumulationen fehlgefalteter Proteine im Gehirn zugrunde liegen, wie die Amyotrophe Lateralsklerose, Chorea Huntington, Morbus Parkinson oder Tauopathien.

Abkürzungsverzeichnis

ACh	Acetylcholin
AChE	Acetylcholinesterase
AChEI	Acetylcholinesterasehemmer
AD	Alzheimer'sche Demenz
AGP	α-1-saueres Glykoprotein
AMPA	α-amino-3-hydroxy-5-methyl-4-isoxazolepropionic acid
APLP	Amyloid-like protein 1
ApoE	Apolipoprotein E
APP	Amyloidvorläuferprotein (engl. Amyloid protein precursor)
Aβ	Amyloid β
AβO	Amyloid β Oligomere
BACE	β-site of APP cleaving enzyme
BHS	Blut-Hirn-Schranke
CSF	Cerebrospinalflüssigkeit
ELISA	Enzyme-linked Immunosorbent Assay
EOAD	early onset AD
fAD	familiäre AD
GABA	γ-Aminobuttersäure
GAG	Glykosaminoglykane
GSK	glycogen synthase kinase
HSA	human serum albumin
LOAD	late onset AD
logBB-Wert	Blut-Gehirn-Gleichgewichtsverteilung
Ion	London
MRT	Magnetresonanztomographie
MWM	Morris Water Maze
NFT	neurofibrillary tangles
NMDA	N-methyl-D-Aspartat
ORT	Object recognition test
pEAβ	pyroglutamate Amyloid β
PET	Positionsemissionstomographie
PKC	Proteinkinase C
PS	Präsenilin
PTM	Posttranslationale Modifikation
QIAD	quantitative determination of interference with aggregate size distribution
sAD	sporadische AD
sFIDA	surface-based Fluorescence Intensity Distribution Analysis
SPR	surface plasmon resonance
Swe	swedisch
$T_{1/2}$	Halbwertszeit
Tg	Transgen
ThT	Thioflavin T
TIRF	Total Internal Reflection

Referenzen

[1] Alzheimer A (1907) Über eine eigenartige Erkrankung der Hirnrinde. *Allgemeine Zeitschrift fur Psychiatrie und Psychisch-gerichtliche Medizin.* **64**, 146-148.

[2] Blennow K, de Leon MJ, Zetterberg H (2006) Alzheimer's disease. *Lancet* **368**, 387-403.

[3] Krysinska K, Sachdev PS, Breitner J, Kivipelto M, Kukull W, Brodaty H (2017) Dementia registries around the globe and their applications: A systematic review. *Alzheimers Dement* **13**, 1031-1047.

[4] Prince M, Wimo A, Guerchet M, Ali G-M, Wu Y-T, Prina M (2015) World Alzheimer Report 2015. The Global Impact of Dementia. An Analysis of Prevalence, Incidence, Costs and Trends. *Alzheimer's Disease International*.

[5] Lista S, Dubois B, Hampel H (2015) Paths to Alzheimer's disease prevention: from modifiable risk factors to biomarker enrichment strategies. *J Nutr Health Aging* **19**, 154-163.

[6] Crous-Bou M, Minguillon C, Gramunt N, Molinuevo JL (2017) Alzheimer's disease prevention: from risk factors to early intervention. *Alzheimers Res Ther* **9**, 71.

[7] Hasnain M, Vieweg WV (2014) Possible role of vascular risk factors in Alzheimer's disease and vascular dementia. *Curr Pharm Des* **20**, 6007-6013.

[8] Imtiaz B, Tolppanen AM, Kivipelto M, Soininen H (2014) Future directions in Alzheimer's disease from risk factors to prevention. *Biochem Pharmacol* **88**, 661-670.

[9] Gorelick PB (2004) Risk factors for vascular dementia and Alzheimer disease. *Stroke* **35**, 2620-2622.

[10] Duara R, Lopez-Alberola RF, Barker WW, Loewenstein DA, Zatinsky M, Eisdorfer CE, Weinberg GB (1993) A comparison of familial and sporadic Alzheimer's disease. *Neurology* **43**, 1377-1384.

[11] Selkoe DJ, Podlisny MB (2002) Deciphering the genetic basis of Alzheimer's disease. *Annu Rev Genomics Hum Genet* **3**, 67-99.

[12] Yoshikai S, Sasaki H, Doh-ura K, Furuya H, Sakaki Y (1990) Genomic organization of the human amyloid beta-protein precursor gene. *Gene* **87**, 257-263.

[13] Karch CM, Cruchaga C, Goate AM (2014) Alzheimer's disease genetics: from the bench to the clinic. *Neuron* **83**, 11-26.

[14] Bergmans BA, De Strooper B (2010) gamma-secretases: from cell biology to therapeutic strategies. *Lancet Neurol* **9**, 215-226.

[15] Sherrington R, Rogaev EI, Liang Y, Rogaeva EA, Levesque G, Ikeda M, Chi H, Lin C, Li G, Holman K, Tsuda T, Mar L, Foncin JF, Bruni AC, Montesi MP, Sorbi S, Rainero I, Pinessi L, Nee L, Chumakov I, Pollen D, Brookes A, Sanseau P, Polinsky RJ, Wasco W, Da Silva HA, Haines JL, Perkicak-Vance MA, Tanzi RE, Roses AD, Fraser PE, Rommens JM, St George-Hyslop PH (1995) Cloning of a gene bearing missense mutations in early-onset familial Alzheimer's disease. *Nature* **375**, 754-760.

[16] Levy-Lahad E, Wasco W, Poorkaj P, Romano DM, Oshima J, Pettingell WH, Yu CE, Jondro PD, Schmidt SD, Wang K, et al. (1995) Candidate gene for the chromosome 1 familial Alzheimer's disease locus. *Science* **269**, 973-977.

[17] Guerreiro RJ, Gustafson DR, Hardy J (2012) The genetic architecture of Alzheimer's disease: beyond APP, PSENs and APOE. *Neurobiol Aging* **33**, 437-456.

[18] Liu CC, Liu CC, Kanekiyo T, Xu H, Bu G (2013) Apolipoprotein E and Alzheimer disease: risk, mechanisms and therapy. *Nat Rev Neurol* **9**, 106-118.

[19] Sperling RA, Aisen PS, Beckett LA, Bennett DA, Craft S, Fagan AM, Iwatsubo T, Jack CR, Jr., Kaye J, Montine TJ, Park DC, Reiman EM, Rowe CC, Siemers E, Stern Y, Yaffe K, Carrillo MC, Thies B, Morrison-Bogorad M, Wagster MV, Phelps CH (2011) Toward defining the preclinical stages of Alzheimer's disease: recommendations from the National Institute on Aging-Alzheimer's Association workgroups on diagnostic guidelines for Alzheimer's disease. *Alzheimers Dement* **7**, 280-292.

[20] McKhann G, Drachman D, Folstein M, Katzman R, Price D, Stadlan EM (1984) Clinical diagnosis of Alzheimer's disease: report of the NINCDS-ADRDA Work Group under the auspices of Department of Health and Human Services Task Force on Alzheimer's Disease. *Neurology* **34**, 939-944.

[21] Jakob-Roetne R, Jacobsen H (2009) Alzheimer's disease: from pathology to therapeutic approaches. *Angew Chem Int Ed Engl* **48**, 3030-3059.

[22] Di Paola M, Macaluso E, Carlesimo GA, Tomaiuolo F, Worsley KJ, Fadda L, Caltagirone C (2007) Episodic memory impairment in patients with Alzheimer's disease is correlated with entorhinal cortex atrophy. A voxel-based morphometry study. *J Neurol* **254**, 774-781.

[23] Braak H, Braak E (1991) Neuropathological stageing of Alzheimer-related changes. *Acta Neuropathol* **82**, 239-259.

[24] Scholl M, Lockhart SN, Schonhaut DR, O'Neil JP, Janabi M, Ossenkoppele R, Baker SL, Vogel JW, Faria J, Schwimmer HD, Rabinovici GD, Jagust WJ (2016) PET Imaging of Tau Deposition in the Aging Human Brain. *Neuron* **89**, 971-982.

[25] Thal DR, Rub U, Orantes M, Braak H (2002) Phases of A beta-deposition in the human brain and its relevance for the development of AD. *Neurology* **58**, 1791-1800.

[26] Ringman JM, Goate A, Masters CL, Cairns NJ, Danek A, Graff-Radford N, Ghetti B, Morris JC (2014) Genetic heterogeneity in Alzheimer disease and implications for treatment strategies. *Curr Neurol Neurosci Rep* **14**, 499.

[27] Oh ES, Savonenko AV, King JF, Fangmark Tucker SM, Rudow GL, Xu G, Borchelt DR, Troncoso JC (2009) Amyloid precursor protein increases cortical neuron size in transgenic mice. *Neurobiol Aging* **30**, 1238-1244.

[28] Meziane H, Dodart JC, Mathis C, Little S, Clemens J, Paul SM, Ungerer A (1998) Memory-enhancing effects of secreted forms of the beta-amyloid precursor protein in normal and amnestic mice. *Proc Natl Acad Sci U S A* **95**, 12683-12688.

[29] Roch JM, Masliah E, Roch-Levecq AC, Sundsmo MP, Otero DA, Veinbergs I, Saitoh T (1994) Increase of synaptic density and memory retention by a peptide representing the trophic domain of the amyloid beta/A4 protein precursor. *Proc Natl Acad Sci U S A* **91**, 7450-7454.

[30] Jonsson T, Atwal JK, Steinberg S, Snaedal J, Jonsson PV, Bjornsson S, Stefansson H, Sulem P, Gudbjartsson D, Maloney J, Hoyte K, Gustafson A, Liu Y, Lu Y, Bhangale T, Graham RR, Huttenlocher J, Bjornsdottir G, Andreassen OA, Jonsson EG, Palotie A, Behrens TW, Magnusson OT, Kong A, Thorsteinsdottir U, Watts RJ, Stefansson K (2012) A mutation in APP protects against Alzheimer's disease and age-related cognitive decline. *Nature* **488**, 96-99.

[31] LaFerla FM, Green KN, Oddo S (2007) Intracellular amyloid-beta in Alzheimer's disease. *Nat Rev Neurosci* **8**, 499-509.

[32] O'Brien RJ, Wong PC (2011) Amyloid precursor protein processing and Alzheimer's disease. *Annu Rev Neurosci* **34**, 185-204.

[33] Nicolas M, Hassan BA (2014) Amyloid precursor protein and neural development. *Development* **141**, 2543-2548.

[34] Kojro E, Fahrenholz F (2005) The non-amyloidogenic pathway: structure and function of alpha-secretases. *Subcell Biochem* **38**, 105-127.

[35] Chow VW, Mattson MP, Wong PC, Gleichmann M (2010) An overview of APP processing enzymes and products. *Neuromolecular Med* **12**, 1-12.

[36] Epis R, Marcello E, Gardoni F, Di Luca M (2012) Alpha, beta-and gamma-secretases in Alzheimer's disease. *Front Biosci (Schol Ed)* **4**, 1126-1150.

[37] Jarrett JT, Berger EP, Lansbury PT, Jr. (1993) The carboxy terminus of the beta amyloid protein is critical for the seeding of amyloid formation: implications for the pathogenesis of Alzheimer's disease. *Biochemistry* **32**, 4693-4697.

[38] Younkin SG (1998) The role of A beta 42 in Alzheimer's disease. *J Physiol Paris* **92**, 289-292.

[39] Portelius E, Bogdanovic N, Gustavsson MK, Volkmann I, Brinkmalm G, Zetterberg H, Winblad B, Blennow K (2010) Mass spectrometric characterization of brain amyloid beta isoform signatures in familial and sporadic Alzheimer's disease. *Acta Neuropathol* **120**, 185-193.

[40] Gremer L, Scholzel D, Schenk C, Reinartz E, Labahn J, Ravelli RBG, Tusche M, Lopez-Iglesias C, Hoyer W, Heise H, Willbold D, Schroder GF (2017) Fibril structure of amyloid-beta(1-42) by cryo-electron microscopy. *Science* **358**, 116-119.

[41] Harigaya Y, Saido TC, Eckman CB, Prada CM, Shoji M, Younkin SG (2000) Amyloid beta protein starting pyroglutamate at position 3 is a major component of the amyloid deposits in the Alzheimer's disease brain. *Biochem Biophys Res Commun* **276**, 422-427.

[42] Gunn AP, Masters CL, Cherny RA (2010) Pyroglutamate-Abeta: role in the natural history of Alzheimer's disease. *Int J Biochem Cell Biol* **42**, 1915-1918.

[43] Kuo YM, Emmerling MR, Woods AS, Cotter RJ, Roher AE (1997) Isolation, chemical characterization, and quantitation of A beta 3-pyroglutamyl peptide from neuritic plaques and vascular amyloid deposits. *Biochem Biophys Res Commun* **237**, 188-191.

[44] Schilling S, Lauber T, Schaupp M, Manhart S, Scheel E, Bohm G, Demuth HU (2006) On the seeding and oligomerization of pGlu-amyloid peptides (in vitro). *Biochemistry* **45**, 12393-12399.

[45] Jawhar S, Wirths O, Bayer TA (2011) Pyroglutamate amyloid-beta (Abeta): a hatchet man in Alzheimer disease. *J Biol Chem* **286**, 38825-38832.

[46] Perez-Garmendia R, Gevorkian G (2013) Pyroglutamate-Modified Amyloid Beta Peptides: Emerging Targets for Alzheimer s Disease Immunotherapy. *Curr Neuropharmacol* **11**, 491-498.

[47] Dammers C, Gremer L, Neudecker P, Demuth HU, Schwarten M, Willbold D (2015) Purification and Characterization of Recombinant N-Terminally Pyroglutamate-Modified Amyloid-beta Variants and Structural Analysis by Solution NMR Spectroscopy. *PLoS One* **10**, e0139710.

[48] Dammers C, Reiss K, Gremer L, Lecher J, Ziehm T, Stoldt M, Schwarten M, Willbold D (2017) Pyroglutamate-Modified Amyloid-beta(3-42) Shows alpha-Helical Intermediates before Amyloid Formation. *Biophys J* **112**, 1621-1633.

[49] Dammers C, Gremer L, Reiss K, Klein AN, Neudecker P, Hartmann R, Sun N, Demuth HU, Schwarten M, Willbold D (2015) Structural Analysis and Aggregation Propensity of Pyroglutamate Abeta(3-40) in Aqueous Trifluoroethanol. *PLoS One* **10**, e0143647.

[50] Dammers C, Schwarten M, Buell AK, Willbold D (2017) Pyroglutamate-modified Abeta(3-42) affects aggregation kinetics of Abeta(1-42) by accelerating primary and secondary pathways. *Chem Sci* **8**, 4996-5004.

[51] AlzheimerResearchForum (2017) Therapeutics, Immunotherapy (passive), N3pG-Aβ Monoclonal Antibody, LY3002813. *http://www.alzforum.org/therapeutics/ly3002813* **Accessed on October 18, 2017.**

[52] Glenner GG, Wong CW (1984) Alzheimer's disease: initial report of the purification and characterization of a novel cerebrovascular amyloid protein. *Biochem Biophys Res Commun* **120**, 885-890.

[53] Haass C, Selkoe DJ (2007) Soluble protein oligomers in neurodegeneration: lessons from the Alzheimer's amyloid beta-peptide. *Nat Rev Mol Cell Biol* **8**, 101-112.

[54] Selkoe DJ (2000) Toward a comprehensive theory for Alzheimer's disease. Hypothesis: Alzheimer's disease is caused by the cerebral accumulation and cytotoxicity of amyloid beta-protein. *Ann N Y Acad Sci* **924**, 17-25.

[55] Wang J, Dickson DW, Trojanowski JQ, Lee VM (1999) The levels of soluble versus insoluble brain Abeta distinguish Alzheimer's disease from normal and pathologic aging. *Exp Neurol* **158**, 328-337.

[56] McLean CA, Cherny RA, Fraser FW, Fuller SJ, Smith MJ, Beyreuther K, Bush AI, Masters CL (1999) Soluble pool of Abeta amyloid as a determinant of severity of neurodegeneration in Alzheimer's disease. *Ann Neurol* **46**, 860-866.

[57] Lue LF, Kuo YM, Roher AE, Brachova L, Shen Y, Sue L, Beach T, Kurth JH, Rydel RE, Rogers J (1999) Soluble amyloid beta peptide concentration as a predictor of synaptic change in Alzheimer's disease. *Am J Pathol* **155**, 853-862.

[58] Naslund J, Haroutunian V, Mohs R, Davis KL, Davies P, Greengard P, Buxbaum JD (2000) Correlation between elevated levels of amyloid beta-peptide in the brain and cognitive decline. *Jama* **283**, 1571-1577.

[59] Wang ZX, Tan L, Liu J, Yu JT (2016) The Essential Role of Soluble Abeta Oligomers in Alzheimer's Disease. *Mol Neurobiol* **53**, 1905-1924.

[60] Wolff M, Zhang-Haagen B, Decker C, Barz B, Schneider M, Biehl R, Radulescu A, Strodel B, Willbold D, Nagel-Steger L (2017) Abeta42 pentamers/hexamers are the smallest detectable oligomers in solution. *Sci Rep* **7**, 2493.

[61] Townsend M, Shankar GM, Mehta T, Walsh DM, Selkoe DJ (2006) Effects of secreted oligomers of amyloid beta-protein on hippocampal synaptic plasticity: a potent role for trimers. *J Physiol* **572**, 477-492.

[62] Walsh DM, Klyubin I, Fadeeva JV, Cullen WK, Anwyl R, Wolfe MS, Rowan MJ, Selkoe DJ (2002) Naturally secreted oligomers of amyloid beta protein potently inhibit hippocampal long-term potentiation in vivo. *Nature* **416**, 535-539.

[63] Hardy JA, Higgins GA (1992) Alzheimer's disease: the amyloid cascade hypothesis. *Science* **256**, 184-185.

[64] Selkoe DJ, Hardy J (2016) The amyloid hypothesis of Alzheimer's disease at 25 years. *EMBO Mol Med* **8**, 595-608.

[65] Hardy J, Selkoe DJ (2002) The amyloid hypothesis of Alzheimer's disease: progress and problems on the road to therapeutics. *Science* **297**, 353-356.

[66] Silvestrelli G, Lanari A, Parnetti L, Tomassoni D, Amenta F (2006) Treatment of Alzheimer's disease: From pharmacology to a better understanding of disease pathophysiology. *Mechanisms of Ageing and Development* **127**, 148-157.

[67] Gauthier S (2002) Advances in the pharmacotherapy of Alzheimer's disease. *CMAJ* **166**, 616-623.

[68] Terry AV, Jr., Buccafusco JJ (2003) The cholinergic hypothesis of age and Alzheimer's disease-related cognitive deficits: recent challenges and their implications for novel drug development. *J Pharmacol Exp Ther* **306**, 821-827.

[69] Mohs RC, Davis KL, Levy MI (1981) Partial reversal of anticholinergic amnesia by choline chloride. *Life Sci* **29**, 1317-1323.

[70] Whitehouse PJ, Price DL, Clark AW, Coyle JT, DeLong MR (1981) Alzheimer disease: evidence for selective loss of cholinergic neurons in the nucleus basalis. *Ann Neurol* **10**, 122-126.

[71] White P, Hiley CR, Goodhardt MJ, Carrasco LH, Keet JP, Williams IE, Bowen DM (1977) Neocortical cholinergic neurons in elderly people. *Lancet* **1**, 668-671.

[72] Birks J (2006) Cholinesterase inhibitors for Alzheimer's disease. *Cochrane Database Syst Rev*, Cd005593.

[73] Cummings JL (2004) Alzheimer's disease. *N Engl J Med* **351**, 56-67.

[74] Hung SY, Fu WM (2017) Drug candidates in clinical trials for Alzheimer's disease. *J Biomed Sci* **24**, 47.

[75] Kumar A, Singh A, Ekavali (2015) A review on Alzheimer's disease pathophysiology and its management: an update. *Pharmacol Rep* **67**, 195-203.

[76] Citron M (2010) Alzheimer's disease: strategies for disease modification. *Nat Rev Drug Discov* **9**, 387-398.

[77] Vassar R (2002) Beta-secretase (BACE) as a drug target for Alzheimer's disease. *Adv Drug Deliv Rev* **54**, 1589-1602.

[78] Folch J, Petrov D, Ettcheto M, Abad S, Sanchez-Lopez E, Garcia ML, Olloquequi J, Beas-Zarate C, Auladell C, Camins A (2016) Current Research Therapeutic Strategies for Alzheimer's Disease Treatment. *Neural Plast* **2016**, 8501693.

[79] Imbimbo BP, Giardina GA (2011) gamma-secretase inhibitors and modulators for the treatment of Alzheimer's disease: disappointments and hopes. *Curr Top Med Chem* **11**, 1555-1570.

[80] May PC, Willis BA, Lowe SL, Dean RA, Monk SA, Cocke PJ, Audia JE, Boggs LN, Borders AR, Brier RA, Calligaro DO, Day TA, Ereshefsky L, Erickson JA, Gevorkyan H, Gonzales CR, James DE, Jhee SS, Komjathy SF, Li L, Lindstrom TD, Mathes BM, Martenyi F, Sheehan SM, Stout SL, Timm DE, Vaught GM, Watson BM, Winneroski LL, Yang Z, Mergott DJ (2015) The potent BACE1 inhibitor LY2886721 elicits robust central Abeta pharmacodynamic responses in mice, dogs, and humans. *J Neurosci* **35**, 1199-1210.

[81] Moussa CE (2017) Beta-secretase inhibitors in phase I and phase II clinical trials for Alzheimer's disease. *Expert Opin Investig Drugs* **26**, 1131-1136.

[82] Barao S, Moechars D, Lichtenthaler SF, De Strooper B (2016) BACE1 Physiological Functions May Limit Its Use as Therapeutic Target for Alzheimer's Disease. *Trends Neurosci* **39**, 158-169.

[83] Anand R, Gill KD, Mahdi AA (2014) Therapeutics of Alzheimer's disease: Past, present and future. *Neuropharmacology* **76 Pt A**, 27-50.

[84] Etcheberrigaray R, Tan M, Dewachter I, Kuiperi C, Van der Auwera I, Wera S, Qiao L, Bank B, Nelson TJ, Kozikowski AP, Van Leuven F, Alkon DL (2004) Therapeutic effects of PKC activators in Alzheimer's disease transgenic mice. *Proc Natl Acad Sci U S A* **101**, 11141-11146.

[85] Singh S, Kushwah AS, Singh R, Farswan M, Kaur R (2012) Current therapeutic strategy in Alzheimer's disease. *Eur Rev Med Pharmacol Sci* **16**, 1651-1664.

[86] Gilman S, Koller M, Black RS, Jenkins L, Griffith SG, Fox NC, Eisner L, Kirby L, Rovira MB, Forette F, Orgogozo JM, Team ANS (2005) Clinical effects of Abeta immunization (AN1792) in patients with AD in an interrupted trial. *Neurology* **64**, 1553-1562.

[87] Panza F, Solfrizzi V, Imbimbo BP, Logroscino G (2014) Amyloid-directed monoclonal antibodies for the treatment of Alzheimer's disease: the point of no return? *Expert Opin Biol Ther* **14**, 1465-1476.

[88] Kulshreshtha A, Piplani P (2016) Current pharmacotherapy and putative disease-modifying therapy for Alzheimer's disease. *Neurol Sci* **37**, 1403-1435.

[89] Gold M (2017) Phase II clinical trials of anti-amyloid beta antibodies: When is enough, enough? *Alzheimers Dement (N Y)* **3**, 402-409.

[90] Ferrero J, Williams L, Stella H, Leitermann K, Mikulskis A, O'Gorman J, Sevigny J (2016) First-in-human, double-blind, placebo-controlled, single-dose escalation study of aducanumab (BIIB037) in mild-to-moderate Alzheimer's disease. *Alzheimers Dement (N Y)* **2**, 169-176.

[91] Sevigny J, Chiao P, Bussiere T, Weinreb PH, Williams L, Maier M, Dunstan R, Salloway S, Chen T, Ling Y, O'Gorman J, Qian F, Arastu M, Li M, Chollate S, Brennan MS, Quintero-Monzon O, Scannevin RH, Arnold HM, Engber T, Rhodes K, Ferrero J, Hang Y, Mikulskis A, Grimm J, Hock C, Nitsch RM, Sandrock A (2016) The antibody aducanumab reduces Abeta plaques in Alzheimer's disease. *Nature* **537**, 50-56.

[92] Janusz M, Zablocka A (2010) Colostral proline-rich polypeptides--immunoregulatory properties and prospects of therapeutic use in Alzheimer's disease. *Curr Alzheimer Res* **7**, 323-333.

[93] Bilikiewicz A, Gaus W (2004) Colostrinin (a naturally occurring, proline-rich, polypeptide mixture) in the treatment of Alzheimer's disease. *J Alzheimers Dis* **6**, 17-26.

[94] Goyal D, Shuaib S, Mann S, Goyal B (2017) Rationally Designed Peptides and Peptidomimetics as Inhibitors of Amyloid-beta (Abeta) Aggregation: Potential Therapeutics of Alzheimer's Disease. *ACS Comb Sci* **19**, 55-80.

[95] Funke SA, Willbold D (2012) Peptides for therapy and diagnosis of Alzheimer's disease. *Curr Pharm Des* **18**, 755-767.

[96] Tjernberg LO, Naslund J, Lindqvist F, Johansson J, Karlstrom AR, Thyberg J, Terenius L, Nordstedt C (1996) Arrest of beta-amyloid fibril formation by a pentapeptide ligand. *J Biol Chem* **271**, 8545-8548.

[97] Tjernberg LO, Lilliehook C, Callaway DJ, Naslund J, Hahne S, Thyberg J, Terenius L, Nordstedt C (1997) Controlling amyloid beta-peptide fibril formation with protease-stable ligands. *J Biol Chem* **272**, 12601-12605.

[98] Funke AS, van Groen T, Kadish I, Bartnik D, Nagel-Steger L, Brener O, Sehl T, Batra-Safferling R, Moriscot C, Schoehn G, Horn AH, Muller-Schiffmann A, Korth C, Sticht H, Willbold D (2010) Oral treatment with the d-enantiomeric peptide D3 improves the pathology and behavior of Alzheimer's Disease transgenic mice. *ACS Chem Neurosci* **1**, 639-648.

[99] Wiesehan K, Buder K, Linke RP, Patt S, Stoldt M, Unger E, Schmitt B, Bucci E, Willbold D (2003) Selection of D-amino-acid peptides that bind to Alzheimer's disease amyloid peptide abeta1-42 by mirror image phage display. *Chembiochem* **4**, 748-753.

[100] van Groen T, Wiesehan K, Funke SA, Kadish I, Nagel-Steger L, Willbold D (2008) Reduction of Alzheimer's disease amyloid plaque load in transgenic mice by D3, A D-enantiomeric peptide identified by mirror image phage display. *ChemMedChem* **3**, 1848-1852.

[101] van Groen T, Kadish, I., Funke, A. S., Bartnik, D., Willbold, D. (2012) Treatment with Aβ42 Binding d-Amino Acid Peptides Reduce Amyloid Deposition and Inflammation in APP/PS1 Double Transgenic Mice. *Advances in Protein Chemistry and Structural Biology* **88**, 133-152.

[102] van Groen T, Kadish I, Funke SA, Bartnik D, Willbold D (2013) Treatment with D3 removes amyloid deposits, reduces inflammation, and improves cognition in aged AbetaPP/PS1 double transgenic mice. *J Alzheimers Dis* **34**, 609-620.

[103] Brener O, Dunkelmann T, Gremer L, van Groen T, Mirecka EA, Kadish I, Willuweit A, Kutzsche J, Jurgens D, Rudolph S, Tusche M, Bongen P, Pietruszka J, Oesterhelt F, Langen KJ, Demuth HU, Janssen A, Hoyer W, Funke SA, Nagel-Steger L, Willbold D (2015) QIAD assay for quantitating a compound's efficacy in elimination of toxic Abeta oligomers. *Sci Rep* **5**, 13222.

[104] Olubiyi OO, Frenzel D, Bartnik D, Gluck JM, Brener O, Nagel-Steger L, Funke SA, Willbold D, Strodel B (2014) Amyloid aggregation inhibitory mechanism of arginine-rich D-peptides. *Curr Med Chem* **21**, 1448-1457.

[105] Elfgen A, Santiago-Schubel B, Gremer L, Kutzsche J, Willbold D (2017) Surprisingly high stability of the Abeta oligomer eliminating all-d-enantiomeric peptide D3 in media simulating the route of orally administered drugs. *Eur J Pharm Sci* **107**, 203-207.

[106] Liu H, Funke SA, Willbold D (2010) Transport of Alzheimer disease amyloid-beta-binding D-amino acid peptides across an in vitro blood-brain barrier model. *Rejuvenation Res* **13**, 210-213.

[107] Jiang N, Leithold LH, Post J, Ziehm T, Mauler J, Gremer L, Cremer M, Schartmann E, Shah NJ, Kutzsche J, Langen KJ, Breitkreutz J, Willbold D, Willuweit A (2015) Preclinical Pharmacokinetic Studies of the Tritium Labelled D-Enantiomeric Peptide D3 Developed for the Treatment of Alzheimer s Disease. *PLoS One* **10**, e0128553.

[108] Aileen Funke S, van Groen T, Kadish I, Bartnik D, Nagel-Steger L, Brener O, Sehl T, Batra-Safferling R, Moriscot C, Schoehn G, Horn AH, Muller-Schiffmann A, Korth C, Sticht H, Willbold D (2010) Oral treatment with the d-enantiomeric peptide D3 improves the pathology and behavior of Alzheimer's Disease transgenic mice. *ACS Chem Neurosci* **1**, 639-648.

[109] Dunkelmann T, Teichmann K, Ziehm T, Schemmert S, Frenzel D, Tusche M, Dammers C, Jürgens D, Langen K-J, Demuth H-U, Shah NJ, Kutzsche J, Willuweit A, Willbold D (2017) Aβ oligomer eliminating compounds interfere successfully with pEAβ (3–42) induced motor neurodegenerative phenotype in transgenic mice. *Neuropeptides*.

[110] Dunkelmann T, Teichmann K, Ziehm T, Schemmert S, Frenzel D, Tusche M, Dammers C, Jurgens D, Langen KJ, Demuth HU, Shah NJ, Kutzsche J, Willuweit A, Willbold D (2017) Abeta oligomer eliminating compounds interfere successfully with pEAbeta(3-42) induced motor neurodegenerative phenotype in transgenic mice. *Neuropeptides*.

[111] Klein AN, Ziehm T, Tusche M, Buitenhuis J, Bartnik D, Boeddrich A, Wiglenda T, Wanker E, Funke SA, Brener O, Gremer L, Kutzsche J, Willbold D (2016) Optimization of the All-D Peptide D3 for Abeta Oligomer Elimination. *PLoS One* **11**, e0153035.

[112] Klein AN, Ziehm T, van Groen T, Kadish I, Elfgen A, Tusche M, Thomaier M, Reiss K, Brener O, Gremer L, Kutzsche J, Willbold D (2017) Optimization of D-peptides for Abeta monomer binding specificity enhances their potential to eliminate toxic Abeta oligomers. *ACS Chem Neurosci*.

[113] Leithold LH, Jiang N, Post J, Ziehm T, Schartmann E, Kutzsche J, Shah NJ, Breitkreutz J, Langen KJ, Willuweit A, Willbold D (2016) Pharmacokinetic Properties of a Novel D-Peptide Developed to be Therapeutically Active Against Toxic beta-Amyloid Oligomers. *Pharm Res* **33**, 328-336.

[114] Schiffter HA (2009) *Pharmakokinetik - Modelle und Berechnungen: mit 25 Tabellen*, Wiss. Verlag-Ges.

[115] Herdegen T (2010) *Kurzlehrbuch Pharmakologie und Toxikologie*, Thieme.

[116] Hein L, Lüllmann H, Mohr K (2014) *Taschenatlas Pharmakologie*, Thieme.

[117] Caldwell J, Gardner I, Swales N (1995) An introduction to drug disposition: the basic principles of absorption, distribution, metabolism, and excretion. *Toxicol Pathol* **23**, 102-114.

[118] Freissmuth M, Offermanns S, Böhm S (2016) *Pharmakologie und Toxikologie: Von den molekularen Grundlagen zur Pharmakotherapie*, Springer Berlin Heidelberg.

[119] Terwel D, Muyllaert D, Dewachter I, Borghgraef P, Croes S, Devijver H, Van Leuven F (2008) Amyloid activates GSK-3beta to aggravate neuronal tauopathy in bigenic mice. *Am J Pathol* **172**, 786-798.

[120] Oddo S, Caccamo A, Shepherd JD, Murphy MP, Golde TE, Kayed R, Metherate R, Mattson MP, Akbari Y, LaFerla FM (2003) Triple-transgenic model of Alzheimer's disease with plaques and tangles: intracellular Abeta and synaptic dysfunction. *Neuron* **39**, 409-421.

[121] Games D, Adams D, Alessandrini R, Barbour R, Berthelette P, Blackwell C, Carr T, Clemens J, Donaldson T, Gillespie F, et al. (1995) Alzheimer-type neuropathology in transgenic mice overexpressing V717F beta-amyloid precursor protein. *Nature* **373**, 523-527.

[122] Jankowsky JL, Fadale DJ, Anderson J, Xu GM, Gonzales V, Jenkins NA, Copeland NG, Lee MK, Younkin LH, Wagner SL, Younkin SG, Borchelt DR (2004) Mutant presenilins specifically elevate the levels of the 42 residue beta-amyloid peptide in vivo: evidence for augmentation of a 42-specific gamma secretase. *Hum Mol Genet* **13**, 159-170.

[123] Garcia-Alloza M, Robbins EM, Zhang-Nunes SX, Purcell SM, Betensky RA, Raju S, Prada C, Greenberg SM, Bacskai BJ, Frosch MP (2006) Characterization of amyloid deposition in the APPswe/PS1dE9 mouse model of Alzheimer disease. *Neurobiol Dis* **24**, 516-524.

[124] Kamphuis W, Mamber C, Moeton M, Kooijman L, Sluijs JA, Jansen AH, Verveer M, de Groot LR, Smith VD, Rangarajan S, Rodriguez JJ, Orre M, Hol EM (2012) GFAP isoforms in adult mouse brain with a focus on neurogenic astrocytes and reactive astrogliosis in mouse models of Alzheimer disease. *PLoS One* **7**, e42823.

[125] Lalonde R, Kim HD, Maxwell JA, Fukuchi K (2005) Exploratory activity and spatial learning in 12-month-old APP(695)SWE/co+PS1/DeltaE9 mice with amyloid plaques. *Neurosci Lett* **390**, 87-92.

[126] Filali M, Lalonde R (2009) Age-related cognitive decline and nesting behavior in an APPswe/PS1 bigenic model of Alzheimer's disease. *Brain Res* **1292**, 93-99.

[127] Rockenstein E, Mallory M, Mante M, Sisk A, Masliaha E (2001) Early formation of mature amyloid-beta protein deposits in a mutant APP transgenic model depends on levels of Abeta(1-42). *J Neurosci Res* **66**, 573-582.

[128] Havas D, Hutter-Paier B, Ubhi K, Rockenstein E, Crailsheim K, Masliah E, Windisch M (2011) A longitudinal study of behavioral deficits in an AbetaPP transgenic mouse model of Alzheimer's disease. *J Alzheimers Dis* **25**, 231-243.

[129] Loffler T, Flunkert S, Havas D, Schweinzer C, Uger M, Windisch M, Steyrer E, Hutter-Paier B (2014) Neuroinflammation and related neuropathologies in APPSL mice: further value of this in vivo model of Alzheimer's disease. *J Neuroinflammation* **11**, 84.

[130] Alexandru A, Jagla W, Graubner S, Becker A, Bauscher C, Kohlmann S, Sedlmeier R, Raber KA, Cynis H, Ronicke R, Reymann KG, Petrasch-Parwez E, Hartlage-Rubsamen M, Waniek A, Rossner S, Schilling S, Osmand AP, Demuth HU, von Horsten S (2011) Selective hippocampal neurodegeneration in transgenic mice expressing small amounts of truncated Abeta is induced by pyroglutamate-Abeta formation. *J Neurosci* **31**, 12790-12801.

[131] Vegh MJ, Heldring CM, Kamphuis W, Hijazi S, Timmerman AJ, Li KW, van Nierop P, Mansvelder HD, Hol EM, Smit AB, van Kesteren RE (2014) Reducing hippocampal extracellular matrix reverses early memory deficits in a mouse model of Alzheimer's disease. *Acta Neuropathol Commun* **2**, 76.

[132] Maguire EA, Gadian DG, Johnsrude IS, Good CD, Ashburner J, Frackowiak RS, Frith CD (2000) Navigation-related structural change in the hippocampi of taxi drivers. *Proc Natl Acad Sci U S A* **97**, 4398-4403.
[133] Maguire EA, Woollett K, Spiers HJ (2006) London taxi drivers and bus drivers: a structural MRI and neuropsychological analysis. *Hippocampus* **16**, 1091-1101.
[134] Morris R (1984) Developments of a water-maze procedure for studying spatial learning in the rat. *J Neurosci Methods* **11**, 47-60.
[135] Morris RG, Garrud P, Rawlins JN, O'Keefe J (1982) Place navigation impaired in rats with hippocampal lesions. *Nature* **297**, 681-683.
[136] Ameen-Ali KE, Wharton SB, Simpson JE, Heath PR, Sharp P, Berwick J (2017) Review: Neuropathology and behavioural features of transgenic murine models of Alzheimer's disease. *Neuropathol Appl Neurobiol* **43**, 553-570.
[137] Leger M, Quiedeville A, Bouet V, Haelewyn B, Boulouard M, Schumann-Bard P, Freret T (2013) Object recognition test in mice. *Nat Protoc* **8**, 2531-2537.
[138] Cohen SJ, Stackman RW, Jr. (2015) Assessing rodent hippocampal involvement in the novel object recognition task. A review. *Behav Brain Res* **285**, 105-117.
[139] Ennaceur A (2010) One-trial object recognition in rats and mice: methodological and theoretical issues. *Behav Brain Res* **215**, 244-254.
[140] Hammond RS, Tull LE, Stackman RW (2004) On the delay-dependent involvement of the hippocampus in object recognition memory. *Neurobiol Learn Mem* **82**, 26-34.
[141] Deacon RM (2013) Measuring motor coordination in mice. *J Vis Exp*, e2609.
[142] Walsh RN, Cummins RA (1976) The Open-Field Test: a critical review. *Psychol Bull* **83**, 482-504.
[143] Seibenhener ML, Wooten MC (2015) Use of the Open Field Maze to measure locomotor and anxiety-like behavior in mice. *J Vis Exp*, e52434.
[144] Rogers DC, Fisher EMC, Brown SDM, Peters J, Hunter AJ, Martin JE (1997) Behavioral and functional analysis of mouse phenotype: SHIRPA, a proposed protocol for comprehensive phenotype assessment. *Mammalian Genome* **8**, 711-713.
[145] Dunham NW, Miya TS (1957) A note on a simple apparatus for detecting neurological deficit in rats and mice. *J Am Pharm Assoc Am Pharm Assoc* **46**, 208-209.
[146] Rodriguez JJ, Olabarria M, Chvatal A, Verkhratsky A (2009) Astroglia in dementia and Alzheimer's disease. *Cell Death Differ* **16**, 378-385.
[147] Grillner S, Robertson B, Stephenson-Jones M (2013) The evolutionary origin of the vertebrate basal ganglia and its role in action selection. *J Physiol* **591**, 5425-5431.
[148] Pappas SS, Leventhal DK, Albin RL, Dauer WT (2014) Mouse models of neurodevelopmental disease of the basal ganglia and associated circuits. *Curr Top Dev Biol* **109**, 97-169.
[149] Wirths O, Bayer TA (2008) Motor impairment in Alzheimer's disease and transgenic Alzheimer's disease mouse models. *Genes Brain Behav* **7 Suppl 1**, 1-5.
[150] Buchman AS, Bennett DA (2011) Loss of motor function in preclinical Alzheimer's disease. *Expert Rev Neurother* **11**, 665-676.
[151] Bouter Y, Dietrich K, Wittnam JL, Rezaei-Ghaleh N, Pillot T, Papot-Couturier S, Lefebvre T, Sprenger F, Wirths O, Zweckstetter M, Bayer TA (2013) N-truncated amyloid beta (Abeta) 4-42 forms stable aggregates and induces acute and long-lasting behavioral deficits. *Acta Neuropathol* **126**, 189-205.
[152] Hsiao K, Chapman P, Nilsen S, Eckman C, Harigaya Y, Younkin S, Yang F, Cole G (1996) Correlative memory deficits, Abeta elevation, and amyloid plaques in transgenic mice. *Science* **274**, 99-102.
[153] Frautschy SA, Yang F, Irrizarry M, Hyman B, Saido TC, Hsiao K, Cole GM (1998) Microglial response to amyloid plaques in APPsw transgenic mice. *Am J Pathol* **152**, 307-317.
[154] Oakley H, Cole SL, Logan S, Maus E, Shao P, Craft J, Guillozet-Bongaarts A, Ohno M, Disterhoft J, Van Eldik L, Berry R, Vassar R (2006) Intraneuronal beta-amyloid aggregates, neurodegeneration, and neuron loss in transgenic mice with five familial Alzheimer's disease mutations: potential factors in amyloid plaque formation. *J Neurosci* **26**, 10129-10140.
[155] Jackson RJ, Rudinskiy N, Herrmann AG, Croft S, Kim JM, Petrova V, Ramos-Rodriguez JJ, Pitstick R, Wegmann S, Garcia-Alloza M, Carlson GA, Hyman BT, Spires-Jones TL (2016) Human tau increases amyloid beta plaque size but not amyloid beta-mediated synapse loss in a novel mouse model of Alzheimer's disease. *Eur J Neurosci* **44**, 3056-3066.
[156] Meissner JN, Bouter Y, Bayer TA (2015) Neuron Loss and Behavioral Deficits in the TBA42 Mouse Model Expressing N-Truncated Pyroglutamate Amyloid-beta3-42. *J Alzheimers Dis* **45**, 471-482.
[157] Wirths O, Breyhan H, Cynis H, Schilling S, Demuth HU, Bayer TA (2009) Intraneuronal pyroglutamate-Abeta 3-42 triggers neurodegeneration and lethal neurological deficits in a transgenic mouse model. *Acta Neuropathol* **118**, 487-496.
[158] van Groen T, Schemmert S, Brener O, Gremer L, Ziehm T, Tusche M, Nagel-Steger L, Kadish I, Schartmann E, Elfgen A, Jurgens D, Willuweit A, Kutzsche J, Willbold D (2017) The Abeta oligomer eliminating D-enantiomeric peptide RD2 improves cognition without changing plaque pathology. *Sci Rep* **7**, 16275.
[159] Kutzsche J, Schemmert S, Tusche M, Neddens J, Rabl R, Jurgens D, Brener O, Willuweit A, Hutter-Paier B, Willbold D (2017) Large-Scale Oral Treatment Study with the Four Most Promising D3-Derivatives for the Treatment of Alzheimer's Disease. *Molecules* **22**.
[160] Wang-Dietrich L, Funke SA, Kuhbach K, Wang K, Besmehn A, Willbold S, Cinar Y, Bannach O, Birkmann E, Willbold D (2013) The amyloid-beta oligomer count in cerebrospinal fluid is a biomarker for Alzheimer's disease. *J Alzheimers Dis* **34**, 985-994.

[161] Kuhbach K, Hulsemann M, Herrmann Y, Kravchenko K, Kulawik A, Linnartz C, Peters L, Wang K, Willbold J, Willbold D, Bannach O (2016) Application of an Amyloid Beta Oligomer Standard in the sFIDA Assay. *Front Neurosci* **10**, 8.

[162] Herrmann Y, Bujnicki T, Zafiu C, Kulawik A, Kuhbach K, Peters L, Fabig J, Willbold J, Bannach O, Willbold D (2017) Nanoparticle standards for immuno-based quantitation of alpha-synuclein oligomers in diagnostics of Parkinson's disease and other synucleinopathies. *Clin Chim Acta* **466**, 152-159.

[163] Herrmann Y, Kulawik A, Kuhbach K, Hulsemann M, Peters L, Bujnicki T, Kravchenko K, Linnartz C, Willbold J, Zafiu C, Bannach O, Willbold D (2017) sFIDA automation yields sub-femtomolar limit of detection for Abeta aggregates in body fluids. *Clin Biochem* **50**, 244-247.

[164] Ziehm T, Brener O, van Groen T, Kadish I, Frenzel D, Tusche M, Kutzsche J, Reiss K, Gremer L, Nagel-Steger L, Willbold D (2016) Increase of Positive Net Charge and Conformational Rigidity Enhances the Efficacy of d-Enantiomeric Peptides Designed to Eliminate Cytotoxic Abeta Species. *ACS Chem Neurosci*.

[165] Leithold LH, Jiang N, Post J, Niemietz N, Schartmann E, Ziehm T, Kutzsche J, Shah NJ, Breitkreutz J, Langen KJ, Willuweit A, Willbold D (2016) Pharmacokinetic properties of tandem d-peptides designed for treatment of Alzheimer's disease. *Eur J Pharm Sci* **89**, 31-38.

[166] Schartmann E, Schemmert S, Ziehm T, Leithold LHE, Jiang N, Tusche M, Jon Shah N, Langen KJ, Kutzsche J, Willbold D, Willuweit A (2017) Comparison of blood-brain barrier penetration efficiencies between linear and cyclic all-d-enantiomeric peptides developed for the treatment of Alzheimer's disease. *Eur J Pharm Sci*.

[167] Van Dorpe S, Bronselaer A, Nielandt J, Stalmans S, Wynendaele E, Audenaert K, Van De Wiele C, Burvenich C, Peremans K, Hsuchou H, De Tré G, De Spiegeleer B (2012) Brainpeps: the blood–brain barrier peptide database. *Brain Structure and Function* **217**, 687-718.

Druckgenehmigung

Title: Aβ oligomer eliminating compounds interfere successfully with pEAβ(3–42) induced motor neurodegenerative phenotype in transgenic mice

Author: Tina Dunkelmann,Kerstin Teichmann,Tamar Ziehm,Sarah Schemmert,Daniel Frenzel,Markus Tusche,Christina Dammers,Dagmar Jürgens,Karl-Josef Langen,Hans-Ulrich Demuth,Nadim Jon Shah,Janine Kutzsche,Antje Willuweit,Dieter Willbold

Publication: Neuropeptides

Publisher: Elsevier

Date: Available online 27 November 2017